NASA Conference Publication 3271

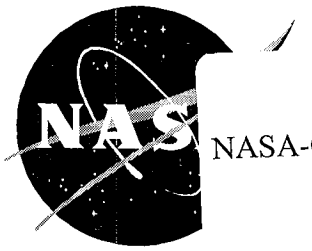

NASA-CP-3271 19940033285

Workshop on Scaling Effects in Composite Materials and Structures

Compiled by
Karen E. Jackson

Proceedings of a workshop jointly sponsored by the National Aeronautics and Space Administration, Washington, D.C., Virginia Polytechnic Institute and State University, Blacksburg, Virginia, and the University of California, San Diego, California, and held at Langley Research Center Hampton, Virginia November 15–16, 1993

July 1994

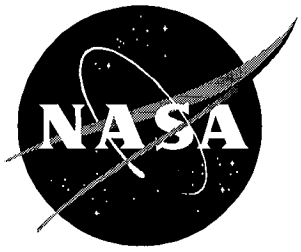

NASA Conference Publication 3271

Workshop on Scaling Effects in Composite Materials and Structures

Compiled by
Karen E. Jackson
Langley Research Center • Hampton, Virginia

Proceedings of a workshop jointly sponsored by the National Aeronautics and Space Administration, Washington, D.C., Virginia Polytechnic Institute and State University, Blacksburg, Virginia, and the University of California, San Diego, California, and held at Langley Research Center Hampton, Virginia November 15–16, 1993

National Aeronautics and Space Administration
Langley Research Center • Hampton, Virginia 23681-0001

July 1994

PREFACE

This document contains the proceedings of the Workshop on Scaling Effects in Composite Materials and Structures held at NASA Langley Research Center, November 15–16, 1993. The workshop was jointly sponsored by NASA, the Engineering Science and Mechanics Department of Virginia Tech, and the Institute for Mechanics and Materials of the University of California at San Diego. Workshop attendees represented government agencies, academia, and the aircraft industry. The objectives of the workshop were to bring together, for the first time, researchers working to identify and characterize size dependent properties of composite materials and structures, to determine the state-of-technology in this field, and to assess the directions and technology shortfalls for future research efforts.

The document contains a brief abstract and presentation materials from each of the technical presentations made during the two-day workshop. While this information is not as complete as might be found in a technical paper, it is suggested that additional information be obtained directly from the individual presenters. The names and addresses of the presenters are provided in the list of attendees.

The use of trade names of manufacturers in this report does not constitute an official endorsement of such products or manufacturers, either expressed or implied, by the National Aeronautics and Space Administration.

Karen E. Jackson
US Army Vehicle Structures Directorate, ARL
NASA Langley Research Center
Hampton, Virginia 23681

INTRODUCTION

The increased application of advanced composite materials in the aircraft industry has raised issues related to scale model technology. For composite materials, it is expensive and time consuming to fabricate and test full-scale components during the design evaluation phase. An obvious alternative might be scale model testing. But, can tests on scale model composite structures be used to predict the behavior of expensive prototypes? This question and other related questions have been the subject of recent research and were addressed during this workshop. Some of the important issues are listed as follows:

> Are the scaling laws developed and validated, which will permit data generated on subscale components to predict full-scale behavior?
>
> What are the issues related to construction of scale models using inhomogeneous, layered composite materials?
>
> What is the significance of size dependent material properties for composite materials?
>
> What level of scaling is necessary for realistic structural problems? Microstructural scaling? Ply-level scaling? Sublaminate-level scaling? Macrostructural scaling?
>
> What are the equations which govern the interactions between the microstructural and macrostructural scales?

The objectives of this workshop were to gather together the leading researchers in scale model research to discuss the state-of-technology, attempt to address some of the issues highlighted previously, and define future directions for scale model research. The presentations were divided into four sessions along the following topic areas: Scaling Effects in (1) Structures, (2) Material Properties, Failure, and Damage Mechanics, and (3) Impact Response.

The ideal technique for constructing scale model composite structures would be to geometrically scale the constituent materials, the fiber and the matrix, or the microstructure. This method, however, is too expensive to be a practical alternative. In lieu of microstructural scaling, several other techniques have been used to fabricate scale model composite structures on the macrostructural level. In **ply-level** scaling, the baseline, or model, laminate stacking sequence is "scaled-up" by simply increasing the number of layers for each angular ply orientation. For example, a baseline 8-ply quasi-isotropic lay-up [+45° /-45° /0° /90°]s is scaled to twice the baseline thickness by doubling the number of plies at each orientation, [+45° 2/-45° 2/0° 2/90° 2]s. Ply-level scaled laminates are constitutively similar in that the in-plane and bending moduli are appropriately scaled.

A second macrostructural scaling technique is called **sublaminate-level** scaling. In this method the laminate thickness is scaled by repeating the baseline stacking sequence as a sublaminate group. For example, the 8-ply quasi-isotropic laminate mentioned previously is "scaled-up" as [(+45°/-45°/0°/90°)]2s using the sublaminate-level scaling approach. Note that the in-plane moduli are scaled appropriately between

two different sized specimens using the sublaminate-level scaling technique, but the flexural moduli are distorted.

Finally, a third technique for scaling composite laminates on the macrostructural level is called **sub-ply level** scaling. In this method, the standard pre-preg ply thickness is scaled by reducing the number of fibers through-the-thickness. For example, a standard graphite-epoxy pre-preg ply, designated Grade 190, has between 12–16 fibers through the thickness of a single ply and is approximately 0.005 inches thick. A Grade 95 graphite-epoxy pre-preg ply has approximately 6–8 fibers through a single ply and is about 0.0025 inches thick. And, a Grade 48 ply has approximately 3–4 fibers through the thickness of a single ply and is approximately 0.00125 inches thick. Thus, a subscale component or structure can be fabricated from the reduced-thickness material. Both ply-level and sublaminate-level scaling techniques can be used in combination with the sub-ply scaling approach. Disadvantages of this technique are the expense of the reduced-thickness material; e.g., the Grade 48 material costs $500 per pound, and only two or three scaled materials may be available.

Previous research has demonstrated that ply-level scaled composite tensile coupons exhibit a reduced ultimate strength with increasing size or scale. Likewise, ply-level scaled flexural beams exhibit the same trend. The magnitude of the "size" effect is dependent on laminate stacking sequence. Generally, laminates containing 0° plies, such as cross-ply or quasi-isotropic lay-ups, show less of the size effect than laminates which contain no 0° plies, such as angle-ply lay-ups. An opposite trend has been observed for sublaminate-scaled tensile coupons. In general, the larger specimens have greater strength than the subscale counterparts. The effect is particularly dramatic for angle ply, ±45° laminates. Ply-level scaled tensile coupons exhibit a linear-elastic response until ultimate failure, with the smaller specimens exhibiting a much greater ultimate strength than the prototype. Sublaminate-level scaled tensile coupons exhibit a classic linear elastic-plastic response, with the larger specimens failing at greater stresses and strains than their subscale counterparts. These findings have promoted modifications to the ASTM standard test methods for determination of shear modulus and strength, since these standards rely on tests of ±45° tensile coupons.

The significance of the research on scaling effects in composite materials is that, in general, current failure criteria do not account for the effect. Strength theories such as maximum stress or strain, or the tensor polynomial criteria are not size dependent. Weibull statistical approaches have been used, but they tend to be material and laminate specific, and therefore not applicable to broad classes of composite materials and laminate stacking sequences. Stress intensity criteria as well as strain energy release rate criteria do incorporate a degree of size dependency. However, the effect is not laminate dependent. A new failure theory or a combination of some of the criteria mentioned previously is required to model the complex issue of size dependent failure mechanics in composite materials.

It is anticipated that continued research on scaling effects in composite materials will lead to the development of validated scaling laws such that data generated on the subscale level can be used to predict the behavior of full-scale components.

FUTURE DIRECTIONS AND NEEDS

1. Develop failure criteria which incorporate statistical methods and combined stress
2. How do we bridge the micro and macro levels?
3. How are scale effects and structural instability related?
4. Ply thickness effects—how do we handle thicker-than-standard plies?
5. Specify resin toughness as a variable?
6. What design techniques can be applied to avoid scale effects?
7. Catalog the design methodology.
8. Study damage characterization and evolution in scaled structures?
9. Determine size effect in the fatigue loading environment?
10. Measure stress concentration at fiber breaks?
11. Incorporate size dependent failure criteria for computer simulation.
12. Examine the sources of scale effects.

CONTENTS

MATERIAL PROPERTIES, FAILURE AND DAMAGE MECHANICS SESSION II

Felton Bartlett, Moderator

IMPACT SESSION

C. C. Poe, Jr., Moderator

List of Attendees

Irving Abel
NASA Langley Research Center
3 Langley Boulevard
M.S. 242
Hampton, VA 23681-0001
Phone: (804)864-2934
FAX: (804)864-7792

Damodar Ambur
NASA Langley Research Center
8 W. Taylor Street
M.S. 190
Hampton, VA 23681-0001
Phone: (804)864-3174

Mark Anstey
Micro Craft, Inc.
3130 N. Armistead Avenue
M.S. 918
Hampton, VA 23666
Phone: (804) 865-7760
FAX: (804) 865-7487

Donald J. Baker
U. S. Army Vehicle Structures Dir.
NASA Langley Research Center
M.S. 190
Hampton, VA 23681-0001
Phone: (804)864-3171
FAX: (804) 864-7791

Felton D. Bartlett, Jr.
U.S. Army Vehicle Structures Dir.
NASA Langley Research Center
M.S. 266
Hampton, VA 23681-0001
Phone: (804) 864-3960

Charles P. Blankenship
NASA Langley Research Center
11 Langley Boulevard
M.S. 118
Hampton, VA 23681-0001
Phone: (804)864-6005

Richard Boitnott
U.S. Army Vehicle Structures Dir.
NASA Langley Research Center
M.S. 495
Hampton, VA 23681-0001
Phone: (804)864-4161
FAX: (804)864-8547

John Botsis, Ph.D.
Dept. of Civil Engineering, Mechanics, and Metallurgy (M/C 246)UIC College of Engineering
Box 4348
Chicago, IL 60680
Phone: (312)996-8260
FAX: (312)996-2426

Eugene J. Brunelle
4006 JEC
Rensselaer Polytechnic Institute
Troy, NY 12180-3590
Phone: (518) 276-6705
FAX: (518) 276-2623

Suzann Burris
Micro Craft, Inc.
3130 N. Armistead Avenue
M.S. 918
Hampton, VA 23666

Ari G. Caliskan
Univ. of Illinois, Chicago
6912 N. Waukesha Ave.
Chicago, IL 60646
Phone: (312)792-0183

Gene Camponeschi
CD/NSWC
CODE 2802
Annapolis, MD 21402
Phone: (410)267-2165

Huey D. Carden
NASA Langley Research Center
12 W. Bush Rd.
M.S. 495
Hampton, VA 23681-0001
Phone: (804)864-4151
FAX: (804)864-8547

Robert V. Doggett
NASA Langley Research Center
3 Langley Boulevard
M.S. 242
Hampton, VA 23681-0001
Phone: (804)864-2934
FAX: (804)864-7792

Edwin Fasanella
Lockheed Engineering and Science Company
144 Research Dr.
Hampton, VA 23666
Phone: (804)766-9630
FAX: (804)766-9601

Donald B. Ford
ED52
Marshall Space Flight Center, AL 35812
Phone: (205) 544-2454
Fax: (205) 544-8110

William T. Freeman, Jr.
NASA Langley Research Center
3 Langley Boulevard
M.S. 241
Hampton, VA 23681-0001
Phone: (804)864-2945

Glenn C. Grimes
Lockheed Advanced Development Company
D/25-43. B/311, P/B-6
P.O. Box 250 Dept. 2543
Sunland, CA 91041
Phone: (818)847-0695
FAX: (818)847-8865

Sathya V. Hanagud, Ph.D.
Professor
School of Aerospace Engineering
Georgia Institute of Technology
Atlanta, GA 30332-0150
Phone: (606) 896-3060
FAX: (606) 894-2760

Martin W. Hargrave
Federal Highway Administration
Turner-Fairbank Highway Res. Ctr.
6300 Georgetown Pike (HSR -20)
Mclean, VA 22101-2296
Phone: (703) 285-2508
FAX: (703) 285-2379

Dan R. Hoad
U.S. Army Vehicle Strucutures Dir.
NASA Langley Research Center
M.S. 266
Hampton, VA 23681-0001
Phone: (804)864-5060

Ron Hoffman
University of Dayton
Research Institute
300 College Park
Dayton, OH 45469-0182
Phone: (513)229-3861
FAX: (513)229-3869

Steve Hooper, Asst. Prof.
Dept. of Aeronautical Engineering
Wichita State University
1845 Fairmount
Wichita, KA 67260-0093
Phone: (316)689-3678
FAX: (316)689-3175

Kailasam Iyer
Army Research Office
P.O. Box 12211
Research Triangle Park, NC 27709-2211
Phone: (919)549-4258
FAX: (919)549-4310

Karen Jackson
U.S. Army Vehicle Structures Dir.
NASA Langley Research Center
M.S. 495
Hampton, VA 23681-0001
Phone: (804)864-4147
FAX: (804)864-8547

David P. Johnson
E.S.M. Dept. 225 Norris Hall
VPI & State University
Blacksburg, VA 24061
Phone: (703)231-4655

Lisa E. Jones
NASA Langley Research Center
12 W. Bush Rd.
M.S. 495
Hampton, VA 23681-0001
Phone: (804)864-4148
FAX: (804)864-8547

Han-Pin Kan
Northrop Corporation
Dept. 3853/63
One Northrop Ave.
Hawthorne, CA 90250
Phone: (310) 332-5285
FAX: (310) 332-6794

George Kardomateas, Ph.D.
Associate Professor
School of Aerospace Engineering
Georgia Institute of Technology
Atlanta, GA 30332-0150
Phone: (404) 894-8198
FAX: (404) 894-9313

Sotiris Kellas
Lockheed Engr & Sciences Co.
NASA Langley Research Center
M.S. 495
Hampton, VA 23681-0001
Phone: (804)864-4150
FAX: (804)864-8547

Andre Lavoie
E.S.M. Dept. 225 Norris Hall
VPI & State University
Blacksburg, VA 24061
Phone: (703)231-7548
FAX: (703)231-4574

James Mack
Micro Craft, Inc.
3130 N. Armistead Avenue
M.S. 918
Hampton, VA 23666
Phone: (804 865-7760
FAX: (804) 865-7487

Ed Martin
Sverdrup Technology Corporation
620 Discovery Drive
Huntsville, AL 35806
Phone: (205) 971-9461
FAX: (205) 971-9475

John Morton
220 Norris Hall
ESM Department
Virginia Tech
Blacksburg, VA 24601
Phone: (703)231-6051
FAX: FAX:(703)231-4574

Alan T. Nettles
MS EH-33
Marshall Space Flight Center
Marshall Space Flight Center, AL 35812
Phone: (205)544-2677
FAX: (205544-7255

Ahmed Noor
University of Virginia
NASA Langley Research Center
3 Langley Blvd. M.S. 210
Hampton, VA 23681-0001
Phone: (804) 864-1978
FAX: (804) 864-8089

Kevin O'Brien
U.S. Army Vehicle Structures Dir.
NASA Langley Research Center
M.S. 188E
Hampton, VA 23681-0001
Phone: (804)864-3465

Reid Phelan
Dept. E20 Bld 600
Newport News Shipbuilding
4101 Washington Ave.
Newport News, VA 23607

S. Leigh Phoenix
Dept. of Theoretical and Applied Mechanics
321 Thurston Hall
Cornell University
Ithaca, NY 14853
Phone: (607)255-8818
FAX: FAX:(607)255-2011

Clarence C. Poe, Jr.
NASA Langley Research Center
2 W. Reid Street
M.S. 188E
Hampton, VA 23681-0001
Phone: (804)864-3467

Martha Robinson
NASA Langley Research Center
12 W. Bush Rd.
M.S. 495
Hampton, VA 23681-0001
Phone: (804)864-4149
FAX: (804)864-8547

Marshall Rouse
NASA Langley Research Center
8 W. Taylor Street
M.S. 190
Hampton, VA 23681-0001

Sam Russell
EH-13
Marshall Space Flight Center
Marshall Space Flight Center, AL 35812
Phone: (205) 544-4411
FAX: (205) 544-9326

Mark Sensmeier
750 Tall Oaks Dr.
#13500-C
Blacksburg , VA 24060
Phone: (703)951-4831
FAX: (703)231-4574

George Simitses
University of Cincinnati
Dept. of Aerospace Engineering and Engineering Mechanics
Mail Location 70
Cincinnati, OH 45221
Phone: (513)556-7069
FAX: (513)556-5038

Richard Skalak, Director
Inst. for Mechanics and Materials
Engineering Bldg. Unit 1, Rm 1603
University of California, San Diego
9500 Gilman Drive, La Jolla, CA 92093
Phone: (619)534-7503
FAX: (619)534-8908

James H. Starnes
NASA Langley Research Center
8 W. Taylor Street
M.S. 190
Hampton, VA 23681-0001
Phone: (804)864-3168

Alrik L. Svenson
Federal Highway Administration
Turner-Fairbank Highway Res. Ctr.
6300 Georgetown Pike (HSR -20)
Mclean, VA 22101-2296

Steve R. Swanson
University of Utah
Dept. Mechanical Engineering
Salt Lake City, Utah 84112
Phone: (801)581-6407
FAX: (801)581-8692

Danniella Muheim Thompson
215 Norris Hall
ESM Dept.
VPI & SU
Blacksburg, VA 24061
Phone: (703)231-7428
FAX: (703)231-4574

Steve Tompkins
NASA Langley Research Center
8 W. Taylor Street
M.S. 188E
Hampton, VA 23681-0001
Phone: (804)864-3096
FAX: (804)864-7893

A. S. D. Wang
Mechanical Engineering Dept.
Drexel University
Philadelphia, PA 19104
Phone: (215)895-2297

Dick Wilkins
Center for Composite Materials
University of Delaware
201 Spencer Laboratory
Newark, DE 19716-3144
Phone: (302)831-1674
FAX: (302)831-8525

Marshall Woodson
Virginia Tech
ESM Department
225 Norris Hall
Blacksburg, VA 24061

Carl Zweben
Advanced Technology Manager
Martin Marietta Astrospace
Bldg. 100 Rm U4018
P.O. Box 8555, Philadelphia PA 19101
Phone: (215) 354-3031
FAX: (215) 354-3040

STRUCTURES SESSION

Jim Starnes, Moderator

DESIGN OF SCALED DOWN STRUCTURAL MODELS

George J. Simitses

Aerospace Engineering and Engineering Mechanics
University of Cincinnati, Cincinnati, OH 45221

Abstract

In the aircraft industry, full scale and large component testing is a very necessary, time consuming and expensive process. It is essential to find ways by which this process can be minimized without loss of reliability. One possible alternative is the use of scaled down models in testing and use of the model test results in order to predict the behavior of the larger system, referred to herein as prototype. The presentation provides justification and motivation for the research study, and it describes the necessary conditions (similarity conditions) for two structural systems to be structurally similar with similar behavioral response. Similarity conditions provide the relationship between a scaled down model and its prototype. Thus, scaled down models can be used to predict the behavior of the prototype by extrapolating their experimental data. Since satisfying all similarity conditions simultaneously is in most cases impractical, distorted models with partial similarity can be employed. Establishment of similarity conditions, based on the direct use of the governing equations, is discussed and their use in the design of models is presented. Examples include the use of models for the analysis of cylindrical bending of orthotropic laminated beam plates, of buckling of symmetric laminated rectangular plates subjected to uniform uniaxial compression and shear, applied individually, and of vibrational response of the same rectangular plates. Extensions and future tasks are also described.

Work supported by the NASA Langley Research Center under Grant NAG-1-1280 and the University of Cincinnati. The NASA technical officer for this Grant is Dr. James H. Starnes, Jr. His encouragement and support are gratefully acknowledged.

OUTLINE

- INTRODUCTION
  - MOTIVATION
  - SIMILARITY CONDITIONS
- EXAMPLES
  - BUCKLING OF CROSS-PLY LAMINATED PLATES
    - * AXIAL COMPRESSION
    - * SHEAR
  - FREQUENCY RESPONSE OF CROSS-PLY LAMINATED PLATES
  - BENDING OF WIDE BEAMS
- CONCLUSIONS AND RECOMMENDATIONS

INTRODUCTION

- MOTIVATION : Aircraft Design
  - Preliminary and Concept Design

    (Mission requirements, expected performance; identification of components and their connection, of manufacturing and of assembly techniques)
  - Detailed Design

    (identification of critical design areas analysis - design and redesign)
  - Verification of the Design

    Large component testing and full scale(prototype) testing
- Manufacturing decisions, predictability of components and management of production process

MOTIVATION (CONT'D)

- C-141A STATIC TEST PROGRAM INCLUDES
  - 8 wing tests
  - 17 fuselage tests
  - 7 empennage tests
  - 6 nacelle and pylon tests
  - etc. ....

- FULL SCALE FATIGUE TESTS ON FOUR SPECIMENS(B,C,D,E)

  C,D,E : goal of four lifetimes

  B : goal of two lifetimes

C-141A FATIGUE TEST SPECIMENS

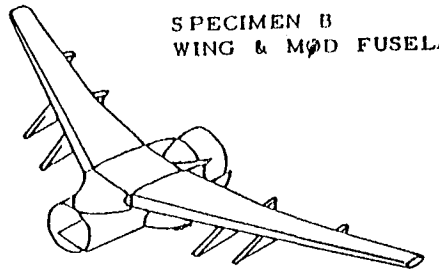

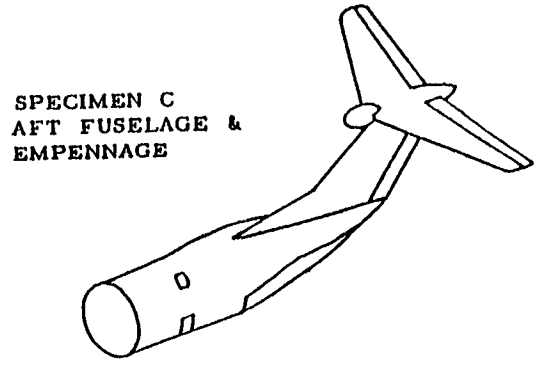

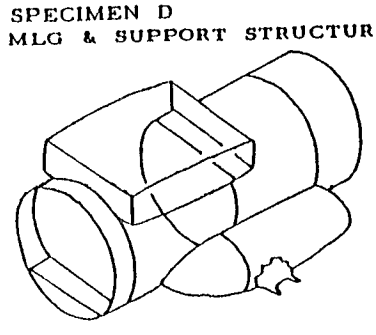

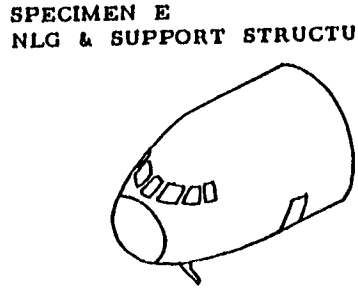

MOTIVATION (CONT'D)

- LIMIT LOAD : *Maximum load that aircraft is expected to encounter.*
- DESIGN LOAD : *Limit Load* × *Safety Factors*

  SAFETY FACTOR ≥ 1.5 (Fitting factors, bearing factors, dynamic etc.)

- THE GOAL IS TO DESIGN AIRCRAFT SUCH THAT THERE ARE NO FAILURES AT LIMIT LOAD
  - NO PART WILL BE STRESSED BEYOND PROPORTIONAL LIMIT OF MATERIAL.
  - NO BUCKLING FAILURE (STATIC & DYNAMIC)
  - ADDITIONAL : FATIGUE, AEROELASTIC INSTABILITY, etc.

THEORY OF SIMILITUDE

$$X_p = \Lambda X_m \quad , \quad X_m = \Lambda^{-1} X_p$$

$$\Lambda = \begin{bmatrix} \lambda_{x1} & 0 & \dots & 0 \\ 0 & \lambda_{x2} & \dots & 0 \\ \vdots & \vdots & \ddots & \vdots \\ 0 & 0 & \dots & \lambda_{xn} \end{bmatrix}$$

SCALE FACTORS :

$$\lambda_{x_i} = \frac{x_{ip}}{x_{im}} \Rightarrow x_{ip} = \lambda_{x_i} x_{im}$$

Two approaches:

- Dimensional Analysis
- Direct Use of Governing Equations

DIRECT USE OF GOVERNING EQUATIONS

$$f(x_{1p}, x_{2p}, x_{3p}, \cdots, x_{np}) = 0 \quad , \quad f(x_{1m}, x_{2m}, x_{3m}, \cdots, x_{nm}) = 0$$

where

x_i : *Geometric, Material properties, and Response parameters.*

$$f(x_{1p}, x_{2p}, x_{3p}, \cdots, x_{np}) \xrightarrow{\Lambda} f(x_{1m}, x_{2m}, x_{3m}, \cdots, x_{nm})$$

$$f(x_{1p}, x_{2p}, x_{3p}, \cdots, x_{np}) = \psi(\lambda_{x_{1p}}, \lambda_{x_{2p}}, \lambda_{x_{3p}}, \cdots, \lambda_{x_{np}}) f(x_{1m}, x_{2m}, x_{3m}, \cdots, x_{nm})$$

$$\psi(\lambda x_{1p}, \lambda x_{2p}, \lambda x_{3p}, \cdots, \lambda x_{np}) = 1$$

(NO SCALE EFFECT CONSIDERED)

Buckling of Symmetric Laminated Cross-Ply Rectangular Plates

$$(B_{ij} = 0 \ , D_{16} = D_{26} = A_{16} = A_{26} = 0)$$
$$(\bar{N}_{xx} \ , \ \bar{N}_{yy} \ , \ \bar{N}_{xy})$$

$$D_{11} w^0_{,xxxx} + 2\bar{D}_{12} w^0_{,xxyy} + D_{22} w^0_{,yyyy} - \bar{N}_{xx} w^0_{,xx} - \bar{N}_{yy} w^0_{,yy} - \bar{N}_{xy} w^0_{,xy} = \rho w^0_{,tt} \qquad (1)$$

$$where \quad \bar{D}_{12} = D_{12} + 2D_{66}$$

B.C's: Simply Supported

at $x = 0, a$

$$w = 0 \quad , \quad M_x = -D_{11} w^0_{,xx} = 0$$

at $y = 0, b$

$$w = 0 \quad , \quad M_y = -D_{22} w^0_{,yy} = 0$$

UNIAXIAL COMPRESSION

$$D_{11}w^0_{,xxxx} + 2\bar{D}_{12}w^0_{,xxyy} + D_{22}w^0_{,yyyy} - \bar{N}_{xx}w^0_{,xx} = 0 \qquad (2)$$

$$w^0 = \sum_{m=1}^{\infty}\sum_{n=1}^{\infty} A_{mn} sin(\frac{m\pi x}{a}) sin(\frac{n\pi y}{b})$$

$$\bar{N}_{xx} = \pi^2[D_{11}(\frac{m}{a})^2 + 2\bar{D}_{12}(\frac{n}{b})^2 + D_{22}(\frac{n}{b})^4(\frac{a}{m})^2] \qquad (3)$$

$$\lambda_{\bar{N}_{xx}} = \lambda_{D_{11}}\frac{\lambda_m^2}{\lambda_a^2} = \lambda_{\bar{D}_{12}}\frac{\lambda_n^2}{\lambda_b^2} = \lambda_{D_{22}}\frac{\lambda_n^4\lambda_a^2}{\lambda_b^4\lambda_m^2} \qquad (4)$$

$$\left.\begin{aligned} \lambda_{K_{xx}} &= \frac{\lambda_{D_{11}}}{\lambda_{E_{22}}\lambda_h^3}\frac{\lambda_m^2}{\lambda_R^2} \\ \lambda_{K_{xx}} &= \lambda_n^2\frac{\lambda_{\bar{D}_{12}}}{\lambda_{E_{22}}\lambda_h^3} \\ \lambda_{K_{xx}} &= \frac{\lambda_{D_{22}}}{\lambda_{E_{22}}\lambda_h^3}\lambda_n^4\lambda_R^2 \end{aligned}\right\} \textit{Three Similarity Conditions Relating Nine Parameters}$$

$$\textit{where} \qquad K_{xx} = \frac{\bar{N}_{xx}b^2}{E_{22}h^3}$$

SHEAR

$$D_{11}w^0_{,xxxx} - 2\bar{D}_{12}w^0_{,xxyy} - D_{22}w^0_{,yyyy} - 2\bar{N}_{xy}w^0_{,xy} = 0$$

$$w^0 = \sum_{m=1}^{\infty}\sum_{n=1}^{\infty} A_{mn} sin(\frac{m\pi x}{a}) sin(\frac{n\pi y}{b})$$

$$\int_0^b\int_0^a [D_{11}w^0_{,xxxx} - 2\bar{D}_{12}w^0_{,xxyy} - D_{22}w^0_{,yyyy} - 2\bar{N}_{xy}w^0_{,xy}] sin(\frac{m\pi x}{a}) sin(\frac{n\pi y}{b}) dxdy = 0 \quad , \quad m,n = 1,2,\cdots\infty \qquad (5)$$

of equations.

$$(\frac{D_{11}}{E_{22}h^3}\frac{m^4}{R^3} + 2\frac{\bar{D}_{12}}{E_{22}h^3}\frac{m^2n^2}{R} + \frac{D_{22}}{E_{22}h^3}Rn^4)A_{mn} = K_s\frac{32mn}{\pi^4}\sum_{p=1}^{\infty}\sum_{q=1}^{\infty} A_{pq}Q_{mnpq} \qquad (6)$$

constraints for

$$m,n = 1,2,\cdots,\infty \quad , \begin{cases} m \pm p = odd \\ n \pm q = odd \end{cases}$$

$$K_s = \frac{\bar{N}_{xy}b^2}{E_{22}h^3} \quad , \quad R = \frac{a}{b} \quad , \quad Q_{mnpq} = \frac{pq}{(m^2-p^2)(n^2-q^2)}$$

SHEAR (CONT'D)

$$\frac{\lambda_{D_{11}}}{\lambda_{E_{22}}\lambda_h^3}\frac{\lambda_m^4}{\lambda_R^3} = \frac{\lambda_{\bar{D}_{12}}}{\lambda_{E_{22}}\lambda_h^3}\frac{\lambda_m^2\lambda_n^2}{\lambda_R} = \frac{\lambda_{D_{22}}}{\lambda_{E_{22}}\lambda_h^3}\lambda_R\lambda_n^4 = \frac{\lambda_{K_s}}{\lambda_{A_{mn}}}\lambda_m\lambda_n\lambda_\Omega$$

where

$$\Omega = \sum_{p=1}^{\infty}\sum_{q=1}^{\infty} A_{pq}Q_{mnpq}$$

Assumption:

$$\lambda_m = \lambda_n = \lambda_p = \lambda_q = 1 \quad \Longrightarrow \quad \lambda_\Omega = 1$$

$$\left.\begin{aligned}
\lambda_{K_s} &= \frac{\lambda_{D_{11}}}{\lambda_{E_{22}}\lambda_h^3\lambda_R^3} \\
\lambda_{K_s} &= \frac{\lambda_{\bar{D}_{12}}}{\lambda_{E_{22}}\lambda_h^3\lambda_R} \\
\lambda_{K_s} &= \frac{\lambda_{D_{22}}}{\lambda_{E_{22}}\lambda_h^3}\lambda_R
\end{aligned}\right\} \textit{Three Similarity Conditions Relating Five Parameters}$$

Summary Of Similarity Conditions

Uniaxial	Shear	
$\lambda_{K_{xx}} = \frac{\lambda_{D_{11}}}{\lambda_{E_{22}}\lambda_h^3}\frac{\lambda_m^2}{\lambda_R^2}$	$\lambda_{K_s} = \frac{\lambda_{D_{11}}}{\lambda_{E_{22}}\lambda_h^3}$	(7)
$\lambda_{K_{xx}} = \lambda_n^2\frac{\lambda_{\bar{D}_{12}}}{\lambda_{E_{22}}\lambda_h^3}$	$\lambda_{K_s} = \frac{\lambda_{\bar{D}_{12}}}{\lambda_{E_{22}}\lambda_h^3}$	(8)
$\lambda_{K_{xx}} = \frac{\lambda_{D_{22}}}{\lambda_{E_{22}}\lambda_h^3}\lambda_n^4\lambda_R^2$	$\lambda_{K_s} = \frac{\lambda_{D_{22}}}{\lambda_{E_{22}}\lambda_h^3}$	(9)

COMPLETE SIMILARITY

$$\lambda_{D_{11}} = \lambda_{D_{22}} = \lambda_{\bar{D}_{12}} \tag{10}$$

$$D_{11} = [(F-1)\psi + 1]\frac{t^3}{12}Q_{11} \implies \lambda_{D_{11}} = \left[\frac{(F_p-1)\psi_p + 1}{(F_m-1)\psi_m + 1}\right]\lambda_t^3\lambda_{Q_{11}}$$

$$D_{22} = [(1-F)\psi + F]\frac{t^3}{12}Q_{11} \implies \lambda_{D_{22}} = \left[\frac{(1-F_p)\psi_p + F_p}{(1-F_m)\psi_m + F_m}\right]\lambda_t^3\lambda_{Q_{11}}$$

$$\bar{D}_{12} = \frac{t^3}{12}(Q_{12} + 2Q_{66}) \implies \lambda_{\bar{D}_{12}} = \left[\frac{Q_{12p} + 2Q_{66p}}{Q_{12m} + 2Q_{66m}}\right]\lambda_t^3$$

where $F = \dfrac{E_{22}}{E_{11}} = \dfrac{Q_{22}}{Q_{11}}$, $M = \dfrac{N+1}{N-1}$ and

$$\psi = \frac{1}{(1+\mathrm{M})^3} + \frac{\mathrm{M(N-3)[M(N-1)+2(N+1)}}{(\mathrm{N}^2-1)(1+\mathrm{M})^3}$$

$$\left[\frac{(F_p-1)\psi_p+1}{(F_m-1)\psi_m+1}\right]\lambda_{Q_{11}} = \left[\frac{(1-F_p)\psi_p+F_p}{(1-F_m)\psi_m+F_m}\right]\lambda_{Q_{11}} = \left[\frac{Q_{12p}+2Q_{66p}}{Q_{12m}+2Q_{66m}}\right]$$

COMPLETE SIMILARITY(CONT'D)

$$f_1(E_{ij}, \nu_{ij}, G_{12}, N) = \left[\frac{(F_p-1)\psi_p+1}{(F_m-1)\psi_m+1}\right]\lambda_{Q_{11}} - \left[\frac{(1-F_p)\psi_p+F_p}{(1-F_m)\psi_m+F_m}\right]\lambda_{Q_{11}} = 0$$

$$f_2(E_{ij}, \nu_{ij}, G_{12}, N) = \left[\frac{(1-F_p)\psi_p+F_p}{(1-F_m)\psi_m+F_m}\right]\lambda_{Q_{11}} - \left[\frac{Q_{12p}+2Q_{66p}}{Q_{12m}+2Q_{66m}}\right] = 0$$

Table 1 *Comparison of shear buckling loads of Kevlar/Epoxy plates with ply - level scaling(complete similarity).*

model	$K_s = \dfrac{N_{xy}b^2}{E_{22}h^3}$			*%Disc.*	
Configuration	*model*	*prototype*	*predicted*	*th.(p)&pr.(p)*	*th.(p)&th.(m)*
$(0_2/90_2)_s$	32.74	32.74	32.74	0.0	0.0
$(0_{10}/90_{10})_s$	32.74	32.74	32.74	0.0	0.0
$(0_{20}/90_{20})_s$	32.74	32.74	32.74	0.0	0.0

$$\%Disc.(th.\&pr.) = 100 \times \frac{|theory - predicted|}{theory}$$

SYSTEM PARAMETERS

Structural Geometry	*Geometry*	$a, b, h(R, h)$
	Material Properties	E_{ij} , ν_{ij} , ρ
	Stacking Sequence	N , $\theta_i(0/90)$
Response	*Mode Parameters*	n , m
	Critical Load	$\bar{N}_{xx}$, $\bar{N}_{yy}$, $\bar{N}_{xy}$

VERSIONS OF SCALED DOWN MODELS

- Distortion in stacking sequence and number of plies (N)
  - ply - level scaling $(0_n/90_n)_s$
  - sublaminate - level scaling $(0/90)_{ns}$
  - general scaling symmetric laminate
    angle ply, quasi- isotropic, cross ply $(0/90/\cdots)$
- Distortion in material properties E_{ij} , ν_{ij} , ρ

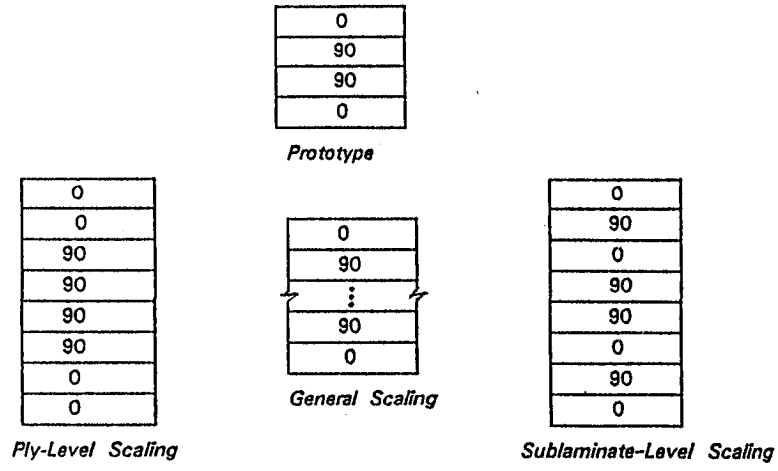

Figure 1 : *Predicted and Theoretical Compressive Buckling Load of the Prototype* $(0/90)_{20s}$ *When* $(0/90/0...)_n$ *Is Used as Model.*

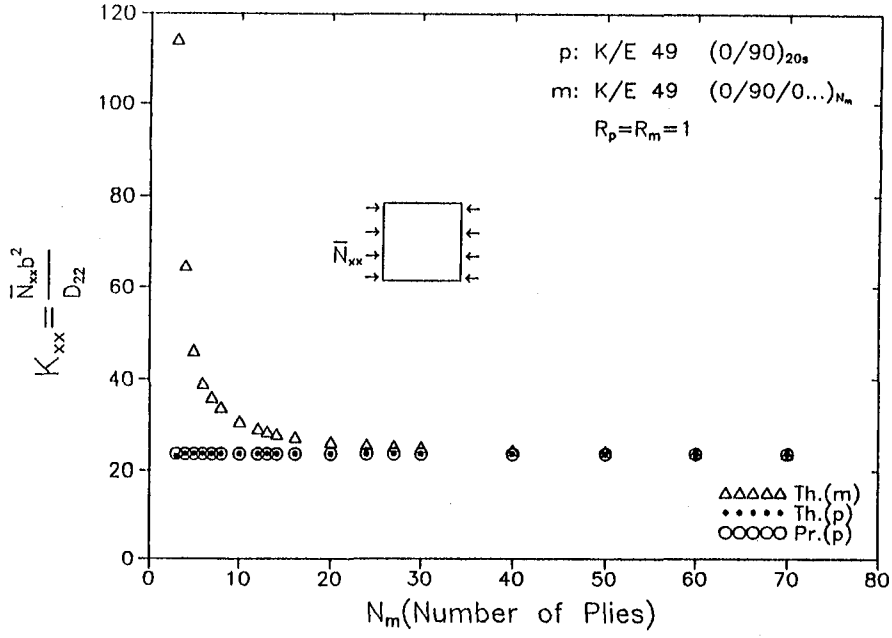

Figure 2 : *Predicted and Theoretical Compressive Buckling Load of the Kevlar/Epoxy Prototype When Model Has Different Material Properties.*

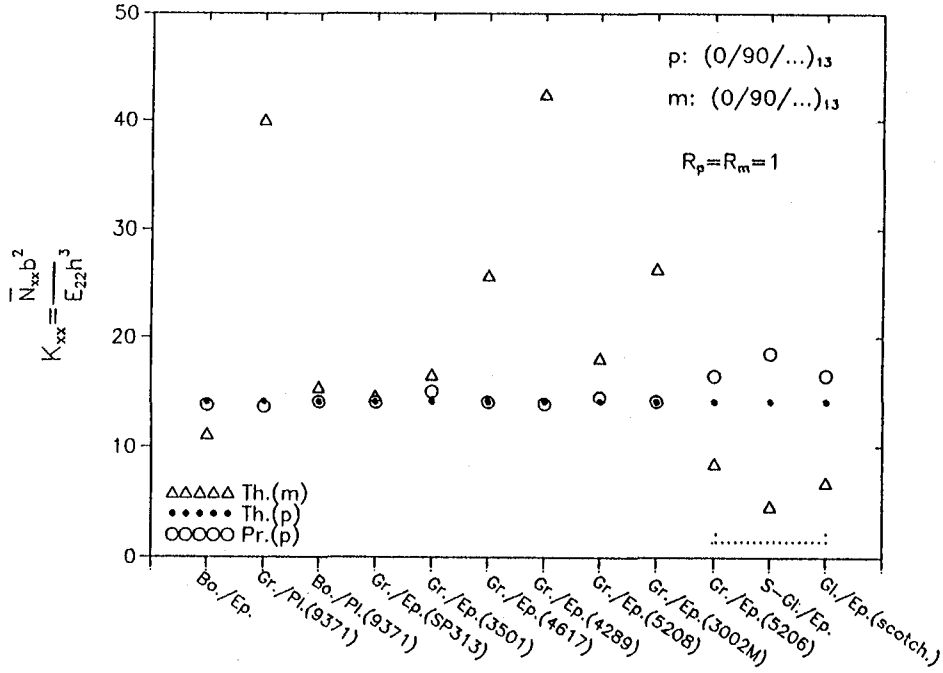

Figure 3 : *Predicted and Theoretical Shear Buckling Load of the Prototype* $(0/90)_{20s}$ *When* $(0/90/0...)_n$ *Is Used as Model.*

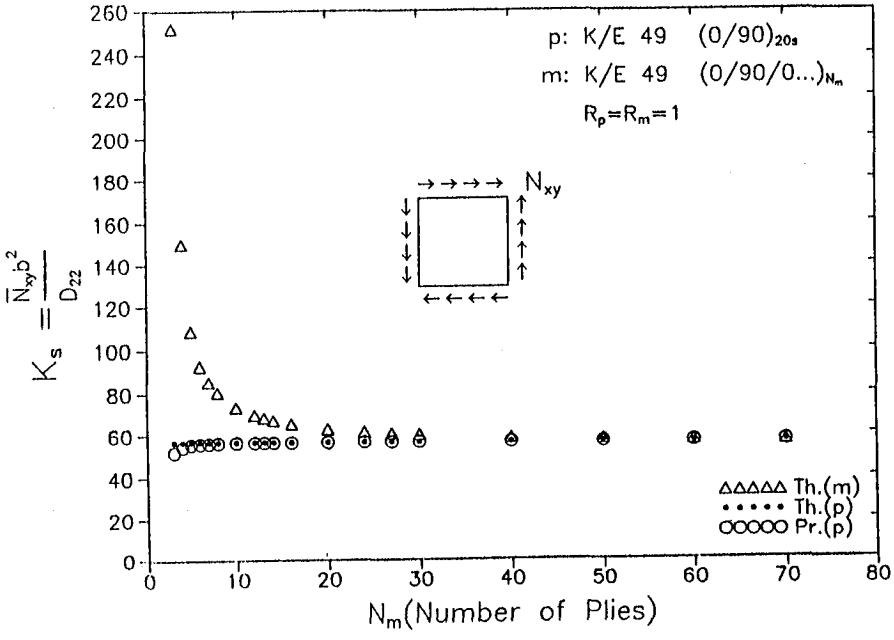

Figure 4 : *Predicted and Theoretical Shear Buckling Load of the Kevlar/Epoxy Prototype When Model Has Different Material Properties.*

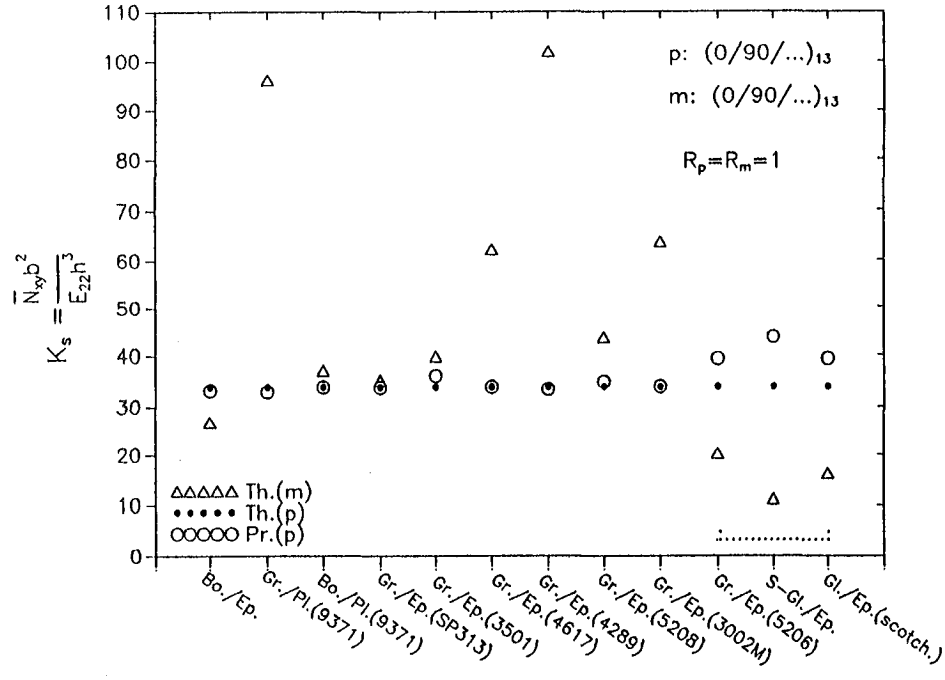

Table 2 *Relaxation in material properties by using isotropic model. Prototype Is Kevlar/Epoxy* $(0/90)_{20s}$

model		$K_{xx} = \frac{N_{xx}b^2}{E_{22}h^3}$			*%Disc.*	
material	R_m	*model*	*prototype*	*predicted*	*th.(p)&pr.(p)*	*th.(p)&th.(m)*
Aluminum	0.705	4.174	14.16	14.16	0.0	70.51
Brass	0.705	4.143	14.16	14.16	0.0	50.80
Copper	0.705	4.149	14.16	14.16	0.0	70.69
Steel	0.705	4.045	14.16	14.16	0.0	71.36
PVC	0.705	4.374	14.16	14.16	0.0	69.1
Polyethylene	0.705	4.760	14.16	14.16	0.0	66.38

model		$K_s = \frac{N_{xy}b^2}{E_{22}h^3}$			*%Disc.*	
material	R_m	*model*	*prototype*	*predicted*	*th.(p)&pr.(p)*	*th.(p)&th.(m)*
Aluminum	0.627	20.22	34.04	34.04	0.0	40.61
Brass	0.627	20.07	34.04	34.04	0.0	41.02
Copper	0.627	20.10	34.04	34.04	0.0	40.97
Steel	0.627	19.63	34.04	34.04	0.0	42.32
PVC	0.627	21.18	34.04	34.04	0.0	37.77
Polyethylene	0.627	23.05	34.04	34.04	0.0	32.28

Figure 5 : *Predicted and Theoretical Natural Frequency of the Prototype* $(0/90)_{20s}$ *When* $(0/90/0...)_n$ *Is Used as Model.*

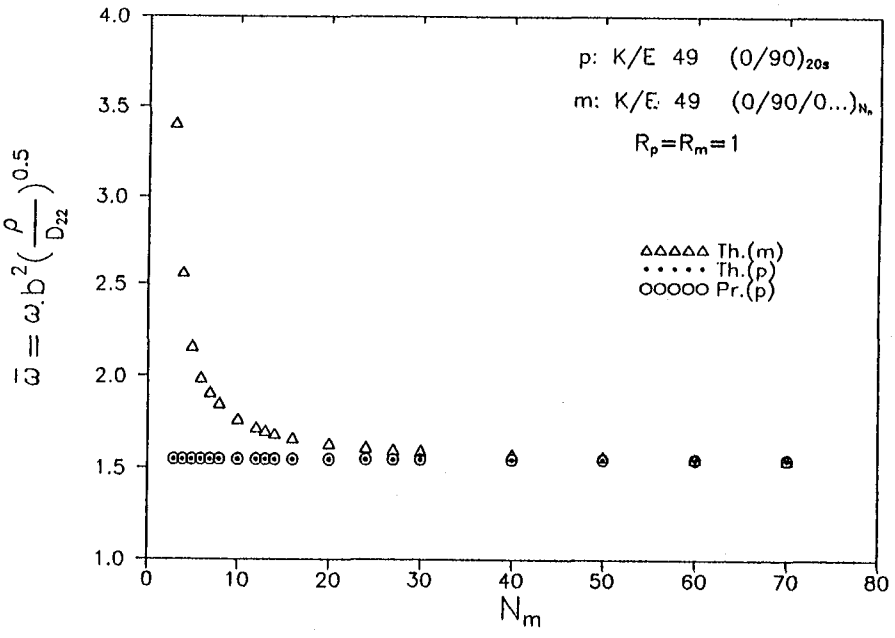

STRESSES

$$\begin{Bmatrix} \sigma_{xx} \\ \sigma_{yy} \\ \tau_{xy} \end{Bmatrix}^{(k)} = \begin{Bmatrix} \bar{Q}_{11} \\ \bar{Q}_{12} \\ \bar{Q}_{14} \end{Bmatrix}^{(k)} \left(u_{,x} + \frac{1}{2} w_{,x}^2 - z w_{,xx} \right) \tag{11}$$

$$\sigma_{xx}{}^{(k)} = \bar{Q}_{11}^{(k)} \left(u_{,x} + \frac{1}{2} w_{,x}^2 - z w_{,xx} \right) \tag{12}$$

Applying similitude theory for the normal stress, σ_{xx},

$$\lambda_{\sigma_{xx}{}^{(k)}} = \lambda_{\bar{Q}_{11}^{(k)}} \left(\frac{\lambda_u}{\lambda_x} + \frac{\lambda_w^2}{\lambda_x^2} - \lambda_z \frac{\lambda_w}{\lambda_x^2} \right) \tag{13}$$

The resulting similarity conditions are

$$\lambda_{\sigma_{xx}{}^{(k)}} = \lambda_{\bar{Q}_{11}^{(k)}} \lambda_u \lambda_x^{-1} \tag{14}$$

$$\lambda_{\sigma_{xx}{}^{(k)}} = \lambda_{\bar{Q}_{11}^{(k)}} \lambda_w^2 \lambda_x^{-2} \tag{15}$$

$$\lambda_{\sigma_{xx}{}^{(k)}} = \lambda_{\bar{Q}_{11}^{(k)}} \lambda_z \lambda_w \lambda_x^{-2} \tag{16}$$

where $\lambda_w = \lambda_x^3 \lambda_q \lambda_{D_{11}}$ and $\lambda_u = \lambda_w \lambda_x \lambda_{B_{11}} \lambda_{A_{11}}^{-1}$

Figure 6 : *Predicted and Theoretical Normal Stress σ_{xx} Distributions in Various Layers of the Prototype G2* $(0/90/0...)_{16}$ *When G4* $(0_3/90_3/0_3/90_3/0_3)$ *Is Used as Model.*

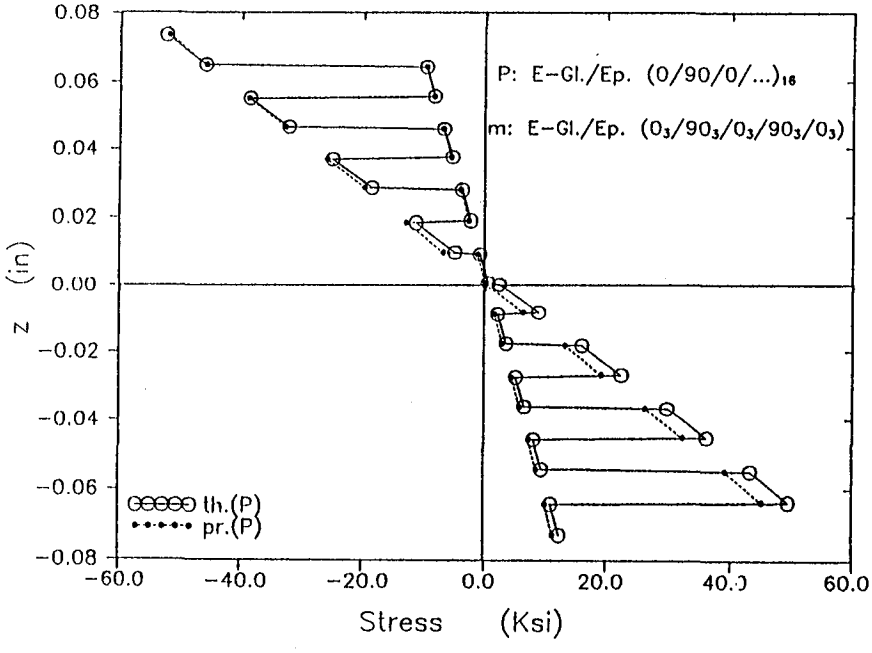

Figure 7 : *Predicted and Theoretical Normal Stress σ_{xx} Distributions in Various Layers of the Prototype K7 $(0_4/90_4/0_4/90_4/0_4)$ When G1 $(0/90/0...)_{16}$ Is Used as Model.*

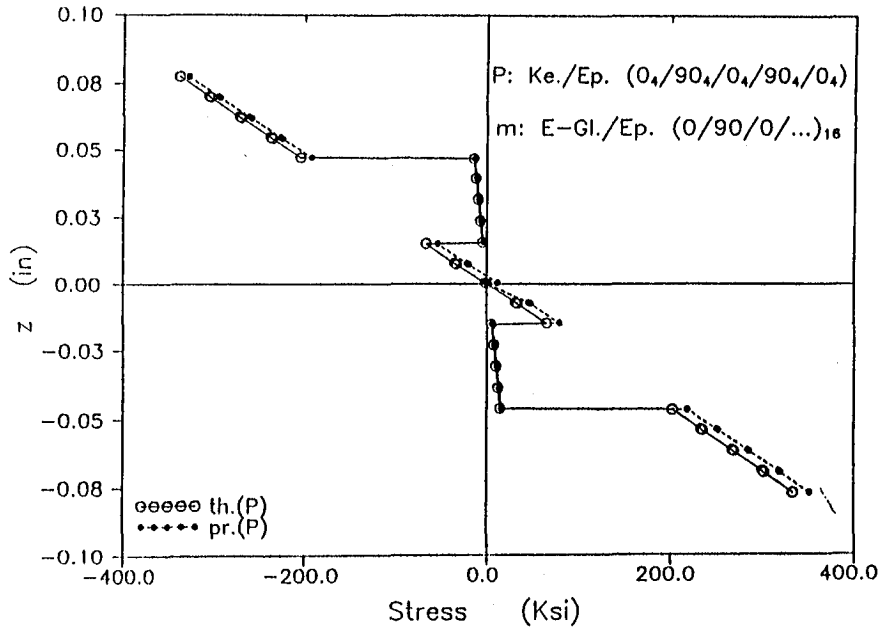

Figure 8 : *Predicted and Theoretical Normal Stress σ_{xx} Distributions in Various Layers of the Prototype K7 $(0_4/90_4/0_4/90_4/0_4)$ When G4 $(0_3/90_3/0_3/90_3/0_3)$ Is Used as Model.*

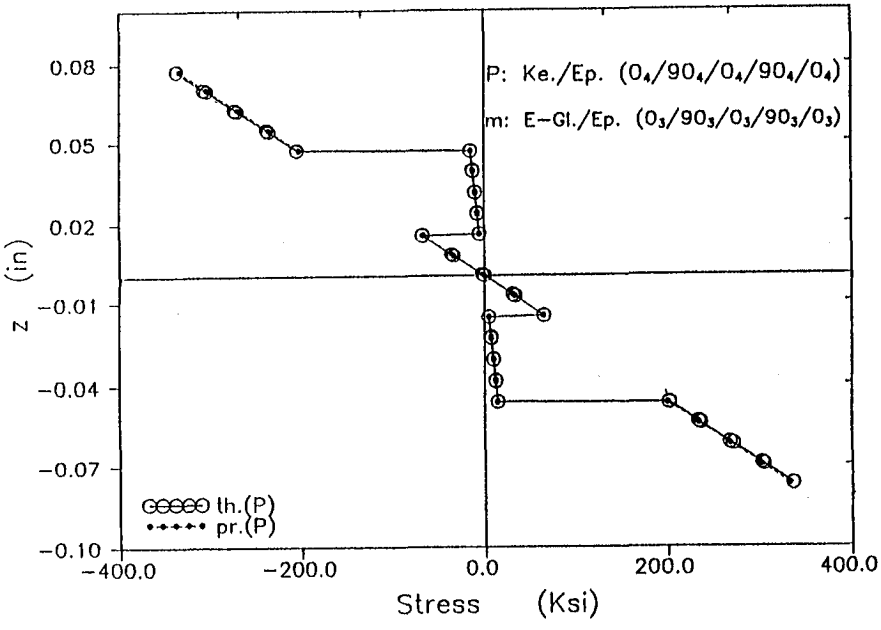

Figure 8 : *Predicted and Theoretical Normal Stress σ_{xx} Distributions in Various Layers of the Prototype K7 $(0_4/90_4/0_4/90_4/0_4)$ When G4 $(0_3/90_3/0_3/90_3/0_3)$ Is Used as Model.*

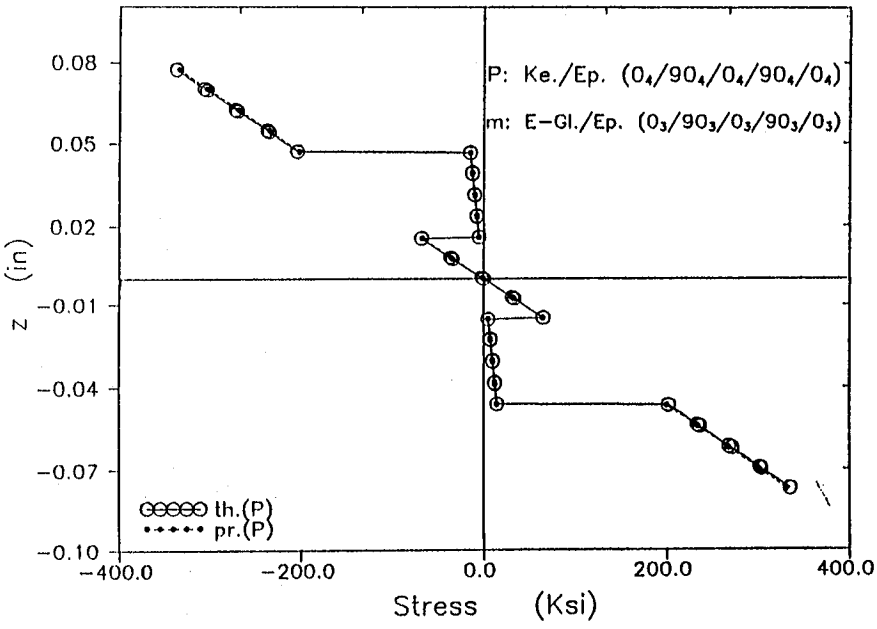

Figure 9 : *Predicted and Theoretical Normal Stress σ_{xx} Distributions in Various Layers of the Prototype G5 $(0/90/0...)_{48}$ When G1 $(0/90/0...)_{16}$ Is Used as Model.*

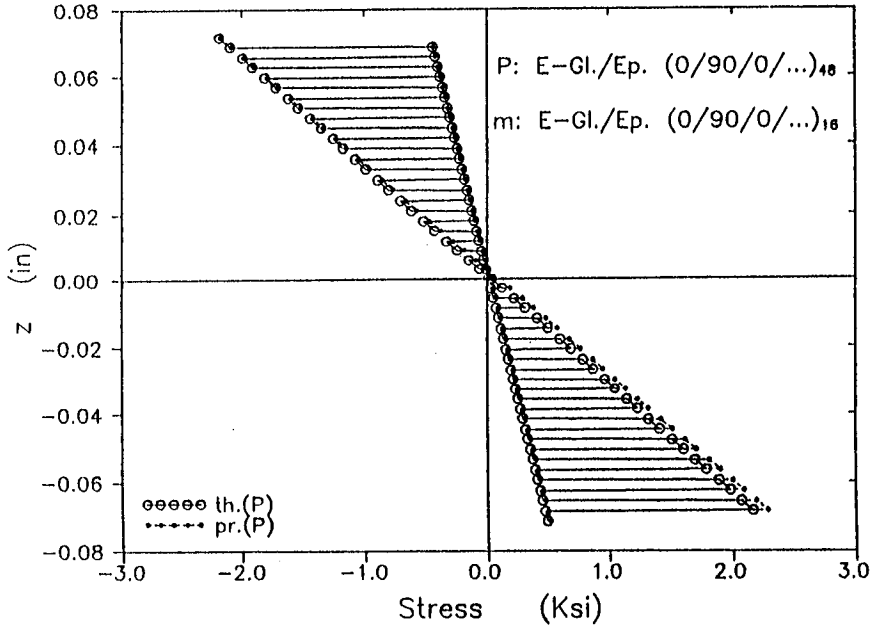

CONCLUSIONS & RECOMMENDATIONS

- There is tremendous freedom in designing distorted scale models because the number of similarity conditions is much smaller than the number of design variables.
- For stress analysis, buckling analysis and vibrations analysis, scaled down models can easily be designed as long as there exists no scale effect.
- If scale effects are completely understood they can be incorporated in the system parameters (modify properties or use functional expression)

CONCLUSIONS & RECOMMENDATIONS (CONT'D)

- Small scale models will not eliminate full scale tests but will definitely reduce the required number of full scale or large component tests.
- Develop the method for designing and employing scale models for more complex systems, i.e stiffened and/or laminated curved configurations.
- Experimental verification of the accuracy of the proposed scaled model.
- Implementation of structural similitude to inelastic and failure analysis of composite structures.

SUB-PLY LEVEL SCALING APPROACH INVESTIGATED FOR GRAPHITE-EPOXY COMPOSITE BEAM-COLUMNS

Karen E. Jackson
U.S. Army Vehicle Structures Directorate, ARL
Landing and Impact Dynamics Branch, SDyD
and
Sotiris Kellas
Lockheed Engineering and Sciences Company

Abstract

Scale model graphite-epoxy composite specimens were fabricated using the "sub-ply level" approach and tested as beam-columns under an eccentric axial load to determine the effect of specimen size on flexural response and failure. The "sub-ply level" approach for constructing scale model composite specimens is a new technique. Previously, scale model composite structures were constructed using two different approaches for sizing the thickness of the specimens. In the ply level approach, the baseline laminate stacking sequence is increased by blocking plies with similar angular orientation together. Thus, using the ply level approach, a baseline 8-ply quasi-isotropic lay-up such as [±45/0/90]s would be scaled up to [$+45_2$/-45_2/0_2/90_2]s for a full-scale specimen with twice the thickness. In the sublaminate level approach, the thickness is increased by repeating a sublaminate group. For example, a full-scale specimen having twice the thickness of the same baseline 8-ply quasi-isotropic laminate would have a [(±45/0/90)]2s lay-up using the sublaminate level approach. Laminates scaled using the sublaminate level technique contain dispersed plies as opposed to blocked ply groups seen with the ply level approach. Both of these techniques have been used to investigate the effect of specimen size on the tensile response and failure of composite coupons [1-5], and the flexural response and failure of composite beam-columns [6-9]. Results of these studies indicate a size effect in strength which depends on the laminate type and scaling technique. In general, ply level scaled composite specimens exhibit a trend of decreasing strength with increasing size. Sublaminate level scaled specimens exhibit the opposite trend, increasing strength with specimen size. Current failure theories for composite materials, such as maximum stress and strain or tensor polynomial theories, cannot predict the size effect.

The ply level and sublaminate level approaches are macroscopic scaling techniques which use standard pre-preg material in construction of both the model and full-scale specimens. Thus, in both approaches the smallest scaling unit is the thickness of a single ply. Ideally, a true replica model composite structure would be fabricated from a geometrically scaled pre-preg material with a scaled microstructure including scaled fiber size, shape and distribution. However, this degree of scaling is impractical at this time due to high cost of producing the pre-preg material.

In the current research project, although the fiber diameters are not scaled, the thickness of the pre-preg material itself has been scaled by adjusting the number of fibers through the thickness of a single ply. Three different grades of graphite-epoxy composite material (AS4/3502) were obtained from Hercules, Inc., in which the number of fibers through the thickness of a single ply was reduced (Grade 190 with 12 to 16 fibers, Grade 95 with 6 to 8 fibers, and Grade 48 with 3 to 4 fibers). Thus, using the sub-ply level approach, a baseline 8 ply quasi-isotropic laminate could be fabricated using either the Grade 48 or Grade 95 material and the corresponding full-scale laminate would be constructed from Grade 95 or standard Grade 190

material, respectively. Note that in the sub-ply level approach, the number of ply interfaces is constant for the baseline and full-scale laminates. This is not true for the ply level and sublaminate level scaled specimens.

The three grades of graphite-epoxy composite material were used to fabricate scale model beam-column specimens with in-plane dimensions of 0.5*n x 5.75*n, where n=1, 2,4 corresponding to 1/4, 1/2, and full-scale factors. Angle ply, cross ply, and quasi-isotropic laminate stacking sequences were chosen for the investigation and the test matrices for each laminate type are given in the following figures. Specimens in each laminate family with the same in-plane dimensions, but different thicknesses were tested to isolate the influence of the thickness dimension on the flexural response and failure. Also, specific lay-ups were chosen with blocked plies and dispersed plies for each laminate type.

The loading configuration is depicted in the following figures. Specimens were subjected to an eccentric axial load until failure. The load offset was introduced through a set of hinges which were attached to the platens of a standard load test machine. Three sets of geometrically scaled hinges were used to ensure that scaled loading conditions were applied. This loading condition was chosen because it promotes large flexural deformations and specimens fail at the center of the beam, away from the grip supports. Five channels of data including applied vertical load, end shortening displacement, strain from gages applied back-to-back at the midspan of the beam, and rotation of the hinge from a bubble inclinometer were recorded for each specimen. The beam-column test configuration was used previously to study size effects in ply level scaled composite specimens of the same material system, sizes, and stacking sequences [6-9]. Thus, a direct comparison between the two scaling approaches is possible. Ply level scaled beam-columns with angle ply, cross ply, and quasi-isotropic lay-ups exhibited no size dependencies in the flexural response, but significant size effects in strength. The reduction in strength with increasing specimen size was not predicted successfully by analysis techniques. It is anticipated that results from this investigation will lead to a better understanding of the strength scale effect in composite structures.

References

1. Kellas, S. and Morton, J.: "Strength Scaling in Fiber Composites," NASA CR 4335, November 1990.

2. Kellas, S.; Johnson, D.; Morton, J.; and Jackson, K. E.: "Scaling Effects in Sublaminate-Scaled Composite Laminates," 34th SDM Conference Proceedings, April 19-21, 1993, La Jolla, CA.

3. Kellas, S. and Morton, J.: "Scaling Effects in Angle-Ply Laminates," NASA CR 4423, February 1992.

4. Kellas, S.; Morton, J.; and Jackson, K. E.: "Damage and Failure Mechanisms in Scaled Angle-Ply Laminates," Fourth Composites Symposium on Fatigue and Fracture, ASTM STP 1156, Stinchcomb, Ed, to be published first quarter, 1993.

5. Kellas, S.; Johnson, David; Morton, J.; and Jackson, K.E.: "Scaling Effects in Sublaminate Scaled Composite Laminates," 34th SDM Conference, April 19-21, 1993, La Jolla, CA.

6. Jackson, K.E.: "Scaling Effects in the Flexural Response and Failure of Composite Beams," *AIAA Journal,* Vol. 30, No. 8, August 1992, pp 2099-2105.

7. Jackson, K. E.; Kellas, S.; and Morton, J.: "Scale Effect in the Response and Failure of Fiber Reinforced Composite Laminates Loaded in Tension and in Flexure." *Journal of Composite Materials,* Vol. 30., No. 8, August 1993.

8. Jackson, K. E.: "Scaling Effects in the Static and Dynamic Response of Graphite-Epoxy Beam-Columns." NASA TM 102697, July 1990.

9. Jackson, K. E.; and Morton, J.: "Analytical and Experimental Evaluation of the Strength Scale Effect in the Flexural Response of Graphite-Epoxy Composite Beams." Proceedings of the 32nd SDM Conference, April 8-10, 1991, Baltimore , MD, AIAA Paper #91-1025

OUTLINE

- INTRODUCTION
  - PROBLEM STATEMENT
  - OBJECTIVES
  - BACKGROUND INFORMATION
- EXPERIMENTAL PROGRAM
- RESULTS
  - NORMALIZED LOAD VS. DEFLECTION PLOTS
  - COMPARISON WITH PREVIOUS EXPERIMENTS
  - COMPARISON WITH LARGE DEFLECTION BEAM ANALYSIS
- CONCLUSIONS

INTRODUCTION

PROBLEM STATEMENT

To Investigate Scaling Effects in the Flexural Response and Failure of Graphite-Epoxy Composite Beam-Columns Fabricated Using the Sub-Ply Level Scaling Technique

OBJECTIVE

To Evaluate the Sub-Ply Level Scaling Approach by Performing Similar Beam-Column Tests That Were Conducted Previously Using Ply Level Scaled Specimens of the Same Material Type and Loading Condition

PAYOFF

Development of Valid Scaling Laws for Composite Materials and Strength Theories Which Incorporate Specimen Size Will Encourage Testing of Scale Model Structures Resulting in Significant Cost Savings

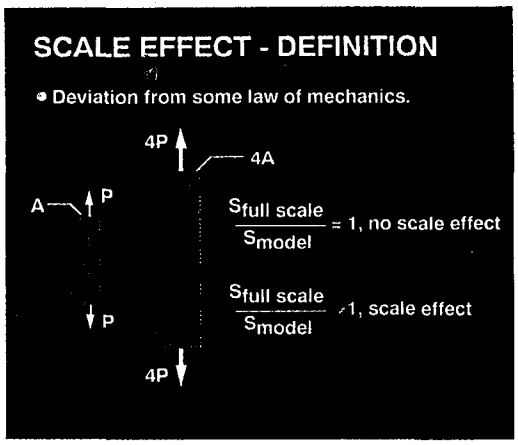

This schematic drawing illustrates the definition of a scale effect as a deviation from some law of mechanics. The example shows a test coupon of cross sectional area A, loaded in tension to a level P. Given a second coupon which is twice the size of the smaller one, the cross sectional area is 4A, and the load level for a comparable stress state is 4P. If the ratio of the strengths of the two samples is equal to 1, then there is no size dependency in strength. If the ratio is not equal to 1, then a scale effect is observed and strength is a function of material volume, or size.

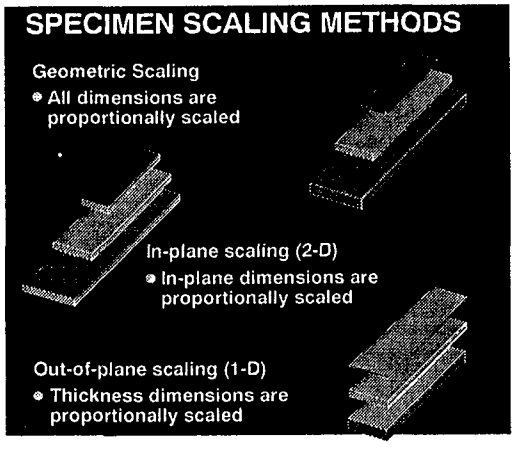

Dimensional scaling may be accomplished by (1) scaling all three dimensions in proportion to a single ratio, (2) scaling the in-plane dimensions alone, while leaving the thickness constant, or (3) scaling the thickness dimension proportionally, and leaving the in-plane dimensions constant. These three methods are called 3D, 2D, and 1D scaling, respectively. The three scaling approaches are depicted in the drawing.

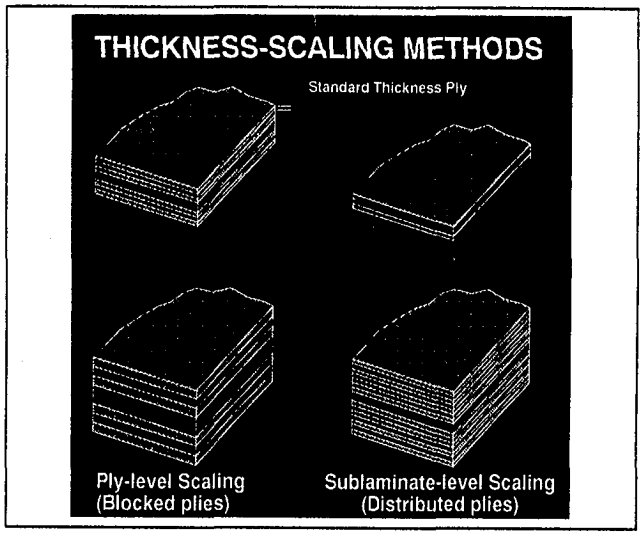

The layered construction of composite materials permits several methods for thickness scaling. The baseline stacking sequence may be scaled by increasing the number of plies for each angluar orientation in the stacking sequence. This method, called ply level scaling, results in blocked ply groups; however, the laminates are both geometrically and constitutively scaled. The baseline stacking sequence may be considered a sub-laminate group and repeated to build up the thickness. This method is called the sublaminate level scaling technique and it results in distributed ply groups. Finally, a reduced thickness pre-preg material can be used to fabricate a scale model of the baseline stacking sequence. This method is the sub-ply level scaling approach.

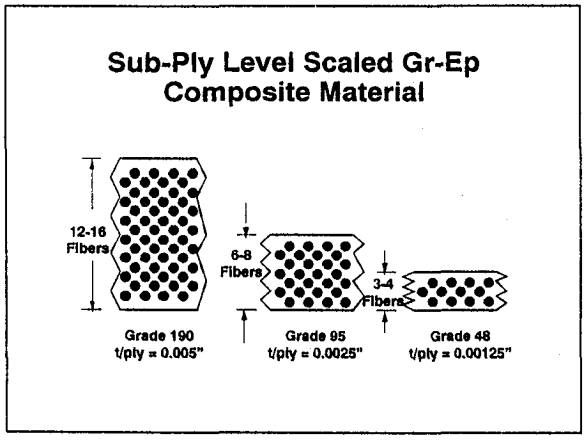

This figure illustrates the difference between various grades of pre-preg material which can be used to fabricate scale model composite structures. The Grade 190 material has approximately 12-16 fibers through the thickness of a single ply, and is the standard 0.0054"/ply material. The Grade 95 is one-half as thick as the Grade 190, and the Grade 48 is one-fourth as thick as the standard. Scale model structures are laminated using the reduced thickness pre-preg material.

Test Matrix of Sub-Ply Level Scaled Angle Ply Beam-Columns

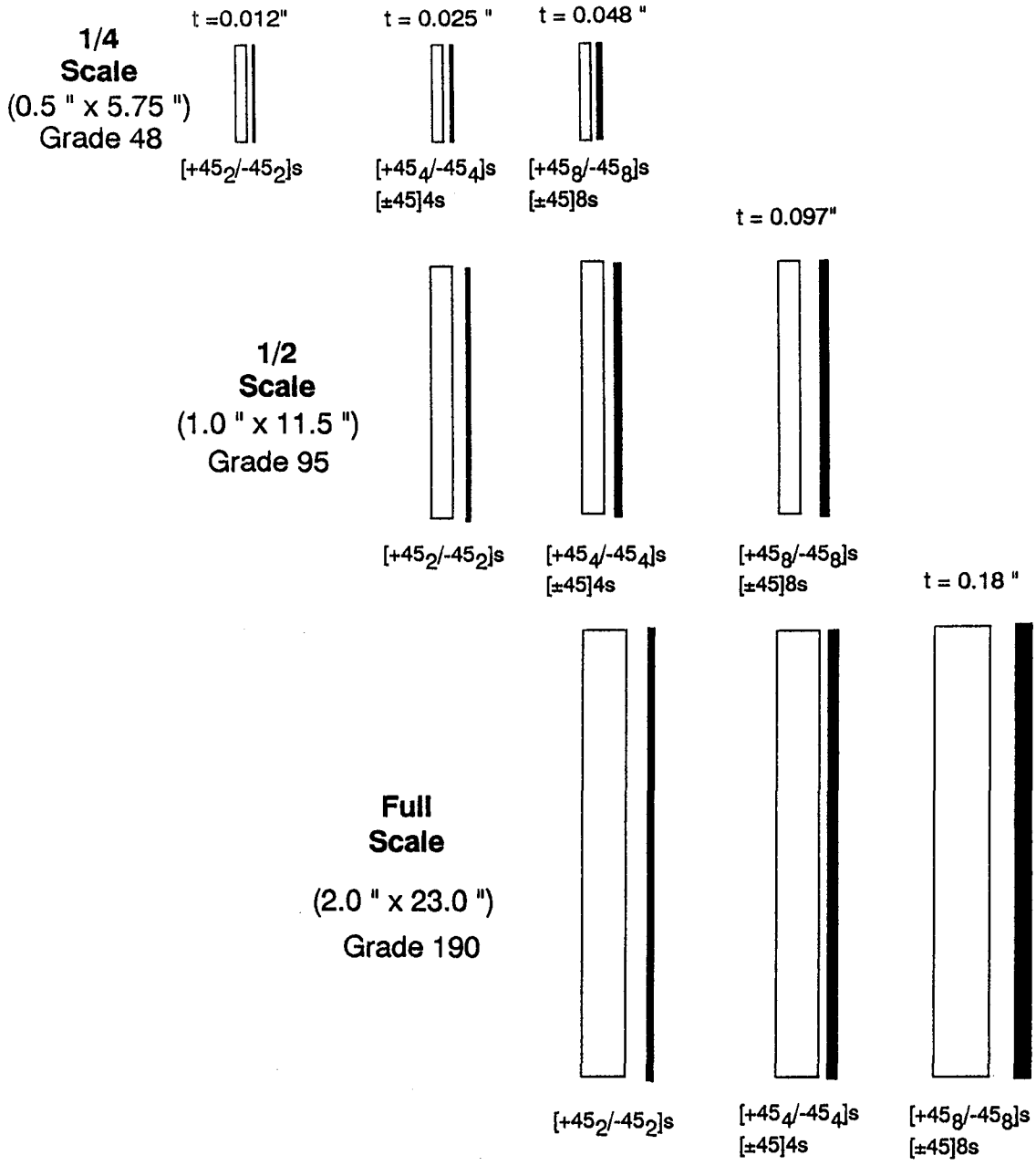

Test Matrix of Sub-Ply Level Scaled Cross Ply Beam-Columns

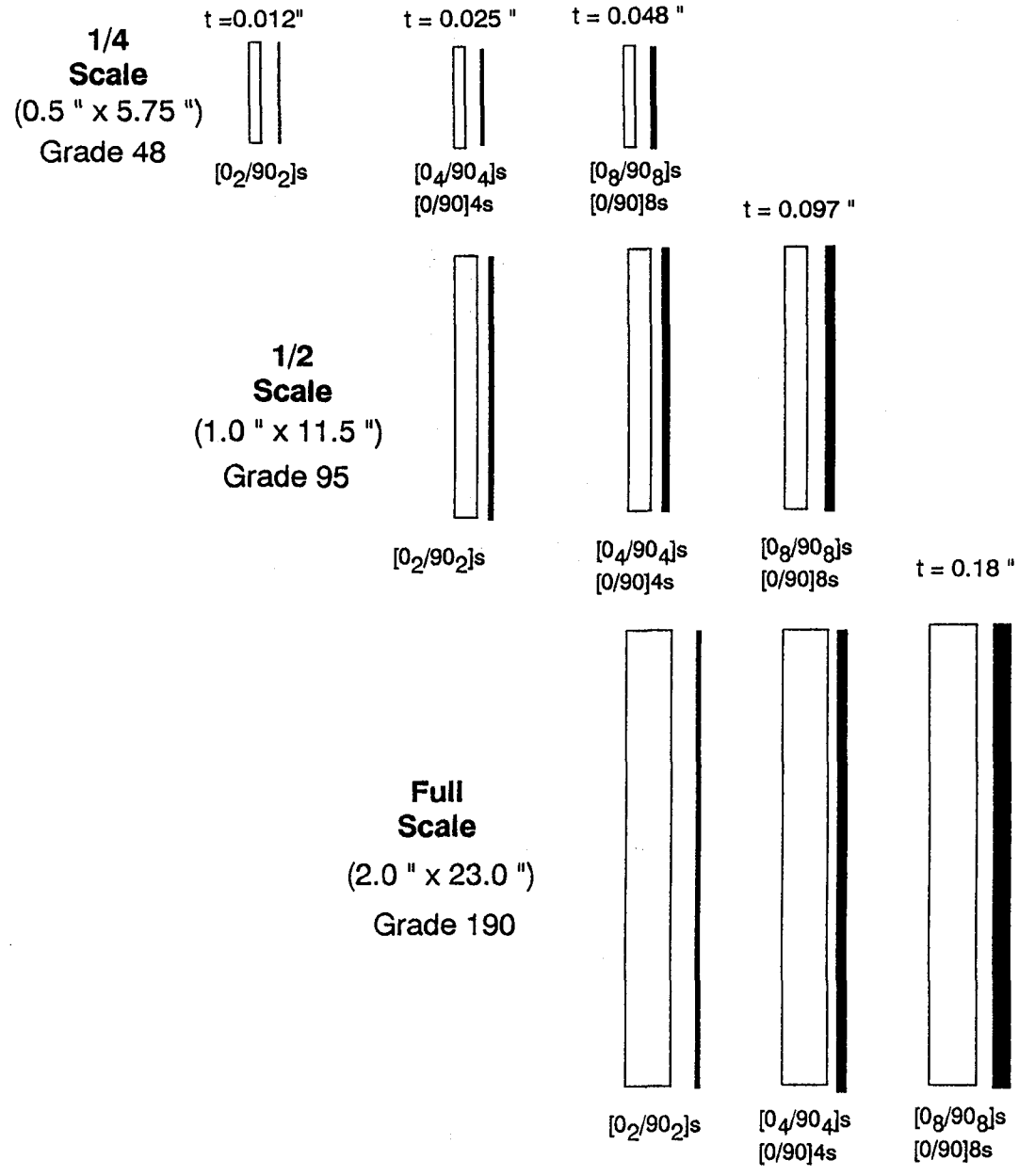

Test Matrix of Sub-Ply Level Scaled Quasi-Isotropic Beam-Columns

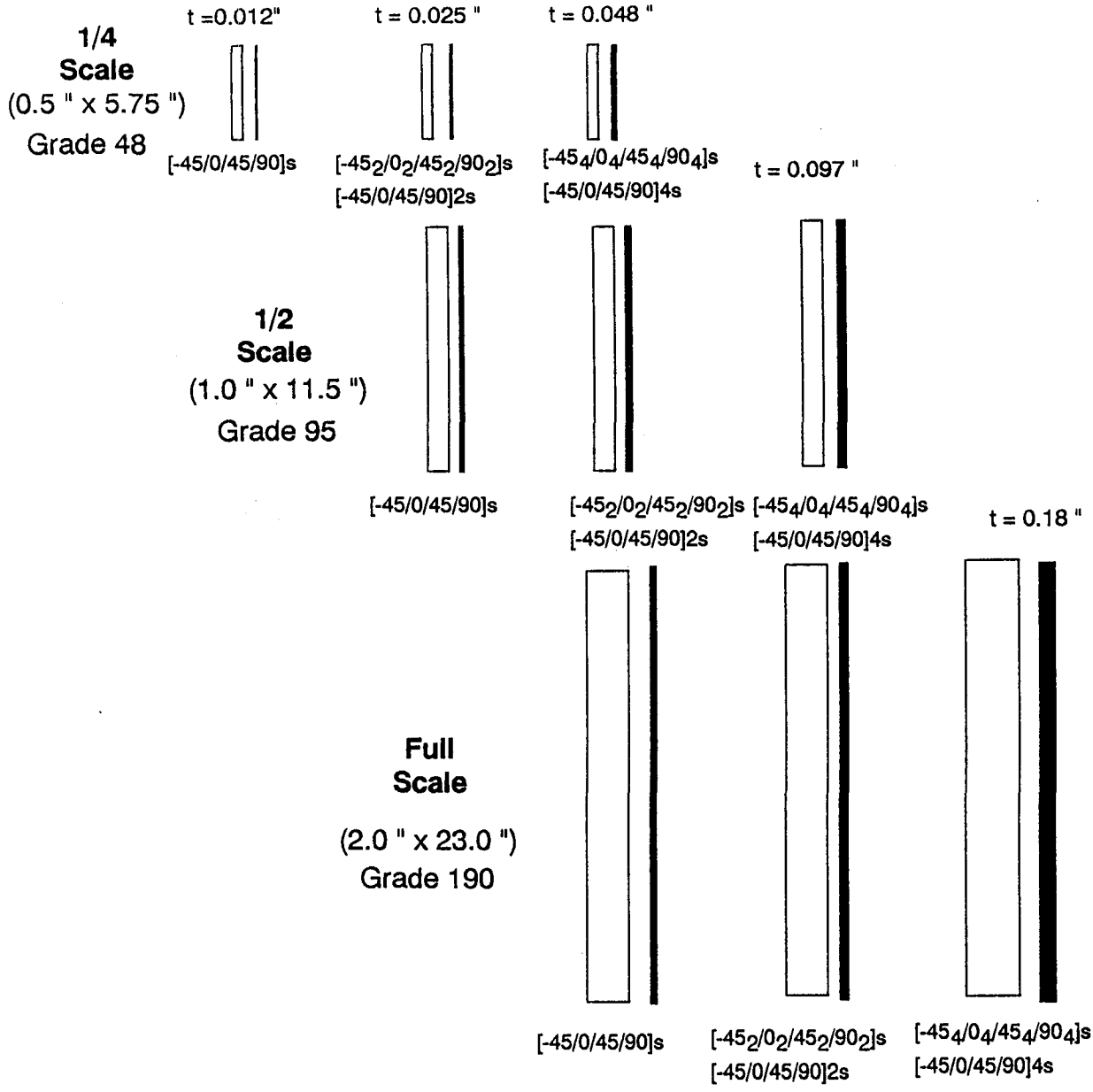

EXPERIMENTAL PROGRAM

LOADING CONFIGURATION

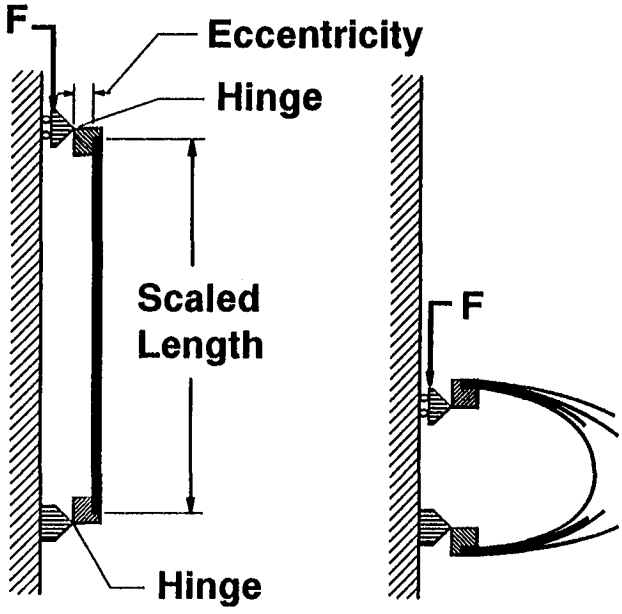

HINGE SUPPORT

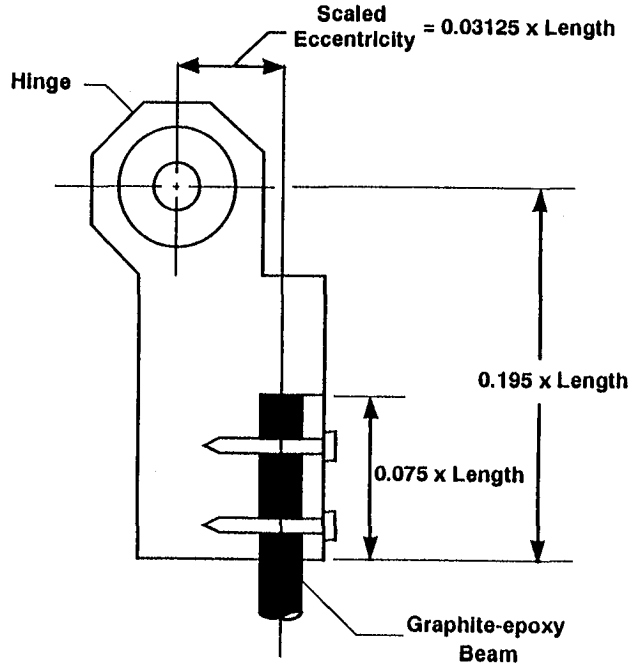

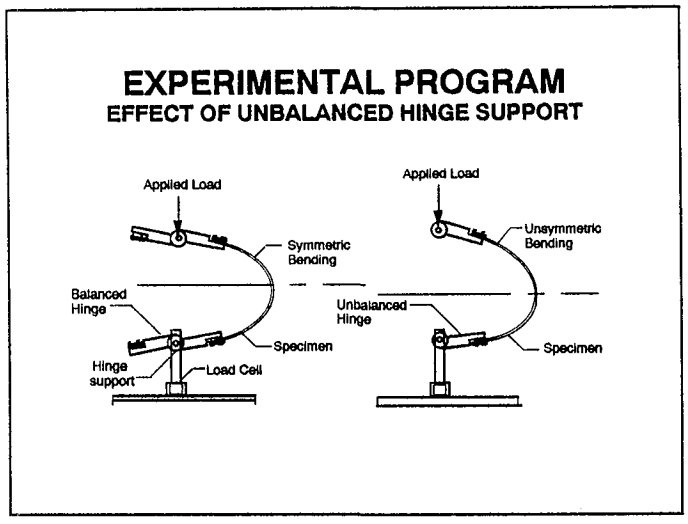

An important aspect of conducting experiments on scaled specimens is to ensure that the loading conditions, boundary conditions, and all other aspects of the experiment are properly scaled. In this case it was necessary to balance the hinge support because the mass of the hinge created an unsymmetric deflection of the beam due to the extra applied inertia load. Once the hinges were balanced, a symmetric deformation shape was observed.

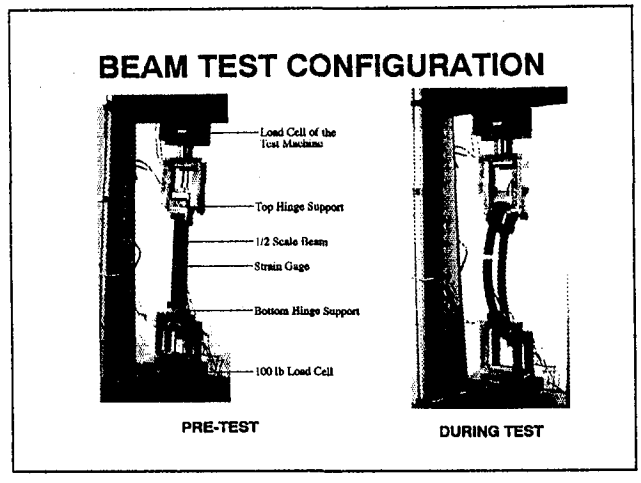

Photographs of the test configuration prior to test and during a test.

NORMALIZED LOAD VS. END DISPLACEMENT

BLOCKED ANGLE PLY LAY-UPS

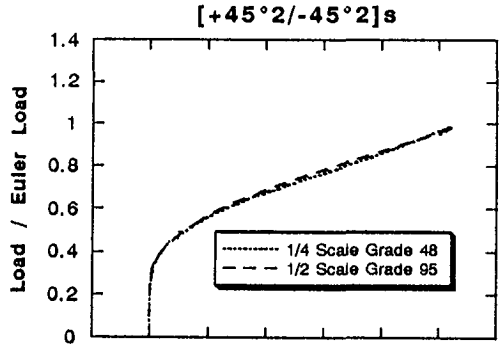

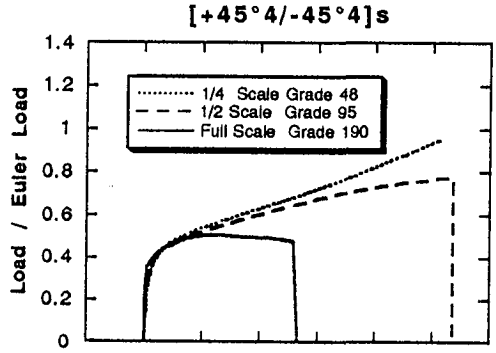

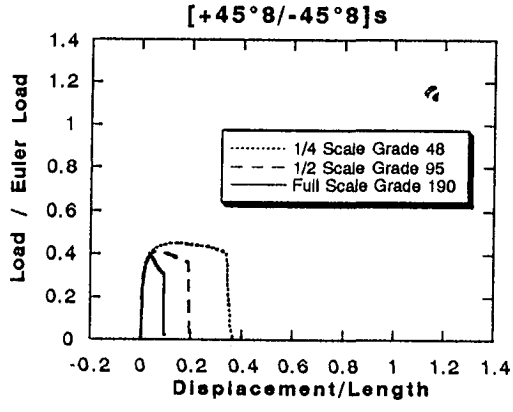

DISTRIBUTED ANGLE PLY LAY-UPS

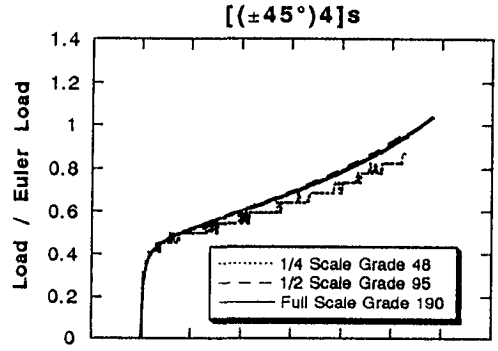

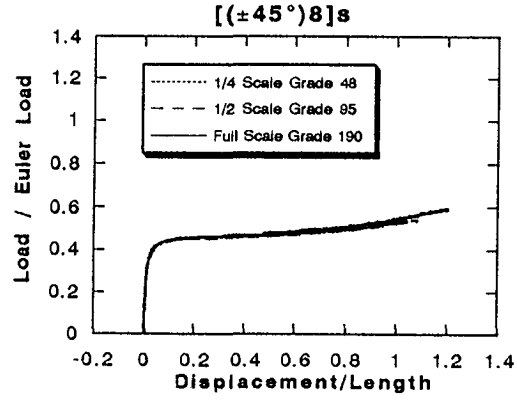

NORMALIZED LOAD VS. END DISPLACEMENT

BLOCKED CROSS PLY LAY-UPS

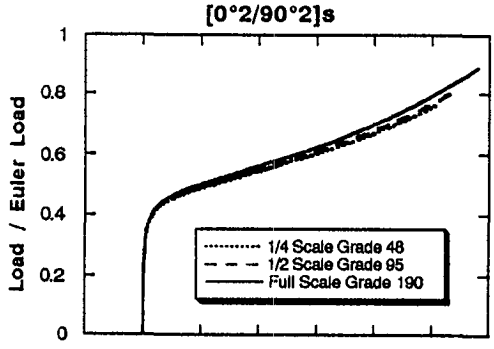

DISTRIBUTED CROSS PLY LAY-UPS

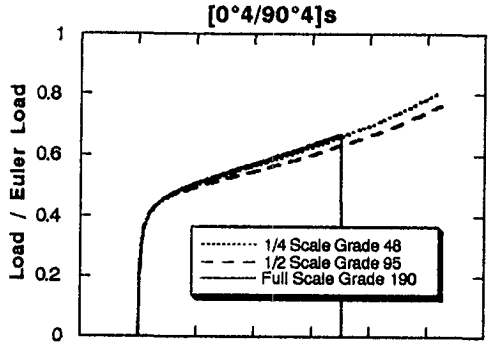

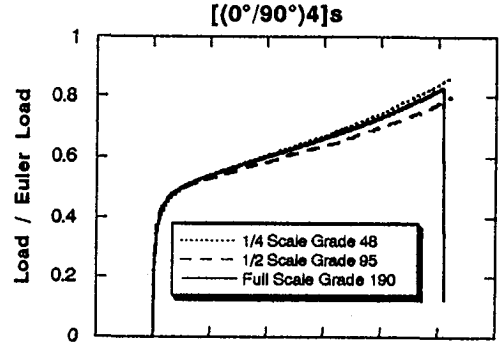

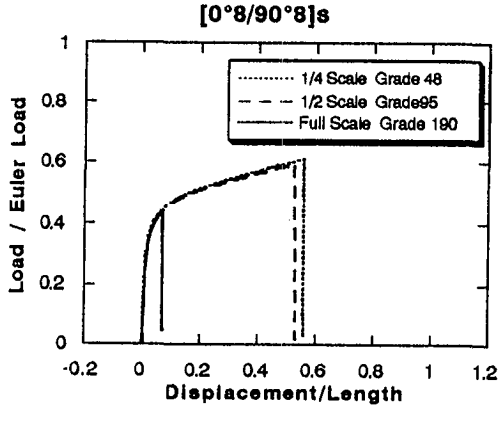

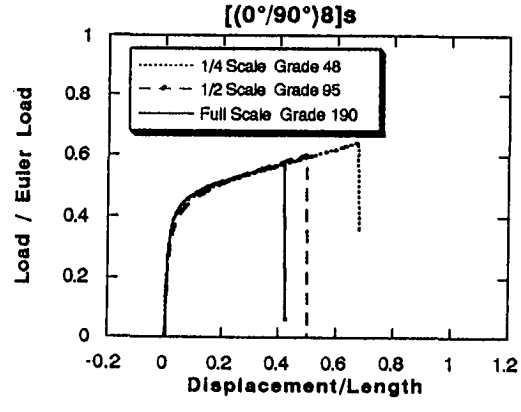

NORMALIZED LOAD VS. END DISPLACEMENT

BLOCKED QUASI-ISOTROPIC LAY-UPS

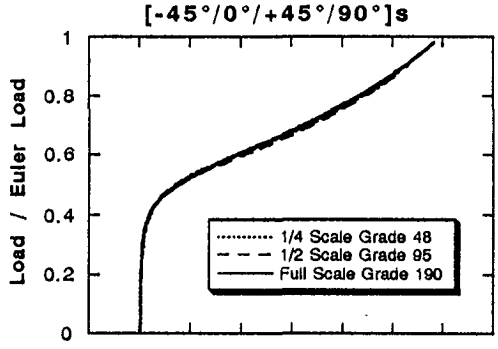

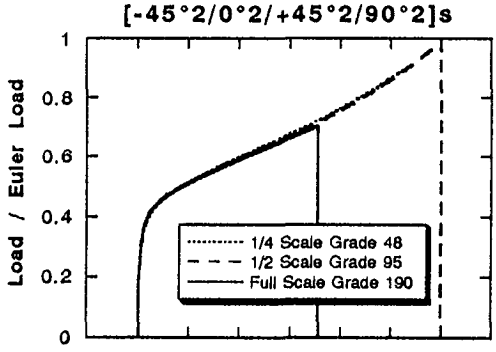

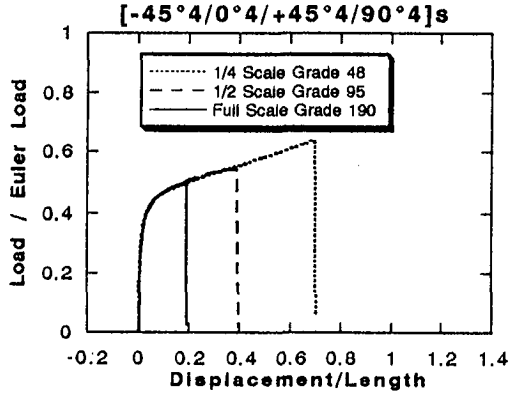

DISTRIBUTED QUASI-ISOTROPIC LAY-UPS

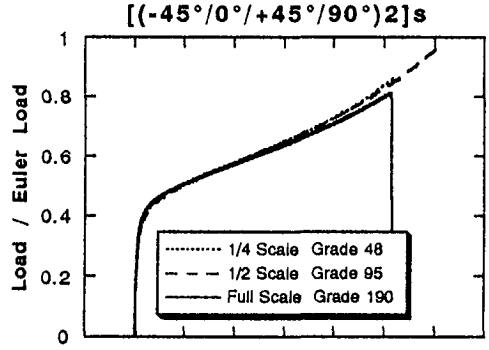

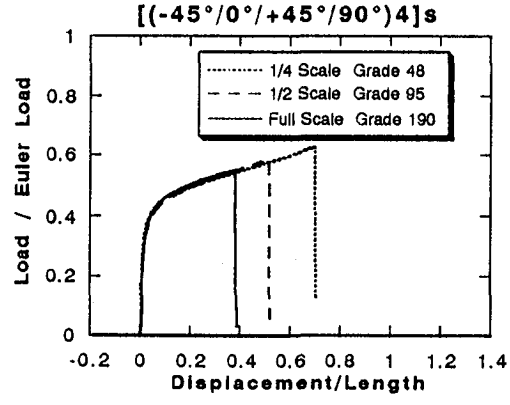

RESULTS
COMPARISON WITH PLY LEVEL SCALED TESTS

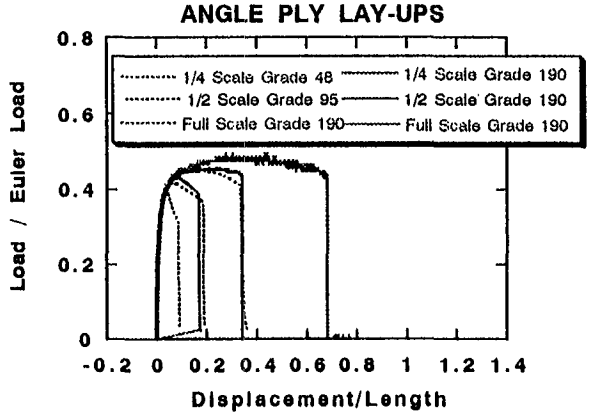

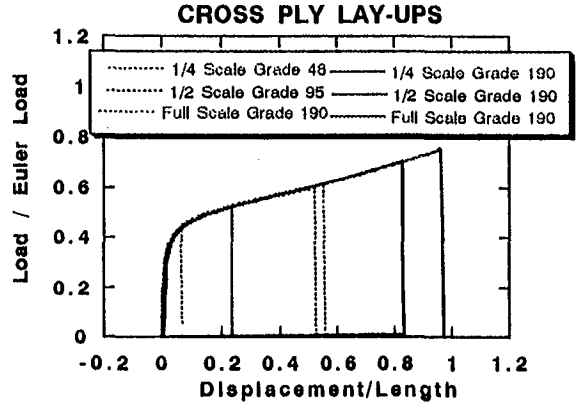

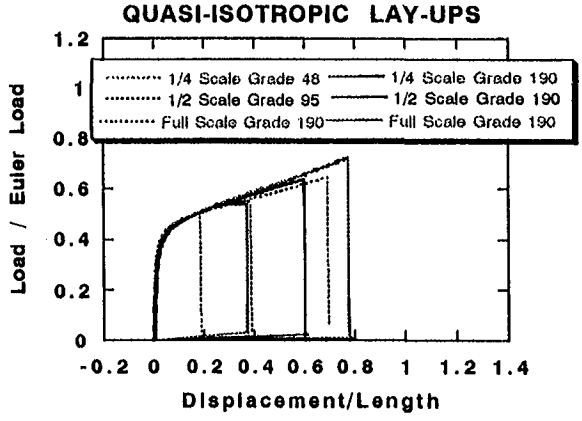

LARGE DEFLECTION BEAM SOLUTION

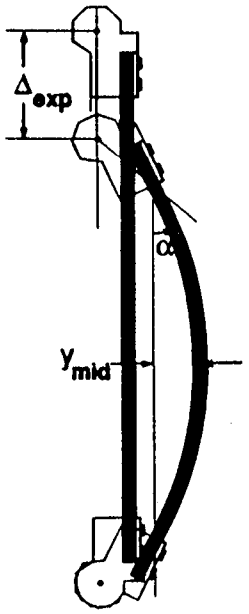

- CLASSICAL "ELASTICA" SOLUTION USING THE EXACT EXPRESSION FOR BEAM CURVATURE
- INCORPORATES HINGED BOUNDARY CONDITIONS
- LINEAR ELASTIC MATERIAL BEHAVIOR
- ONE DIMENSIONAL
- SOLUTION ALGORITHM PREDICTS ROTATION ANGLE, END DISPLACEMENT, AND TRANSVERSE DISPLACEMENT FOR INCREASING LOAD INCREMENTS
- STRESS ANALYSIS CALCULATES STRAINS AND PLY STRESSES
- COMPOSITE FAILURE CRITERIA INCLUDING MAX STRAIN, MAX STRESS, AND TSAI-WU APPLIED TO PREDICT FAILURE

RESULTS

COMPARISON OF FULL-SCALE RESPONSE WITH LARGE DEFLECTION ANALYSIS

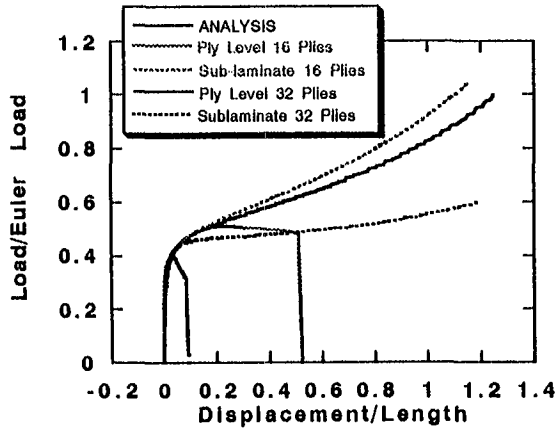

ANGLE PLY

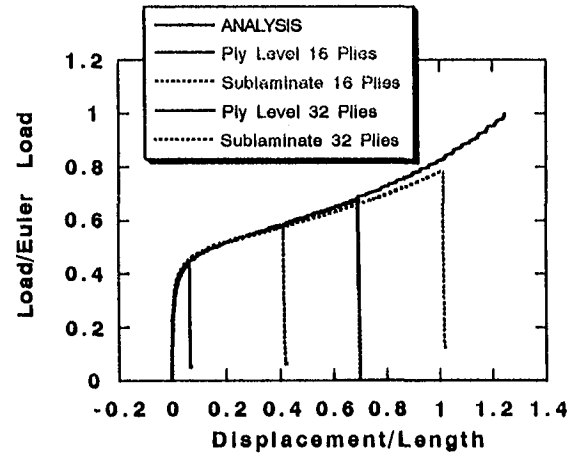

CROSS PLY

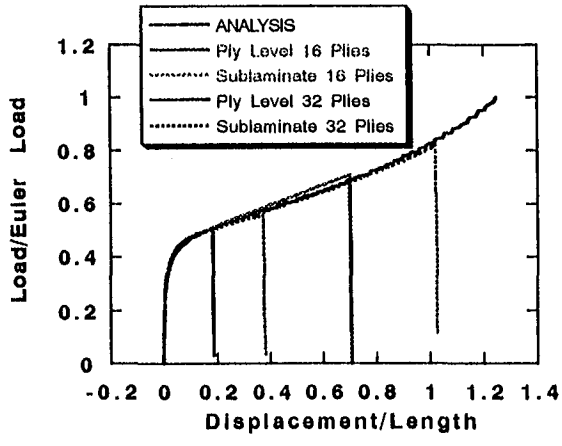

QUASI-ISOTROPIC

CONCLUSIONS

- Sub-Ply Level Scaled Beam-Columns, Tested Under Flexural Loads, Exhibited Size Effects in Response and Failure, with the Magnitude Depending on Absolute Size and Lay-up
- Strength Scale Effects Were Amplified for the Sub-Ply Level Beams Compared to the Ply Level Specimens Tested in an Earlier Study
- A Large Deflection "Exact" Solution Compared Well with the Experimental Beam Responses for Fiber Dominated Lay-ups
- The Sub-Ply Level Scaling Approach Does Not Alleviate the Strength Scale Effect in Flexure

EFFECTS OF SCALE IN PREDICTING GLOBAL STRUCTURAL RESPONSE

H. P. Kan
R. B. Deo

Northrop Aircraft Division
Department 3853/63
One Northrop Avenue
Hawthorne, CA 90250

ABSTRACT

In the course of previous composite structures test programs, the need for and the feasibility of developing analyses for scale-up effects has been demontrated. The analysis techniques for scale-up effects fall into two categories. The first category pertains to developing analysis methods independently for a single, unique failure mode in composites, and using this compendium of analysis methods together with a global structural model to identify and predict the response and failure mode of full-scale built-up structures. The second category of scale-up effects pertains to similitude in structural validation testing. In this latter category, dimensional analysis is used to develop scale-up laws that enable extrapolation of sub-scale component test data to full-scale structures. This paper decribes the approach taken and some developments accomplished in the first category of analysis for scale-up effects. Layup dependence of composite material properties severely limits the use of the dimensional analysis approach and these limitations are illustrated by examples.

This work was performed under NASA/Northrop Contract NAS1-18842, entitleed "Innovative Composite Fuselage Structures."

Outline

- INTRODUCTION
- BACKGROUND
- SCALING OF SIMPLE TENSION LAMINATE
- BUCKLING OF NARROW LAMINATE PLATE
- BUCKLING OF CYLINDRICAL SHELL
- SUMMARY

Introduction

- HIGH COST OF COMPOSITE STRUCTURAL TESTS NECESSITATE TEST OF COUPONS, ELEMENTS AND SUBSCALE STRUCTURES
- SCALING LAWS REQUIRED TO DESIGN SUBSCALE STRUCTURES CAPABLE OF SIMULATING FULL-SCALE STRUCTURAL BEHAVIOR AND TO INTERPRET SUBSCALE STRUCTURAL TEST RESULTS
- METHODOLOGY ALSO NEEDED TO PREDICT BUILT-UP FULL-SCALE STRUCTURAL RESPONSE USING COUPON AND ELEMENT LEVEL TEST DATA

Objectives

- DEVELOP SCALING LAWS TO PREDICT FULL-SCALE STRUCTURAL RESPONSE USING SCALE MODEL TEST DATA
  - — Principles of Similitude
  - — Static Response to Failure
- DEVELOP A METHODOLOGY AND THE REQUISITE ANALYSES TO PREDICT FULL-SCALE STRUCTURAL RESPONSE USING TEST DATA FROM SIMPLE SPECIMENS
  - — Building Block Approach
  - — Static Response to Failure

General Requirements – Principles of Similitude

- STRUCTURAL BEHAVIOR FULLY DESCRIBED BY A STRUCTURAL MECHANICS MODEL
- ALL SCALING PARAMETERS DEFINED BY DIMENSIONAL ANALYSIS
- ALL PHYSICAL PARAMETERS SCALABLE
- NO SCALING CONFLICT EXISTS

Application of Principles of Similitude to Composite Structures – Limitations

- LIMITED CLOSED FORM STRUCTURAL MECHANICS MODELS AVAILABLE
  - — Only Local Analysis Models Available
  - — No Reliable Failure Prediction Method
- NOT ALL PARAMETERS CAN BE SCALED ACCORDING TO SCALING RULES
  - — Thickness
  - — Stiffness, Rigidities

Alternative Approach – Building Block Approach

- DETAILED FINITE ELEMENT MODEL FOR THE STRUCTURE
  - — Load Distribution Within Structure
  - — Critical Locations
  - — Competing Failure Modes
- LOCAL STRESS ANALYSIS FOR FAILURE PREDICTION
  - — Joints
  - — Holes, Cutouts
  - — Substructures
  - — Structure Details
- ENVIRONMENTAL EFFECTS
  - — Material Property Change
  - — Failure Mode Change
- FAILURE SEQUENCE PREDICTION
- CORRELATION WITH TEST DATA

Building Block Approach

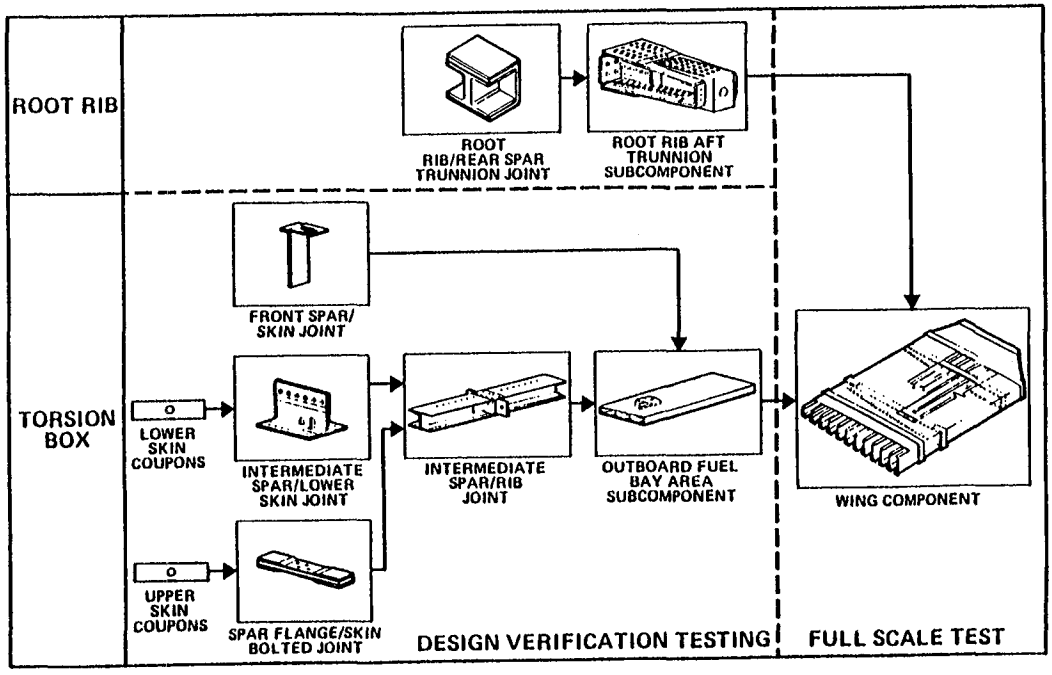

Post-Impact Compression Strength Scale Up

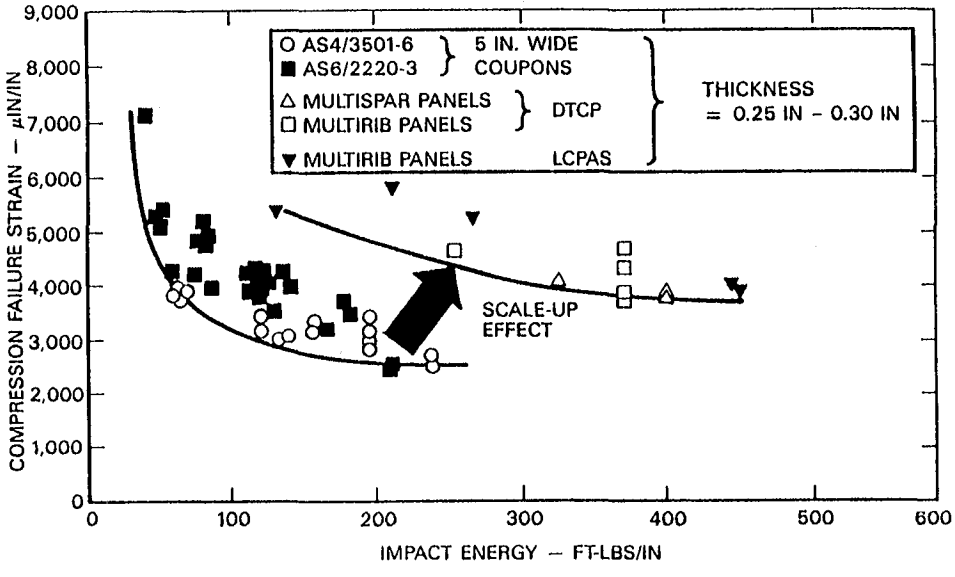

Alternative Approach – Principles of Similitude for Structures Where Closed Form Solution Available

- DEFINE OBJECTIVE OF SCALING – MAY REQUIRE DIFFERENT SET OF SCALING RULES FOR DIFFERENT PURPOSES
  - — Failure Load Simulation
  - — Structural Response Simulation
- DEFINE OVERALL SCALING PARAMETER
  i.e. 1/5 Model, 1/10 Model
- DEFINE SCALING RULES FOR MATERIAL PROPERTIES
- OBTAIN SCALING RULES FOR SELECTED PARAMETERS USING DIMENSIONAL ANALYSIS
  i.e. Length, Width, Thickness, Radius
- RESULTS IN PROBLEM SPECIFIC SPECIALIZED SCALING LAWS

Scaling of Simple Tension Laminate

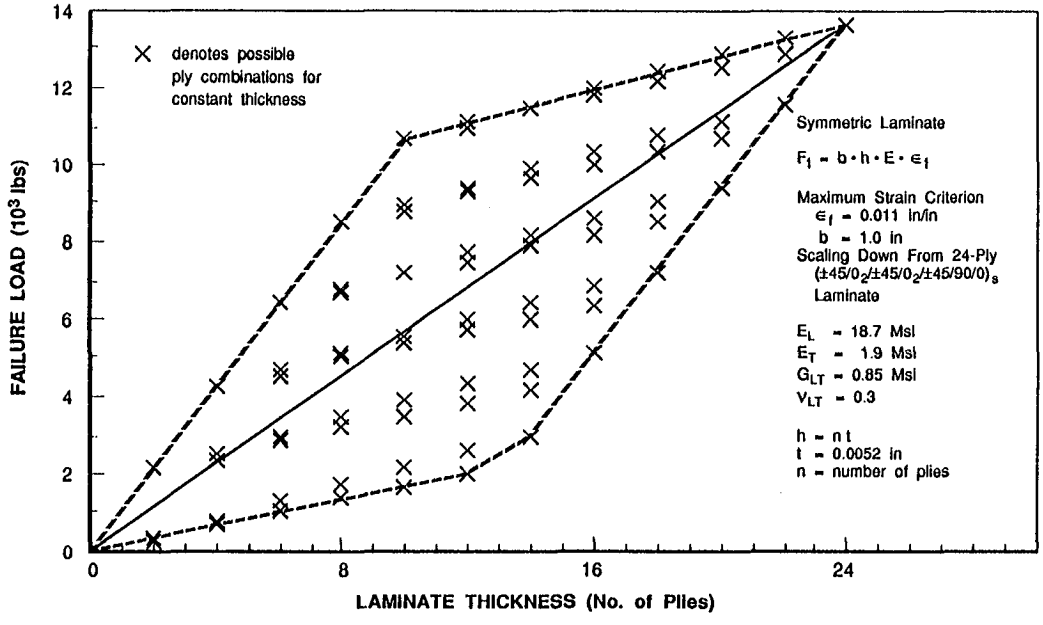

Buckling of Narrow Laminate

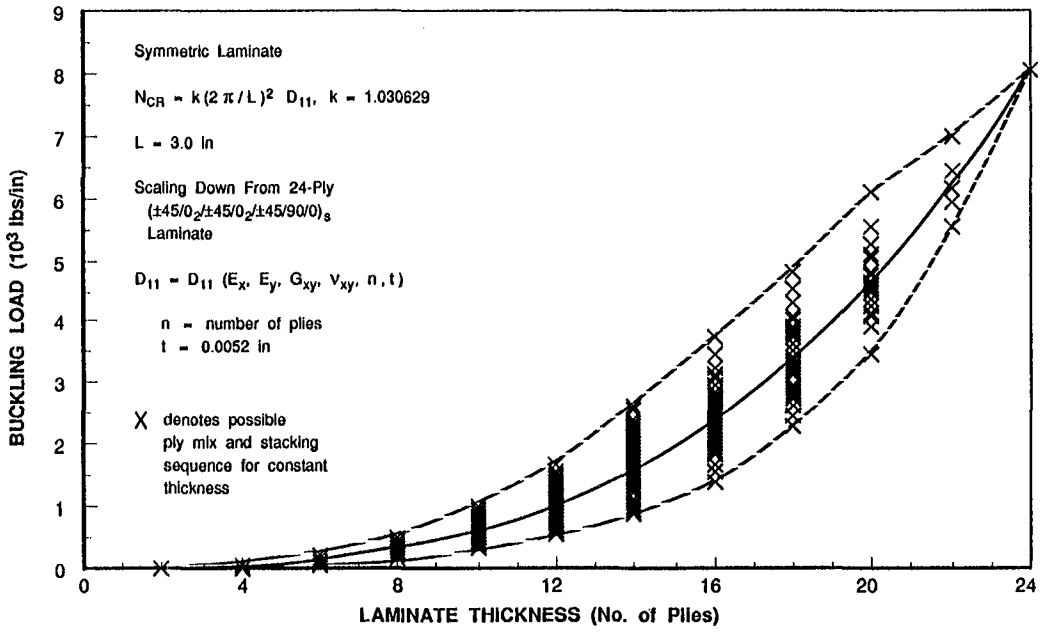

Failure of Rectangular Plate Under Uniform Pressure

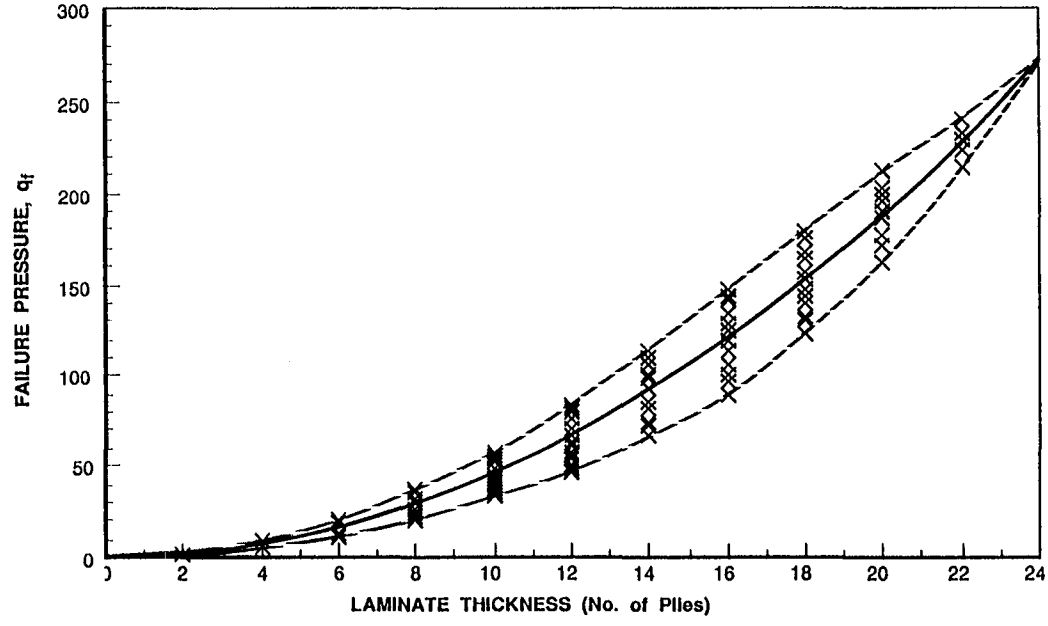

Buckling of Simply Supported Plate

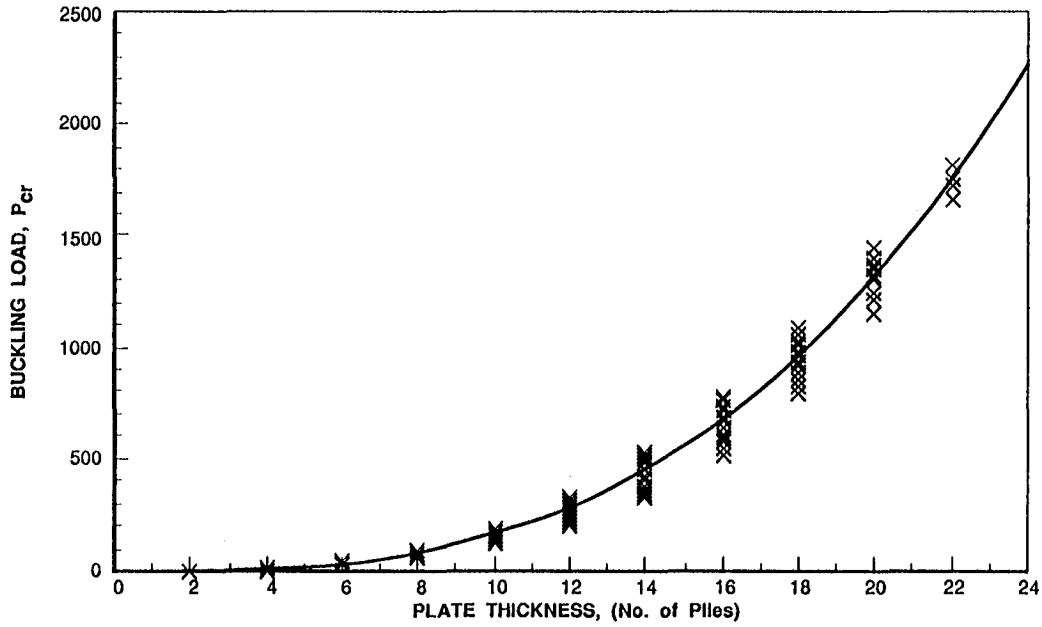

Specialized Scaling Technique

- OBJECTIVE: PREDICT BUCKLING LOAD FOR LARGE CYLINDRICAL SHELLS BASED ON CURVED PANEL TESTS

$$N_{CR} = \frac{2}{R}(EDt)^{1/2}$$

- SCALING PARAMETERS:

$$R_r = \frac{1}{P_r}\left(E_r D_r t_r\right)^{1/2}$$

$$t_r = \frac{\left(R_r P_r\right)^2}{E_r D_r}$$

$$E_r = \frac{\left(R_r P_r\right)^2}{t_r D_r}$$

$$D_r = \frac{\left(R_r P_r\right)^2}{E_r t_r}$$

- USE ISOTROPIC CASE FOR FIRST ESTIMATE
- USE ORTHOTROPIC SHELL BUCKLING EQUATIONS TO DETERMINE PARAMETERS ITERATIVELY
- USE CURVED PANEL BUCKLING EQUATIONS TO OBTAIN EQUIVALENT WIDTH

Iterative Procedure for Scale Model Shell

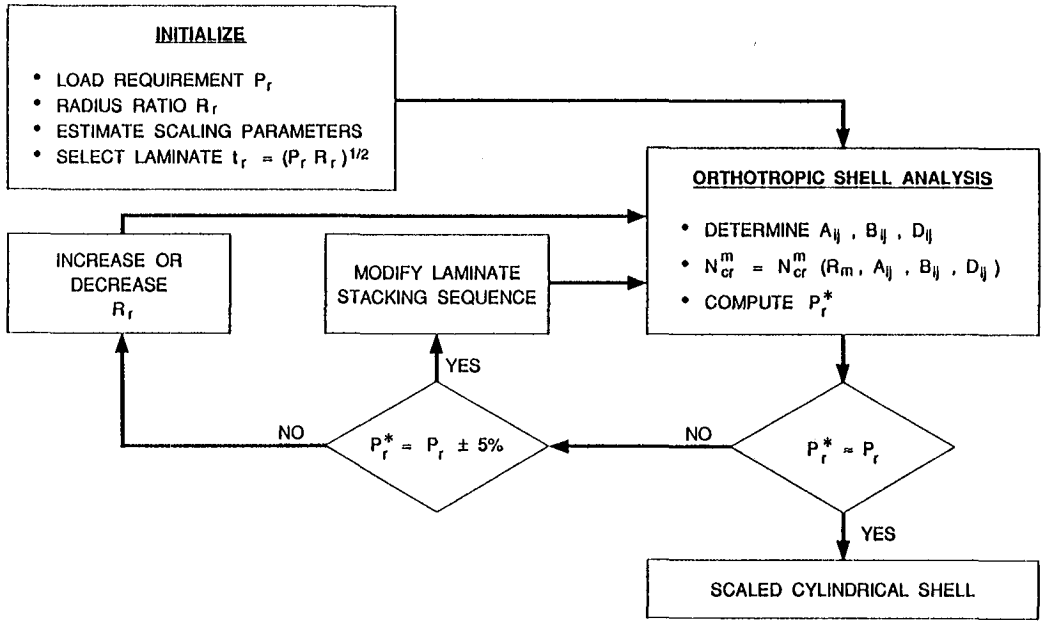

Equivalent Curved Panel

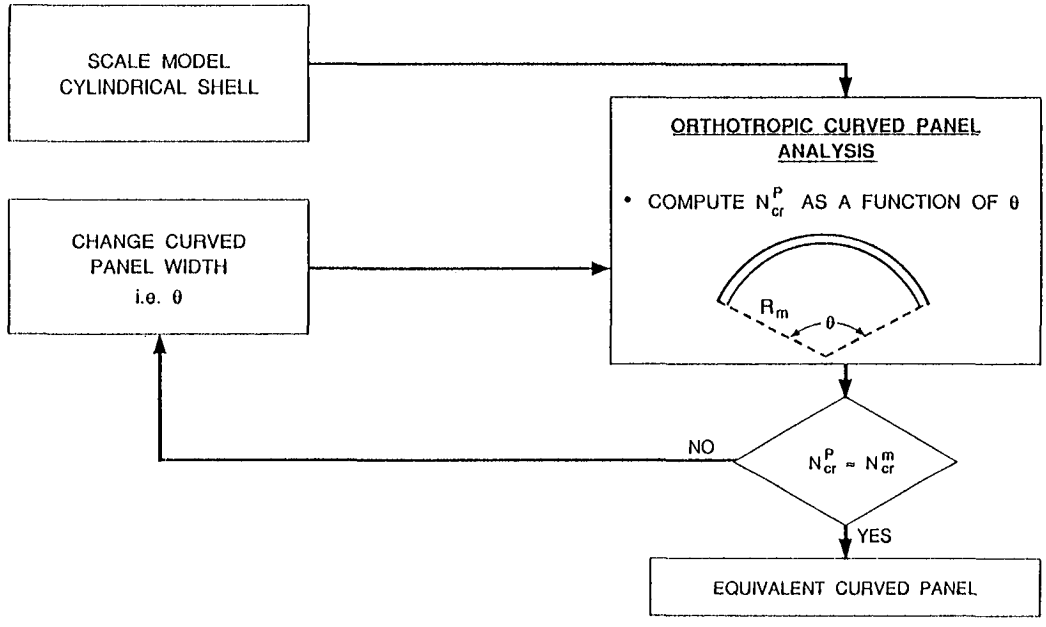

Scaling Example

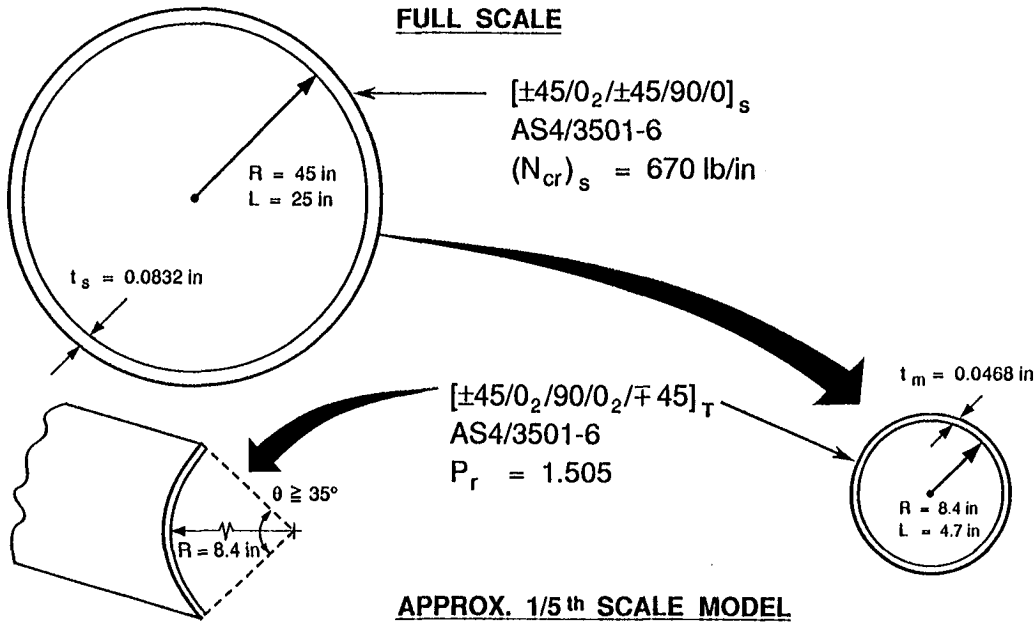

Summary

- REVIEWED ANALYTICAL TECHNIQUES FOR SCALE-UP EFFECTS
- SUMMARIZED ADVANTAGES AND LIMITATIONS OF PRINCIPLES OF SIMILITUDE
- FORMULATED ANALYTICAL PROCEDURE FOR DESIGN SCALE MODELS FOR AXIALLY COMPRESSED COMPOSITE CYLINDER
- OUTLINED A BUILDING-BLOCK APPROACH

SCALING, ELASTICITY, AND C.L.P.T.

Eugene Brunelle
Rensselaer Polytechnic Institute
Troy, NY

ABSTRACT 1

The first few viewgraphs describe the general solution properties of linear elasticity theory which are given by the following two statements:

(i) For stress B.C. on S_σ and zero displacement B.C. on S_u the altered displacements u_i^* and the actual stresses τ_{ij} are elastically dependent on Poisson's Ratio ν alone: thus the actual displacements are given by $u_i = \mu^{-1} u_i^*$.

(ii) For zero stress B.C. on S_σ and displacement B.C. on S_u the actual displacements u_i and the altered stresses τ_{ij}^* are elastically dependent on Poisson's Ratio ν alone: thus the actual stresses are given by $\tau_{ij} = E\tau_{ij}^*$.

ABSTRACT 2

The remaining viewgraphs describe the minimum parameter formulation of the general classical laminate theory plate problem as follows:

The general CLT plate problem is expressed as a 3 x 3 system of differential equations in the displacements u, v and w. The eighteen (six each) A_{ij}, B_{ij} and D_{ij} system coefficients are ply-weighted sums of the transformed reduced stiffnesses $(\bar{Q}_{ij})_k$; the $(\bar{Q}_{ij})_k$ in turn depend on six reduced stiffnesses $(Q_{ij})_k$ and the material and geometry properties of the k^{th} layer.

This paper develops a method for redefining the system coefficients, the displacement components (u,v,w) and the position components (x,y) such that a minimum parameter formulation is possible. The pivotal steps in this method are (i) the reduction of $(\bar{Q}_{ij})_k$ dependencies to just two constants $Q^* = (Q_{12} + 2Q_{66})/(Q_{11}Q_{22})^{1/2}$ and $F_* = (Q_{22}/Q_{11})^{1/2}$ in terms of ply-independent reference values Q_{ij}, (ii) the reduction of the remaining portions of the A, B and D coefficients to non-dimensional ply-weighted sums (with 0 to 1 ranges) that are independent of Q^* and F_* and (iii) the introduction of simple coordinate stretchings for u, v, w and x,y such that the process is neatly completed.

A SNEAK PREVIEW OF :

GENERAL SOLUTION PROPERTIES

OF LINEAR ELASTICITY THEORY

CONSIDER $(\lambda+\mu)\dfrac{\partial^2 u_j}{\partial x_i \partial x_j} + \mu \dfrac{\partial^2 u_i}{\partial x_j \partial x_j} + B_i = 0$

$$T_{ij} = \lambda \frac{\partial u_k}{\partial x_k}\delta_{ij} + \mu\left(\frac{\partial u_i}{\partial x_j} + \frac{\partial u_j}{\partial x_i}\right)$$

USE: $\begin{cases} f_1(\nu) = \dfrac{\lambda+\mu}{\mu} = (1-2\nu)^{-1} \\ f_2(\nu) = \dfrac{\lambda}{\mu} = 2\nu(1-2\nu)^{-1} \end{cases}$

IN ADDITION TO u_i AND T_{ij} WE INTRODUCE:

$$u_i^* = \mu u_i$$

AND

$$T_{ij}^* = \mu^{-1} T_{ij}$$

CASE I : $u_i^* = \mu u_i$

$$f_1(\nu)\,\partial^2 u_j^*/\partial x_i \partial x_j + \partial^2 u_i^*/\partial x_j \partial x_j + B_i = 0$$

$$T_{ij} = f_2(\nu)\,\delta_{ij}\,\partial u_k^*/\partial x_k + \partial u_i^*/\partial x_j + \partial u_j^*/\partial x_i$$

① FOR ARBITRARY STRESS B.C. ON S_σ AND HOMOG. DISP. B.C. ON S_u, u_i^* AND T_{ij} ARE ELASTICALLY DEPENDENT ON ONLY POISSON'S RATIO ν : THUS $u_i = \mu^{-1} u_i^*$.

② USING A WEIGHTED STRAIN ENERGY DENSITY $U^* = \mu U$, A VARIATIONAL PRINCIPLE IN u_i^* EXISTS WITH JUST ONE ELASTIC CONSTANT (POISSON'S RATIO ν).

③ THERE ARE GENERALIZED THEOREMS (IN u_i^*) OF MAXWELL, CASTIGLIANO AND RAYLEIGH & BETTI.

CASE II : $T^*_{ij} = \mu^{-1} T_{ij}$ AND $B_i = 0$

$$f_1(\nu)\, \partial^2 u_j / \partial x_i \partial x_j + \partial^2 u_i / \partial x_j \partial x_j = 0$$

$$T^*_{ij} = f_2(\nu)\, \delta_{ij}\, \partial u_k / \partial x_k + \partial u_i / \partial x_j + \partial u_j / \partial x_i$$

(1) FOR HOMOG. STRESS B.C. ON S_σ AND ARBITRARY DISP. B.C. ON S_u, u_i AND T^*_{ij} ARE ELASTICALLY DEPENDENT ON ONLY POISSON'S RATIO ν : THUS $T_{ij} = \mu T^*_{ij}$

NOTE : IN APPROX. THEORIES OF RODS, BEAMS, PLATES AND SHELLS MOST PROBLEMS ARE "CASE I-LIKE" AS WE WILL SEE IN THE "FEATURE-PRESENTATION".

A Minimum Parameter Formulation of the General CLT Plate Problem

E.J. Brunelle*

$$A_{11}U_{,xx}+2A_{16}U_{,xy}+A_{66}U_{,yy}+A_{16}V_{,xx}$$
$$+(A_{12}+A_{66})V_{,xy}+A_{26}V_{,yy}-B_{11}W_{,xxx}$$
$$-3B_{16}W_{,xxy}-(B_{12}+2B_{66})W_{,xyy}-B_{26}W_{,yyy}=0$$

$$A_{16}U_{,xx}+(A_{12}+A_{66})U_{,xy}+A_{26}U_{,yy}$$
$$+A_{66}V_{,xx}+2A_{26}V_{,xy}+A_{22}V_{,yy}-B_{16}W_{,xxx}$$
$$-(B_{12}+2B_{66})W_{,xxy}-3B_{26}W_{,xyy}-B_{22}W_{,yyy}=0$$

$$D_{11}W_{,xxxx}+4D_{16}W_{,xxxy}+4D_{26}W_{,xyyy}+D_{22}W_{,yyyy}$$
$$+2(D_{12}+2D_{66})W_{,xxyy}-B_{11}U_{,xxx}-3B_{16}U_{,xxy}$$
$$-(B_{12}+2B_{66})U_{,xyy}-B_{26}U_{,yyy}-B_{16}V_{,xxx}$$
$$-(B_{12}+2B_{66})V_{,xxy}-B_{22}V_{,yyy}-3B_{26}V_{,xyy}=p(x,y)$$

$$A_{ij}=\sum_{k=1}^{N}(\bar{Q}_{ij})_k(z_k-z_{k-1}) \qquad B_{ij}=\sum_{k=1}^{N}(\bar{Q}_{ij})_k(z_k^2-z_{k-1}^2)/2$$

$$D_{ij}=\sum_{k=1}^{N}(\bar{Q}_{ij})_k(z_k^3-z_{k-1}^3)/3$$

$$\bar{Q}_{11}=Q_{11}m^4+2(Q_{12}+2Q_{66})m^2n^2+Q_{22}n^4$$
$$\bar{Q}_{22}=Q_{11}n^4+2(Q_{12}+2Q_{66})m^2n^2+Q_{22}m^4$$
$$\bar{Q}_{16}=(Q_{11}-(Q_{12}+2Q_{66}))m^3n+((\cdots)-Q_{22})mn^3$$
$$\bar{Q}_{26}=(\quad"\quad\quad")mn^3+(\quad"\quad\quad")m^3n$$

AND A COMBINATION OF TERMS :

$$\bar{Q}_{12}+2\bar{Q}_{66}=(Q_{12}+2Q_{66})(m^4+n^4)$$
$$+[3(Q_{11}+Q_{22})-4(Q_{12}+2Q_{66})]m^2n^2$$

* Rensselaer Polytechnic Institute

RETAIN THESE DEFINITIONS: $F_* = (Q_{22}/Q_{11})^{1/2}$

$Q^* = (Q_{12}+2Q_{66})/(Q_{11}Q_{22})^{1/2}$ $\quad Q^* = \epsilon Q^* + (1-\epsilon)Q^*$

$\therefore$ $Q_{ij}/(Q_{11}Q_{22})^{1/2}$ TERMS ARE GIVEN BY:

$$\bar{Q}_{11}/(\ )^{1/2} = F_*^{-1} m^4 + 2Q^* m^2 n^2 + F_* n^4$$

$$\bar{Q}_{22}/(\ )^{1/2} = F_*^{-1} n^4 + 2Q^* m^2 n^2 + F_* m^4$$

$$\bar{Q}_{16}/(\ )^{1/2} = (F_*^{-1} - Q^*) m^3 n + (Q^* - F_*) m n^3$$

$$\bar{Q}_{26}/(\ )^{1/2} = (F_*^{-1} - Q^*) m n^3 + (Q^* - F_*) m^3 n$$

$$(\bar{Q}_{12}+2\bar{Q}_{66})/(\ )^{1/2} = Q^*(m^4+n^4) + [3(F_*^{-1}+F_*) - 4Q^*] m^2 n^2$$

THUS FOR A GIVEN LAYER ALL Q_{ij} EFFECTS REDUCE TO A Q^* AND F_* DEPENDENCE!

$D_{11}W_{,XXXX}$ AS A PROTOTYPE EXPRESSION.

$$D_{11}/(Q_{11}Q_{22})^{1/2} = \frac{1}{3}\sum_{k=1}^{N}\left[\frac{(Q_{11})_k}{(Q_{11}Q_{22})^{1/2}} m_k^4 + \frac{(Q_{12}+2Q_{66})_k}{(Q_{11}Q_{22})^{1/2}} m_k^2 n_k^2 + \frac{(Q_{22})_k}{(Q_{11}Q_{22})^{1/2}} n_k^4\right](Z_k^3 - Z_{k-1}^3)$$

TO USE F_* AND Q^* DEFINITIONS FOR ALL LAYERS LET $(Q_{11})_k = q_{1k} Q_{11}$, $(Q_{22})_k = q_{2k} Q_{22}$ AND

$$(Q_{12}+2Q_{66})_k = q_{3k}(Q_{12}+2Q_{66})$$

THUS WE HAVE: $D_{11}/(Q_{11}Q_{22})^{1/2} = \frac{1}{3}F_*^{-1}\sum_{k=1}^{N} q_{1k}\, m_k^4 (z_k^3 - z_{k-1}^3)$

$$+\frac{2}{3}Q^*\sum_{k=1}^{N} q_{3k}\, m_k^2\, n_k^2 (z_k^3 - z_{k-1}^3) + \frac{1}{3}F_*\sum_{k=1}^{N} q_{2k}\, n_k^4 (z_k^3 - z_{k-1}^3)$$

NOTE THAT SUMS JUST DEPEND ON WEIGHTED (q_{ik}) STACKING SEQUENCE TERMS!

FURTHER: IF $T = z_N$ THEN THE "SUMS/T^3" ARE DIMENSIONLESS AND ARE ALL $\leq$ UNITY!

$\Longrightarrow$ NOW INTRODUCE ℓ AND P SUCH THAT:

$x_* = \ell x$ AND $y_* = \ell y$ AND

$$p(x,y) = P\, p_o(x,y)$$

THUS NOTE THAT

$$\frac{D_{11} W_{,xxxx}}{P} = \underbrace{\frac{D_{11}}{T^3(Q_{11}Q_{22})^{1/2}}}_{\tilde{D}_{11}} \underbrace{\left[\frac{T^3(Q_{11}Q_{22})^{1/2} W(x,y)}{P\ell^4}\right]_{,x_*x_*x_*x_*}}_{W^*_{,x_*x_*x_*x_*}}$$

A SCALED DEFLECTION!

IF WE CAN SCALE ALL OTHER TERMS IN THE 3 EQUIL. EQNS. WITHOUT CONFLICTS THEN THE SCALING PROCESS WILL BE COMPLETE AND SUCCESSFUL!

HOWEVER IT SHOULD BE CLEAR THAT THE SYMMETRIC ANGLE-PLY PLATE IS NOW IN SCALED FORM SINCE THE ONLY UNKNOWN IS W^*. THUS IN OUR NOTATION:

$$\widetilde{D}_{11} W^*_{,x^*x^*x^*x^*} + 4\widetilde{D}_{16} W^*_{,x^*x^*x^*y^*} + 4\widetilde{D}_{26} W^*_{,x^*y^*y^*y^*}$$

$$+ 2\underbrace{\left(\widetilde{D}_{12} + 2\widetilde{D}_{66}\right)}_{D^*} W^*_{,x^*x^*y^*y^*} + \widetilde{D}_{22} W^*_{,y^*y^*y^*y^*} = P_o(x^*, y^*)$$

WHERE $W^* = \left(\dfrac{T^3 (Q_{11}Q_{22})^{1/2}}{P l^4}\right) W$

NOTE THAT THE RAW W^* OUTPUT FOR A PARTICULAR PROBLEM (ONE COMPUTER RUN) IS CONVERTED TO AS MANY SOLUTIONS IN "REAL SPACE" AS DESIRED BY JUST MULTIPLYING THE RAW W^* BY THE CHOSEN VALUES OF T, P, l AND $Q_{11}Q_{22}$. THAT IS TO SAY, A 4-FOLD INFINITY OF SOLUTIONS!

THUS PARAMETER STUDIES CAN BE ECONOMICALLY MADE.

TO FIND SCALING FOR U AND V

LOOK AT EQUIL. EQNS. WE SEE THAT:

$A_{ij}\,U_{,rs}$ (OR $A_{ij}\,V_{,rs}$) AND $B_{ij}\,W_{,rst}$ (MUST MATCH)

AND

$D_{ij}\,W_{,rst}$ AND $B_{ij}\,U_{,rst}$ (OR $B_{ij}\,V_{,rst}$) (MUST MATCH)

WHERE (REMEMBER THE "T" FACTOR)

$$A_{ij} = T\sum_{k=1}^{N}(\bar{Q}_{ij})_k \frac{(z_k - z_{k-1})}{T} \qquad B_{ij} = \frac{T^2}{2}\sum_{k=1}^{N}(\bar{Q}_{ij})_k \frac{(z_k^2 - z_{k-1}^2)}{T^2}$$

$$D_{ij} = \frac{T^3}{3}\sum_{k=1}^{N}(\bar{Q}_{ij})_k \frac{(z_k^3 - z_{k-1}^3)}{T^3}$$

EXPANDING THE MATCHING CONDITIONS

ON THE LAST TRANSPARENCY WE HAVE:

$$\sum_{k=1}^{N}(\bar{Q}_{ij})_k \frac{(z_k - z_{k-1})}{T(Q_{11}Q_{22})^{1/2}} \frac{\partial^2 u (Q_{11}Q_{22})^{1/2} T}{\partial r^* \partial s^* \ell^2 P}$$

$$\frac{1}{2}\sum_{k=1}^{N}(\bar{Q}_{ij})_k \frac{(z_k^2 - z_{k-1}^2)}{T^2(Q_{11}Q_{22})^{1/2}} \frac{\partial^3 w (Q_{11}Q_{22})^{1/2} T^2}{\partial r^* \partial s^* \partial t^* \ell^3 P}$$

(MUST MATCH!)

AND

$$\frac{1}{3}\sum_{k=1}^{N}(\bar{Q}_{ij})_k \frac{(z_k^3 - z_{k-1}^3)}{T^3(Q_{11}Q_{22})^{1/2}} \frac{\partial^4 w (Q_{11}Q_{22})^{1/2} T^3}{\partial q^* \partial r^* \partial s^* \partial t^* \ell^4 P}$$

$$\frac{1}{2}\sum_{k=1}^{N}(\bar{Q}_{ij})_k \frac{(z_k^2 - z_{k-1}^2)}{T^2(Q_{11}Q_{22})^{1/2}} \frac{\partial^3 u (Q_{11}Q_{22})^{1/2} T^2}{\partial r^* \partial s^* \partial t^* \ell^3 P}$$

(MUST MATCH!)

UPON COMPARING WE SEE THAT

$$U^* = \left(\frac{T^2 (Q_{11} Q_{22})^{1/2}}{\ell^3 P}\right) U \qquad V^* = \left(\frac{T^2 (Q_{11} Q_{22})^{1/2}}{\ell^3 P}\right) V$$

AND

$$W^* = \left(\frac{T^3 (Q_{11} Q_{22})^{1/2}}{\ell^4 P}\right) W$$

$\Longrightarrow$ NOTE THAT THE OUTPUT FOR A SINGLE (ONE COMPUTER RUN) PROBLEM U^*, V^* AND W^* CAN BE CONVERTED INTO A 4-FOLD INFINITY OF SOLUTIONS BY SIMPLE MULTIPLICATIONS PERFORMED ON THE OUTPUT DATA SET!

EXPERIMENTAL OBSERVATIONS OF SCALE EFFECTS ON BONDED AND BOLTED JOINTS IN COMPOSITE STRUCTURES

Glenn C. Grimes
Lockheed Advanced Development Company

ABSTRACT

OBJECTIVE: To observe size (scale) effects in 1) fiber dominated laminates and bolted joints, 2) adhesive (matrix) dominated bonded joints with fiber dominated laminate adherends, and 3) matrix dominated laminates.

SCOPE: Selected literature on scale effects is reviewed with comments and test data from one source that is analyzed for predicted and actual scale effects utilizing uniaxial loaded static strength, spectrum fatigue residual strength, and spectrum fatigue lifetime test results. Causes of scale effects are discussed, the results are summarized, and conclusions are made.

DETAILED OBSERVATIONS:

In Reference 1, Verette and Labor show the results of experimentally observed scale effects on fiber dominated graphite/epoxy solid laminates under static and spectrum fatigue uniaxial loading. The large size specimens had a test volume 16 times that of the small size specimens. The scale effects reduction of the large scale vs. the small scale specimens is -4.5% for static strength, -8.0% for tension dominated spectrum fatigue residual strength, and -3.2% for compression dominated spectrum fatigue residual strength. Their conclusion is that there is no strength reduction scale effect since these values fall within experimental scatter.

In Reference 1, Verette and Labor utilize a size effects equation for predicting scale effects that is developed by Halpin, Jerina, and Johnson in Reference 2. It is based on the idea that the likelihood of serious flaws occurring increases as the volume of a composite specimen increases.

In Reference 3, Jeans, Grimes, and Kan studied many thousands of bonded and bolted joints under static and spectrum fatigue loading in several severe environments. A large number of standard size and a small number of large size bonded and bolted joints are studied at RTW conditions. Appendix A details the results of 14 test series of bonded joints covering 243 individual specimens. Some RTD specimens are included. Of these data, 8 test series at RTW covering 96 specimens are utilized in studying the effects of size on bonded joints under RTW static and fatigue conditions. In addition, from Reference 3, RTD and RTW bolted joint test data is extracted as shown in

Appendix B and analyzed for size effects. Five of the nine test series are used in the study covering 59 specimens at RTW conditions.

An adhesives test evaluation performed in Reference 3 is shown utilizing a double overlap bonded joint specimen. This data illustrates the extreme detrimental effects that absorbed moisture has on bonded joint strength when composite adherends are used.

The Reference 3 standard and large scale bonded joints (composite-to-titanium) configurations are shown, followed by the data being analyzed for scale effects in the next four charts. The estimated (calculated) and the actual (experimentally observed) scale effects are shown along with other pertinent data. For static strength the estimated scale factor is 0.93, whereas, the actual value is 1.39, indicating that the large size joint is better than the small size joint. In tension dominated fatigue most of the specimens failed in fatigue before reaching 2 lifetimes; i.e., the scale factors were calculated and measured based on the lifetimes survived instead of residual strength. With an estimated scale factor or 0.71 lifetimes and an actual value of 0.60, significant scale effects occurred. For static compression loading, the estimated scale effects value is 0.92, whereas, the actual value is 1.34; i.e., the large bonded joints were significantly better than the small bonded joints. In compression dominated fatigue most of the specimens survived 2 lifetimes of spectrum fatigue so the residual strength data is analyzed. The estimated scale factor is 0.82 while the actual is 1.54, illustrating again that the large size joints are better than the small size joints.

The standard and large size bolted joint configurations are shown, followed by the RTW static and fatigue test data taken from Reference 3 on these joints. For static tension loaded RTW bolted joints the estimated (calculated) scale factor is 0.94, whereas, the actual test scale factor is 0.87, which is probably reasonable correlation even though the scale factor reduction is small. For the RTW tension dominated fatigue data (comparison #1) the estimated scale factor is 0.94 versus the actual test value of 1.02, also reasonable correlation, but not much of a scale factor exists. For RTW tension dominated fatigue (comparison #2), the estimated scale factor is 0.890 and the actual scale factor is 1.01, again reasonable correlation. However, there is not much of a scale factor.

A summary of these scale factors is next shown. These show that for the failure mode that occurs, i.e., bondline cohesive failure in bonded joints and net (through the hole) tension failure in bolted joints, there are no significant strength reduction scale factors for static loading of RTW bonded and RTW bolted joints. In addition there is no significant residual strength scale effect reduction in RTW bonded joints in compression dominated fatigue and in tension dominated fatigue RTW bolted joints. There is a significant fatigue lifetime scale factor in tension dominated fatigue RTW bonded joints. In this latter case much fatigue wearout occurs in the bondline during testing.

Causes of scale effects follow in the next chart, showing that the most likely conditions for scale effects are quality issues.

SUMMARY

The following discussion is based on large scale strength divided by small scale strength, unless otherwise noted. For fiber dominated solid laminates of RTW graphite/epoxy, no significant reduced scale effects strengths are observed for static strength and fatigue residual strength. For RTW bonded joints with fiber dominated adherends, no significant scale effects strength reductions are observed for tension and compression static strength and for compression dominated fatigue residual strength. However, for RTW tension dominated fatigue bonded joints, a significant lifetime reduction scale effect is observed. No significant scale effects strength reductions are observed for static tension and tension dominated fatigue residual strength of RTW bolted joints. Data from References 1 and 3 are analyzed for scale effects using the Reference 2 equation. For the bonded joints with fiber dominated adherends, significant strength increase scale effects are observed for static tension, static compression, and compression dominated fatigue. This latter effect is probably caused by the fact that the large bonded joints are more efficient than the small ones as shown in Reference 5.

Fiber dominated and matrix dominated tension loaded laminates from Reference 4 exhibited significant scale factors in the next chart. This is in contrast to the Reference 1 and 3 data. Apparently the quality of the Reference 4 large scale specimen panels is significantly lower than that of the small scale specimen panels. This is shown in Reference 4 by NDI, and physical property testing showing matrix cracking and an increase in void content. In some cases the large scale specimens exhibited changes in failure modes compared to those observed in the small scale specimens.

A list of causes of significant scale factors is presented showing the most frequently occurring ones as judged by the author. The fact that these causes are dominated by quality issues is in agreement with the Reference 4 results.

CONCLUSIONS

Scale effects occur most of the time as a result of the large scale specimens having lower quality than those of the small scale specimen. If there is sufficient time and money to 1) select the proper materials, 2) develop good and consistent processing, and 3) solve the design and tooling problems for the large scale parts, there will not be scale effects in most cases.

Exceptions could be: 1) large, multi-material parts that have significant, manufacturing induced, thermal stresses, 2) moisture sensitive bonded joints that exhibit substantial fatigue lifetime wearout, 3) complicated multiple load path, large scale parts that have not had adequate building block test development or FEM analysis, and 4) full (large) size structural prototyping that is done quickly in the development cycle without adequate M&P development and building block structural test development.

Where scale effects do occur, the equation from Reference 1 seems to be adequate for estimation.

The specimens tested in References 1 and 3 had the benefit of well developed and established, high quality and consistent fabrication methods that resulted in consistent high quality test data that was analyzed for this paper.

LIST OF REFERENCES

1. Verette, R.M. and Labor, J.D., "Structural Criteria for Advanced Composites", AFFDL-TR-76-142, Vol. I, Final Report, March 1977.

2. Halpin, J.C., Jerina, K.L., and Johnson, T.A., "Characterization of Composites for the Purpose of Reliability Evaluation", in Analysis of Test Methods for High Modulus Fibers and Composites, ASTM STP521, ASTM, 1973, pp. 5-64, J.M. Whitney, Editor.

3. Jeans, L.L., Grimes, G.C. and Kan, H.P., "Fatigue Spectrum Sensitivity Study of Advanced Composite Materials", Volumes I, II, and III, AFWAL-TR-80-3130, December 1980.

4. Jackson, K.E., Kellas, S., and Morton, J., "Scale Effects in the Response and Failure of Fiber Reinforced Composite Laminates Loaded in Tension and Flexure", Journal of Composite Materials, Volume 26, No. 18, 1992.

5. Grimes, G.C., Ranger, K.W., and Brunner, M.D., "Element and Subcomponent Tests", Composites-Volume 1 of Engineered Materials Handbook, Technical Chairman, Theodore J. Reinhart, ASM, International, 1987, pp. 328-344.

APPENDIX A
BONDED JOINTS (Reference 3)

TEST SERIES	ENVIR-ONMENT	LOAD DIR.	LOAD FREQ. OR RATE	LIFE-TIMES	TRUNCA-TION[1]	MAX SPECT. LD, (LBS)[2]	Weibull Parameters[3,4] α (α_L)	B^5 (B_L)[6]	B^5 (B_L)[6]	$N_x(t)^5$ (T)[6]	NO. OF SPEC.
					- LS Bonded Joints - Ten. (W) -						
76S-RTW(T)	RTW	Ten.	-	Static	-	-	15.47	17,705	17,113	14,796	7
76F-RTW(TD)	RTW	T.D.	5Hz	2	9/2	12,300	- (3.92)	(no survivors) (1.42)	(1.25)	- (0.70)	3
					- LS Bonded Joints - COMPR. (W) -						
76S-RTW(C)	RTW	Compr.	-	Static	-	-	-	-23,578	-	-	3
76F-RTW(CD)	RTW	C.D.	5Hz	2	9/2	-12,300	-	-23,329	-	-	3
					- Std. Bonded Joints - Ten (W) -						
60-RTW(T)	RTW	Ten.	-	Static	-	-	19.83	7088	6970	6222	20
ϕ 107-RTW(TD)	RTW	T.D.	5Hz	2	9/2	5000 *(13/20)	4.93 (0.95)	4905 (4.82)	4586 (3.40)	2906 (0.32)	20
107-1-RTW(TD)	RTW	T.D.	5Hz	2	9/2	5000 *(11/20)	5.57 (3.04)	7051 (2.37)	6643 (2.13)	4433 (1.01)	20
					- Std. Bonded Joints - Compr. (W) -						
61-RTW(C)	RTW	Compr.	-	Static	-	-	14.97	-9797	-9582	-8244	20
112-RTW(CD)	RTW	C.D.	5Hz	2	9/2	-5850 *(15/20)	6.25 (1.42)	-8433 (4.70)	-7996 (3.72)	-5579 (0.76)	20
					- Std. Bonded Joints - Ten (Dry) -						
1-(RTD)(T) (30 spec)	RTD	Ten	-	Static	-	-	10.37	11,408	11,190	9007	30
3-(RTD)(TD) (29 spec)	RTD	Ten	5Hz	2	9/2	5850	8.63	9922	9692	7467	29
					- Std. Bonded Joints - Compr (Dry) -						
2-(RTD)(C)	RTD	Compr.	-	Static	-	-	13.72	-13,121	-12,892	-10,942	40
10-(RTD)(CD)	RTD	Compr.	5Hz	2	9/2	-5850	10.20	-11,838	-11,458	-9183	20
#, ϕ 10A-(RTD)(CD)	RTD	Compr.	5HZ	2	9/2	-5850 *(7/8)	9.02	-11,238	-10,636	-8287	8

* (survivors/total no.) specimens
\# 8 spec. total but only 7 survived
ϕ poor quality: high void content, adhesive and laminate

NOTES: [1] 9/2 denotes 9g max. load, 1/2g to 2g peaks truncated

[2] Based on stress level factors of 0.90 for RTD bonded joints and 0.77 for RTW bonded joints because of their fatigue sensitivity.

[3] Weibull residual strength values are shown first with fatigue lifetime Weibull values shown in parentheses.

[4] Weibull parameters based on 2 parameter Weibull distribution methodology.

[5] lbs/in

[6] (T) = Lifetimes

APPENDIX 3

BOLTED JOINTS (Reference 3)

TEST SERIES	ENVIR-ONMENT	LOAD DIR.	LOAD FREQ./ RATE	LIFE-TIMES	TRUNCA-TION[1]	MAXIMUM SPECTRUM[2] LOAD (lbs/in)	Weibull Parameters on R.S.[3]				NO OF SPEC
							α[4]	β[4] lbs/in	β[4] lbs/in	$N_x(t)$[4] lbs/in	
*14 (STD)	RTD	Ten.	-	Static	-	-	24.98	10,159	10,025	9,161	20
14-1 (STD)	RTD	Ten.	-	Static	-	-	50.22	12,730	12,646	12,092	20
*15 (STD)	RTD	Ten.	5Hz	2	9/2	6,500	15.06	9,990	9,831	8,466	40
15-1 (STD)	RTD	Ten.	5Hz	2	9/2	6,500	71.23	12,623	12,565	12,174	40
62 (STD)	RTW	Ten.	-	Static	-	-	13.39	12,047	11,764	9,944	22
115 (STD)	RTW	Ten.	5Hz	2	9/2	6,500	16.10	12,168	11,919	10,365	20
72-SRTW (LS)	RTW	Ten.	-	Static	-	-	48.16	20,651	20,427	19,494	7
72-FRTW-1(LS)	RTW	Ten.	5Hz	2	9/2	7,571	43.36	20,835	20,584	19,543	7
72-FRTW-2(LS)	RTW	Ten.	5Hz	2	9/2	7,571 (1/2LT) 13,286 (3/2LT)	-	20,645[5]	-	-	3

NOTES: [1] 9/2 denotes 9g maximum load, 1/2-2g peaks truncated

[2] Based on stress level factors determined to be 1.00 for bolted joints

[3] Weibull values for residual strength

[4] Weibull parameters based on 2 parameter Weibull distribution methodology

[5] Mean value of 3 specimens; no Weibull statics computed. Used baseline values for comparison.

* Poor quality: Receiving Inspection showed fiber strength below specification.

EXPERIMENTAL OBSERVATIONS OF SCALE EFFECTS ON BONDED AND BOLTED JOINTS IN COMPOSITE STRUCTURES

- OBJECTIVE: To Observe Size(Scale) Effects in Uniaxial Loaded:
  - Fiber Dominated Laminates and Bolted Joints
  - Adhesive(Matrix) Dominated Bonded Joints with Fiber Dominated Laminate Adherends
  - Matrix Dominated Laminates
- SCOPE: From Selected Literature on Scale Effects in Composite Structures, Test Data is Analyzed for:
  - Estimated(Predicted) Scale Effects
  - Actual Scale Effects Observed
  - Causes of Scale Effects are Discussed
  - Results are Summarized
  - Conclusions are Made

SIZE EFFECTS ON GRAPHITE/EPOXY TENSILE SPECIMENS

[0/+45/90]4S AS/3501–5 TAPE

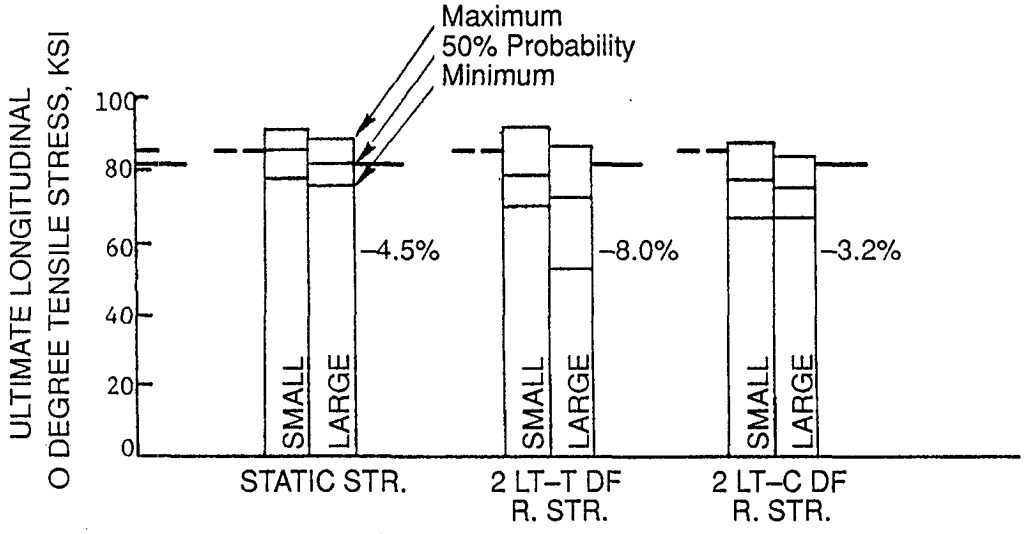

Ref. 1: Verette, R. M. and Laber, J. D., "Structural Criteria for Advanced Composites", AFFDL–TR–76–142, Vol. I Final Report, March 1977

SIZE EFFECTS EQUATION

$$\beta_{large} = \frac{\beta_{small}}{(V_{large}/V_{small})^{\frac{1}{\alpha}}} \quad \text{or} \quad \frac{\beta_L}{\beta_S} = \frac{1}{(V_L/V_S)^{\frac{1}{\alpha}}}$$

where

β = characteristic strength

V = volume within which failure can occur

α = Weibull Shape parameter

Ref. 1: Verette, R. M. and Laber, J. D., "Structural Criteria for Advanced Composites", AFFDL–TR–76–142, Vol. I Final Report, March 1977

Ref. 2: Halpin, J. C., Jerina, K. L., and Johnson, T. A., "Characterization of Composites for the Purpose of Reliability Evaluation" in Analysis of Test Methods for High Modulus Fibers and Composites, ASTM STP 521, ASTM, 1973, pp. 5–64, J. M. Whitney, Editor

SPECIMEN FOR ADHESIVES EVALUATION

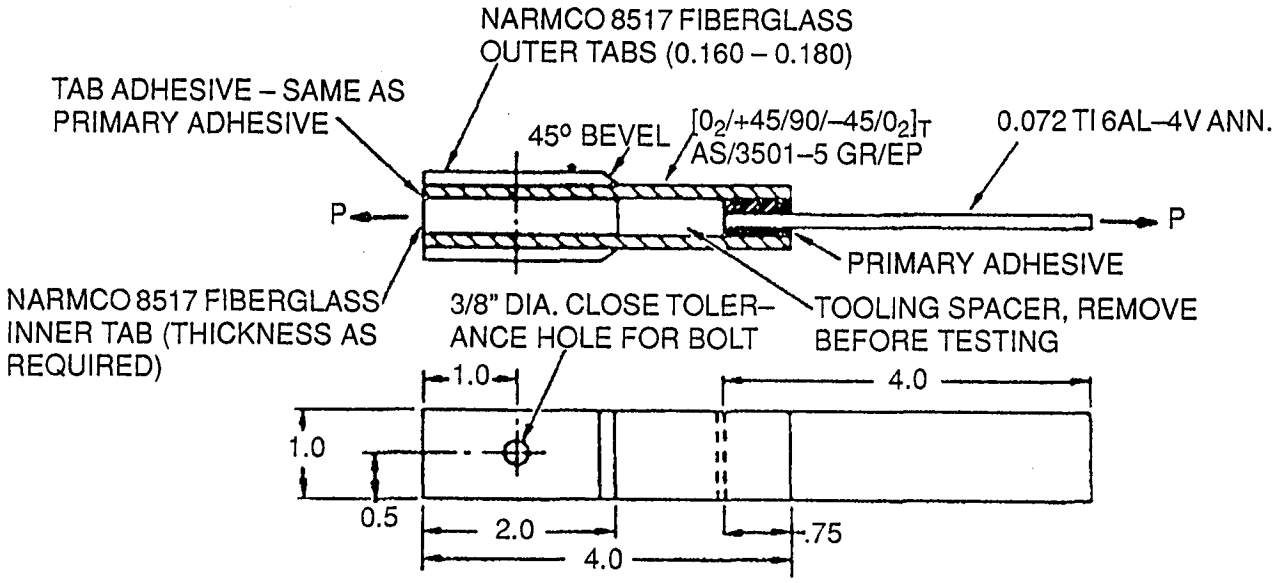

Ref. 3: Jeans, L.L., Grimes, G. C., and Kan, H. P., "Fatigue Spectrum Sensitivity Study of Advanced Composite Materials", Vols. I,II, and III, AFWAL–TR–80–3130, Dec. 1980.

ADHESIVES EVALUATION DATA

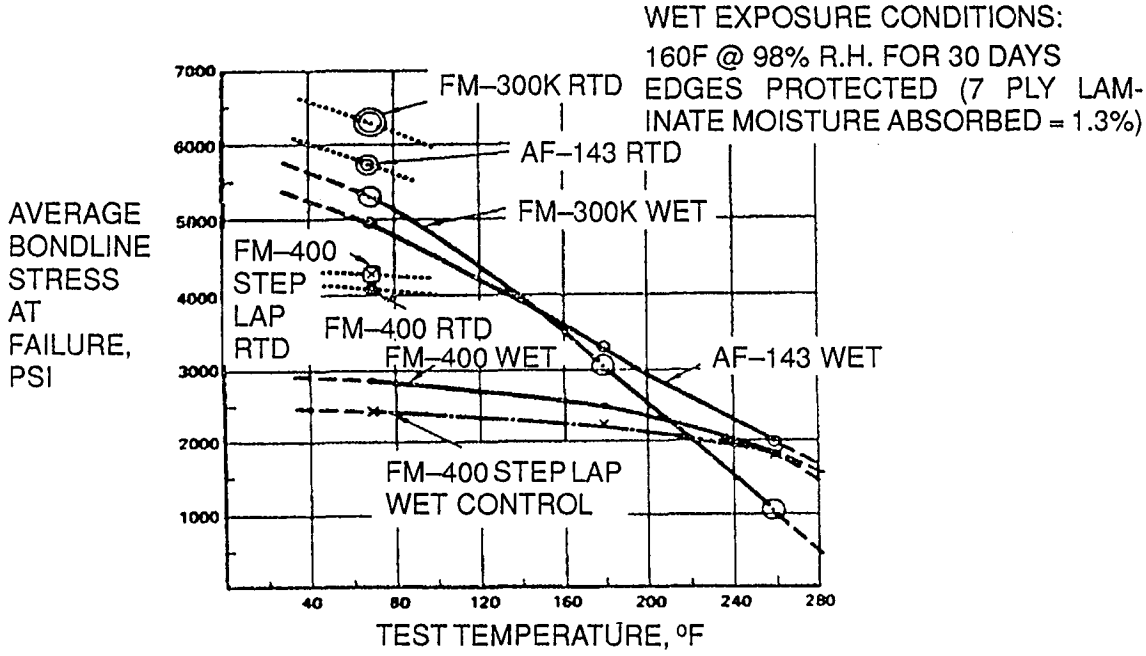

Ref. 3: Jeans, L.L., Grimes, G. C., and Kan, H. P., "Fatigue Spectrum Sensitivity Study of Advanced Composite Materials", Vols. I,II, and III, AFWAL–TR–80–3130, Dec. 1980.

STANDARD SIZE BONDED JOINT SPECIMEN

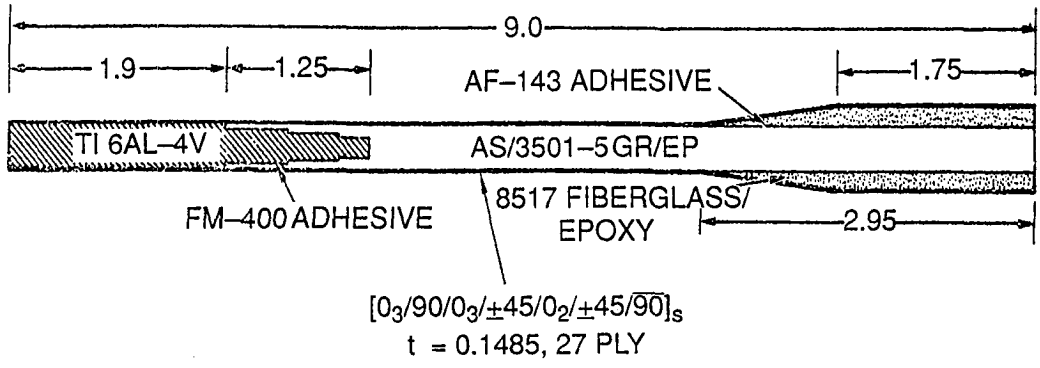

SPECIMEN 1 INCH WIDE

Ref. 3: Jeans, L.L., Grimes, G. C., and Kan, H. P., "Fatigue Spectrum Sensitivity Study of Advanced Composite Materials", Vols. I,II, and III, AFWAL–TR–80–3130, Dec. 1980.

LARGE SIZE BONDED JOINT SPECIMEN

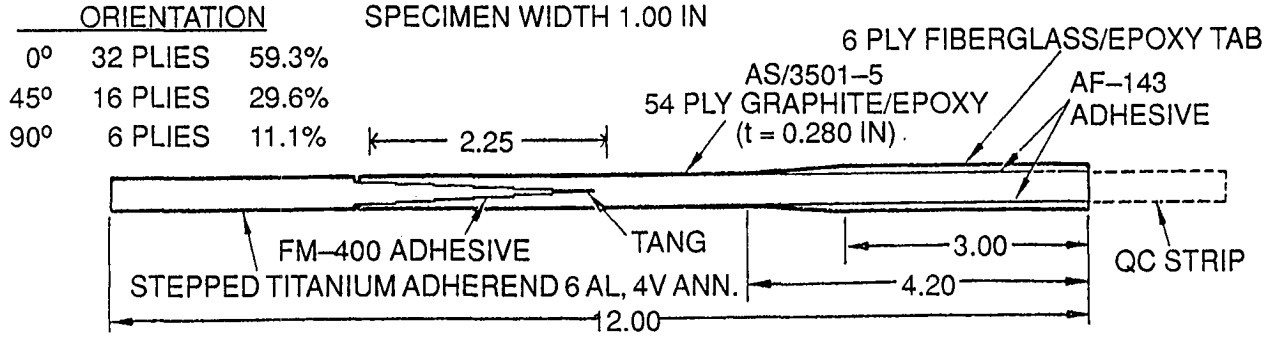

Ref. 3: Jeans, L.L., Grimes, G. C., and Kan, H. P., "Fatigue Spectrum Sensitivity Study of Advanced Composite Materials", Vols. I,II, and III, AFWAL–TR–80–3130, Dec. 1980.

STATIC TENSION LOADED

STANDARD AND LARGE SIZE BONDED JOINTS** – RTW

$V_L/V_S = 3.387,\ V_S/V_L = 0.295$

Test Series	No. of Specimens	Test Volume, in^3	Static Strength* Weibull Parameters	Static Strength Scale Factor $\hat{\beta}_L/\hat{\beta}_S$
STD–60–ST	20	0.186	$\hat{\alpha}_S^* = 19.83$ $\hat{\beta}_S^* = 7088$ lbs/in $(\hat{\beta}_S^*)_{BL} = 2835$ psi $(\hat{\beta}_S^*)_{LAM} = 47,731$ psi	Est. 0.93 Act. 1.39 } Bondline
LS–76–ST	7	0.630	$\hat{\alpha}_S^* = 15.47$ $\hat{\beta}_S^* = 17,705$ lbs/in $(\hat{\beta}_S^*)_{BL} = 3934$ psi $(\hat{\beta}_S^*)_{LAM} = 63,232$ psi	Est. 0.93 Act. 1.32 } Laminate

** Ref. 3

TENSION DOMINATED FATIGUE LOADED

STANDARD AND LARGE SIZE BONDED JOINTS* – RTW

$V_L/V_S = 3.387,\ V_S/V_L = 0.295$

Test Series	No. of Specimens Total/Survived	Test Volume, in^3	Fatigue Spectrum Maximum Loading (2 Lifetimes–Baseline)	Static Residual Strength & (Lifetime) Weibull Parameters	Fatigue (Lifetime) Scale Factor $\hat{\beta}_L/\hat{\beta}_S$
STD–107–1–FT	20/11	0.186	$N_X^t = 5000$ lbs/in $f_{BL}^s = 2000$ psi $f_{LAM}^t = 33,670$ psi	$\hat{\alpha}_F = 5.57(3.04)$ $\hat{\beta}_F = 7051$ lbs/in (2.37) $(\hat{\beta}_F)_{BL} = 2820$ psi (2.37) $(\hat{\beta}_F)_{LAM} = 47,482$ psi (2.37)	Est. (0.71) Act. (0.60) } Bondline
LS–76–FT	3/0	0.630	$N_X^t = 12,300$ lbs/in $f_{BL}^s = 2733$ psi $f_{LAM}^t = 43,928$ psi	$\hat{\alpha}_F = —(3.92)$ $\hat{\beta}_F = —(1.42)$ $(\hat{\beta}_F)_{BL} = —(1.42)$ $(\hat{\beta}_F)_{LAM} = —(1.42)$	Est. (0.71) Act. (0.60) } Laminate

* Ref. 3

STATIC COMPRESSION LOADED

STANDARD AND LARGE SIZE BONDED JOINTS* – RTW

$V_L/V_S = 3.387,\ V_S/V_L = 0.295$

Test Series	No. of Specimens	Test Volume, in^3	Static Strength* Weibull Parameters	Static Strength Scale Factor $\hat{\beta}_L/\hat{\beta}_S$
STD–61–SC	20	0.186	$\hat{\alpha}_S^* = 14.97$ $\hat{\beta}_S^* = -9797$ lbs/in $(\hat{\beta}_S^*)_{BL} = 3919$ psi $(\hat{\beta}_S^*)_{LAM} = -65,973$ psi	Est. 0.922 Act. 1.337 } Bondline
LS–76–SC	3	0.630	$\hat{\alpha}_S^* =$ — [1] $\hat{\beta}_S^* = -23,578$ lbs/in [1] $(\hat{\beta}_S^*)_{BL} = 5240$ psi [1] $(\hat{\beta}_S^*)_{LAM} = -84,207$ psi	Est. 0.922 Act. 1.276 } Laminate

[1] Assumed Equal to Mean Value
* Ref 3

COMPRESSION DOMINATED FATIGUE LOADED

STANDARD AND LARGE SIZE BONDED JOINTS** – RTW

$V_L/V_S = 3.387,\ V_S/V_L = 0.295$

Test Series	No. of Specimens Total/Survived	Test Volume, in^3	Fatigue Spectrum Maximum Loading (2 Lifetimes–Baseline)	Static Residual Strength* & (Lifetime) Weibull Parameters	Fatigue Residual Str. Scale Factor $\hat{\beta}_L/\hat{\beta}_S$
STD–112–FC	20/15	0.186	$N_x^c = -5850$ lbs/in $f_{BL}^s = 2340$ psi $f_{LAM}^c = -39,394$ psi	$\hat{\alpha}_S^* = 6.25(1.42)$ $\hat{\beta}_S^* = -8433$ lbs/in (4.70) $(\hat{\beta}_S^*)_{BL} = 3373$ psi (4.70) $(\hat{\beta}_S^*)_{LAM} = -56,788$ psi (4.70)	Est. 0.82 Act. 1.54 } Bondline
LS–76–FC	3/3	0.630	$N_x^c = -12,300$ lbs/in $f_{BL}^s = 2733$ psi $f_{LAM}^c = -43,929$ psi	$\hat{\alpha}_S^* =$ — $\hat{\beta}_S^* = -23,329$ lbs/in $(\hat{\beta}_S^*)_{BL} = 5184$ psi $(\hat{\beta}_S^*)_{LAM} = -83,318$ psi	Est. 0.82 Act. 1.47 } Laminate

** Ref. 3

STANDARD SIZE BOLTED JOINT SPECIMEN

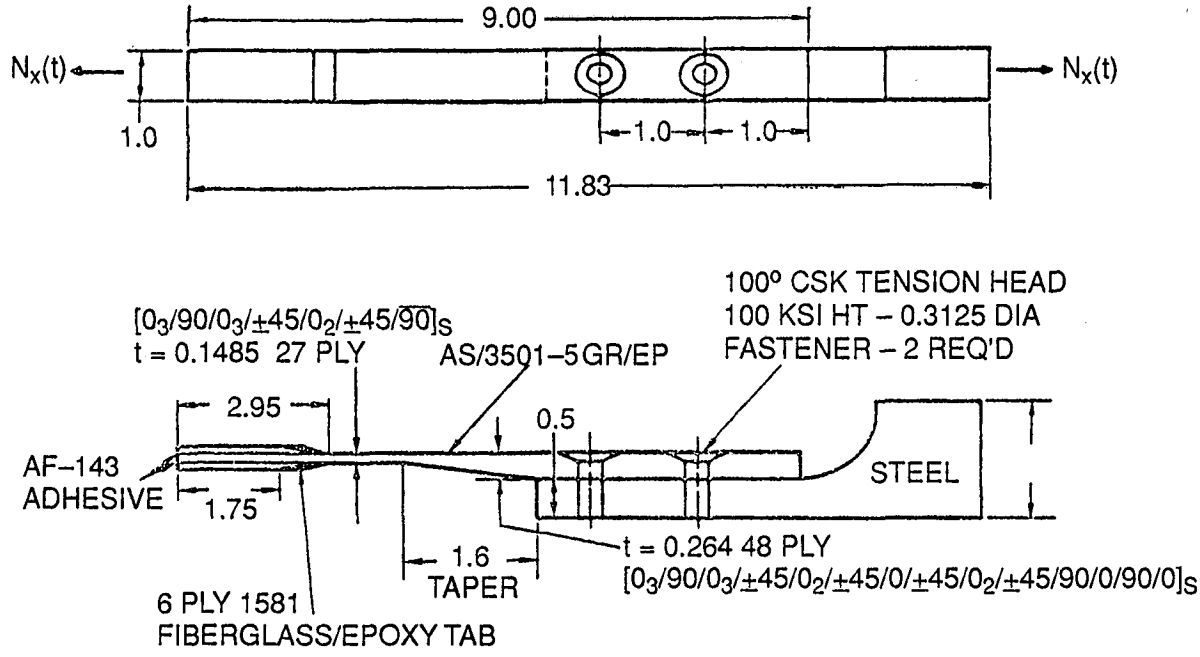

Ref. 3: Jeans, L.L., Grimes, G. C., and Kan, H. P., "Fatigue Spectrum Sensitivity Study of Advanced Composite Materials", Vols. I,II, and III, AFWAL–TR–80–3130, Dec. 1980.

LARGE SIZE BOLTED JOINT SPECIMEN

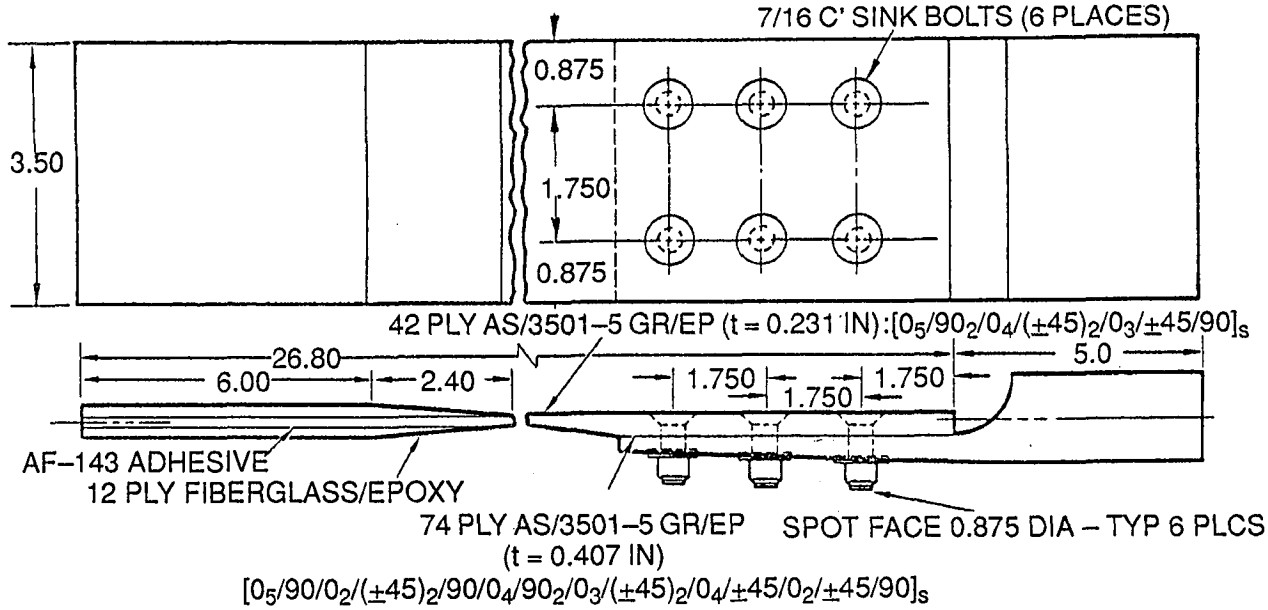

Ref. 3: Jeans, L.L., Grimes, G. C., and Kan, H. P., "Fatigue Spectrum Sensitivity Study of Advanced Composite Materials", Vols. I,II, and III, AFWAL–TR–80–3130, Dec. 1980.

STATIC TENSION LOADED

STANDARD AND LARGE SIZE BOLTED JOINTS**– RTW

$V_L/V_S = 6.493,\ V_S/V_L = 0.154$

Test Series	No. of Specimens	Test Volume, in^3	Static Strength* Weibull Parameters	Static Strength Scale Factor $\hat{\beta}_L/\hat{\beta}_S$
STD–62–ST	22	2.694	$\hat{\alpha}_S^* = 13.39$ $\hat{\beta}_S^* = 12,047$ lbs/in $(\hat{\beta}_S^*)_{BRG} = 129,817$ psi $(\hat{\beta}_S^*)_{NT} = 66,375$ psi $(\hat{\beta}_S^*)_{LAM} = 81,125$ psi	Est. 0.941 Act. 0.874 } Net Tension (Thru–Bolt Holes) Est. 0.941 Act. 0.521 } Bearing
LS–72–ST	7	17.492	$\hat{\alpha}_S^* = 48.16$ $\hat{\beta}_S^* = 20,651$ lbs/in $(\hat{\beta}_S^*)_{BRG} = 67,658$ psi $(\hat{\beta}_S^*)_{NT} = 57,987$ psi $(\hat{\beta}_S^*)_{LAM} = 89,398$ psi	Est. 0.941 Act. 1.102 } Laminate Tension (Away From Joint)

** Ref. 3

TENSION DOMINATED FATIGUE LOADED (COMPARISON #1)

STANDARD AND LARGE SIZE(1) BOLTED JOINTS**– RTW

Test Series	No. of Specimens	Test Volume, in^3	Fatigue Spectrum Maximum Loading (2 Lifetimes–Baseline)	Static Residual Strength* Weibull Parameters	Fatigue Residual Strength Scale Factor $\hat{\beta}_L/\hat{\beta}_S$
STD–115–FT	20	2.694	$N_X^t = 6500$ lbs/in $f_{BRG}^t = 70,043$ psi $f_{NT}^t = 35,813$ psi $f_{LAM}^t = 43,771$ psi	$\hat{\alpha}_S^* = 16.10$ $\hat{\beta}_S^* = 12,168$ lbs/in $(\hat{\beta}_S^*)_{BRG} = 131,121$ psi $(\hat{\beta}_S^*)_{NT} = 67,041$ psi $(\hat{\beta}_S^*)_{LAM} = 81,939$ psi	Est. 0.939 Act. 1.018 } Net Tension (Thru–Bolt Holes)
LS–72–F1T	7	17.492	$N_X^t = 7571$ lbs/in $f_{BRG}^t = 24,804$ psi $f_{NT}^t = 24,802$ psi $f_{LAM}^t = 32,775$ psi	$\hat{\alpha}_S^* = 43.36$ $\hat{\beta}_S^* = 20,835$ lbs/in $(\hat{\beta}_S^*)_{BRG} = 68,268$ psi $(\hat{\beta}_S^*)_{NT} = 68,254$ psi $(\hat{\beta}_S^*)_{LAM} = 90,195$ psi	Est. 0.939 Act. 0.521 } Bearing Est. 0.939 Act. 1.101 } Laminate Tension (Away from Joint)

** Ref. 3

Note 1: $V_L/V_S = 6.493,\ V_S/V_L = 0.154$

TENSION DOMINATED FATIGUE LOADED (COMPARISON #2)

STANDARD AND LARGE SIZE(2) BOLTED JOINTS** – RTW

Test Series	No. of Specimens	Test Volume, in^3	Fatigue Spectrum Maximum Loading (2 Lifetimes – Baseline)	Static Residual Strength* & (Lifetime) Weibull Parameters	Fatigue Residual Str. Scale Factor $\hat{\beta}_L/\hat{\beta}_S$
STD–115–FT	20	2.694	N^t_X = 6500 lbs/in f^t_{BRG} = 70,043 psi f^t_{NT} = 35,813 psi f^t_{LAM} = 43,771 psi	$\hat{\alpha}_{\beta^*_S}$ = 16.10 $\hat{\beta}_{\beta^*_S}$ = 12,168 lbs/in $(\hat{\beta}_{\beta^*_S})_{BRG}$ = 131,121psi $(\hat{\beta}_{\beta^*_S})_{NT}$ = 67,041 psi $(\hat{\beta}_{\beta^*_S})_{LAM}$ = 81,939 psi	Est. 0.890 Act. 1.009 } NT
LS–72–F2T	3	17.492	N^t_X = 7571lbs/in ($1/2$ LT) = 13,286lbs/in ($1\,1/2$ LT) f^t_{BRG} = 24,804psi($1/2$ LT) = 43,528psi ($1\,1/2$ LT) f^t_{NT} = 24,802psi ($1/2$ LT) = 43,524psi ($1\,1/2$ LT) f^t_{LAM} = 32,775psi ($1/2$ LT) = 57,515psi ($1\,1/2$ LT)	$\hat{\alpha}_{\beta^*_S}$ = — $\hat{\beta}_{\beta^*_S} \approx$ 20,645 lbs/in (mean) $(\hat{\beta}_{\beta^*_S})_{BRG} \approx$ 67,638 psi (mean) $(\hat{\beta}_{\beta^*_S})_{NT} \approx$ 67,632 psi (mean) $(\hat{\beta}_{\beta^*_S})_{LAM} \approx$ 89,372 psi (mean)	Est. 0.890 Act. 0.516 } BRG Est. 0.890 Act. 1.091 } LAM TEN.

** Ref. 3

Note 1: $V_L/V_S = 6.493$, $V_S/V_L = 0.154$

SUMMARY OF BONDED JOINT SCALE FACTORS

$V_L/V_S = 3.387,\ V_S/V_L = 0.295$

Loading Mode	Bondline Strength		Bondline Fatigue Lifetime	
	Estimated $\frac{\beta_L}{\beta_S}$	Actual $\frac{\beta_L}{\beta_S}$	Estimated $\frac{(LT)_L}{(LT)_S}$	Actual $\frac{(LT)_L}{(LT)_S}$
Static Tension–Strength	0.93	1.39	—	—
Tension Dom. Fatigue–Lifetimes	—	—	0.71	0.60
Static Compression–Strength	0.92	1.34	—	—
Compression Dom. Fatigue–Residual Strength	0.82	1.54	—	—

SUMMARY OF BOLTED JOINT SCALE FACTORS

Loading Mode	Net Tension* (Thru The Bolt Holes)	
	Estimated $\frac{\beta_L}{\beta_S}$	Actual $\frac{\beta_L}{\beta_S}$
Static Tension–Strength	0.941	0.874
Tension Dom. Fatigue(#1)–Residual Strength	0.939	1.018
Tension Dom. Fatigue(#2)–Residual Strength	0.890	1.009

*strength

NORMALIZED STRENGTH VERSUS SPECIMEN SIZE FOR LAMINATES B & D LOADED IN TENSION

LAMINATE B – Q I – Fiber Dominated
LAMINATE D – Angle Ply – Matrix Dominated

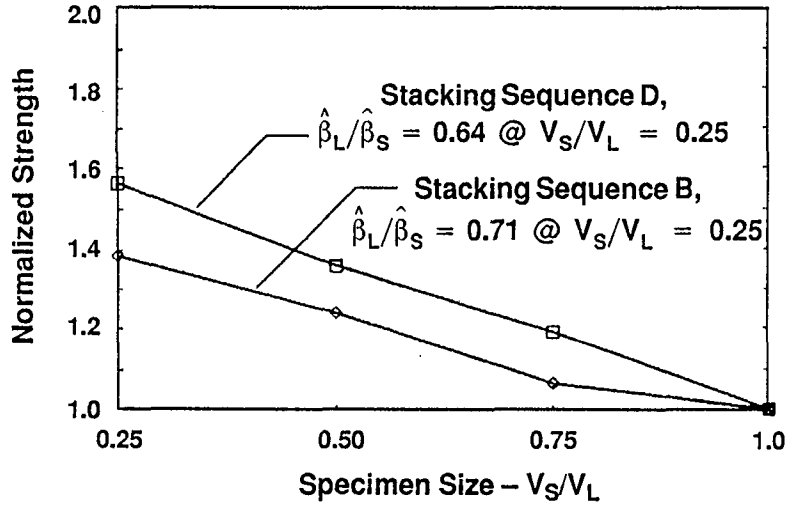

Ref. 4: Jackson, K. E., Kellas, S., Morton, J., "Scale Effects in the Response and Failure of Fiber Reinforced Composite Laminates Loaded in Tension and Flexure", JOCM, Vol. 26, No. 18, 1992.

CAUSE OF SCALE EFFECTS

- MATERIALS QUALITY
  - Large Variation in Fiber Areal Weight
  - Large Variation in Resin Content
  - Material Received with High Moisture Content
  - Low Fiber Strength
  - ⊖ Changes in Resin Formulation without Notifying User
- PROCESSING QUALITY
  - ⊖ Improper Storage and Inaccurate Out–Time Records
  - ⊖ Overage Prepreg in Storage
  - ⊖ Layup in High Humidity Areas
  - Rate of Heat–Up During Cure is Too Slow
  - Recommended or Best Cure Cycle Not Used
  - ⊖ Vacuum/Pressure Bag Breaks Before Cure is Complete
  - ⊖ Improper Use of, or Using the Wrong Kind of, Peel Plies

CAUSE OF SCALE EFFECTS(CONT.)

- POSSIBLE SIZE EFFECTS

  ⊖ • Poor Quality Tooling

  ⊖ • Autoclaves and Presses with Poor Temperature/ Pressure Controls

  • Multiple Load Paths that are not Considered in Design

  ⊖ • Lack of a Building Block Development Test Effort for Experimental Characterization

  ⊖ • Differences in Environmental Exposure and Effects

  • Differences in Structural Efficiency*

  • Thermal Stresses

*See Ref. 5

⊖ These are most likely to occur

SUMMARY AND CONCLUSIONS

- SUMMARY
  - Except for Jackson in Ref. 4, the Largest Solid Laminate Scale Effects Observed were –8% Based on Strength.
  - In Bonded Joints the Largest Scale Effects Observed were +54% Based on Strength and –40% Based on Lifetimes.
  - In Bolted Joints the Largest Scale Effects Observed were –13% and +2%.
- CONCLUSIONS
  - Most Strength Reduction Scale Effects Observed in Composites and Bonded Joints are Related to Quality Variations, Although, Differences in Environmental Exposure and its Effects may Affect Some Results. More Efficient* Large Joints had an Effect.
  - The Effects of Moisture on Bonded Joint Fatigue Lifetimes Show Definite Lifetime Reduction Scale Effects.
  - Significant Strength Reduction Scale Effects were not Observed in Bolted Joints.

* See Ref. 5

SUMMARY AND CONCLUSIONS(CONT.)

- CONCLUSIONS(CONT.)
  - Significant Strength Increase* Scale Effects are Observed on Static Tension and Compression and Compression Dominated Fatigue RTW Bonded Joints.
  - Strength Reduction Scale Effects Can Occur When:
    - Large, Multiple Material Parts Have High Manufacturing Induced Thermal Stresses.
    - Large Bonded Joints are Moisture Sensitive.
    - Large, Complicated, Multiple Load Path Parts have not had Adequate Building Block Test Development or FEM Analysis.
    - Large(Full) Size Structural Prototyping is Done Quickly in the Development Cycle Without Adequate M&P and Structural Building Block Test Development.
  - The Equation from References 1 and 2 Does Work When Scale Effects Occur.
  - The Specimen Data Analyzed from References 1 and 3 had the Benefit of Consistent High Quality.

* See Ref. 5

LIST OF REFERENCES

1. Verette, R. M. and Labor, J. D., "Structural Criteria for Advanced Composites", AFFDL–TR–76–142, Vol. I, Final Report, March 1977.
2. Halpin, J. C., Jerina, K. L. and Johnson, T. A., "Characterization of Compoistes for the Purpose of Reliability Evaluation", in Analysis of Test Methods for High Modulus Fibers and Composites, ASTM STP521, ASTM, 1973, pp. 5–64, J. M. Whitney, Editor.
3. Jeans, L. L., Grimes, G. C. and Kan, H. P., "Fatigue Spectrum Sensitivity Study of Advanced Composite Materials", Volumes I, II, and III, AFWAL–TR–80–3130, December 1980.
4. Jackson, D. E., Kellas, S. and Morton, J., "Scale Effects in the Response and Failure of Fiber Reinforced Composite Laminates Loaded in Tension and Flexure", Journal of Composite Materials, Volume 26, No. 18, 1992.
5. Grimes, G. C., Ranger, K. W. and Brunner, M. D., "Element and Subcomponent Tests," Composites – Volume 1 of Engineered Materials Handbook, Technical Chairman, T. J. Reinhart, ASM, International, 1987, pp. 328–344.

MATERIAL PROPERTIES, FAILURE AND DAMAGE MECHANICS

Session I

John Morton, Moderator

The Effects of Specimen Scale on the Compression Strength of Composite Materials

Gene Camponeschi
Composite Materials Program Office

CARDEROCKDIV, NSWC
Formerly, DTRC

Abstract

This paper presents a number of observations on the effect of specimen scale on the compression response of composite materials. Work on this topic was motivated by observations that thick-walled, unstiffened carbon reinforced cylinders subjected to hydrostatic pressure were not reaching inplane laminate stress levels at failure expected from coupon level properties, while similar cylinders reinforced with fiberglass were. Results from a study on coupon strength of [0/0/90] laminates, reinforced with AS4 carbon fiber and S2 glass fiber are presented, and show that compression strength is not a function of material or specimen thickness for materials that have the same laminate quality (autoclave cured quality.) Actual laminate compression strength was observed to decrease with increasing thickness, but this is attributed to fixture restraint effects on coupon response.

The hypothesis drawn from the coupon level results is further supported by results from a compression test on a thick carbon reinforced coupon in a fixture with reduced influence on specimen response, and from a hydrostatic test on an unstiffened carbon reinforced cylinder subjected to hydrostatic pressure with end closures designed to minimize their effect on cylinder response.

Compression Response of Composite Coupons and Cylinders

CARDEROCKDIV NSWC

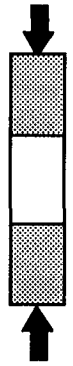

[0/0/90]

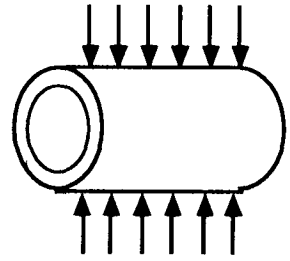

[0/0/90]

	Strength	Strength
Carbon	150 ksi	80 - 120 ksi ?
Glass	120 ksi	100 - 130 ksi √

The focus of the work to be discussed was to address the issue of translating material properties from the coupon level to the structural element level. Small scale hydrostatic collapse tests on composite cylinders have not reached pressures expected from coupon level test on [0/0/90]carbon reinforced composite laminates, but have reached expected levels for fiberglass reinforced materials.

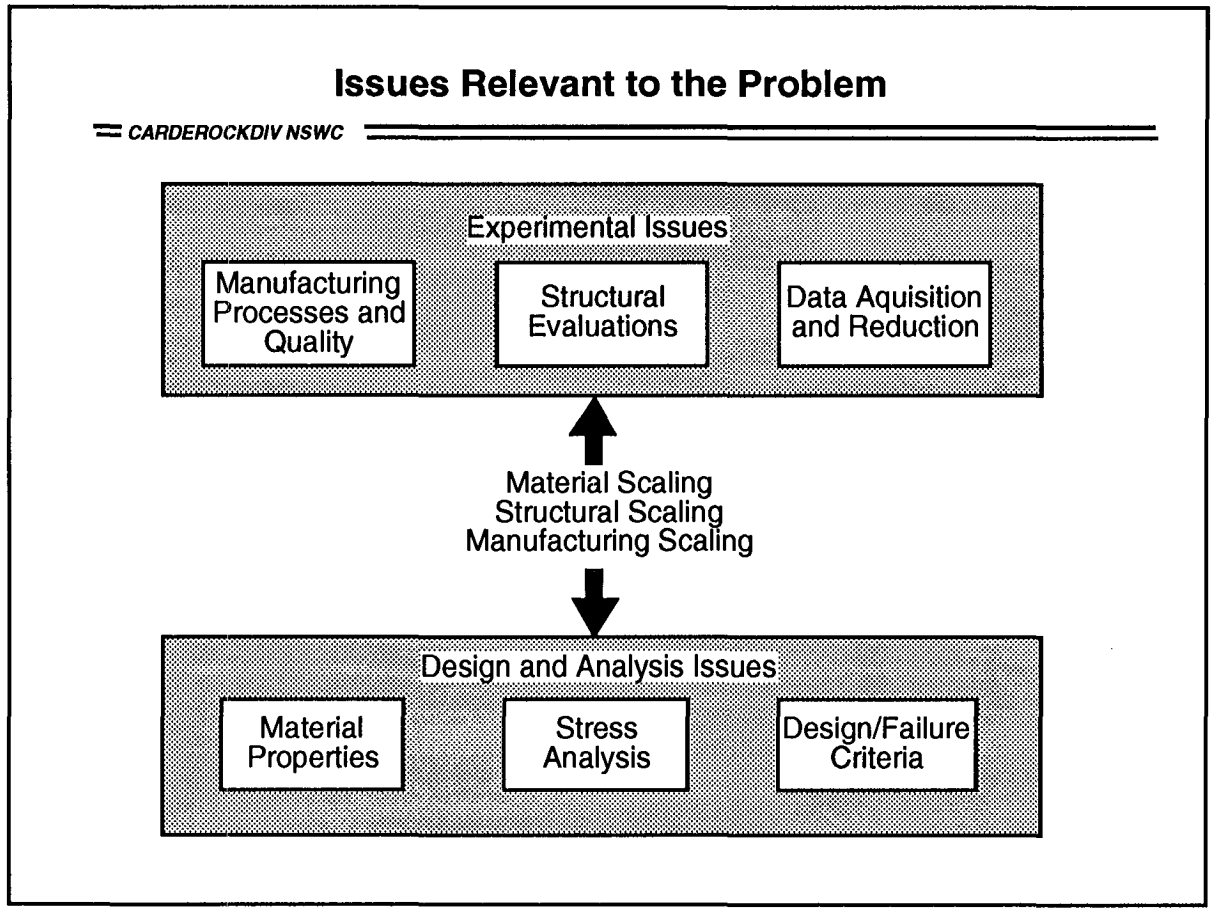

Many factors can influence the translation of material properties to structural response, and in this work specific focus is on the issue of material property scaling. Do strength and stiffness properties of composites change when going from small scale coupons to structural test components.

Objective

CARDEROCKDIV NSWC

Determine the 3-D elastic constants, strength, and failure mechanisms for thick-section composite materials

Are theories for the prediction of 3-D laminate properties accurate?

Are existing failure theories applicable to thick composites?

AS4/3501-6 **S2 glass/3501-6**

$[0]_{48}$ $[0]_{96}$ $[0]_{192}$

$[0_2/90]_{8s}$ $[0_2/90]_{16s}$ $[0_2/90]_{32s}$

The specific objectives of the research are outlined above. Two material systems, in two laminate configurations, and in three thicknesses were tested. Both material systems were 0.005 mil, 12 inch wide prepreg tape, autoclave cured in flat panels for coupon preparation. The 48 ply laminates were nominally 0.25 inches thick, the 96 ply were nominally 0.5 inches thick, and the 192 ply were nominally 1.0 inches thick. All panels were cured in one step, with a cure cycle designed to avoid any temperature excursions or exotherm during the cure. All panels were C-scanned after fabrication, found to be of high-quality, and destructive tests showed FVF of ~ 60% and void contents of 0-1%.

Thick-Section Compression Test Fixture

CARDEROCKDIV NSWC

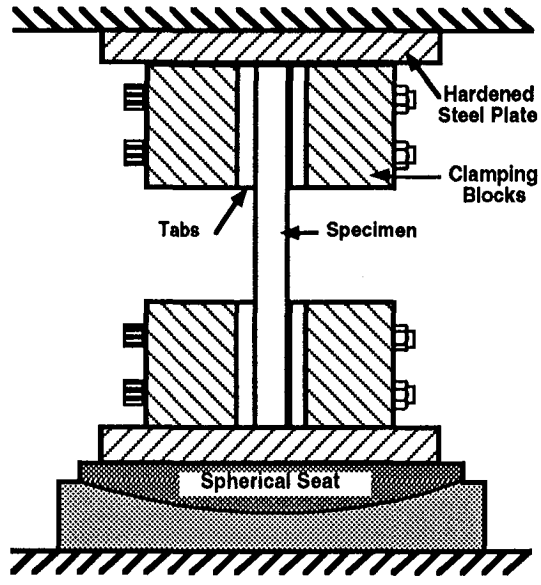

A uniaxial compression test fixture was designed to be scalable to the three specimen geometries of concern, and transferred load into the specimen through end-loading. Tabs of the same material as the specimen were bonded to the specimens, and specimen ends, width, and tab surfaces were machined flat, parallel and perpendicular within 0.001 inches.

Compression Modulus as a Function of Thickness

CARDEROCKDIV NSWC

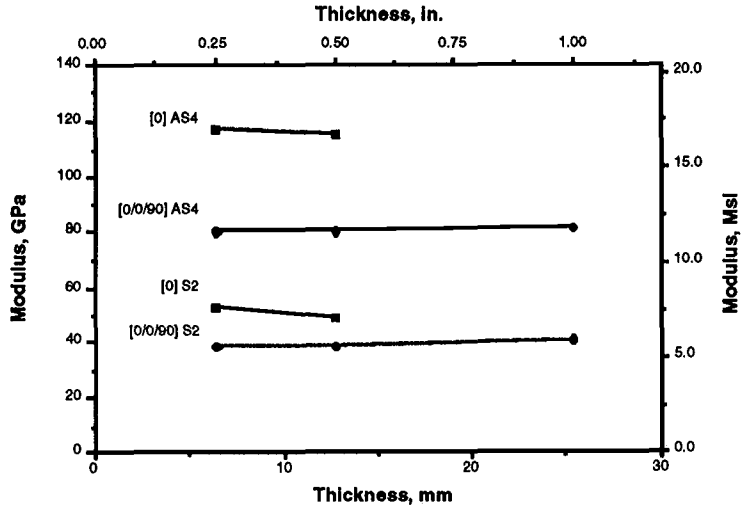

Inplane, longitudinal compression modulus of the two laminates and two materials tested were found to be insensitive to specimen thickness. Likewise, inplane an through-thickness Poisson's ratios were found to be insensitive to specimen thickness. Through-thickness Poisson's ratios were also found to be very nonlinear elastic.

Compression Strength as a Function of Thickness

CARDEROCKDIV NSWC

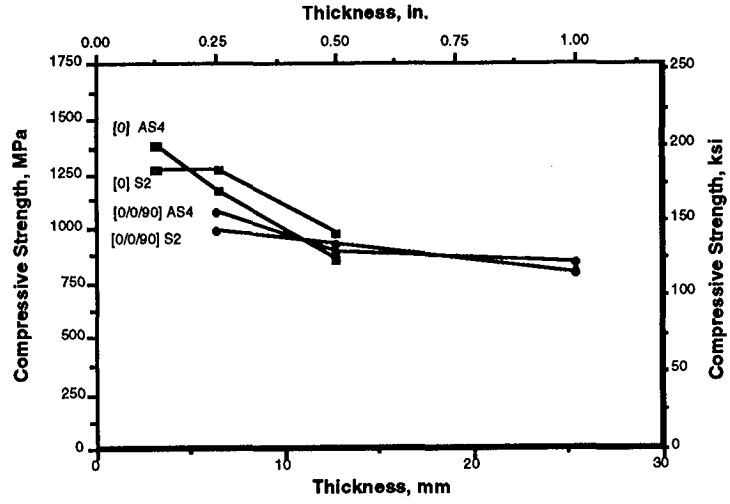

Unlike the elastic constants, inplane, longitudinal compression strength was found to decrease with increasing specimen thickness. The [0] strength results were not considered acceptable since all failures occurred at the specimen ends at the location of load introduction. The [0/0/90] laminate strengths were considered acceptable, and a drop in strength of 20% was seen between the 0.25 inch and 1.0 inch laminates for both materials.

Location of [0/0/90] Laminate Failures

CARDEROCKDIV NSWC

Location of gage section / tab termination region failures

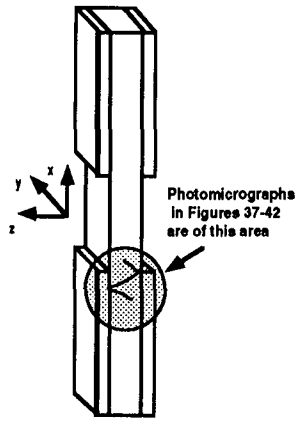

Although all of the thick-section[0/0/90] laminate compression failures were within the specimen gage section, they initiated at the tab/gage-section transition point, where the tabs and block compression fixture terminated. Since this is a region of stress concentration and geometric transition, an analysis to investigate the effect of these factors was conducted. The focus of this investigation was to determine the extent of the influence of the geometry/stress concentration effects on compression strength, with increasing specimen thickness.

Determine Δz in Terms of Specimen/Fixture Combination

CARDEROCKDIV NSWC

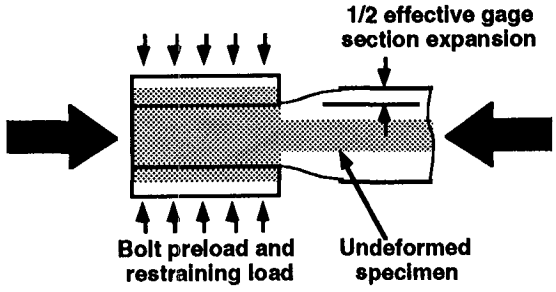

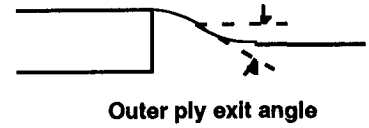

Free gage section expansion

+ preload contraction

- specimen expansion within clamps

This graphic depicts the geometry of the outer laminate plies in the region of transition between the tabs and the gage-section. Poisson expansion takes place in the unsupported gage-section, and this expansion is restrained within the block portion of the test fixture due to the fixture clamping bolts. The outer ply geometry results in fibers that are misaligned with respect to the principal loading axis of the specimen, that could effectively reduce the compression strength of the specimen. The through-thickness expansion that occurred in the gage-section increased with increasing specimen thickness; therefore, an analysis was performed that included this effect in the determination of compression strength.

Kink Band Failure Theories Accounting For Fiber Misalignment

CARDEROCKDIV NSWC

$$\sigma_{ult} = K_t \frac{k}{\phi_o}$$ Argon, 1972

$$\sigma_{ult} = K_t \left[\frac{\gamma_y}{\phi_o + \gamma_y}\right] G$$ Budiansky, 1983

ϕ_o = waviness and expansion

G = 0.6 initial G

K_t = 2.0 and 1.2

k = 11,000 psi

γ_y =2.0 %

Two kink band based compression failure criteria were used in the evaluation of the effect of fixture effects on the failure of the thick-section composites. Both criteria include the effect of fiber misalignment on compression strength. For the purposes of this work, the misalignment term in each equation was defined to include initial fiber waviness and misalignment due to the through-thickness Poisson's expansion. The initial fiber waviness was determined optically on the actual laminates used in this study and was found to be independent of laminate thickness.

Summary of Compression Strength Analysis

CARDEROCKDIV NSWC

- **Determine effective gage section expansion**
  SOM solution for fixture and clamping effect
- **Determine outer ply geometry**
  FEA with effective expansion as uniform displacement BC
- **Determine effect of fiber misalignment on composite strength**
  Argon and Budiansky solutions

A three part solution was used in the compression strength analysis. The first part was used to determine the gage-section free expansion due to Poisson's ratio compared to the expansion within the fixture clamping blocks. This information was then used to determine the boundary conditions for a finite element analysis used to determine outer ply geometry. The outer ply exit angle from the finite element analysis was then used in the closed form kink band failure criteria to determine compression strength as a function of specimen thickness.

Strength Versus Thickness, S2 Glass/Epoxy

CARDEROCKDIV NSWC

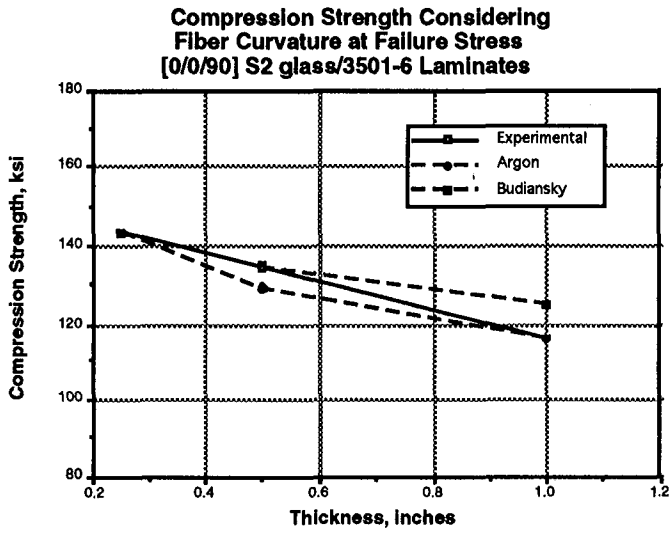

A plot of experimental and theoretical compression strength versus thickness for the S2/epoxy shows the 20% drop in strength observed experimentally is predicted theoretically.

Strength Versus Thickness, Carbon/Epoxy

CARDEROCKDIV NSWC

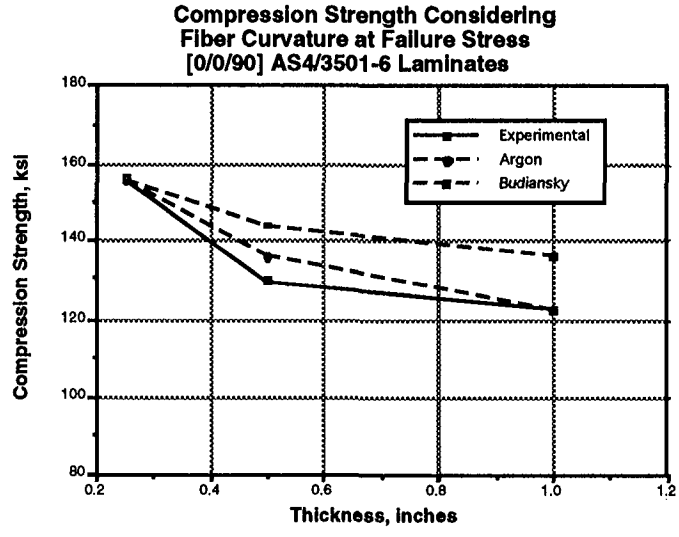

A plot of experimental and theoretical compression strength versus thickness for the carbon/epoxy shows the same pattern as the S2/epoxy results. These results indicate that the drop in compression strength observed experimentally can be attributed to fixture induced restraint effects. A failure theory that accounts for laminate expansion that occurs in the through-thickness direction and the observed laminate failure mechanism follow the experimental trends.

Sphere Joint and Specimen Cross-Section

CARDEROCKDIV NSWC

Sphere Joint Cross-Section

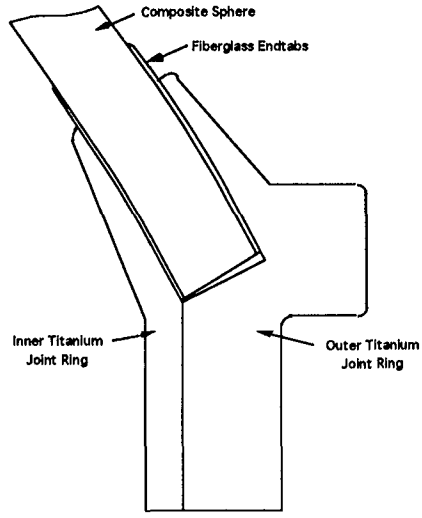

Test Specimen Cross-Section

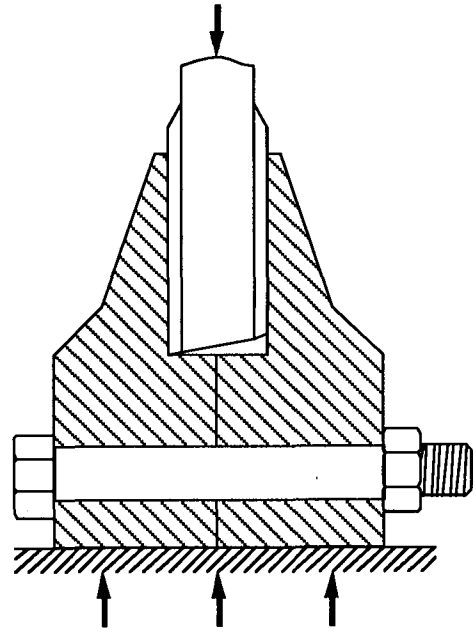

Following the work on uniaxial compression strength, an ARPA program looking at composites for a Man-Rated Demonstration Article (MRDA) was initiated. In this program a titanium-composite sphere joint was evaluated in uniaxial compression. The titanium fixture is similar to typical end-loading block compression fixtures, with the exception of the tapered cross section of the blocks. A 0.78 inch thick, 4 inch wide, 10 inch long, quasi-isotropic AS4/3501-6 test specimen was loaded to failure in this compression test fixture. The specimen failure occurred in the center of the gage section, at 89,000 psi and a strain of 13,000 micro inches/inch. This result is almost identical to results expected from 0.1 inch thick coupons for the same material in a D3410 Procedure B test method. This further demonstrates the claim that compressive properties are independent of thickness. In this test fixture stress concentration and fixture restraint effects are minimized due to the tapered titanium fixture cross-section.

Stress-Strain Results for Test to Failure

CARDEROCKDIV NSWC

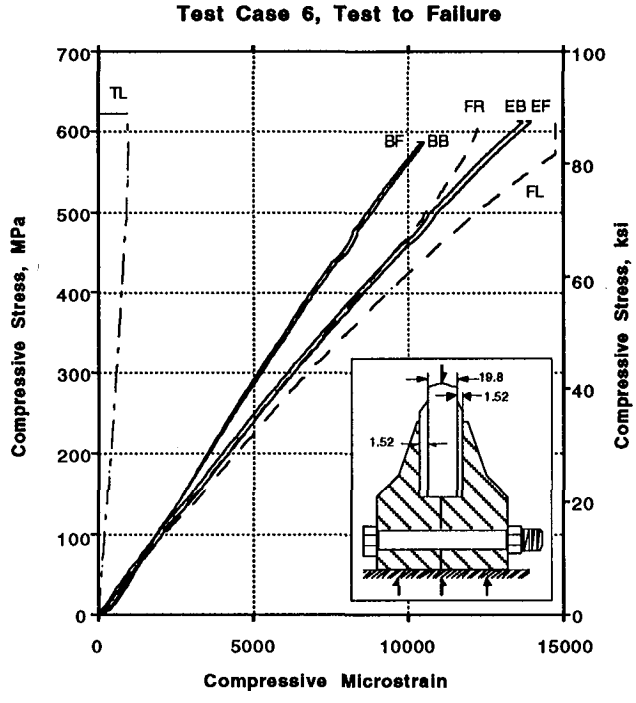

This slide shows a graph of the stress/strain response for the specimen described in the previous slide.

Oak Ridge National Labs Cylinder Tests

CARDEROCKDIV NSWC

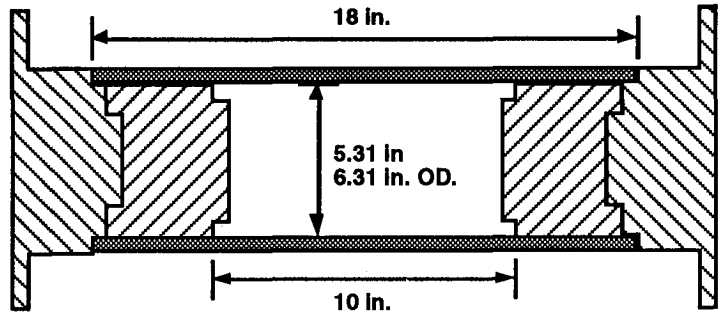

- IM6/ERL-2258 Carbon Epoxy (~1.4% voids)
- 2:1 hoop/longitudinal fiber ratio
- Linear taper, unique end plugs vs. constant radius, standard plugs
- Plug design to make full contact on taper at design collapse pressure
- Inner layer hoop stress at 20,000 psi 194 ksi (ply-level stress analysis)
- Cylinder unfailed at 20,000 psi, inner hoop strain ~ 9000 $\mu\varepsilon$

Blake and Starbuck, Hydrostatic Pressure Testing of Graphite/Epoxy Cylinder C6-1, ORNL/ATD-64, July 1992

This slide summarizes the results from a thick-section carbon/epoxy cylinder test conducted at the Oak Ridge National Lab. End closures specially designed to minimize stress concentration effects on the cylinder allowed this cylinder to perform at collapse pressures expected from typical thin section coupon compression strengths. This data again supports the notion that with adequate attention to joint and detail areas in small scale structures, composite material properties show no effect of scaling.

Material Scaling Issue for Composites?

CARDEROCKDIV NSWC

When material quality is consistent, scaling of uniaxial composite material properties is not an issue at the coupon level and above.

Material quality is a key qualifier in the above statement. For instance, in timber construction a specific set of guidelines are established for grading lumber, and design allowables are defined and used based on this grading system.

Based on the results presented in this report, uniaxial composite properties show no scale effects, provided the material quality at the large scale are the same as at the small scale.

Conclusions

CARDEROCKDIV NSWC

- **Elastic constants unchanged with thickness**
- **Failure mechanisms unchanged with thickness**
  - kink band failures predominate
  - kink band theories need development
- **Strength of autoclave cured AS4 and S2 Epoxy laminates unchanged with thickness**
- **Joint element and small scale structural tests have shown material properties are the same at other scales.**
- **Scaling issues are of concern for joints, details, and structural level designs and not materials for = quality**

Conclusions from the work presented in this report are clearly summarized in this slide.

BIBLIOGRAPHY

Camponeschi, E. T. J., Gillespie, J. W., Jr., and Wilkins, D. J., "Kink-Band Failure Analysis of Thick Composites in Compression," *Journal of Composite Materials*, 1993, 27(8).

Camponeschi, E. T., Jr., "Compression of Composite Materials: A Review", *Fatigue and Fracture of Composite Materials (Third Conference),* ASTM STP 1110, T.K. O'Brien, Ed., ASTM, 1991, pp. 550-580.

Camponeschi, E. T., Jr., "Compression Response of Thick-Section Composite Materials," DTRC Rep. No. SME-90-60, Nov., 1990.

Camponeschi, E. T., Jr., "Lamina Waviness Levels in Thick Composites and its Effect on Their Compression Strength," Proceedings of ICCM 8, 1991, Tsai and Springer, SAMPE.

Camponeschi, E. T., Jr., Bohlmann, R. E., Hall, J., and Carr, T. T., "Effect of Assembly Fit-Up Gaps on the Compression Response of Thick-Section Carbon/Epoxy Composites", *Compression Response of Composite Structures,* ASTM STP, ASTM, Accepted for Publication.

Blake, H. W. and Starbuck, J. M., "Hydrostatic Pressure Testing of Graphite/Epoxy Cylinder C6-1," Oak Ridge National Laboratory Rep. No. ORNL/ATD-64, July, 1992.

On Nature's Scaling Effects

Dick J. Wilkins, University of Delaware

Abstract

This presentation afforded the opportunity to look back in the literature to discover scaling effects in nature that might be relevant to composites. Numerous examples were found in nature's approaches to wood, teeth, horns, leaves, eggs, feathers, etc. Nature transmits tensile forces rigidly with cohesive bonds, while dealing with compression forces usually through non-compressible hydraulics. The optimum design scaling approaches for aircraft were also reviewed for comparison with similitude laws. Finally, some historical evidence for the use of Weibull scaling in composites was reviewed.

References included:

Morrison, Powers of Ten
Fuller, Critical Path
D'arcy Thompson, On Growth and Form
Dinwiddie, Wood
French, Invention and Evolution
Vogel, Life's Devices
Gordon, New Science of Strong Materials (and Structures)
Shanley, Weight-Strength Analysis of Aircraft Structures
Bullock, Eisenmann, Weibull, Statistical Scaling
Karbhari, Issues of Scale in Composites Fracture and Design

Morrison, Powers of Ten

- Familiar - 6 orders - 100m to .1mm
- Span - 10**25 to10**-16=10**42
- Atoms Don't Scale

Fuller, Critical Path

- Balanced Tensive & Compressive Forces
- Tensile - resists rigidly with 3 crystalline, max cohesive bonds
- Compressive - double-bonded, flexibly hinged, non-compressible hydraulics

D'arcy Thompson, On Growth and Form

- Forces: $S=f(l^2)$, $V=f(l^3)$, $W=f(kl^3)$
- Similitude
  - Table of Sizes
  - Froude's Law
- Applications
  - Teeth

D'arcy Thompson, On Growth and Form (cont.)

- Horns
- Leaves
- Eggs

Dinwiddie, Wood

- Structure

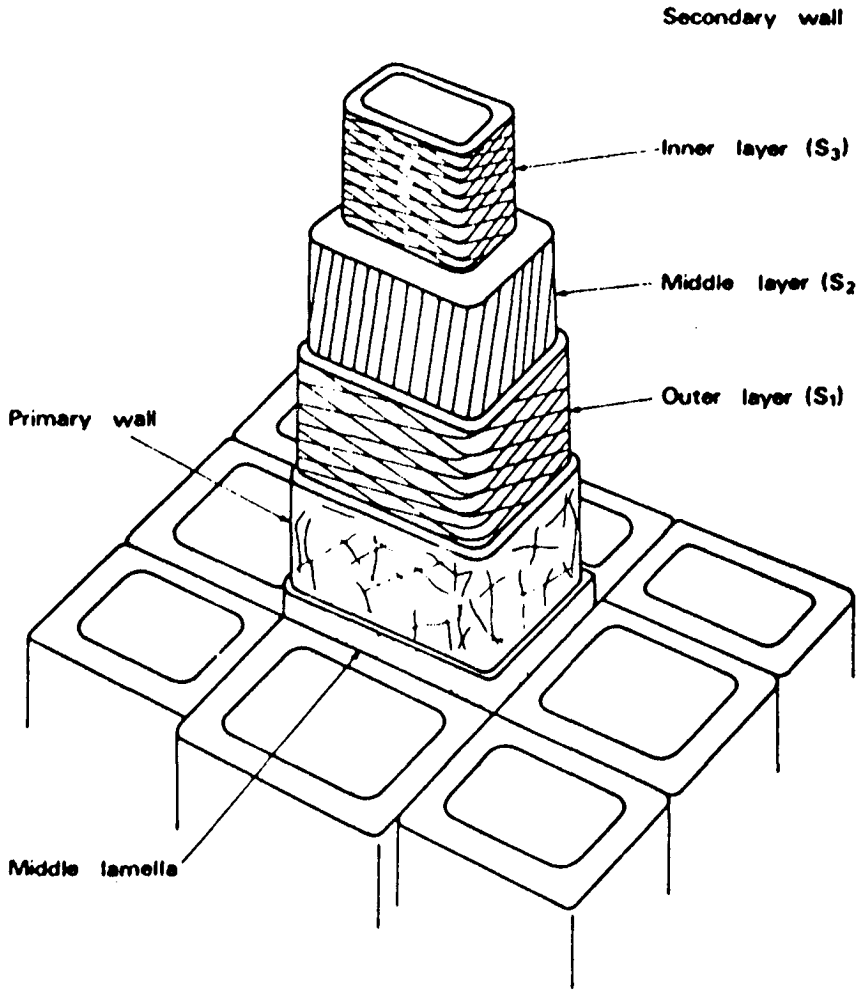

Simplified structure of the cell wall showing orientation of microfibrils in each of the major wall layers (BRE diagram: © Crown Copyright)

French, Invention and Evolution

- Self-Sustaining Lengths
- Structure of a Feather

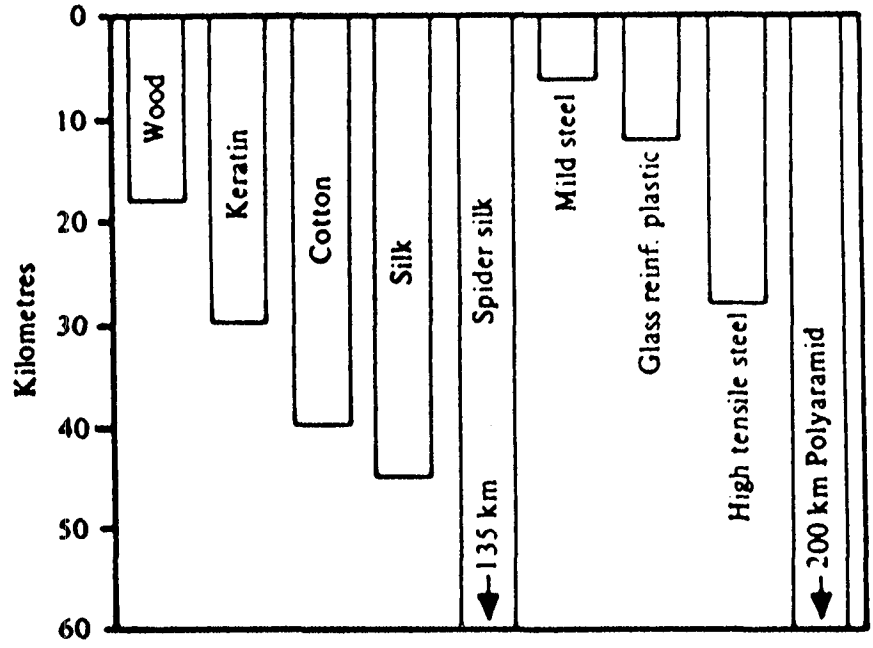

Lengths of materials able to sustain their own weight.

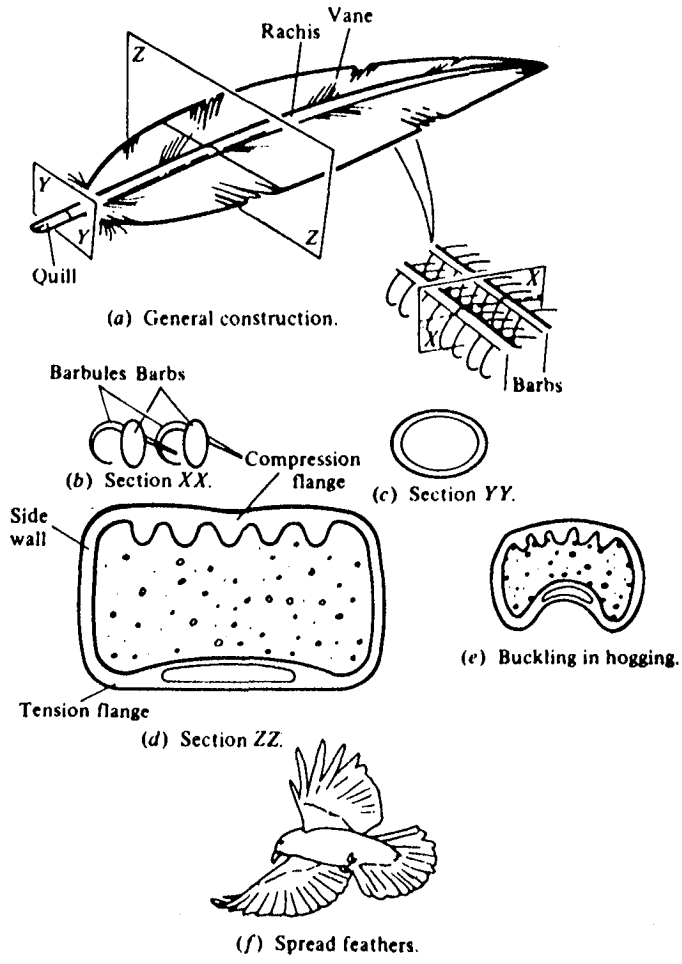

Structure of a feather.

Vogel, Life's Devices

- **Scaling Factors**
- **Skeletons**
- **Modulus, Strength, Strain, Energy Storage**
- **Leaf Structure**
- **Load Sharing**
- **Energy Cost of Moving**

RELATIVE MAGNITUDES IN MAMMALIAN DESIGN: SCALING FACTORS FOR THE ALLOMETRIC EQUATION, $y = bx^a$. THE INDEPENDENT VARIABLE, x, IS THE CUBE ROOT OF BODY MASS; THE UNITS ARE SI (KILOGRAMS, SECONDS, METERS, WATTS). DATA EXCERPTED FROM PETERS (1983) AND SCHMIDT-NIELSEN (1984).

y	a	b
Surface area	1.95	0.11
Skeletal mass (terrestrial)	3.25	0.0608
Skeletal mass (cetaceans)	3.07	0.137
Muscle mass	3.00	0.45
Metabolic rate	2.25	4.10
Effective lung volume	3.09	0.0000567
Frequency of breathing	−0.78	0.892
Heart mass	2.94	0.0058
Frequency of heartbeat	−0.75	4.02
Kidney mass	2.55	0.00732
Liver mass	2.61	0.033
Brain mass (nonprimates)	2.10	0.01
Brain mass (humans)	1.98	0.085

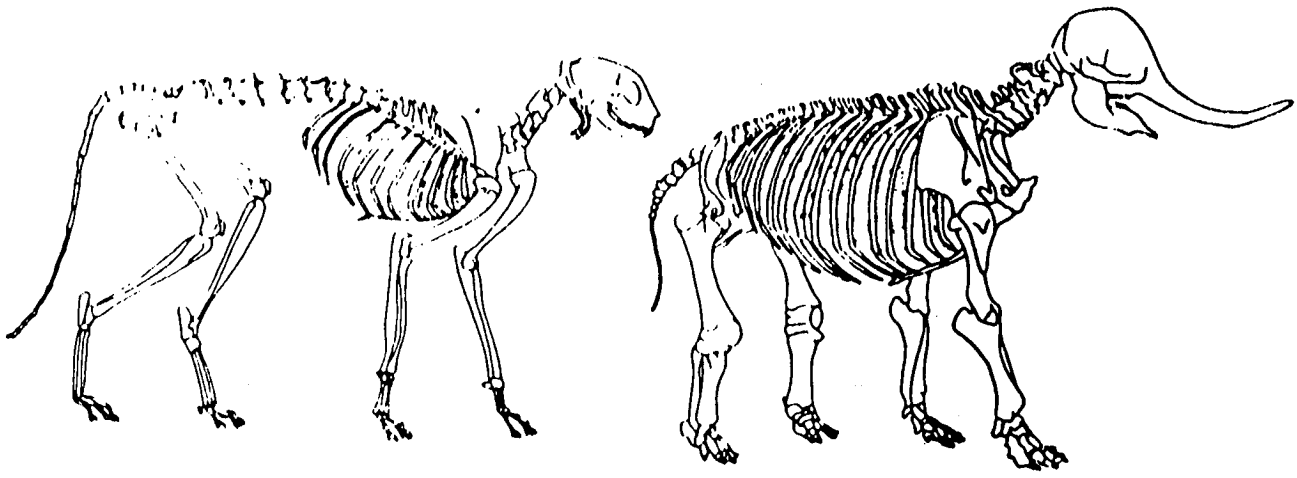

The skeletons of a cat (left) and an elephant (right), drawn approximately the same size. There's no trouble telling one from the other! Notice, in particular, the differences in both shape and position of the bones of the legs.

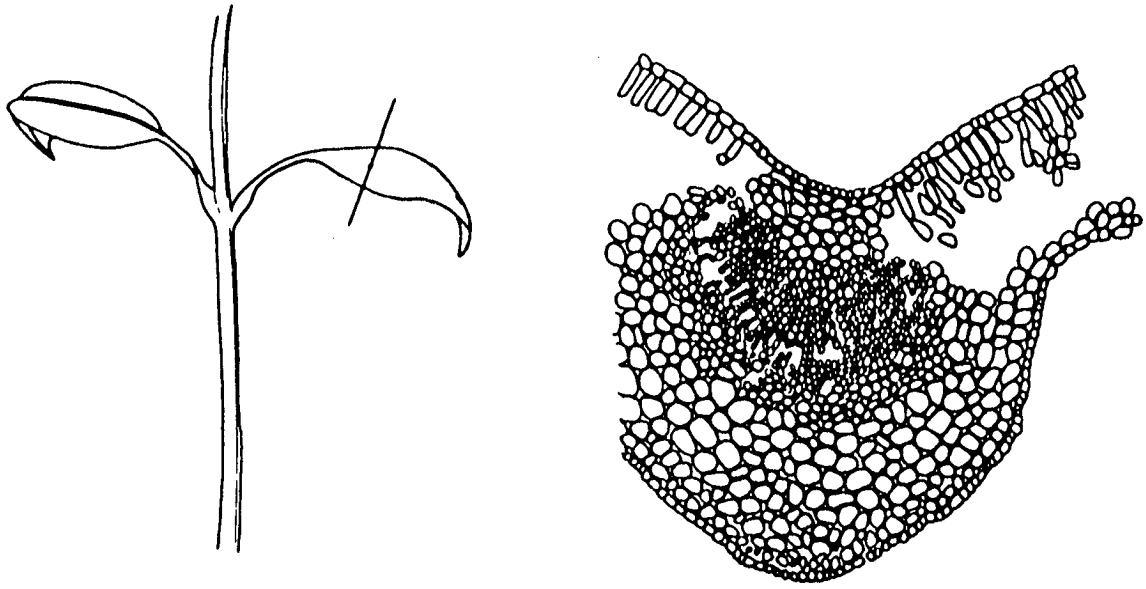

A leaf and its petiole act as a cantilever beam. The upper part is loaded in tension and the lower in compression. At right is a cross section through the midrib of a leaf—the large cells near the bottom are nearly spherical and liquid-filled; the smaller ones further up are elongate and fibrous.

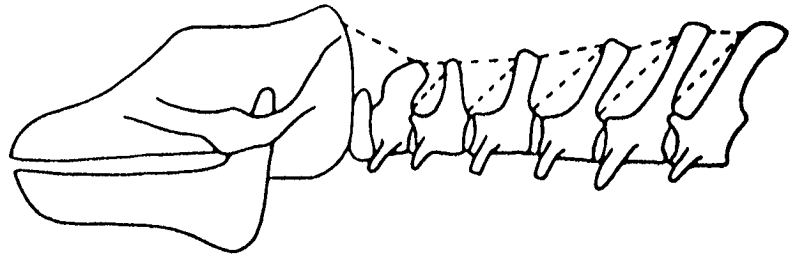

The head and cervical vertebrae of a mammal—the latter are the compression-resisting elements of a cantilever. The minimal tension-resisting components have been drawn in with dashed lines; the real array of muscles and tendons is more complex.

Gordon, New Science of Strong Materials

- Theoretical Strength
  - strain=10-20%
  - stress=E/10-E/5
- Toughness
  - sigy=1x to 5x sigx
  - Interfaces as Crack Stoppers

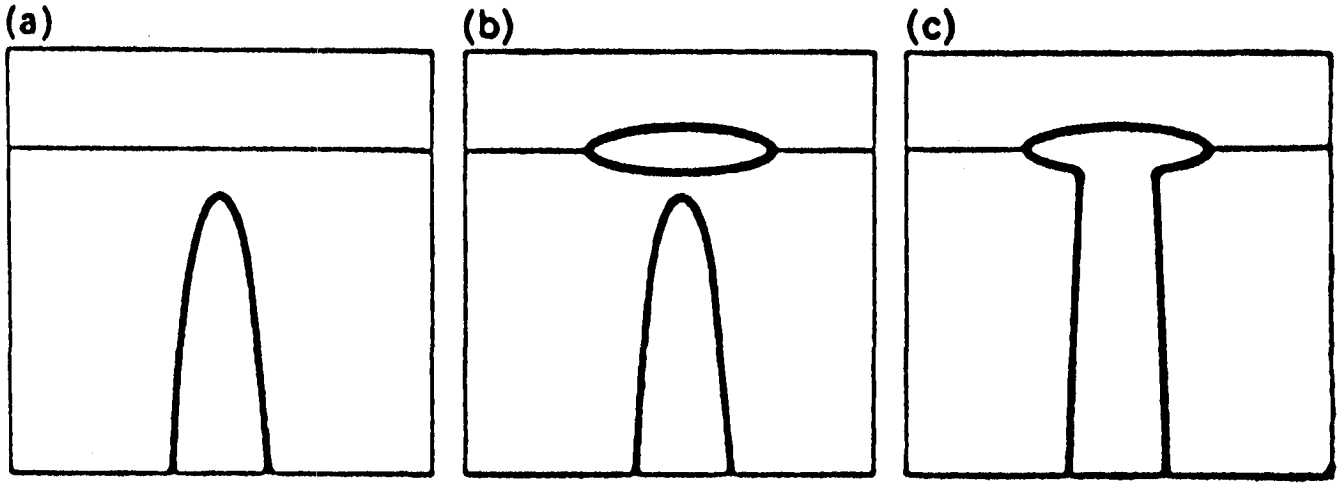

Cook-Gordon mechanism for stopping cracks at a weak interface.
(a) Crack approaches a weak interface.
(b) Interface breaks ahead of main crack.
(c) T-shaped crack-stopper. In practice the crack is usually diverted, as in Plate 11.

Gordon, New Science of Strong Materials (and Structures) (cont.)

- Relative Weight-Cost
- Efficiency

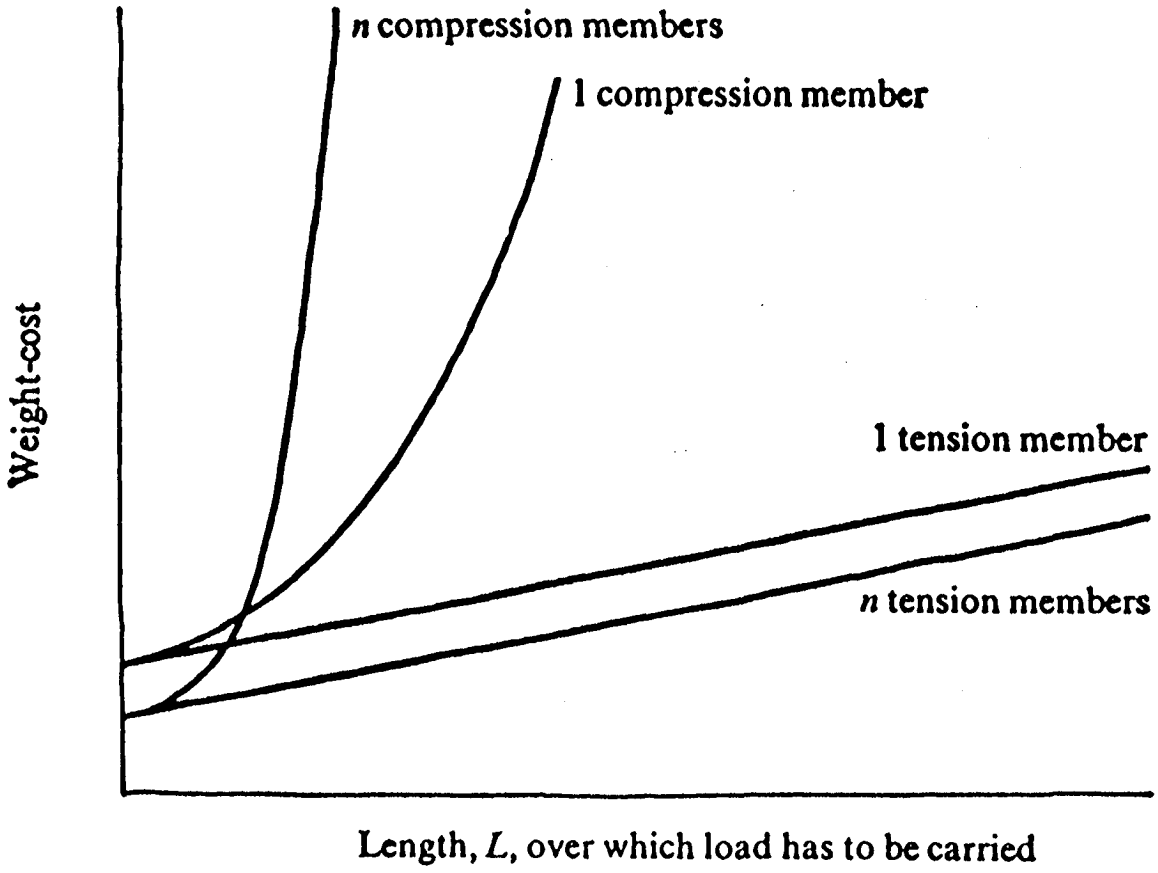

Diagram illustrating the relative weight-cost of carrying a given load over a distance L.

Shanley, Weight-Strength Analysis of Aircraft Structures

- Optimum Design - Minimum Wt to Carry Given Load
- Structural Index = P/ab

Bullock, Eisenmann, Weibull, Statistical Scaling

- Weibull Strength
- Scatter Affects Strength
- Complexity
- Volume
- Stress Distribution Effects
- Weibull Predicts

HERE'S HOW STRENGTH IS CALCULATED

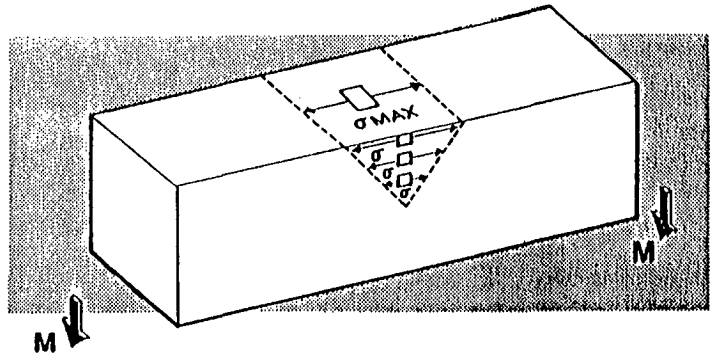

Probability of Survival	$P_S = e^{-\int_{Volume} \left(\frac{\sigma}{\beta}\right)^{\alpha} dV}$	Weibull
	$P_S = \begin{cases} 1, & \text{if } \sigma_{max} < F_{ult} \\ 0, & \text{if } \sigma_{max} > F_{ult} \end{cases}$	Classical

MATERIAL SCATTER AFFECTS STRENGTH

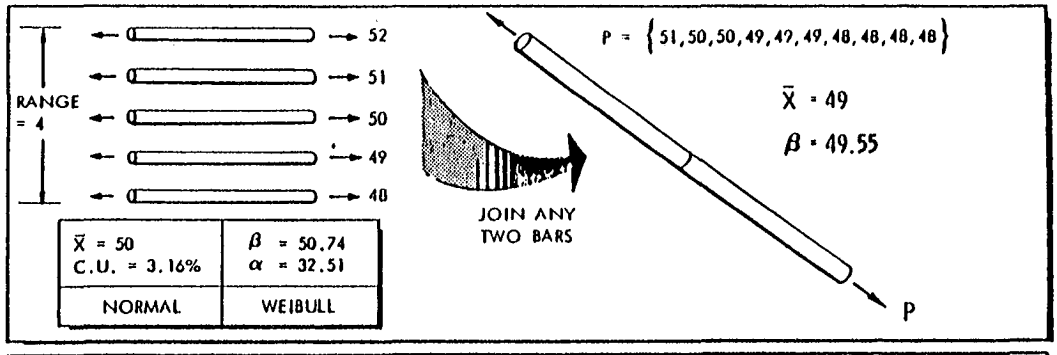

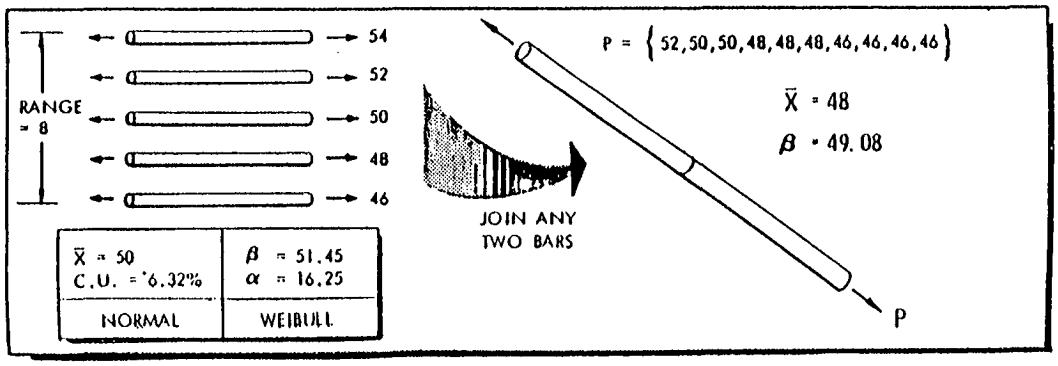

INCREASED COMPLEXITY LOWERS STRENGTH

IF THE STRENGTH OF A COUPON CONTAINING A SINGLE HOLE IS GIVEN AS σ_1,

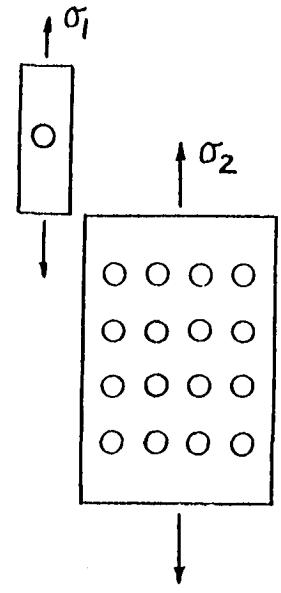

THEN FOR A SET OF N UNIFORMLY STRESSED HOLES THE STRENGTH OF THE COUPON IS GIVEN BY

$$\frac{\sigma_2}{\sigma_1} = \left(\frac{1}{N}\right)^{1/\alpha}.$$

FOR $N = 16$, AND $\alpha = 30$;

$$\frac{\sigma_2}{\sigma_1} = \left(\frac{1}{16}\right)^{1/30} = 0.912$$

VOLUME INCREASE LOWERS STRENGTH

FOR A UNIFORM STRESS FIELD,

$$P_S = e^{-\int \left(\frac{\sigma}{\beta}\right)^{\alpha} dV} = e^{-V\left(\frac{\sigma}{\beta}\right)^{\alpha}}$$

FOR TWO DIFFERENT VOLUMES UNDER UNIFORM STRESS,

$$P_{S_1} = e^{-V_1\left(\frac{\sigma_1}{\beta}\right)^{\alpha}} \quad \& \quad P_{S_2} = e^{-V_2\left(\frac{\sigma_2}{\beta}\right)^{\alpha}},$$

WHERE α AND β ARE MATERIAL PROPERTIES.

FOR EQUAL PROBABILITIES OF FAILURE,

$$P_{S_1} = P_{S_2}, \text{ SO } -V_1\left(\frac{\sigma_1}{\beta}\right)^{\alpha} = -V_2\left(\frac{\sigma_2}{\beta}\right)^{\alpha}$$

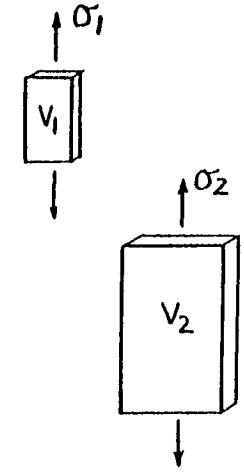

OR $$\frac{\sigma_2}{\sigma_1} = \left(\frac{V_1}{V_2}\right)^{1/\alpha}.$$ FOR $\frac{V_1}{V_2} = \frac{1}{50}$, AND $\alpha = 30$, $\frac{\sigma_2}{\sigma_1} = \left(\frac{1}{50}\right)^{1/30} = 0.878$

STRESS GRADIENTS MUST BE ACCOUNTED FOR...

$$P_S = e^{-\int_{VOL} \left(\frac{\sigma}{\beta}\right)^{\alpha} dV}$$

WHERE σ IS TYPICALLY A $f(X,Y,Z)$.

TENSION: σ = CONSTANT

LET'S COMPARE A $[0]_6$ TENSILE COUPON WITH A $[0]_{15}$ FLEXURE SPECIMEN.

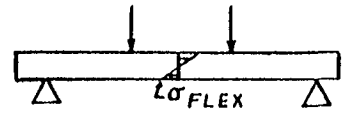

FLEXURE: $\sigma = f(X,Y,Z)$

$$\frac{\sigma_{FLEX}}{\sigma_{TEN}} = \left[2(\alpha+1)^2 \frac{V_{TEN}}{V_{FLEX}}\right]^{\frac{1}{\alpha}}$$

FOR $V_{TEN} = V_{FLEX}$, AND $\alpha = 30$;

$$\frac{\sigma_{FLEX}}{\sigma_{TEN}} = \left[2(30+1)^2 \left(\frac{1}{1}\right)\right]^{1/30} = 1.29$$

WEIBULL CORRECTLY PREDICTS FAILING STRENGTH

[0] NARMCO 5208/T300 GRAPHITE - EPOXY	CLASSICAL STRENGTH THEORIES	WEIBULL	TEST RESULT
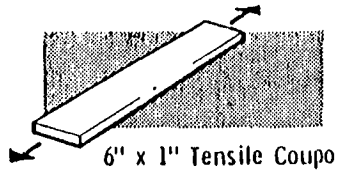 6" x 1" Tensile Coupon Test	207 KSI	207 KSI	207 KSI
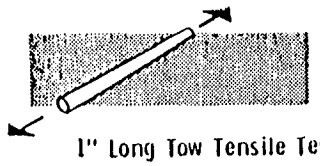 1" Long Tow Tensile Test	207 KSI	259 KSI	252 KSI
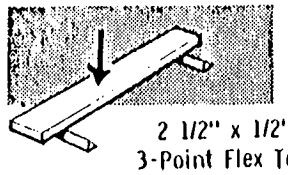 2 1/2" x 1/2" 3-Point Flex Test	207 KSI	277 KSI	280 KSI

Karbhari, Issues of Scale in Composites Fracture and Design

- Scope
- Scales
- Hierarchy
- Inherent Scaling
- Strength vs Fiber Size
- Load vs Diameter

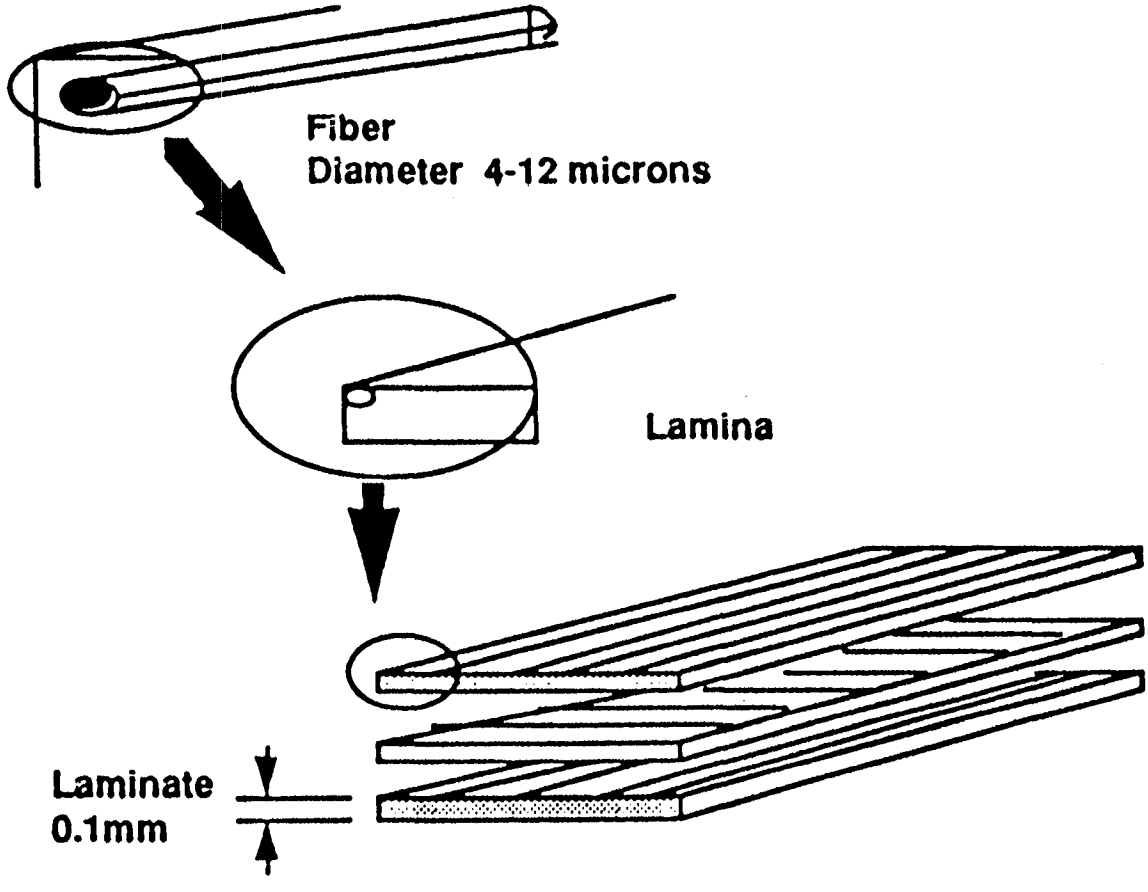

Inherent scaling in a composite

Table 2.1: Mechanics of Composites - Structural scale levels of applicability

Methods / Disciplines	Structural Scale Levels
Continuum Theory	Infinitesimal
Micromechanics	Interphase thickness, Fiber length and diameter
Macromechanics	Ply thickness
Combined stress failure criteria	Ply thickness
Laminate Theory	Laminate thickness
Structural mechanics	Laminate thickness Element size
Life / strength prediction (Durability)	Fiber diameter and length Ply thickness

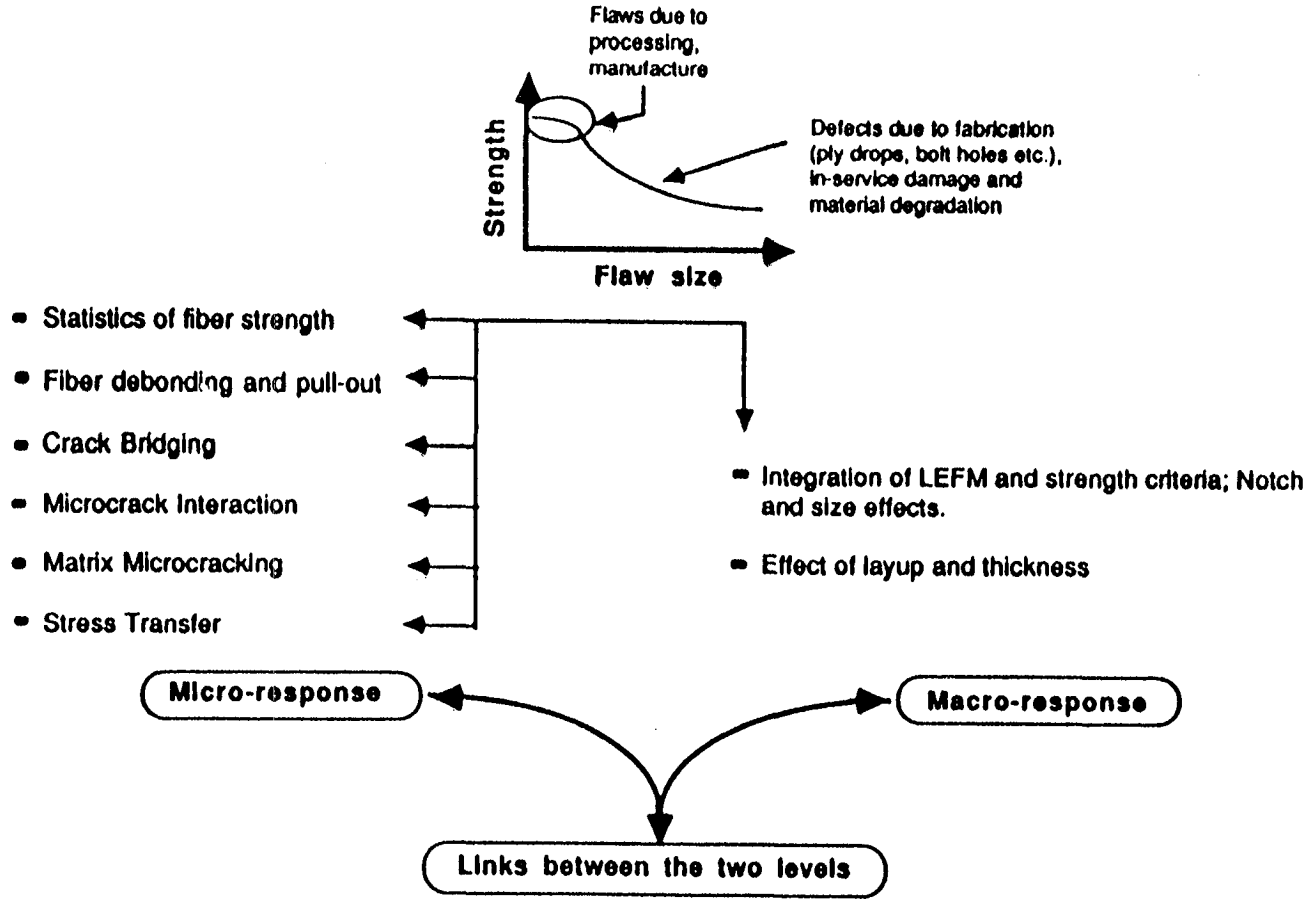

Classification of investigations

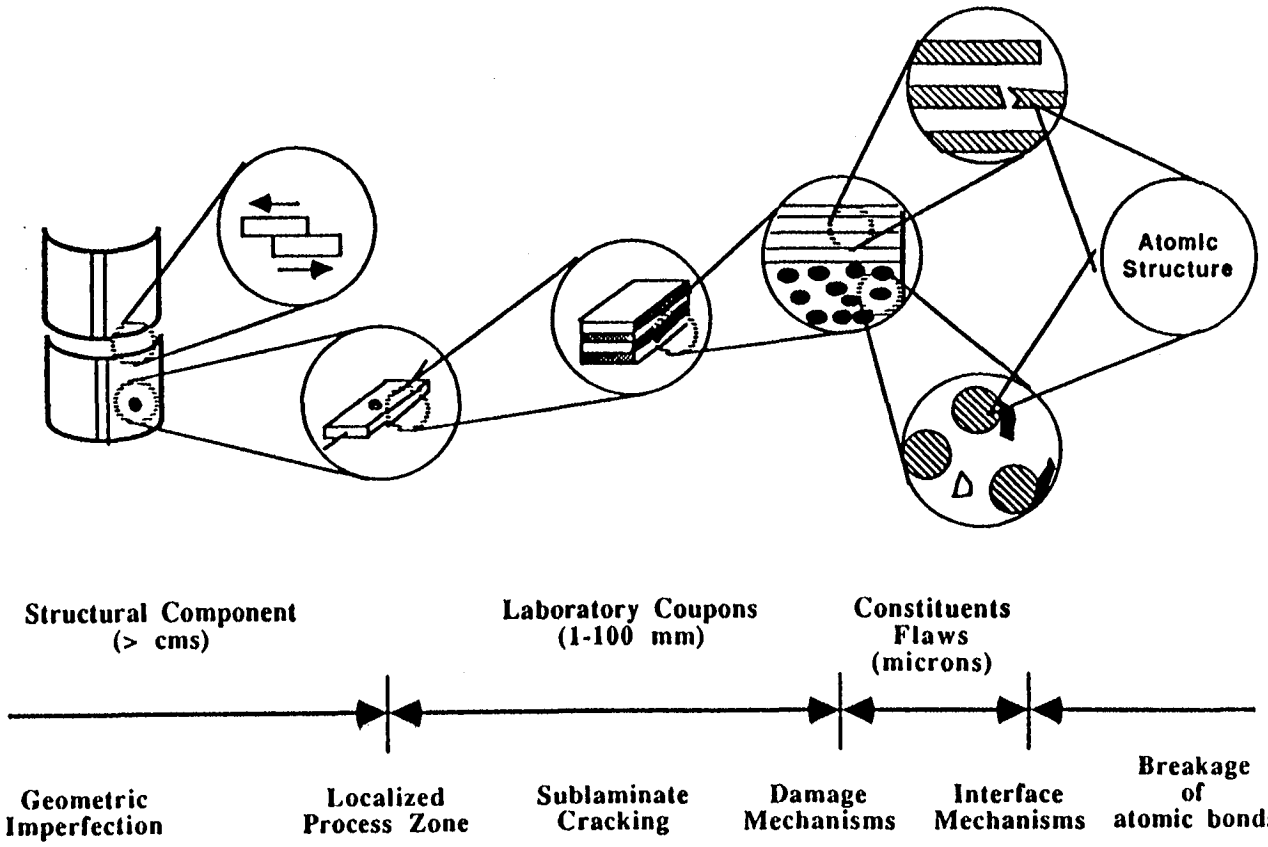

Levels of scale in composites (after A.S.D. Wang)

Summary

- **Atoms Don't Scale**
- **Fibers Don't Scale**
- **Nature Can Help Explain Composites Scaling**

STRENGTH CHARACTERISTICS AND CRACK GROWTH BEHAVIOR OF A COMPOSITE WITH WELL ALIGNED FIBERS*

J. Botsis, C. Beldica, A. Caliskan and D. Zhao
Department of Civil Engineering,
Mechanics & Metallurgy
2095 ERF, 842 W. Taylor Str.
University of Illinois at Chicago
Chicago, IL 60607

Abstract

Continuous fiber composites have shown tremendous promise in industrial applications. Their microstructures, however, are very complex and in many instances difficult to characterize. In this project, the fracture characteristics of a specially made fiber reinforced composite with different fiber spacing are investigated. The experimental results so far have shown that after an initial transient phase the crack speed reaches a steady phase, i.e., independent of the crack length. Within the steady crack growth phase debonding along the fibers in the bridging zone grows in a self-similar manner. During the steady phase the energy dissipation per cycle is constant. Afterwards, an increase of the energy dissipation is observed that is accompanied by a decrease in crack speed. This latter tend is presumed to be the result of relatively large amounts of energy dissipated in the bulk of the specimen. Using appropriate Green's function and computer simulations, the stress intensity factor at the crack tip is evaluated for various cases of bridging stresses. In this way the effects of specimen size and fiber spacing on the overall fracture behavior of the composite system are analyzed. The steady crack speed and the steady rate of debonding have a similar power dependence on stress level. Dimensional analysis demonstrates that the particular fracture process is not governed by dimensional invariance but on the detailed micromechanisms in the bridging zone.

STRENGTH CHARACTERISTICS AND CRACK GROWTH BEHAVIOR OF A COMPOSITE WITH WELL ALIGNED FIBERS

John Botsis, et. al

outline

- introduction
  - *motivation and objectives*
  - *approach*
- experimental methods
  - *materials and specimens*
  - *loading conditions*
- experimental results
- analysis
  - *stress intensity factor simulations*
  - *dimensional analysis*
- conclusions

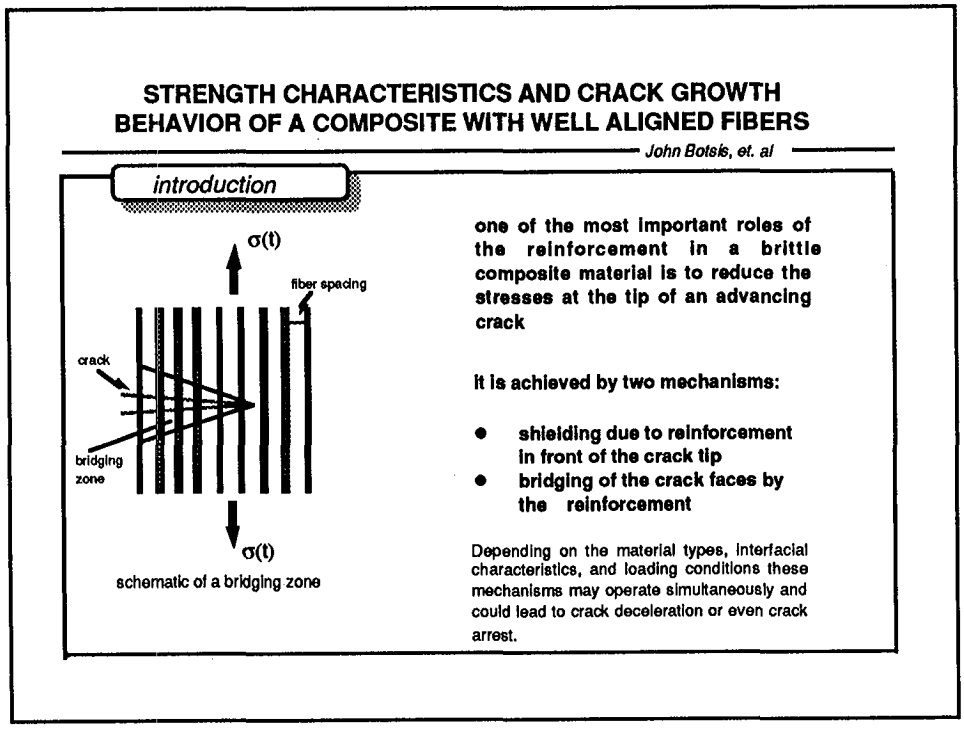

- One of the most important roles of the reinforcement in a brittle composite material is to reduce the stresses and strains at the tip of an advancing crack. This is usually achieved through two mechanisms. (i). the first one is from a shielding effect that the reinforcement ahead of the crack tip imposes on the stress and strain fields around the crack tip. (ii). the second and more important results from bridging of the crack faces by the reinforcing particles, fibers, whiskers, etc. A typical bridging zone in a fiber reinforced composite is shown on the left hand side of this slide.

STRENGTH CHARACTERISTICS AND CRACK GROWTH BEHAVIOR OF A COMPOSITE WITH WELL ALIGNED FIBERS

John Botsis, et. al

introduction

Significant work has been reported on the effects of the reinforcement and bridging on the stress intensity factor and crack growth characteristics of composite materials*.

Most of this work is concerned with deriving expressions for toughness and stresses at the crack tip for cracks that would exhibit either non - steady or steady state growth characteristics.

However, experimental works on the effects of fiber spacing and loading conditions on crack bridging, fiber debonding, and crack growth characteristics have been limited.

*Marshall, Cox and Evans (1985). Budiansky, Hutchinson and Evans (1986). Hori and Nemat-Nasser (1987). Budiansky and Amazigo (1989). Hutchinson and Jensen (1990). Yang, Tsai, Quin, Mura, Shibata and Mori (1991). Rubinstein and Xu (1992).

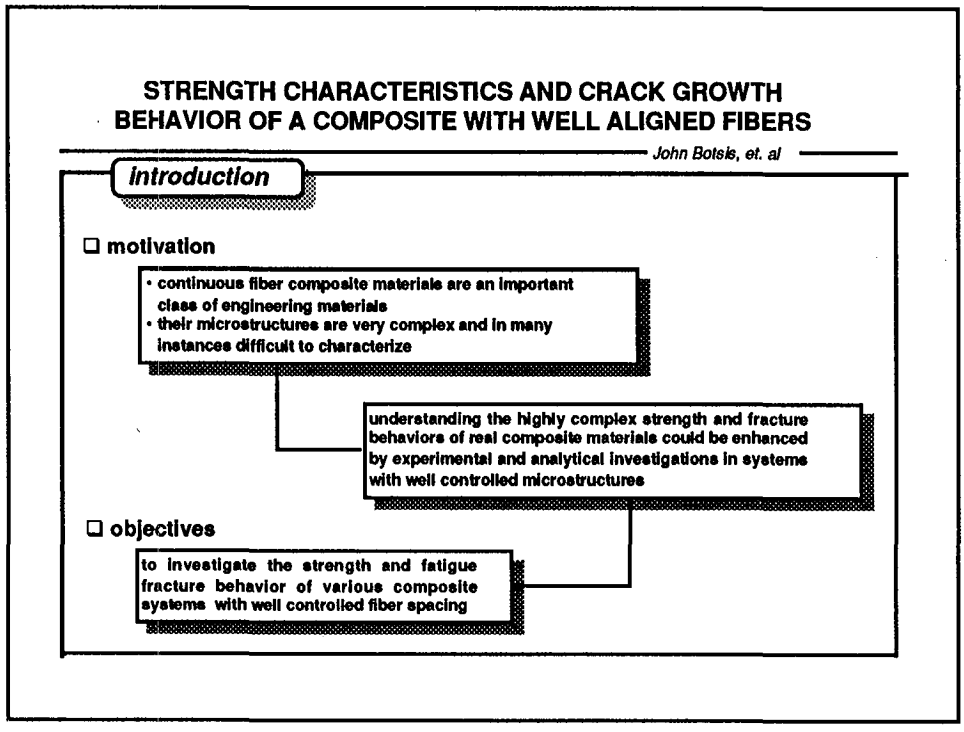

- In this paper, results of fatigue crack growth on a specially made composite material are reported. The matrix material was an epoxy and the reinforcement consisted of long aligned fibers that were approximately spaced at equal distances from each other. The properties of the constituent materials were chosen in such a way that the fibers were sufficiently stronger than the matrix. As a result, it is expected that the fibers in the bridging zone of the crack do not fail and thus, all fibers in the zone contribute to the fracture behavior of the composite specimen.

STRENGTH CHARACTERISTICS AND CRACK GROWTH BEHAVIOR OF A COMPOSITE WITH WELL ALIGNED FIBERS

John Botsis, et. al

approach

- choose the properties of the constituent materials in such a way that the fibers (glass, carbon, kevlar) are sufficiently stronger than the matrix
- choose a transparent matrix material (epoxy) and keep the fibers at equal distances from each other
- prepare composite specimens with long aligned fibers along one direction

→ the fibers in the bridging zone do not fail and thus, all fibers in the zone contribute to the fracture behavior of the composite specimen. Debonding and any other damage can be observed during testing

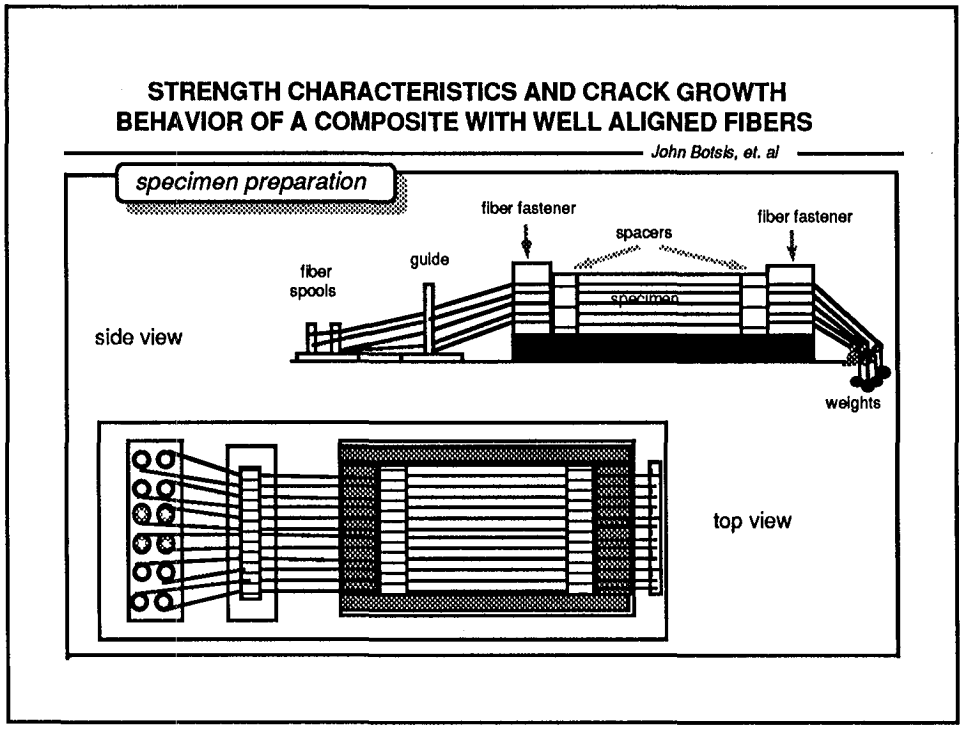

- This slide illustrates the mold used for specimen preparation. Note that composites with various layers of fibers can be prepared with specific fiber spacing.
- The material used in the present studies was a glass and epoxy, unidirectional, single lamina composite.
- The Young moduli for the constituent materials were, E_f =72.5 GPa for the glass, and E_m = 3.5 GPa for the matrix.
- This particular matrix material was transparent, which facilitated in situ optical observation.
- Specimens were prepared from E - glass fibers with 0.40 mm in diameter and an epoxy resin matrix.
- The matrix material was a mixture of Eiclorhidrin - Bisfenol resin and Hysol PZA - B hardener in a ratio of 4:1 by weight.

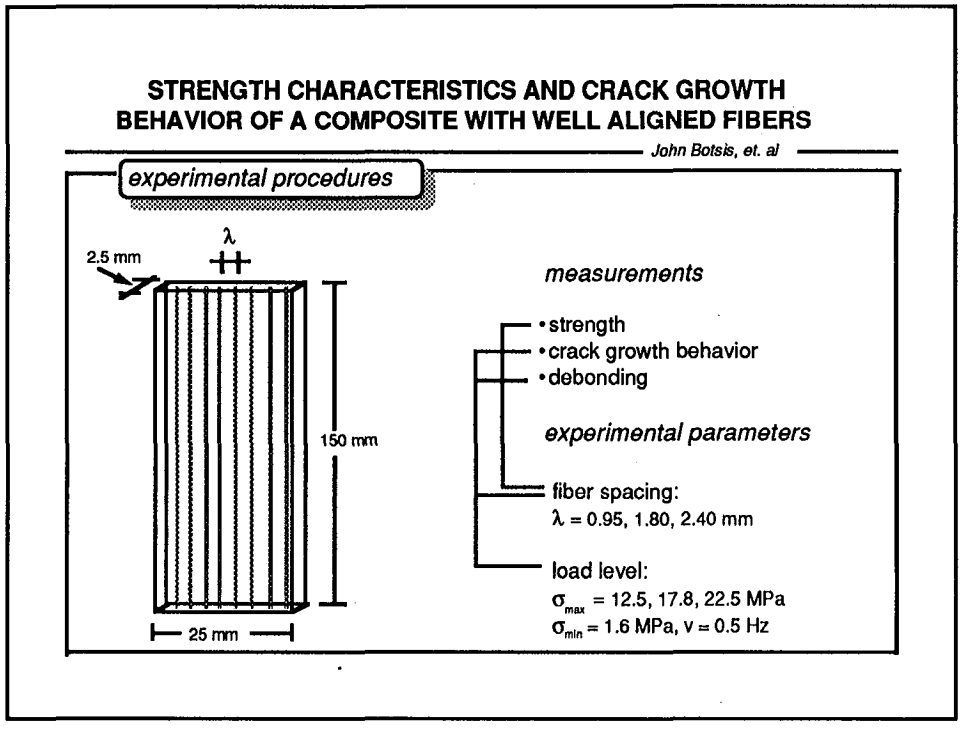

- **A schematic of a specimen used in these studies is shown here.**
- **For strength measurements ram tests were performed on specimens with different fiber spacing.**
- **In the fatigue testing, a 60° angle notch of 2 mm depth was milled at the middle of the specimen edge. In all specimens, the distance from the notch tip to the first fiber was about 1 mm.**
- **Tension-tension fatigue experiments were performed on a dual servohydraulic Instron Mechanical Testing System at room temperature and laboratory environment.**
- **All experiments were load controlled with a sinusoidal waveform function.**
- **Measurements of crack growth and the extent of debonding were monitored during the experiment with a traveling optical microscope.**
- **A light beam was configured at an angle to the specimen's plane to distinguish the debonding that appeared as a relatively brighter area along the fibers within the bridging zone.**

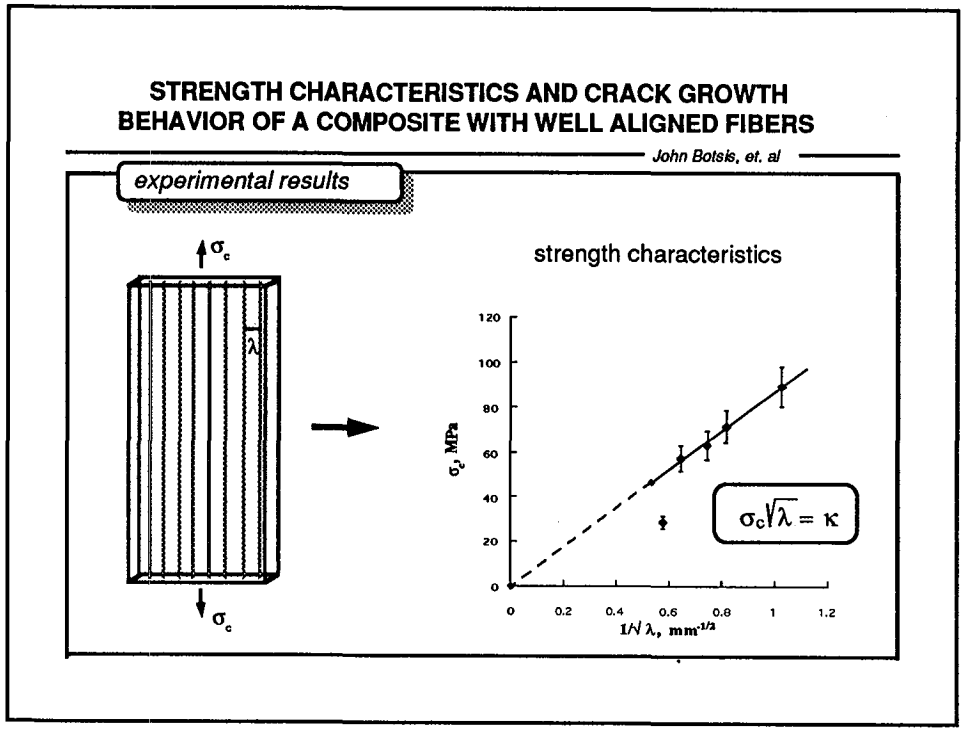

- For strength measurements ram tests were performed on specimens with different fiber spacing (λ = 0.95, 1.5, 1.8, 2.4, and 3.5 mm).
- It is very important to note that for λ = 0.95, 1.5, 1.8, 2.4 mm the product of the composite strength σ_c and the square root of fiber spacing is constant.
- A deviation from this relationship was observed for larger fiber spacing.
- Note that these observations agree with the mixture rule for strength.
- Moreover, as it is shown later, steady state crack speed was observed only in the specimens where $\sigma_c\sqrt{\lambda} = k$.

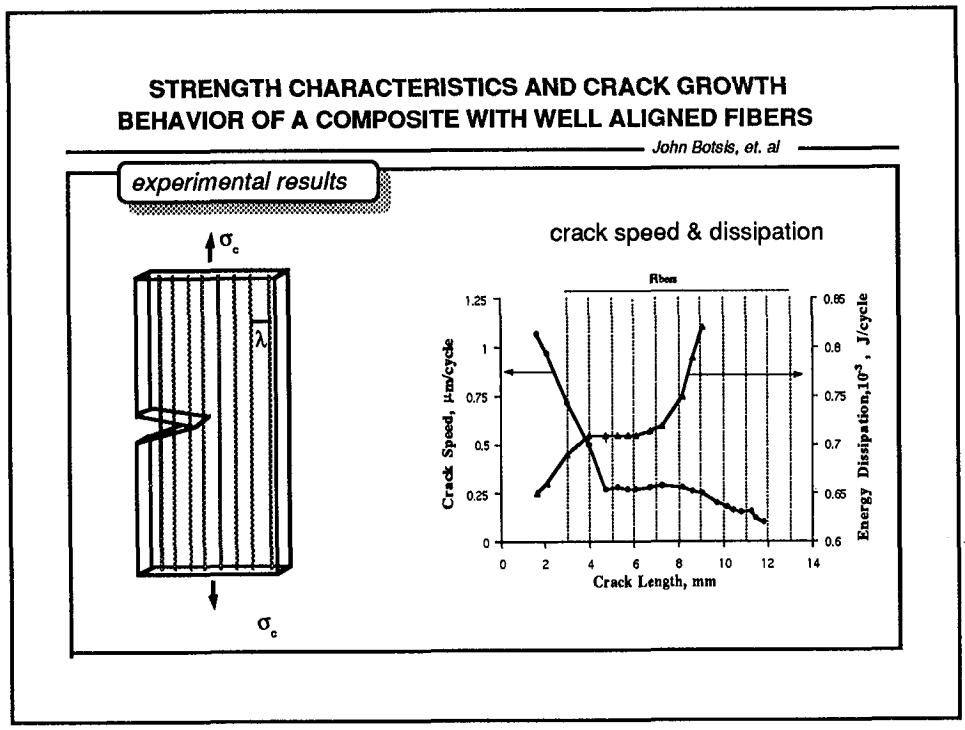

- This slide shows the crack growth behavior as well as the rate of energy dissipation during fatigue of a notched specimen.
- In all cases examined in the present work, the time to crack initiation largely depended upon the applied load. That is, the lower the stress level the longer the time to crack initiation. After crack initiation, a significant decrease of the crack speed was observed. This behavior was due to the fiber in front of the crack and its effect on the stress field around the crack tip. It has been reported that an inclusion with higher stiffness than the surrounding material, in front of a crack, lowers the stress intensity factor at the crack tip.
- In all cases investigated the crack speed reached a constant value. Moreover, the rate of energy dissipation was constant during the steady state crack growth.
- After the steady state growth, crack speed decreased while the dissipation increased. This behavior may be due to changes in energy absorption mechanisms of the system (bridging zone versus matrix material).

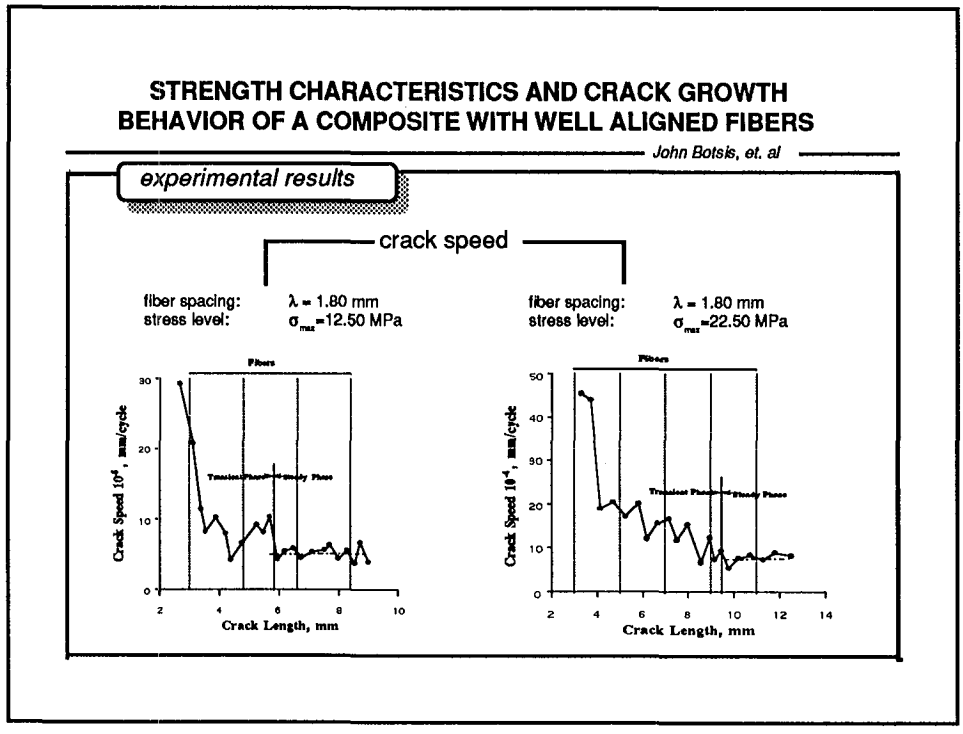

- The crack propagation rates plotted against the crack length in specimens with the same fiber spacing and different load levels are shown.
- Note that after a decrease the crack speed reached steady values.
- The fluctuations around a constant crack speed, observed in the steady phase may be due to an experimental error in the measurements of crack length and/or the various mechanisms of dissipation in the bridging zone and the fibers ahead of the crack tip.
- Moreover, variations in their center to center distances may have contributed to the observed small oscillations around a mean steady speed.

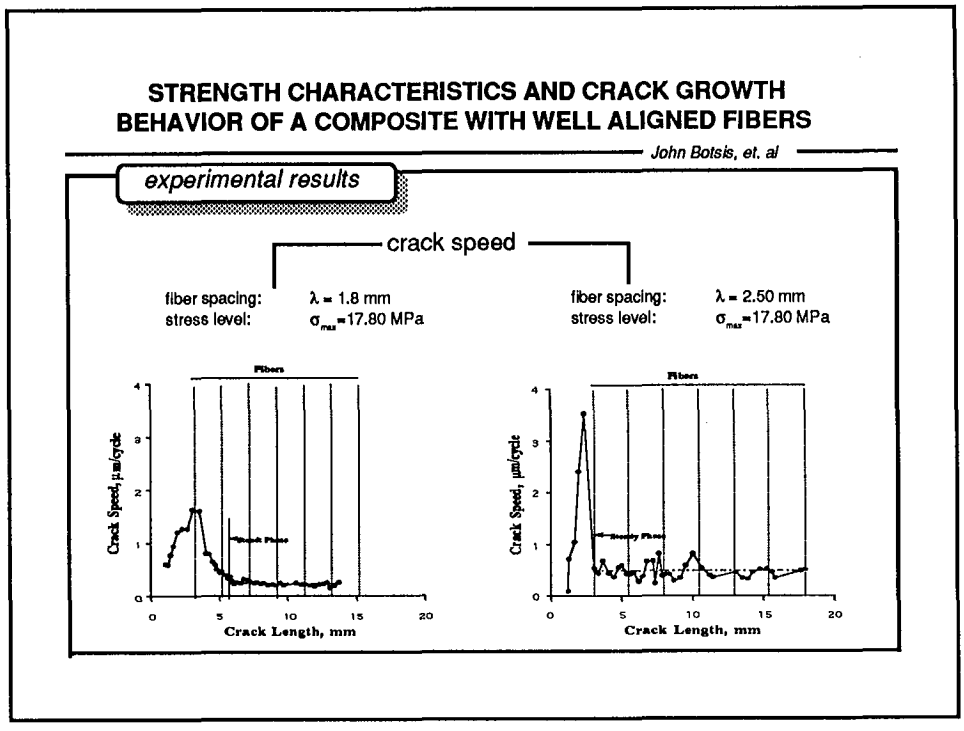

- The crack propagation rates plotted against the crack length in specimens with different fiber spacing and the same load levels are shown.
- Note that after a decrease the crack speed reached steady values.
- The fluctuations around a constant crack speed, observed in the steady phase may be due to an experimental error in the measurements of crack length and/or the various mechanisms of dissipation in the bridging zone and the fibers ahead of the crack tip.
- Moreover, variations in their center to center distances may have contributed to the observed small oscillations around a mean steady speed.

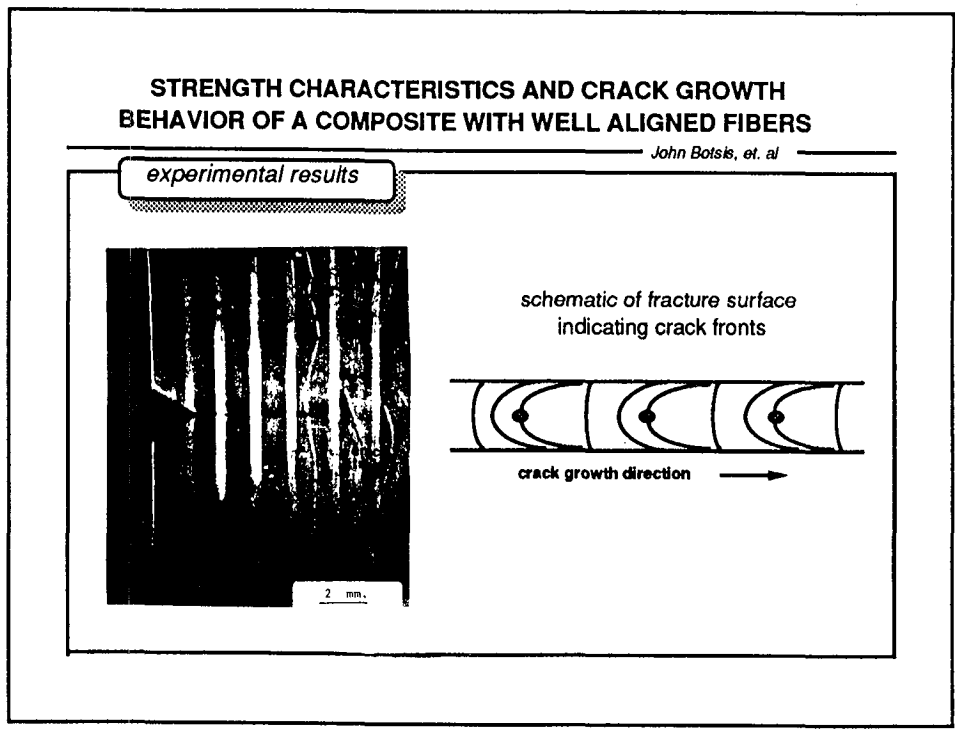

- A typical configuration of the crack and the associated extent of debonding along the fibers is shown in the photograph displayed in in the left hand side of this slide.
- It is interesting to note here that debonding is smaller on fibers closer to the crack tip. In situ optical observations indicated that, in all specimens fatigued under different loading conditions, the crack was bridged by all fibers behind the crack.
- A schematic of the fracture surface indicating the crack front around and between fibers is shown in the right hand side. In all cases, the crack front was not straight. Instead, a curved crack front was seen with the curvature being much larger when the crack was near to a fiber.
- The curvature of the crack front is a manifestation of the effects of the fiber ahead of the crack front and its effect on the stress field. At a particular fiber, debonding started when the center of the crack front ran into a fiber.

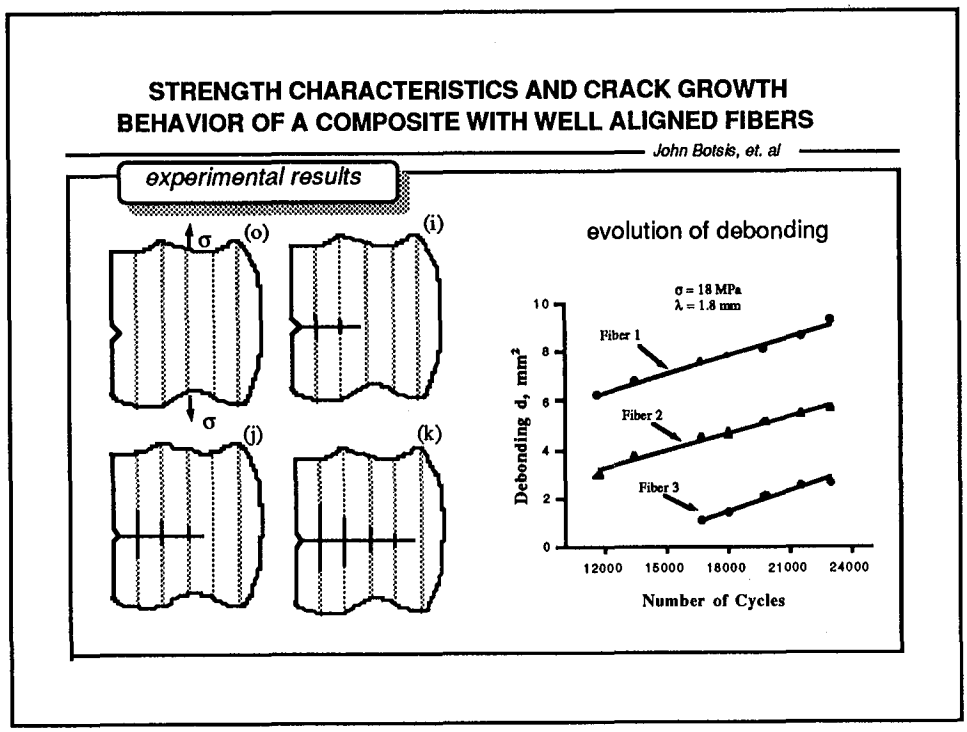

- Schematics of the bridging zone at consecutive configurations are shown in the left hand side of this slide.
- The evolution of debonding d, defined as $d = \pi LD$, where L is the debonding length and D is the fiber diameter on fibers within the bridging zone as a function of cycle number in a typical specimen, is shown in the right hand side. Regarding these data two important statements can be made.
- First, debonding vs. cycle number at each fiber in the bridging zone may be approximated with a straight line. This implies that, along with the crack speed, the rate of debonding at every fiber reached a steady growth mode.
- Second, for each loading condition the slopes of debonding vs. cycle number are equal. Thus, the rate of debonding was the same in every fiber of a given specimen and the evolution of the bridging zone was self- similar.
- Within the resolution of the observations, fiber debonding was the dominant mechanism of energy dissipation. Fiber friction, and filament fracture may have contributed to energy dissipation; however, they were not recorded in the present studies.

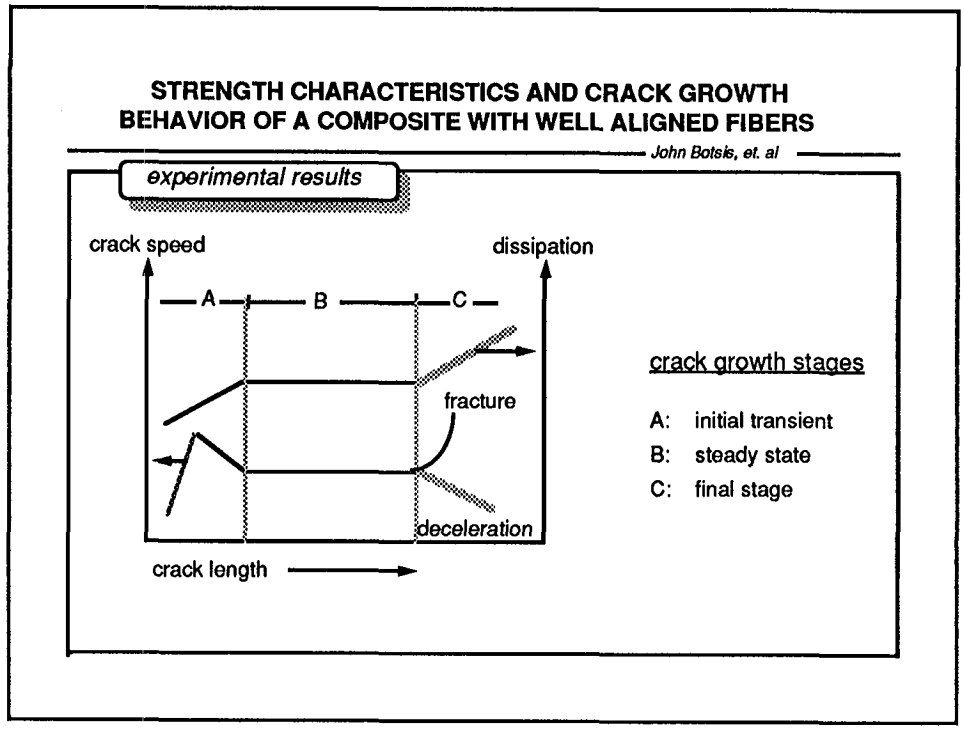

- The experimental results reported in this paper demonstrated that after a decrease, the crack speed reached a steady state. Although the speed at the steady phase was an increasing function of the applied load, the results of the present work implied that the stress state at the crack tip is independent of the crack length. Instead, it depended upon local parameters around the close vicinity of the crack tip and the applied load. Thus, for a particular fiber spacing, the remote applied stress seemed to be the controlling factor of the steady crack speed.
- Schematics of crack growth behavior and energy dissipation per cycle are displayed in this slide.
- Note that at the steady state, not only the crack speed was constant but also the energy dissipation per cycle.
- After the steady state, two types of behavior where observed. (i) increase in crack speed followed by a specimen fracture. (ii) decrease in crack speed and increase in energy dissipation.
- In this work, analysis of the experimental data will be limited to the steady state regime only.

STRENGTH CHARACTERISTICS AND CRACK GROWTH BEHAVIOR OF A COMPOSITE WITH WELL ALIGNED FIBERS

John Botsis, et. al

analysis

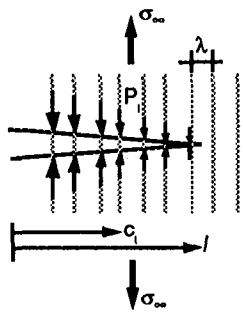

$$K_t = K(\sigma_\infty, l) - \sum_{i=1}^{n} K_i^f(P_i, c_i) + \Delta K$$

$$K(\sigma_\infty, l) = \int_0^l \frac{2\sigma_\infty}{\sqrt{\pi l}} F\left(\frac{x}{l}, \frac{l}{B}\right) dx$$

$$K_i^f(P_i, c_i) = \frac{2P_i}{\sqrt{\pi l}} F\left(\frac{c_i}{l}, \frac{l}{B}\right)$$

$$\Delta K \longrightarrow 0$$

$$F\left(\frac{x}{l}, \frac{l}{B}\right) = \frac{3.52\left(1-\frac{x}{l}\right)}{\left(1-\frac{l}{B}\right)^{3/2}} - \frac{4.35-5.28\frac{x}{l}}{\left(1-\frac{l}{B}\right)^{1/2}} + \left[\frac{1.30-0.30\left(\frac{x}{l}\right)^{3/2}}{\sqrt{1-\frac{x}{l}}} + 0.83 - 1.76\frac{x}{l}\right]\left[1-\left(1-\frac{x}{l}\right)\frac{l}{B}\right]$$

- To correlate the steady crack speed and the steady rate of debonding, the total stress intensity factor K_t, at the crack tip should be evaluated for the particular specimen geometry and bridging zone.
- For a crack bridged by fibers, it is assumed that the principle of superposition applies and that the level of residual stresses is relatively small.
- The stress intensity factor may be evaluated by employing standard Green's functions.
- The correction ΔK is due to the presence of the fiber ahead of the crack tip. For a cracked specimen with the particular reinforcement evaluation of ΔK is beyond the scope of this work. It has been reported, however, that an inclusion of radius r with higher modulus than the matrix material, located in front of the crack tip, does not contribute to the stress intensity factor when the distance between the crack tip and the center of the inclusion is greater than 2r (Rubinstein, 1986). Although the configuration of the inclusion investigated by Rubinstein was different, it is assumed that the same trends on the magnitude of total stress intensity factor would exist in this case as well. Thus, for the fiber spacing employed in these studies and considering that the crack tip was located in the middle of two consecutive fibers, ΔK was presumed negligible.

STRENGTH CHARACTERISTICS AND CRACK GROWTH BEHAVIOR OF A COMPOSITE WITH WELL ALIGNED FIBERS

John Botsis, et. al

analysis

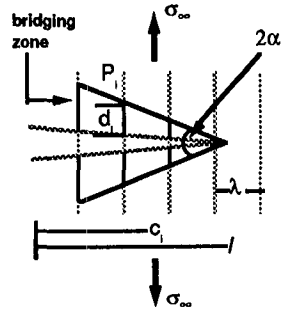

assumptions

- $P_i = b_1 d_i^m$

  $d_i = b_2(l - c_i)$

  $b_2 = \tan\alpha = \text{constant}$

- $P_i = \beta(l - c_i)^m$

  $\beta = b_1 b_2^m$

- Calculation of the stress intensity factor due to the remote load for an unbridged crack does not possess any particular difficulty. However, the contribution of the fibers to K_t can be evaluated only if the forces carried by the fibers are known. These quantities cannot be easily evaluated experimentally. Thus, one is led to assuming some distribution of tractions in the fibers that are compatible with the observed fracture phenomenon (Marshall, et. al, 1985, Cox and Marshall, 1991).
- In the present work, it is considered that at the steady crack growth phase, Kt is constant. Accordingly, various distributions of the forces were simulated.

STRENGTH CHARACTERISTICS AND CRACK GROWTH BEHAVIOR OF A COMPOSITE WITH WELL ALIGNED FIBERS

John Botsis, et. al

analysis

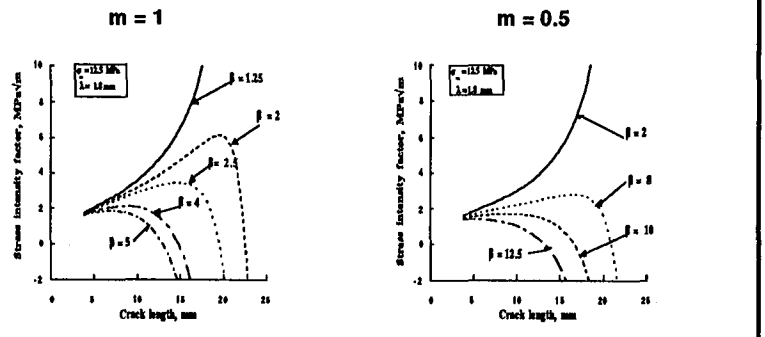

- Evolution of K_t as a function of crack length for various values of the proportionality constant β and two values of the exponent m.
- Note that under the adopted assumptions the total stress intensity factor did not reach constant level.

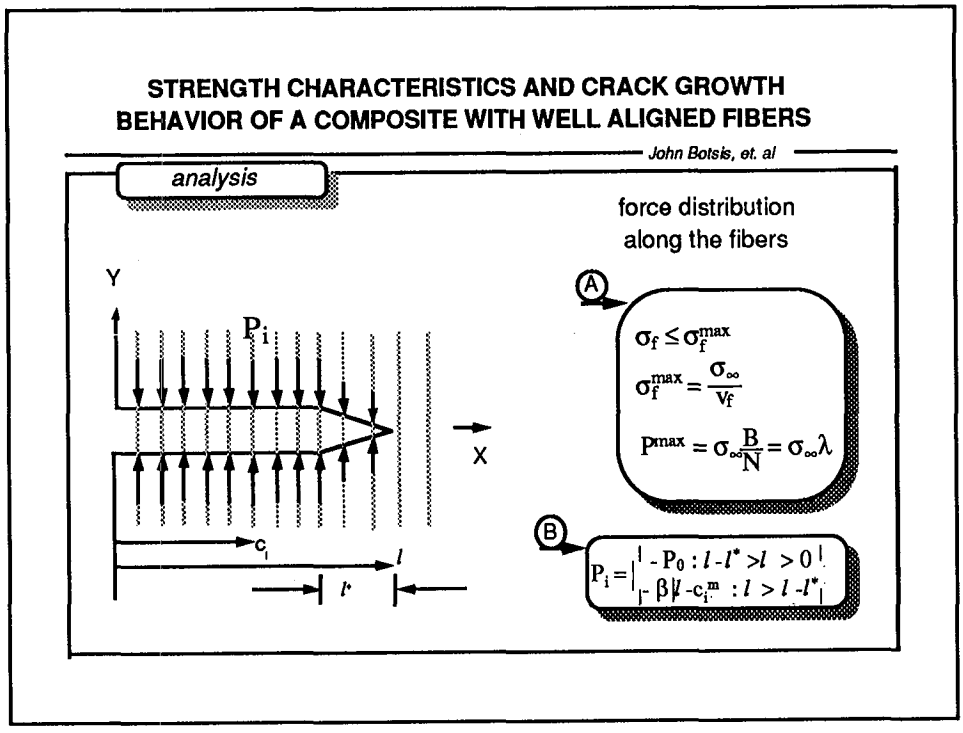

- In the next stage of the simulations, the force distribution in the fibers was described by two relations that are shown in the left hand side of this slide.
- In terms of these assumptions, the bridging zone is separated into two regions (left hand side). The first one is distinguished by a constant stress distribution and the second one by a linear dependence on debonding.

STRENGTH CHARACTERISTICS AND CRACK GROWTH BEHAVIOR OF A COMPOSITE WITH WELL ALIGNED FIBERS

John Botsis, et. al

analysis

finite geometry

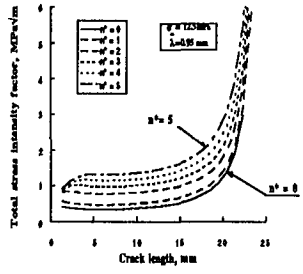

semi-infinite geometry

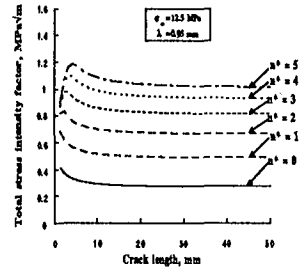

- **Since the value of the proportionality constant β, is unknown, simulations were performed for different values of β. Under the assumptions presented before and for a given applied load,changing the proportionality constant implies changing the magnitude of *l**, i.e., the number of fibers n*. Note that *l** and n* do not depend on the crack length.**
- **The plots presented in this slide show that in all cases, K_t is constant in a certain interval of crack length.**
- **However, the extent of the interval where K_t is constant and the level of K_t change with β.**

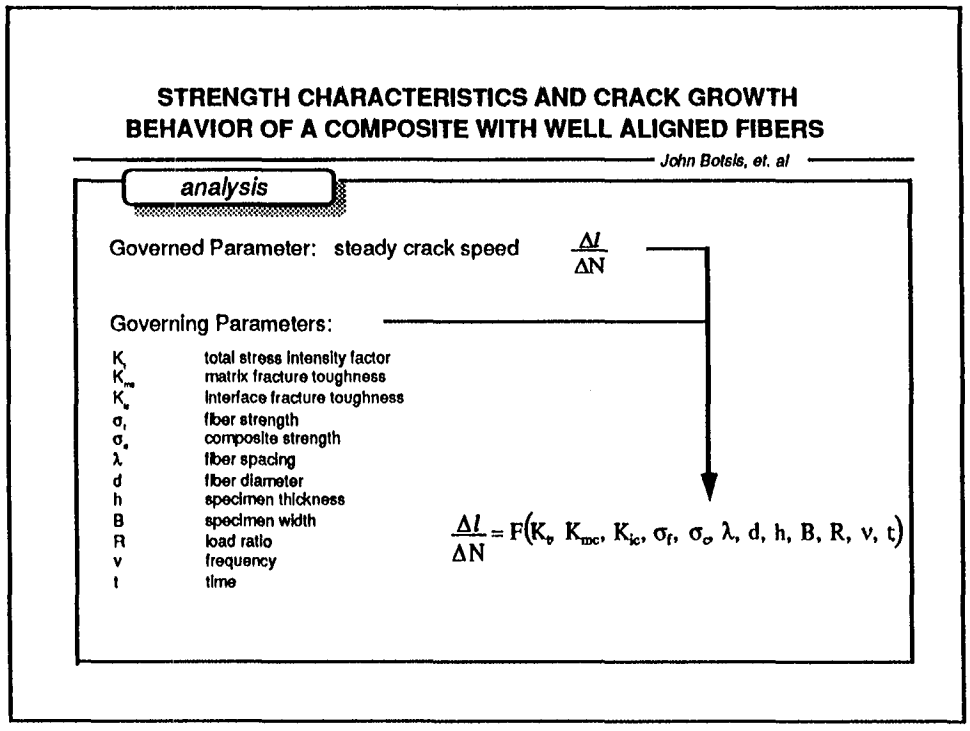

- **Analysis of the experimental data on crack speed was carried out using dimensional analysis.**
- **The governed parameter is the crack speed and the governing parameters are listed in the left hand side of this slide.**

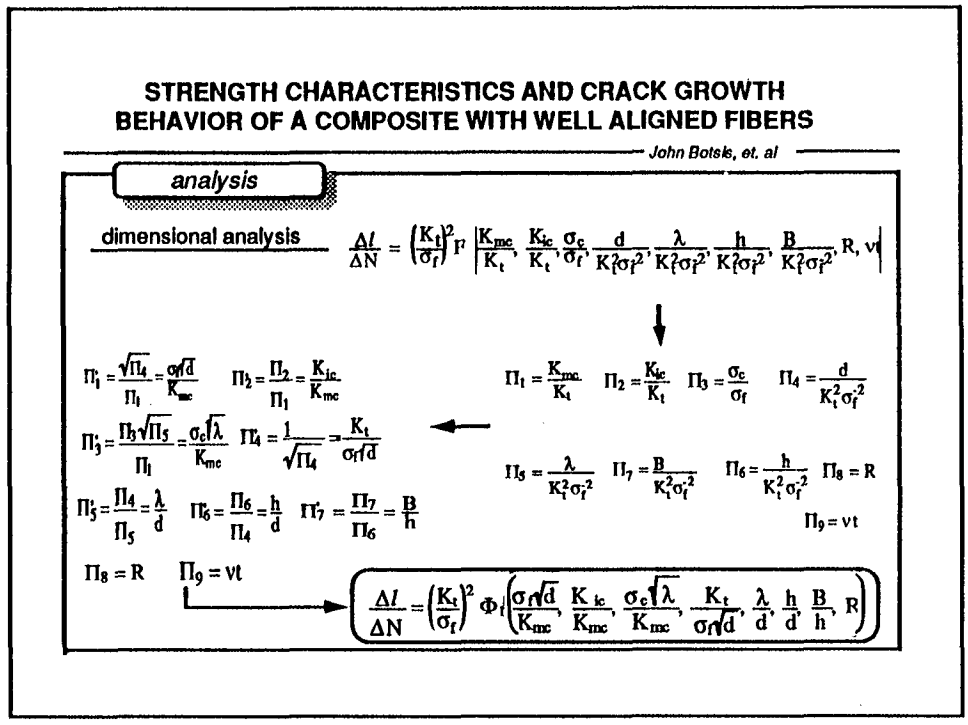

- The fundamental set of parameters were the total stress intensity factor K_t, the the fiber strength σ_f, and time t.
- Accordingly an initial set of Π parameters can be identified. These parameters were combined and the resulting new set of independent Π parameters were used for further analysis.
- The crack speed is then related to the new Π parameters.

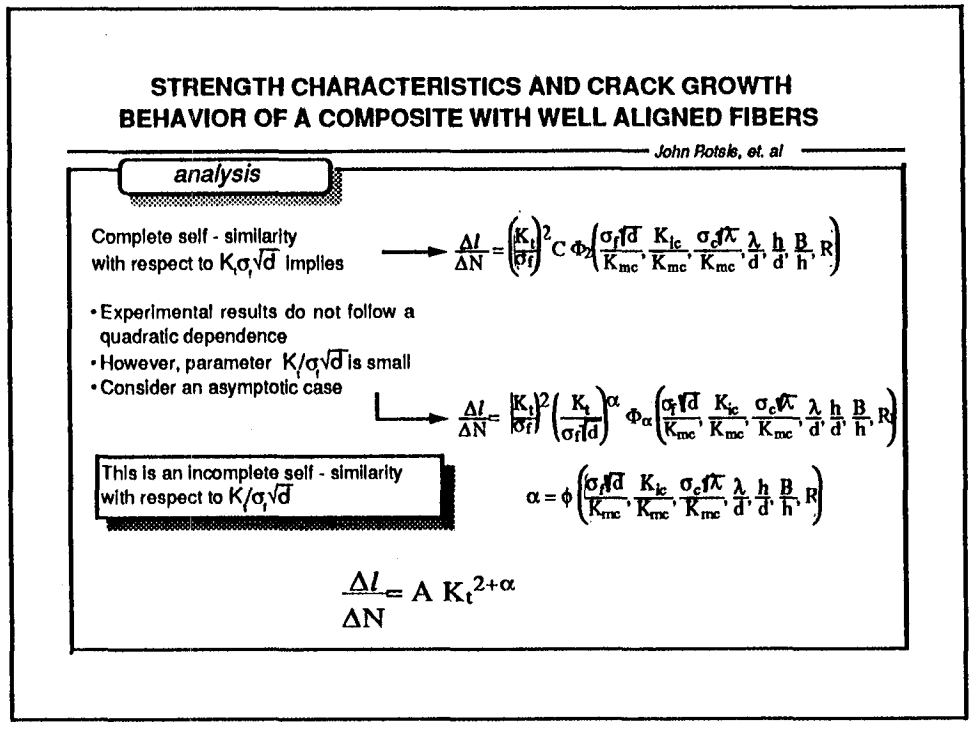

- **The parameter $K_t/\sigma_f\sqrt{d}$ is small. Threfore, complete self - similarity with respect to this parameter would imply a quadratic dependence of the crack speed on K_t. The experimental results, however, do not follow such a dependence.**
- **That leads to considering an incomplete self - similarity (Barenblatt, 1980) with respect to $K_t/\sigma_f\sqrt{d}$ that results in a power rule with an exponent of $2+\alpha$.**
- **Note that the exponent α cannot be determined from dimensional analysis. It depends on the Π parameters that enter the function Φ_α.**

STRENGTH CHARACTERISTICS AND CRACK GROWTH BEHAVIOR OF A COMPOSITE WITH WELL ALIGNED FIBERS

John Botsis, et. al

analysis

$$\frac{\Delta l}{\Delta N} = A_1(K_t)^{m_1} \qquad \frac{\Delta d}{\Delta N} = A_2(\sigma\sqrt{r})^{m_2}$$

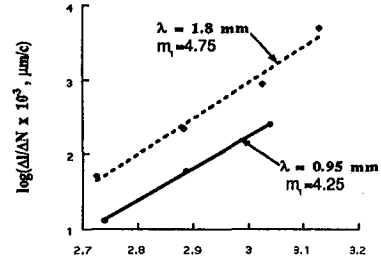

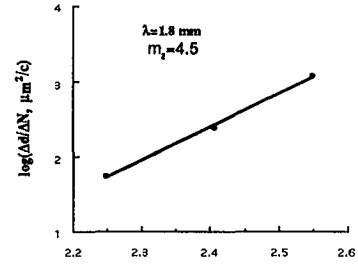

- The experimental data on the steady crack speed and the steady evolution of debonding were correlated with power laws.
- Here $\Delta l/\Delta N$ and $\Delta d/\Delta N$ refer to the steady crack speed and debonding, respectively, observed in a specimen fatigued under a certain stress level. A_1, A_2, m_1, and m_2 are parameters that may depend on the properties of the constituent materials. They can be evaluated by linear regression analysis on a Log - Log plane.
- The straight lines in slide represent the right hand side of equations. The data points are steady speeds and the steady values of debonding.
- It is worth noting that for different fiber spacing the values of the exponents were very close and that the exponent for the rate of debonding was approximately equal to that for crack growth.
- This result agrees with the self - similar evolution characteristics of debonding observed experimentally.

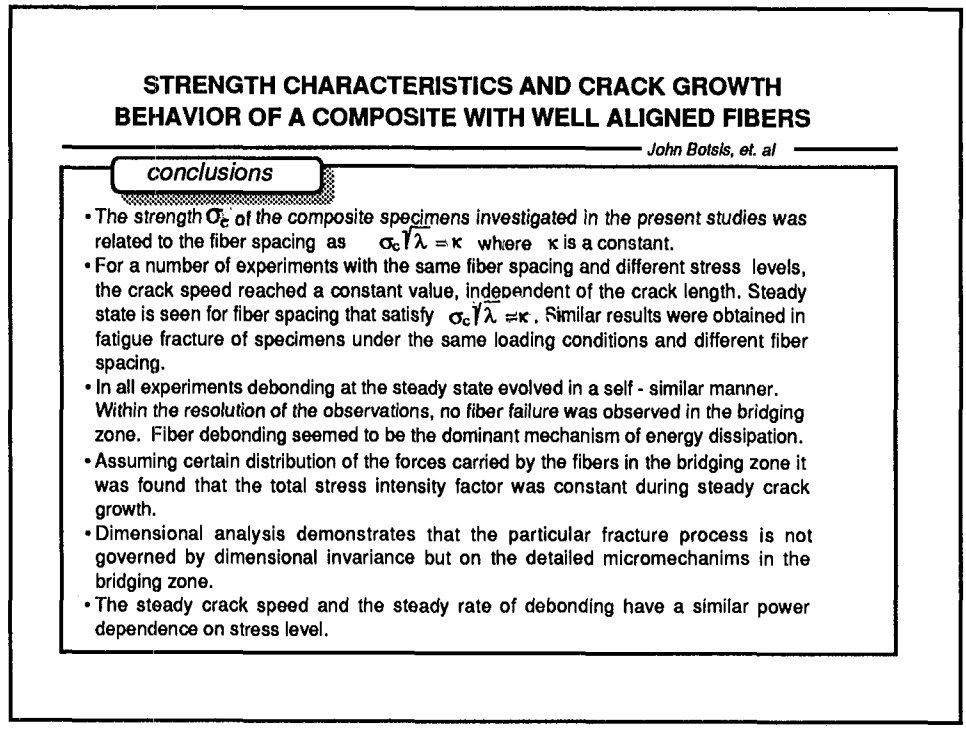

- **Steady state is the result of a balance between the energy available for the process and the energy required for process. It takes place when the boundary conditions and microstructure prevent the system from reaching equilibrium. Thus, the system settles down to a steady state. In the particular case investigated herein, a steady state is manifested by the constancy of the crack speed and rate of debonding.**
- **The steady state of crack growth and debonding suggested a form of self - similarity in space and time and the existence of certain stabilization processes in fracture of the composite material investigated in this work.**
- **The results of the present studies demonstrate that a steady fracture process in composites is an important physical phenomenon that needs to be fully understood and characterized. In the particular fracture process reported herein, irreversible process occurred mostly behind the crack tip and across the entire crack length.**

Acknowledgment

The authors wish to acknowledge the financial support from the AFOSR under grant 92-J-0493.

Damage and Strength of Composite Materials: Trends, Predictions, and Challenges

T. Kevin O'Brien
Vehicle Structures Directorate
U.S. Army Research Laboratory
NASA Langley Research Center
Hampton, Virginia

ABSTRACT

Research on damage mechanisms and ultimate strength of Composite Materials relevant to scaling issues will be addressed. The use of fracture mechanics and Weibull Statistics to predict scaling effects for the onset of isolated damage mechanisms will be highlighted. The ability of simple fracture mechanics models to predict trends that are useful in parametric or preliminary design studies will be reviewed. The limitations of these simple models for complex loading conditions will also be noted. The difficulty in developing generic criteria for the growth of these mechanisms needed in progressive damage models to predict strength will be addressed. A specific example for a problem where failure is a direct consequence of progressive delamination will be explored. A Damage Threshold/Fail-safety concept for addressing composite damage tolerance will be discussed.

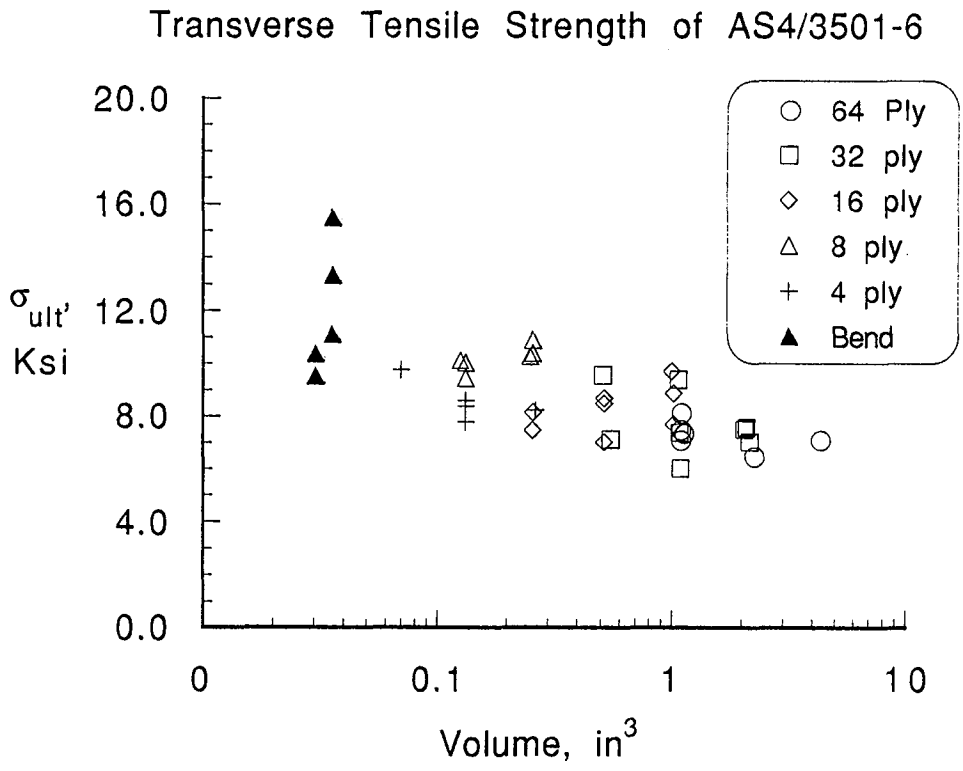

WEIBULL SCALE LAW

$$\frac{(\sigma_{ult})_1}{(\sigma_{ult})_2} = \left(\frac{V_2}{V_1}\right)^{1/m}$$

Where **V = Volume Stressed**

σult = Strength

m = Shape Parameter

WEIBULL STRENGTH DISTRIBUTION

$$P(\sigma) = 1 - \exp^{-\left(\frac{\sigma}{\sigma_c}\right)^m}$$

Where $P(\sigma)$ = Probability of failure at stress level, σ

σ_c = Characteristic Strength

m = Shape Parameter

which yields

$$\ln\left[\ln\left(\frac{1}{1-P(\sigma)}\right)\right] = m \ln\sigma + b$$

where

$$b = -m \ln\sigma_c$$

and for a median ranking of data from i to n

$$P(\sigma) = \frac{(i-1) + 0.7}{n + 0.4}$$

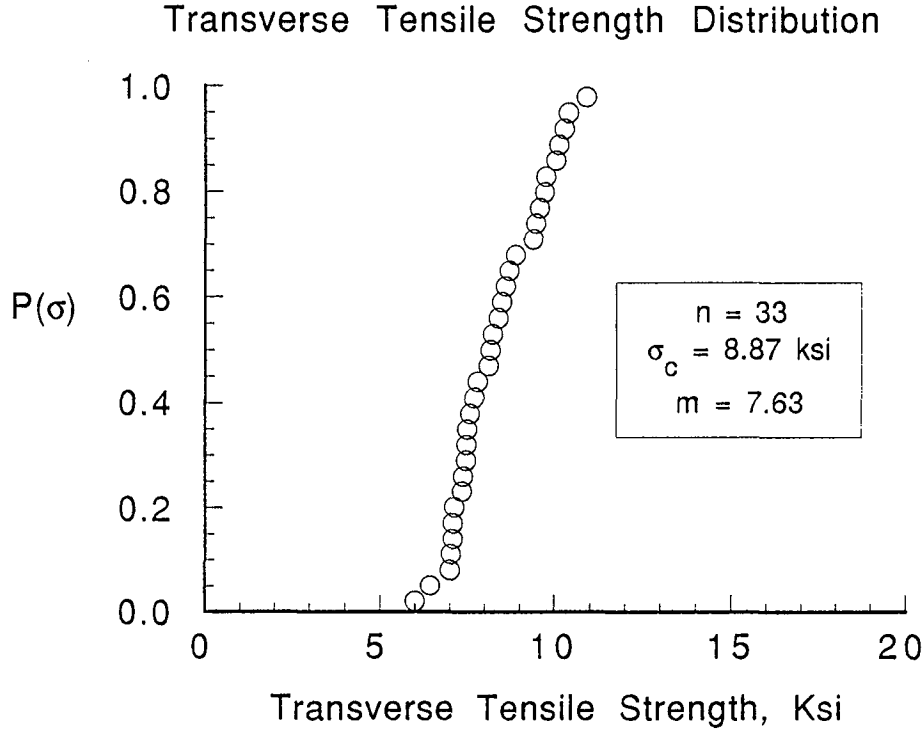

LOCAL VOLUME IN THREE POINT BEND TESTS

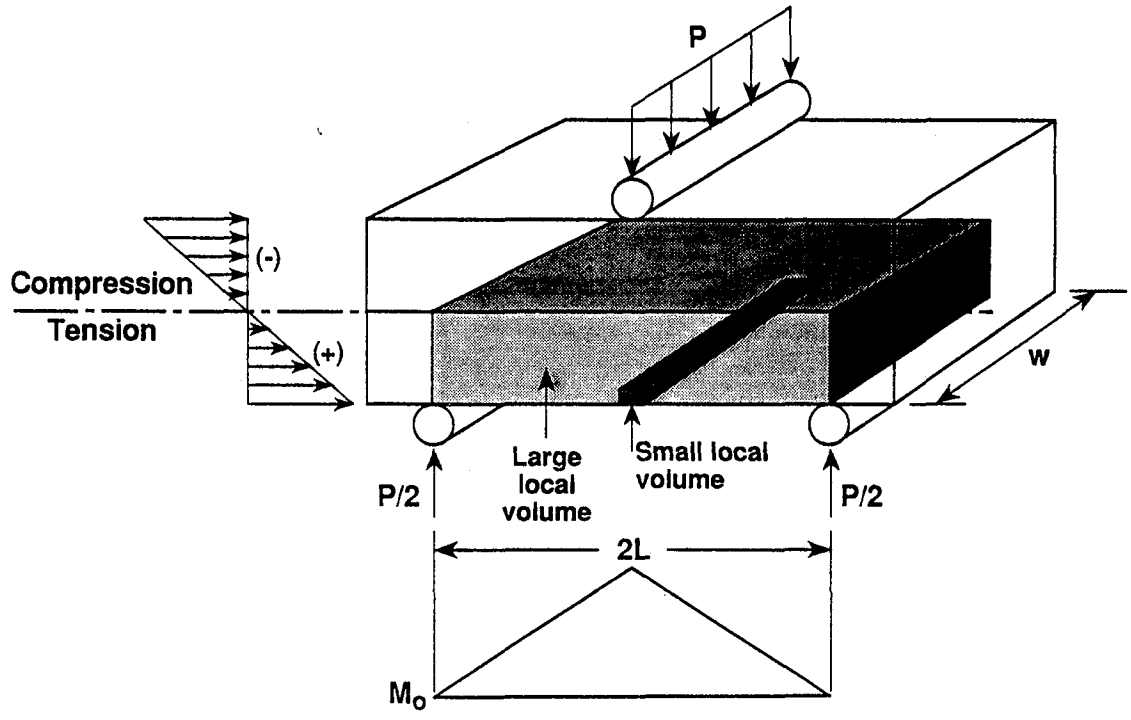

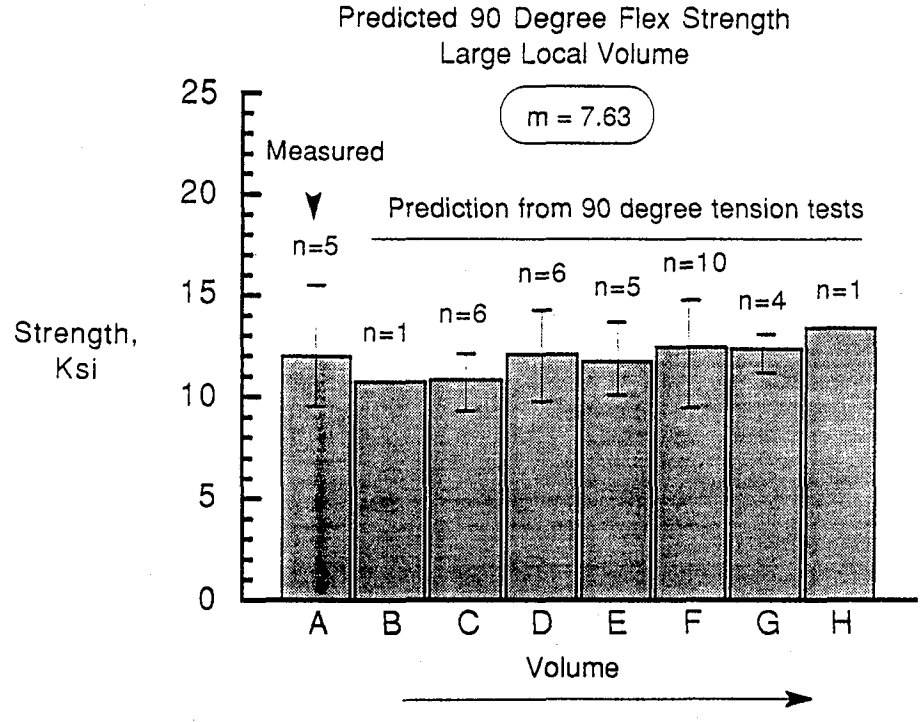

ANALYSIS OF IN-PLANE LAMINA STRESSES

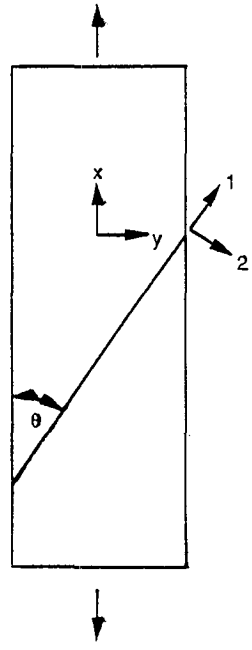

- IN-PLANE STRESSES CALCULATED IN -θ DEGREE PLIES OF $(0/\theta/-\theta)_S$ GRAPHITE EPOXY LAMINATES
- IN-PLANE STRESSES TRANSFORMED INTO LAMINA COORDINATE SYSTEM
- σ_{22} AND τ_{12} CALCULATED
  - IN LAMINATE INTERIOR (LPT)
  - NEAR FREE EDGE (Q3D FEM)

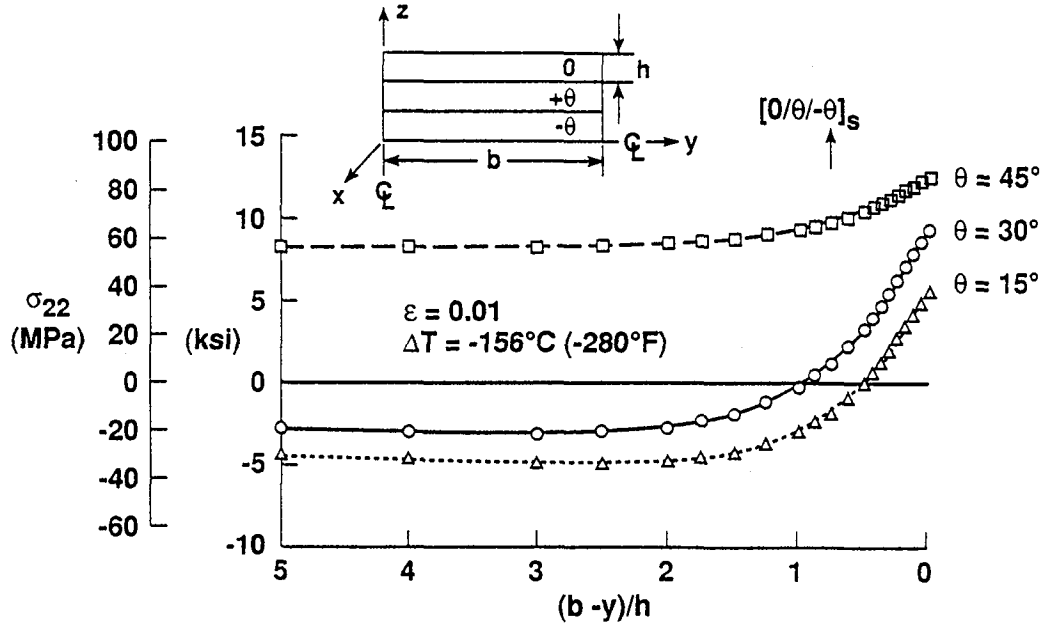

In-plane normal stress near the free edge of the -θ degree ply in $[0/\theta/-\theta]_S$ graphite epoxy laminate.

SOURCES OF DELAMINATION IN UNNOTCHED LAMINATES

EDGE DELAMINATION

$$G = \frac{\varepsilon^2 t}{2}\left(E_{lam} - E^*\right)$$

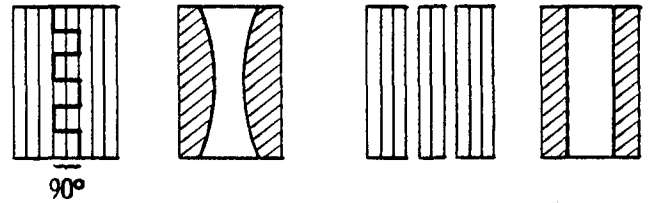

LOCAL DELAMINATION FROM MATRIX CRACKS

$$G = \frac{P^2}{4w^2}\left[\frac{1}{E_{LD}\,t_{LD}} - \frac{1}{E_{lam}\,t}\right]$$

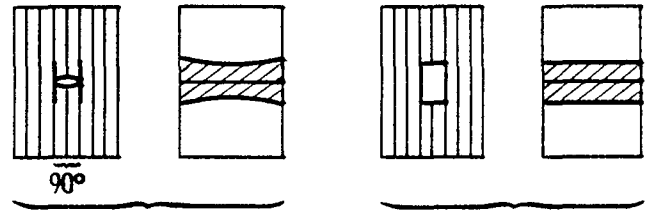

SCHEMATIC OF FRACTURE SEQUENCES IN $[\pm 25/90_n]_s$ LAMINATES

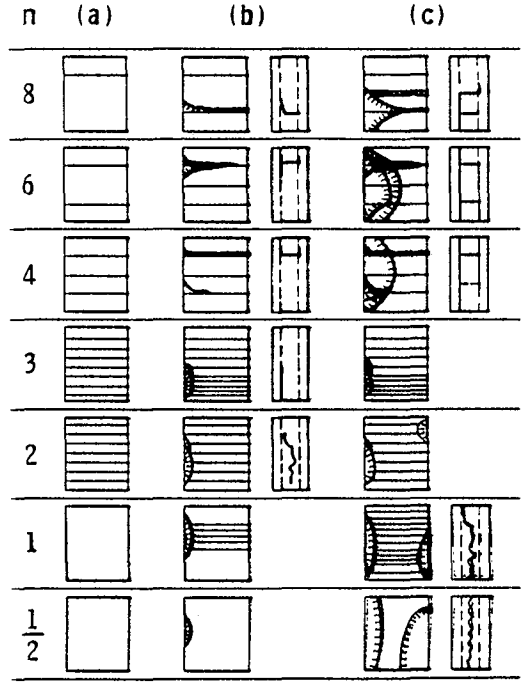

DELAMINATION ONSET IN $[\pm 25/90_n]_s$ LAMINATES

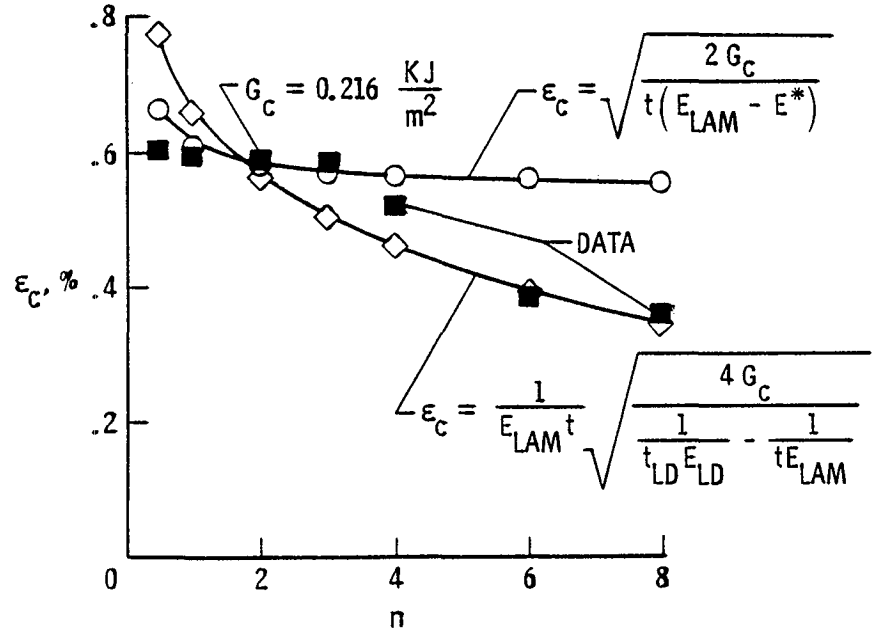

DELAMINATION FRACTURE MODES

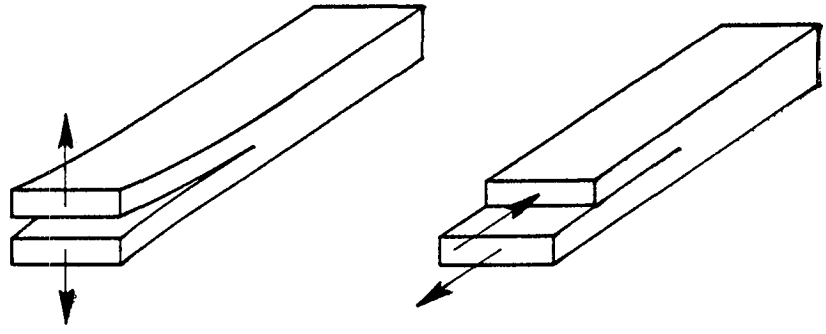

MODE I

INTERLAMINAR TENSION

MODE II

INTERLAMINAR SHEAR

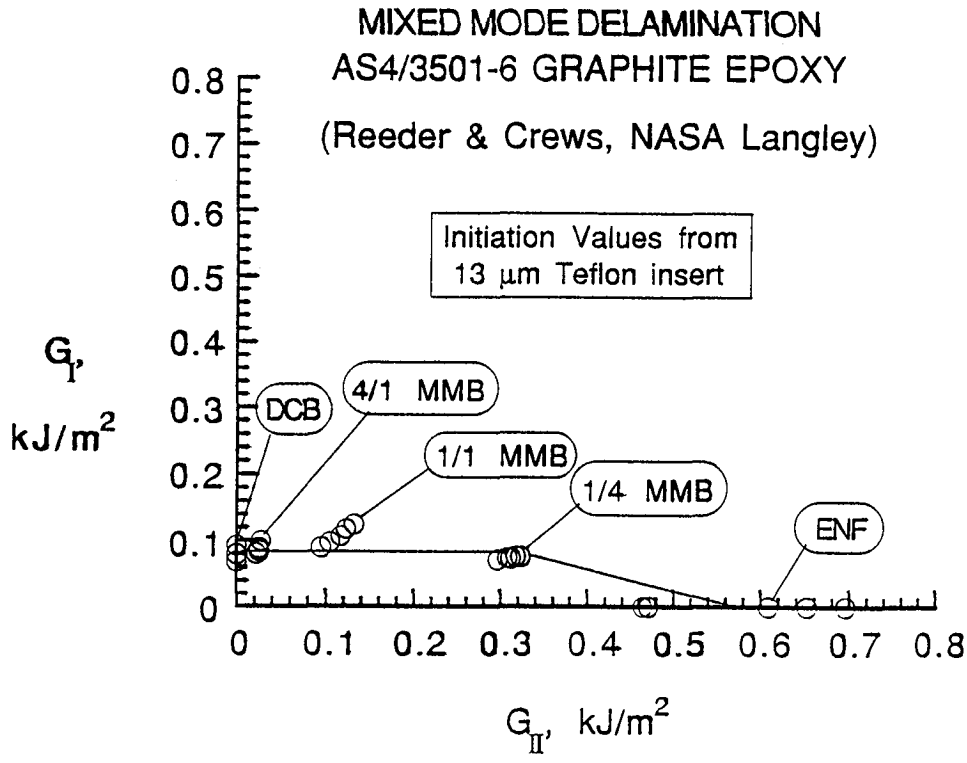
MIXED MODE DELAMINATION
AS4/3501-6 GRAPHITE EPOXY
(Reeder & Crews, NASA Langley)
Initiation Values from
13 μm Teflon insert
DCB
4/1 MMB
1/1 MMB
1/4 MMB
ENF
G_I, kJ/m^2
G_{II}, kJ/m^2
0.8
0.7
0.6
0.5
0.4
0.3
0.2
0.1
0
0 0.1 0.2 0.3 0.4 0.5 0.6 0.7 0.8

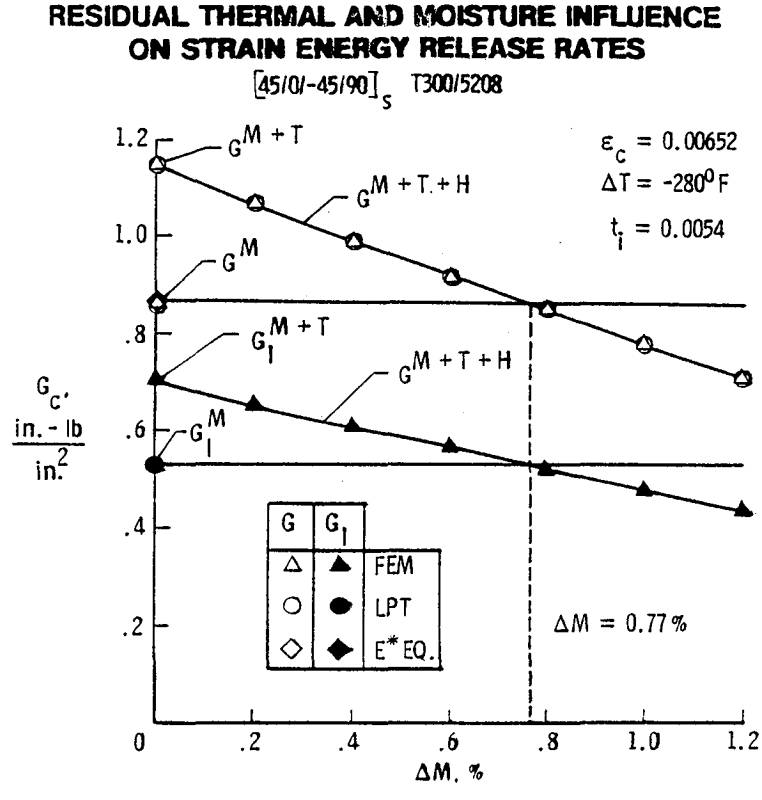
RESIDUAL THERMAL AND MOISTURE INFLUENCE
ON STRAIN ENERGY RELEASE RATES
$[45/0/-45/90]_S$ T300/5208
G^{M+T}
G^{M+T+H}
G^M
G_I^{M+T}
G_I^{M+T+H}
G_I^M
$\varepsilon_c = 0.00652$
$\Delta T = -280^0$F
$t_i = 0.0054$
G_c, in.-lb/in.^{2}
G | G_I
FEM
LPT
E* EQ.
$\Delta M = 0.77\%$
1.2
1.0
.8
.6
.4
.2
0 .2 .4 .6 .8 1.0 1.2
ΔM, %

EFFECT OF RESIDUAL THERMAL AND MOISTURE ON THE MIXED-MODE STRAIN ENERGY RELEASE RATE PERCENTAGE

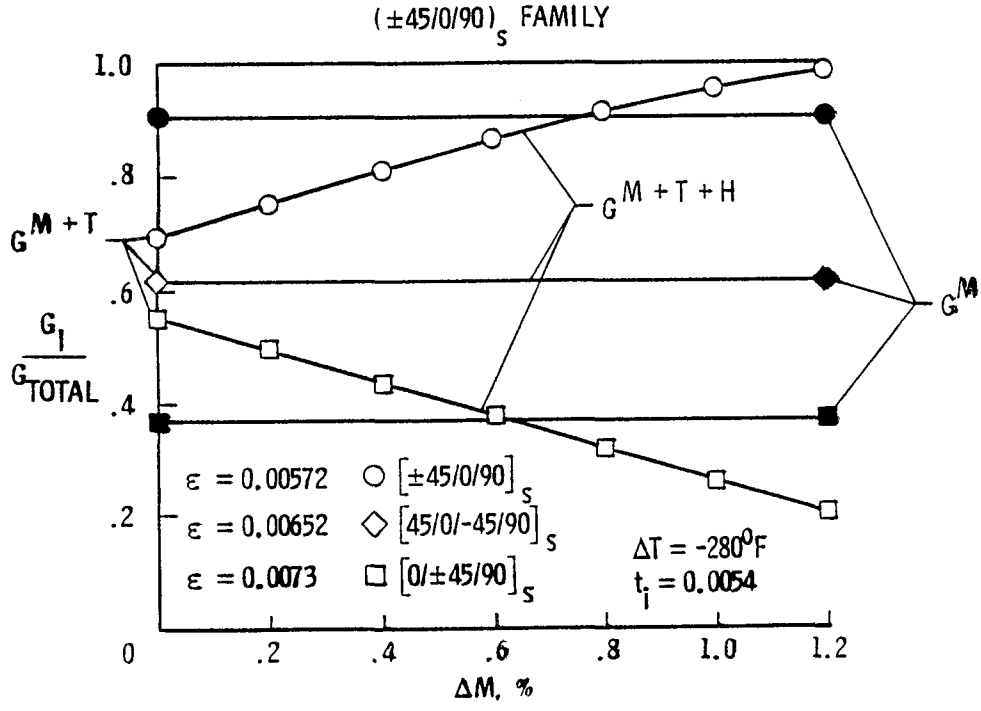

SKETCH OF RADIOGRAPH & MICROGRAPH SHOWING DELAMINATION IN θ/-θ INTERFACE OF $(0_2/\theta_2/-\theta_2)_S$ LAMINATE

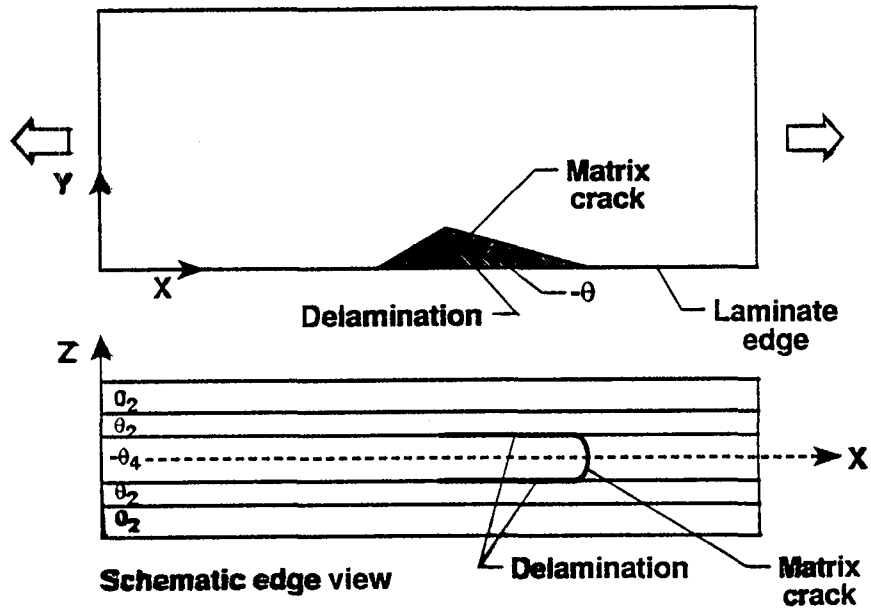

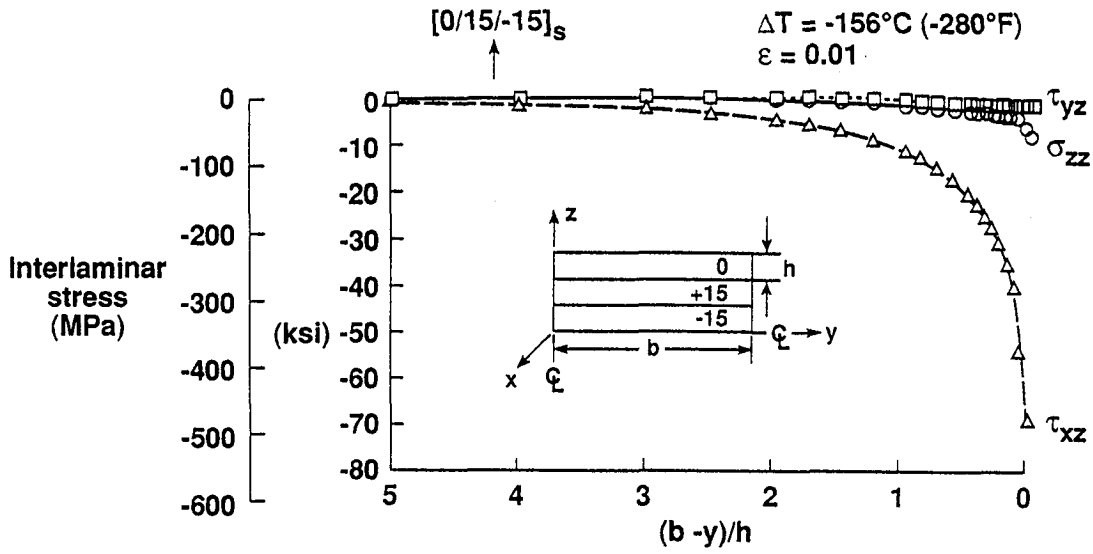

Interlaminar stresses near the free edge in the 15/-15 interface of a $[0/15/-15]_S$ graphite epoxy laminate.

NORMALIZED INTERLAMINAR NORMAL STRESS IN 15/-15 INTERFACE DUE TO MATRIX CRACK IN -15 PLY OF $(0/15/-15)_S$ LAMINATE

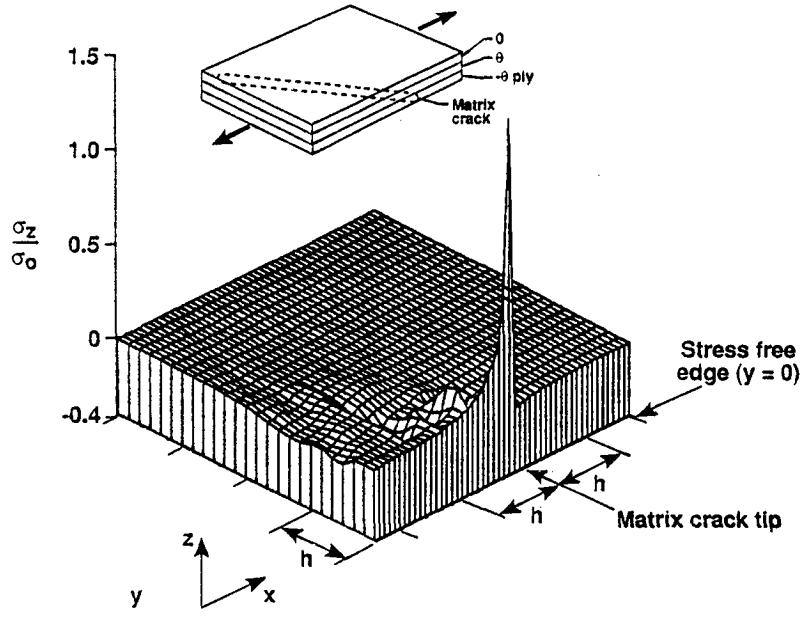

SCHEMATIC OF STAIRCASE DAMAGE PATTERN FOR AN IMPACTED COMPOSITE PLATE

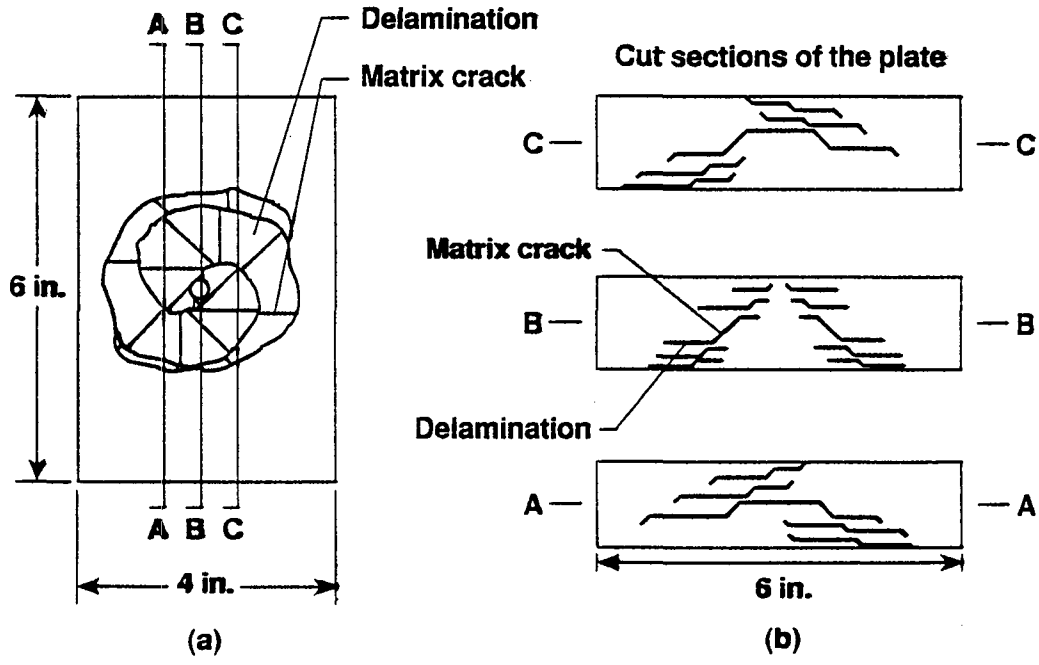

ANALYSIS OF DELAMINATION IN CROSS PLY LAMINATES INITIATING FROM IMPACT INDUCED MATRIX CRACKING

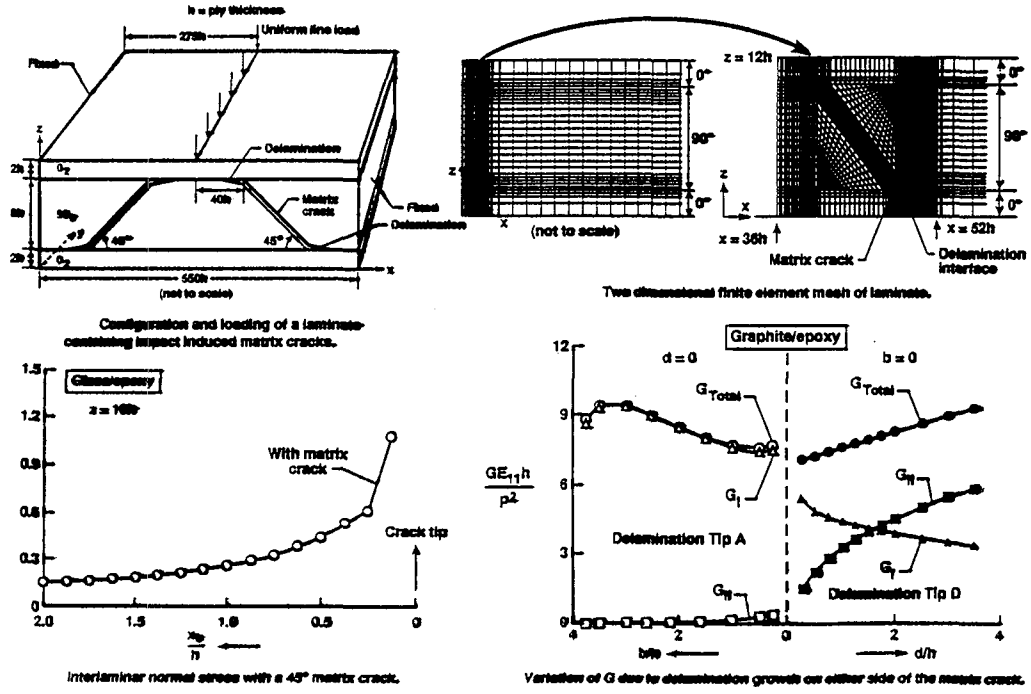

STRAIN ENERGY RELEASE RATE FOR LOCAL DELAMINATION ONSET

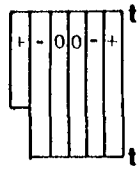

$$G = \frac{\sigma^2 t_{LAM}^2}{2} \left(\frac{1}{E_{LD} t_{LD}} - \frac{1}{E_{LAM} t_{LAM}} \right)$$

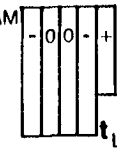

Under constant σ_{MAX}, as local delaminations accumulate through-the-thickness, G changes for each case.

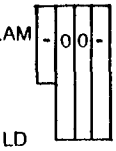

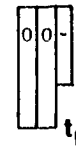

$\therefore$ <u>for the l^{th} case</u>

$$G_l(N) = m \log N_l + G_c = \frac{\sigma_{MAX}^2 t_{LAM}^2}{2} \left(\frac{1}{t_{LD} E_{LD}} - \frac{1}{t_{LAM} E_{LAM}} \right)_l$$

LOCAL STRAIN CONCENTRATIONS DUE TO DELAMINATIONS FROM MATRIX CRACKS

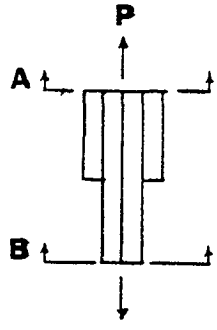

From equilibrium $P_A = P_B = P$

From Hooke's law $P = EA\varepsilon$ where A = wt

$$\therefore K_\varepsilon = \frac{\varepsilon_B}{\varepsilon_A} = \frac{E_A t_A}{E_B t_B}$$

Section A ~ undamaged laminate (LAM)

Section B ~ locally delaminated region (LD)

$$\therefore K_\varepsilon = \frac{t_{LAM} E_{LAM}}{t_{LD} E_{LD}}$$

Typically $E_{LD} > E_{LAM}$

$t_{LD} < t_{LAM}$

LOCAL STRAIN CONCENTRATIONS DUE TO THROUGH-THE-THICKNESS ACCUMULATION OF LOCAL DELAMINATIONS $[\pm 45/0]_S$ E-GLASS EPOXY X751/50

Case	1	2	3	4
	+45/-45 interface +	+45/-45 interface +	-45/0 interface +	-45/0 interface
Through-thickness condition	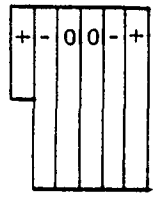	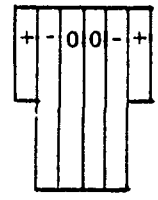	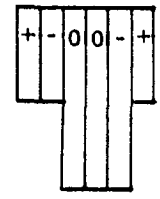	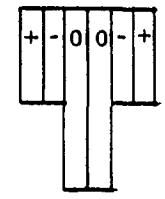
K_ε	1.119	1.281	1.473	1.729

FATIGUE LIFE PREDICTION $[\pm 45/0]_S$ GRAPHITE/GLASS EPOXY HYBRID

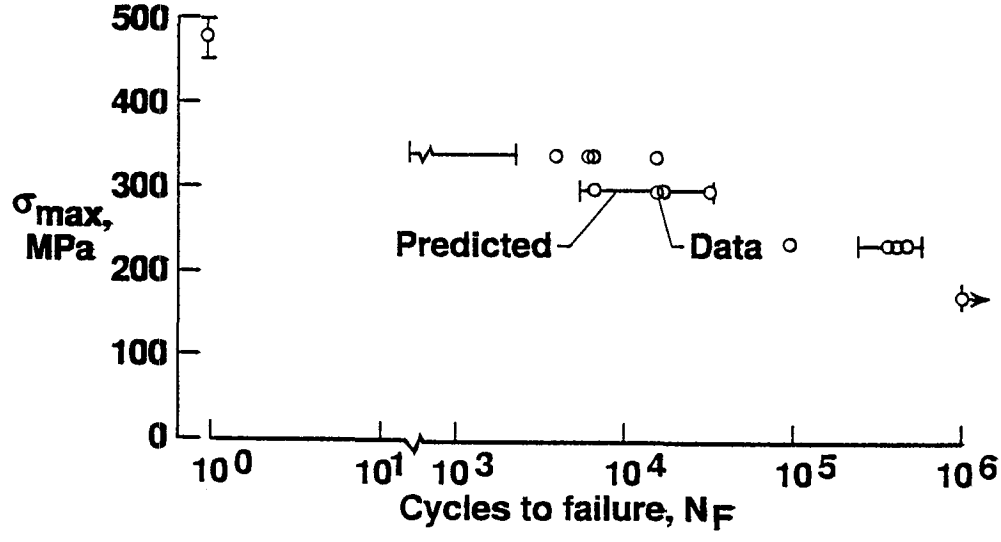

CONCLUSIONS

I. Composite strength can be predicted with scaling laws if

   A) A single damage mechanism is responsible for ultimate failure

   B) All loadings (thermal, mechanical, hygroscopic) and stress components (tension and shear) responsible for this damage mechanism are considered

II. For composite materials and structures, ultimate failure typically results from a progression of damage events

III. Progressive damage models must be developed to achieve composite strength scaling, requiring:

   A) Determination of damage sequence

   B) Incorporating the influence of internal stress free boundaries due to matrix cracking and delamination

   C) Determination of load redistribution as damage progresses

MATERIAL PROPERTIES, FAILURE AND DAMAGE MECHANICS

Session II

Felton Bartlett, Moderator

EFFECTS OF PLY THICKNESS ON THERMAL CYCLE INDUCED DAMAGE AND THERMAL STRAIN

Stephen S. Tompkins
Materials Division
NASA Langley Research Center
Hampton, VA 23681-0001

Abstract

An experimental study was conducted to determine the effects of ply thickness in composite laminates on thermally induced cracking and changes in the coefficient of thermal expansion, CTE. A graphite-epoxy composite material, P75/ERL 1962, in thin (1 mil) and thick (5 mils) prepregs was used to make cross-ply laminates, $[(0/90)_n]_s$, with equal total thickness (n=2, n=10) and cross-ply laminates with the same total number of plies (n=2). Specimens of each laminate configuration were cycled up to 1500 times between -250°F and 250°F. Thermally induced microdamage was assessed as a function of the number of cycles as was the change in CTE. The results showed that laminates fabricated with thin-plies microcracked at significantly different rates and reached significantly different equilibrium crack densities than the laminate fabricated with thick-ply and n=2. The CTE of thin-ply laminates was less affected by thermal cycling and damage than the CTE of thick-ply laminates. These differences are attributed primarily to differences in interply constraints. Observed effects of ply thickness on crack density was qualitatively predicted by a combined shear-lag stress/energy method.

OUTLINE

- Background
- Study objective
- Materials and test procedures
- Experimental results
- Analytical results
- Summary of Findings

REQUIREMENTS FOR HIGH PRECISION SPACECRAFT

- High stiffness
- Low thermal expansion
- Low weight
- Long life
- Predictable and acceptable end-of-life properties
- Environmental durability

EFFECTS OF THE THERMAL CYCLING ENVIRONMENT

- Most all spacecraft subjected to thermal cycling
  - Temperature ranges from -265^{O}F to 250^{O}F
  - Lifetime exposures up to 30 years (175,000 cycles)

- Thermal cycling can induce damage in high stiffness Gr/Ep composites
  - Damage accumulation can affect material properties

- Thin-ply material is of interest for weight savings
  - Current experience largely for thick-ply composites
  - Ply thickness affects composite laminate properties and behavior

STUDY OBJECTIVE

- Determine the effects of ply thickness on the damage induced by thermal cycling and the resulting changes in the thermal expansion behavior of polymer composites for space applications.

The standard 5-mil prepreg used to fabricate composite laminates is being replaced by thinner, 1- to 3-mil, prepreg in many material designs for additional weight savings (ref. 1 and 2) in space structures. The comparative properties and performance of laminates fabricated from the thinner prepreg and those fabricated with the standard thickness prepreg are fundamental questions that must be addressed as materials are replaced.

The properties and response to mechanical loads of composite laminates with different ply thicknesses have been found to be different (refs. 3-5). Laminates with the same materials and configuration but fabricated with different ply thicknesses do not have the same mechanical properties. While the stiffnesses are the same for the two materials, the transverse strengths are significantly different. This was attributed to both a material volume effect, ref. 4, and a ply constraint effect, ref. 6.

Reference 5 established that damage induced by mechanical fatigue is dependent upon laminate thickness. Reference 7 showed similar results for high modulus fibers subjected to limited thermal fatigue. The difference in the induced damage has been attributed to differences in inter-ply constraints, where the constraint was highest within thin ply laminates.

The objective of this study was to investigate the effects of ply thickness on thermally induced microdamage and the resulting changes in the CTE after a large number of thermal cycles. A high modulus continuous graphite fiber composite material, representative of spacecraft materials, was used in this study.

SCHEMATIC DIAGRAM OF $[(0/90)_n]_s$ LAMINATES

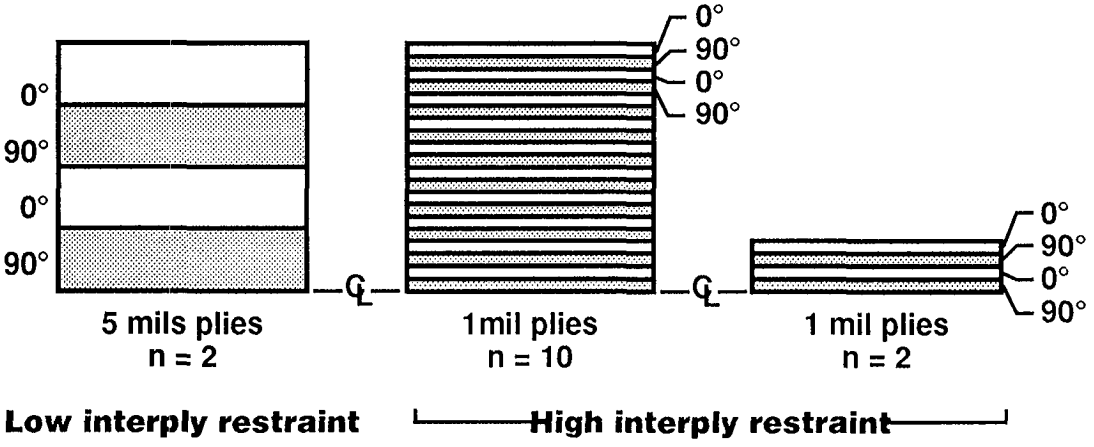

This figure shows schematic diagrams of the $[(0/90)_n]_s$ laminates of P75/ERL 1962 graphite epoxy composite material used in this study. Laminates were fabricated using 5-mil plies with n=2 and using 1-mil plies with n=10 and n=2. This resulted in laminates with the same total thickness (n=2 and n=10), but with different ply thicknesses, and laminates with the same total number of plies (n=2).

PHOTOMICROGRAPHS OF $[(0/90)_n]_s$ LAMINATES

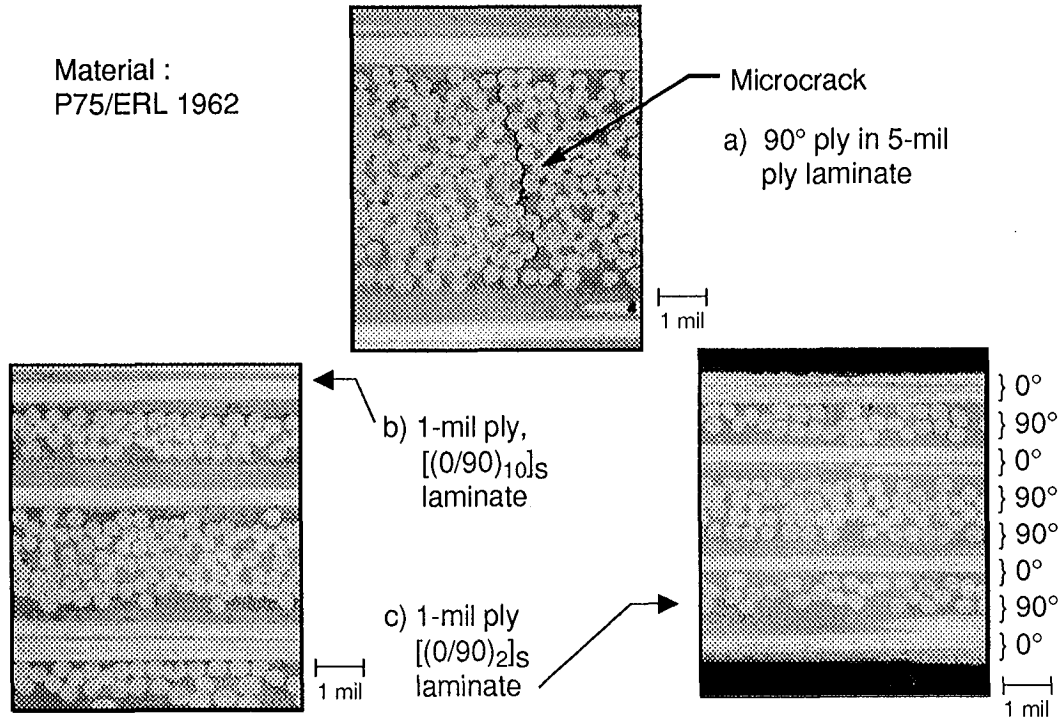

Photomicrographs of the cross section of each of the laminates tested are shown in this figure. The percent fiber volume contents of the laminates made with the thick- and thin-plies were about 53% and 58% respectively. Figure (a) shows a microcrack in the 5-mil ply laminate after 10 thermal cycles. For this study, a microcrack was counted only if the crack extended at least half way across the thickness of a ply. Also, only cracks in the middle two 90^{o} plies were counted. The specimens in photomicrographs (b) and (c) were in the as-fabricated condition. Microcrack densities, number/inch, were determined by counting microcracks over the middle inch along the polished edge using an optical microscope at a magnification of 400X.

SCHEMATIC DIAGRAM OF THERMAL CYCLING CHAMBER AND TYPICAL TEMPERATURE HISTORY

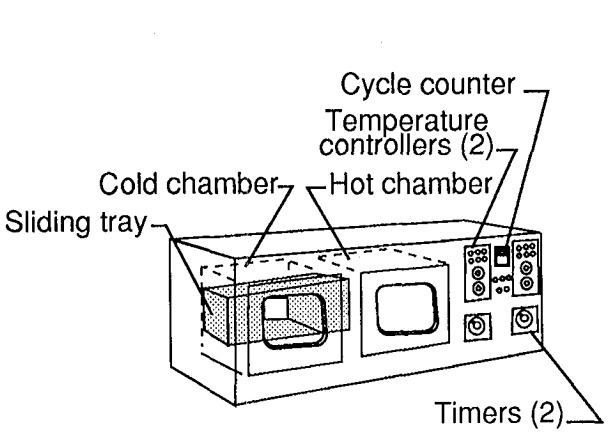

a) Thermal cycling chamber

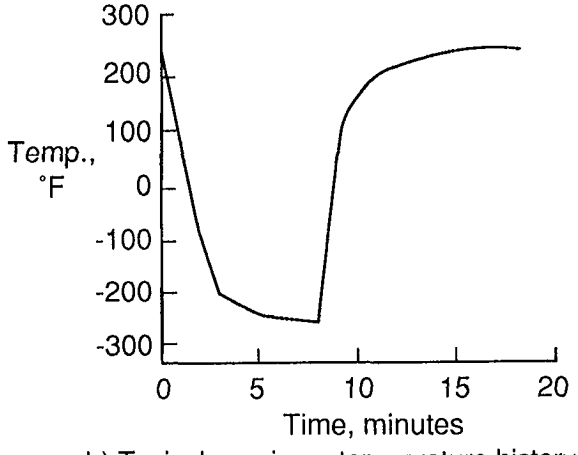

b) Typical specimen temperature history

A schematic diagram of the thermal cycling apparatus used for this study is shown in figure (a). The apparatus consists of a hot chamber heated with electric resistance heaters and an adjacent cold chamber cooled with liquid nitrogen. Specimens were moved from the hot to the cold chamber on a sliding tray. A typical temperature history of a specimen during a cycle between 250^{o}F to -250^{o}F is shown in figure (b).

MICROCRACK DENSITY IN $[(0/90)_n]_S$ LAMINATES

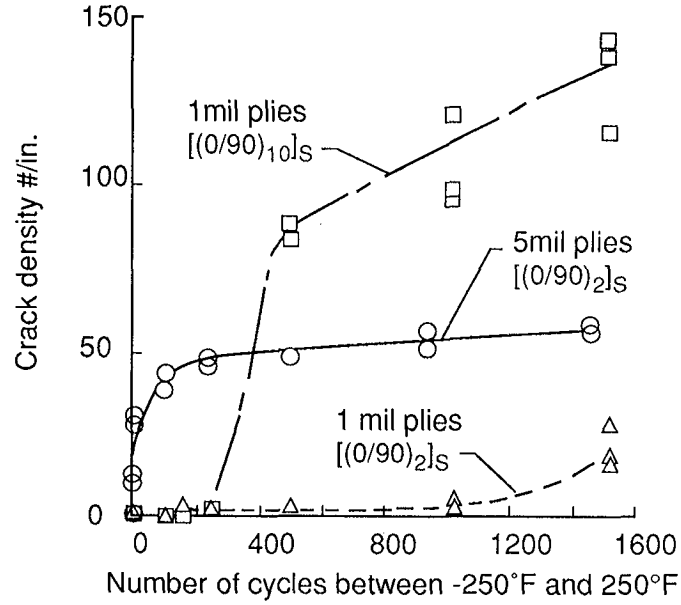

This figure shows the change in the crack densities of the middle 90^o plies in each of the laminates tested. The 5-mil ply laminate cracked as soon as cycling began and reached a near plateau at about 50 cracks/inch after about 200 cycles. The thin-ply laminates behaved very differently. The thin-ply laminate with n=10 did not begin microcracking until after about 200 cycles, then cracks formed very rapidly. This laminate reached a crack density of about 140 cracks/inch after about 1550 cycles and still had a high crack density increase rate. The thin-ply with n=2 had less than 5 cracks/inch even after about 1000 cycles. The density reached about 20 cracks/inch after about 1500 cycles.

The large differences in the crack densities in the thin- and thick-ply laminates are attributed to the fact that the thin plies are more constrained by adjacent plies than the thick plies. This restricts the straining of the plies which resulted in a high stress required for cracking and delayed crack initiation. The constraint also does not allow the stress relief by cracking to extend far from the crack as in the thicker plies, thus resulting in a higher crack density. The difference in the cracking in the two thin-ply laminates is not understood and is under investigation.

THERMAL EXPANSION BEHAVIOR AFTER THERMAL CYCLING $[(0/90_2]_S$

5-mil Ply

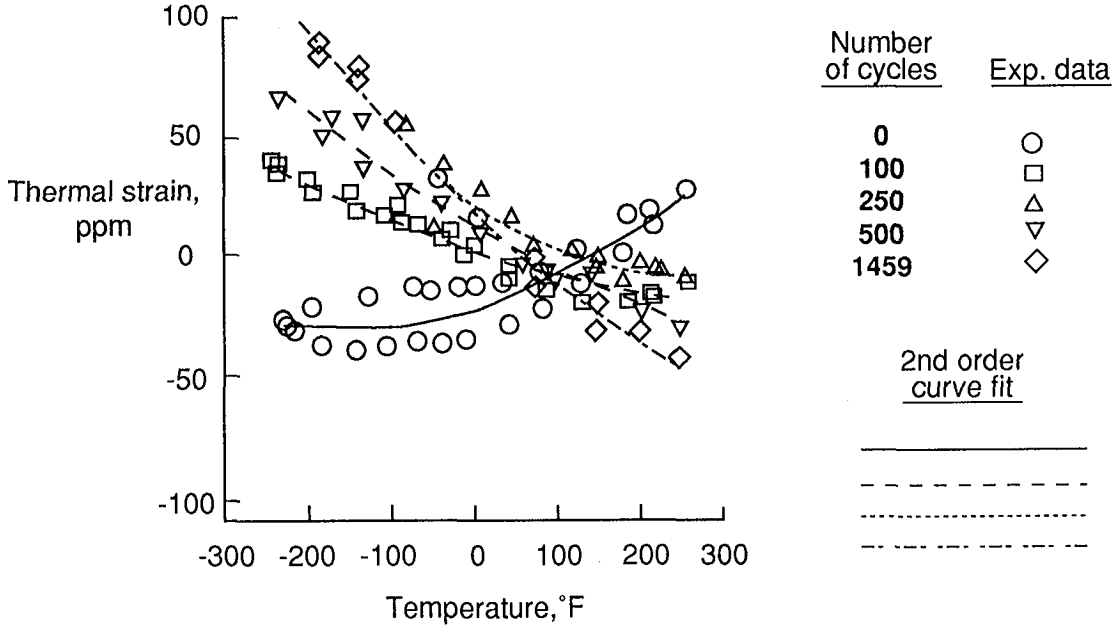

This figure shows the thermal expansion of the P75/ERL 1962 $[(0/90)_2]_S$ 5-mil laminate before and after thermal cycling. As the crack density increases, the thermal expansion becomes dominated by the 0^o plies of the laminate. The thermal expansion of the laminate approached that of the unidirectional laminate.

RESIDUAL CTE FOR $[(0/90)_n]_s$ LAMINATES

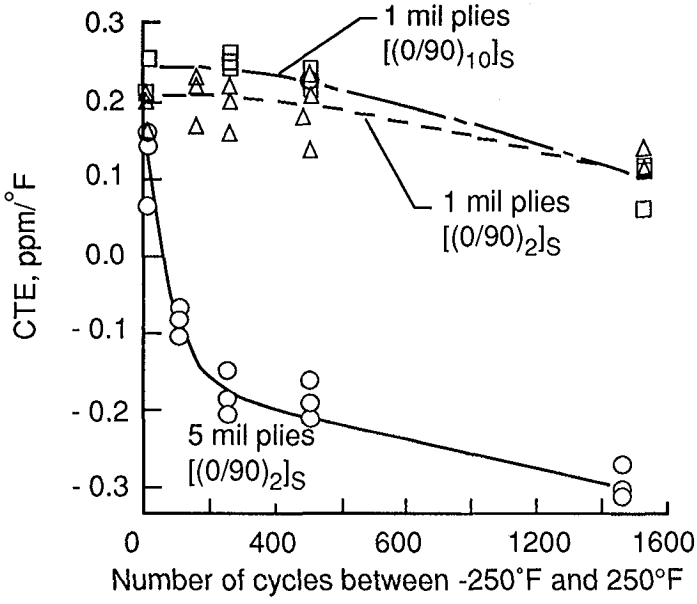

The effects of thermal cycling on the CTE of the thick- and thin-ply laminates are shown in this figure. For the thick-ply laminate, the CTE changes from a positive value to a negative value and approaches the longitudinal lamina value of -0.531 ppm/^{o}F. The CTEs of both of the thin-ply laminates, however, were not significantly changed after 500 cycles even though the crack density in the thin-ply, n=10, was very large. The near constant CTEs were attributed to the constraint of the cracked plies imposed by the adjacent plies. As thermal cycling continued, the crack density increased and the effects of the constraining adjacent plies were reduced. This resulted in a decrease in the CTE in all of the laminates. After about 1500 cycles, both of the thin-ply laminates approached about the same value, 0.1 ppm/^{o}F, half of the initial value. The CTE of the thick-ply laminate also decreased but to an average value of -0.295 ppm/^{o}F, down from the value of -0.193 ppm/^{o}F at 500 cycles and the initial value of 0.111 ppm/^{o}F.

DEPENDENCE OF MICROCRACKING ON CTE OF $[(0/90)_n]_S$ LAMINATES

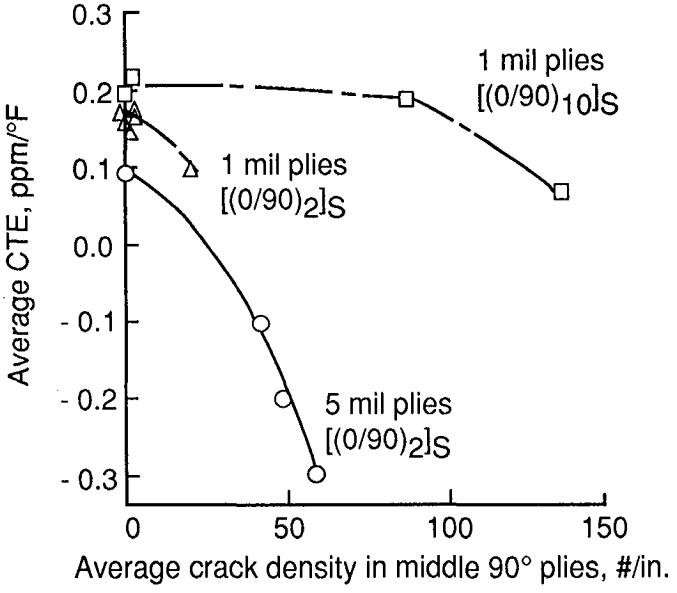

This figure shows the CTE of each of the laminates as a function of the microcrack density. These data seem to indicate that once microcracks begin to accumulate, the initial rates of change of CTE with microcracking are about the same for the thin- and thick-ply laminates with the same number of plies (n=2). The rate of change of the CTE with microcracking for the thin-ply laminate with n=10 is very small up to a crack density of about 90, after which the rate begins to increase.

ANALYTICAL MODEL

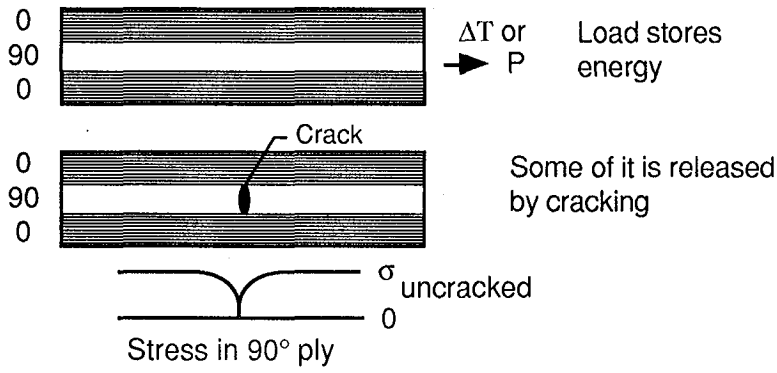

In central (90°) ply

- Crack forms if $\Delta G > G_c$
  (ΔG = Strain energy released)
- Compute ΔG using shear lag approximation of stress state with crack
- Critical strain energy varied as the transverse strength varied with thermal cycling

This figure shows a schematic of the analytical model developed in ref. 8 to predict transverse matrix cracks in a composite laminate subjected to cyclic thermal load. Shear lag stress approximations and a simple energy-based fracture criteria are used to predict crack density as a function of temperature. Predictions of crack density as a function of thermal cycling are accomplished by assuming that fatigue degrades the material's inherent resistance to cracking.

PREDICTED EFFECTS OF PLY THICKNESS AND THERMAL CYCLING ON CRACK DENSITY

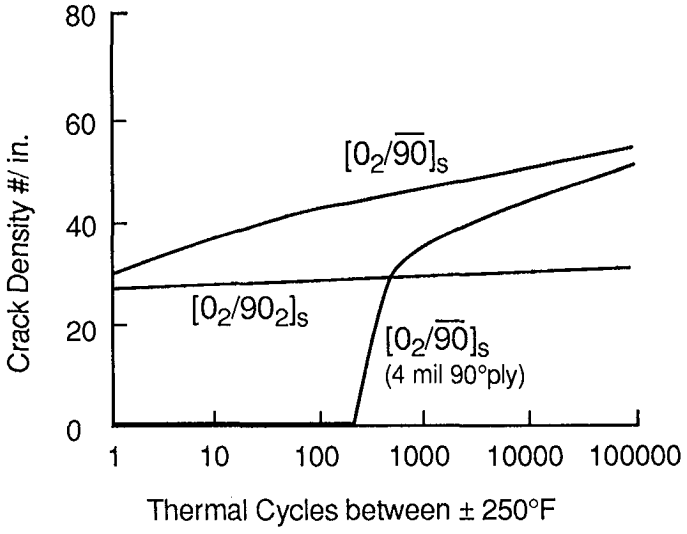

- Damage increases with cycling.
- No saturation limit.
- Smaller thickness delays initiation, more cracks.

This figure shows the effects of ply thickness and long term cycling on crack density. The amount of damage increases as the number of thermal cycles are increased. Also, note that none of the laminates reach an equilibrium crack level. As shown previously, the laminates with the thinner plies have a delayed crack initiation and ultimately a higher crack density as compared to the laminate with thicker plies.

PREDICTED EFFECTS OF PLY THICKNESS AND THERMAL CYCLING ON LAMINATE CTE

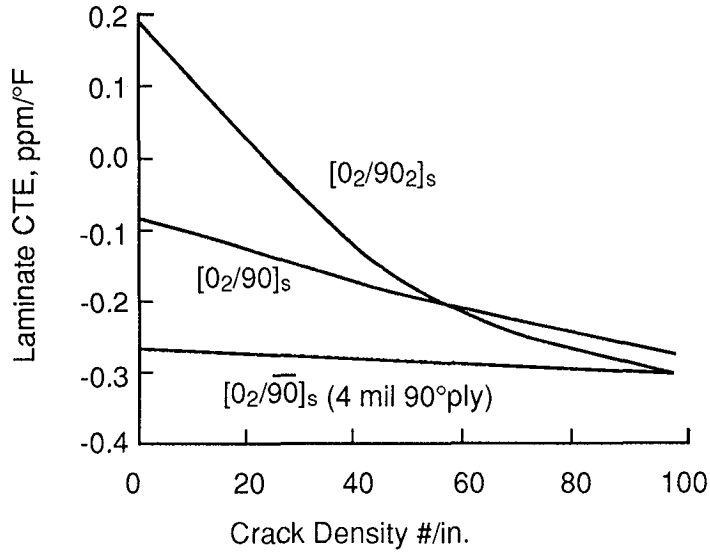

- Cracks significantly affect CTE
- Laminate CTE less affected for thin plies

These analytical data show that the effects of cracks on laminate CTE can be very significant. The CTE of the laminate with the thicker middle layer is much more sensitive to cracking than that of the thin-ply laminates.

SUMMARY OF FINDINGS

- Microcracking:
  - Onset of microcracking in thin-ply laminates delayed relative to thick- ply laminates
  - For equal total thicknesses, thin-ply laminates reach higher crack densities than thick-ply laminates

- Coefficient of thermal expansion:
  - CTE of thin-ply laminates less affected by thermal cycling than the CTE of thick-ply laminates

- Observed effects of ply thickness on crack density qualitatively predicted by a combined shear-lag stress/energy method

FUTURE PLANS

- Continue thermal exposures of thin-ply specimens.
- Apply analytical model to exposed laminate configurations.
- Extend analysis (under grant) to include angle-ply laminates.
- Determine range of applicability of results to several types of composite material systems.

References

1. Kulick, Shel (1992): Dimensionally Stable, Graphite-Fiber Reinforced Composite Mirror Technology. SPIE Vol. 1693 Surveillance Technologies II, pp. 313-317.

2. Kilpatrich, M. C. and Girard, J. D. (1992): Design of a Precise and Stable Composite Telescope Structure for the Ultraviolet Coronagraph Spectrometer (UVCS), SPIE Vol. 1690, Design of Optical Instruments pp. 197-215.

3. Kellas, S. and Morton, J. (1992): Scaling Effects in Angle-Ply Laminates. NASA CR-4423.

4. O'Brien, T. K. and Salpekar, S. A. (1992): Scale Effects on the Transverse Tensile Strength of Graphite Epoxy Composite. NASA TM 107637.

5. Crossman, F. W. and Wang, A. S. D. (1982): "The Dependence of Transverse Cracking and Delamination on Ply Thickness in Graphite/Epoxy Laminates". Damage in Composite Materials, ASTM STP 775, K. L. Reifsnider, Ed., American Society for Testing and Materials, pp. 118-139.

6. Kellas, Sotiris, et al (1993): Scaling Effects in Sublaminate-scaled Composite Laminates. AIAA 34th SDM Conference, La Jolla, CA. April 19-21, 1993.

7. Manders, P. W. and Maas, D. R. (1990): Thin Carbon Fiber Prepregs for Dimensionally Critical Structures. SPIE Proceedings Vol. 1303, Advances in Optical Structure Systems, pp. 536-545.

8. McManus, H. L.; Bowles, D. E.; and Tompkins, S. S. (1993): Prediction of Thermal Cycling Induced Matrix Cracking. Presented at the American Society for Composites 8th Technical Conference on Composite Materials, Cleveland, Ohio.

SCALING EFFECTS OF DEFECTS IN FIBER-REINFORCED COMPOSITES

A. S. D. Wang
Drexel University
Philadelphia, PA 19104

ABSTRACT

Material defects may be introduced willingly or unwillingly during material manufacturing and structural component fabrication stages. Their presence in the material plays a dominant role in determining the material's strength and the associate failure mechanisms. In the sense that the size and the number of defects may increase with the volume of the material, the effect of dimensional scaling may manifest itself in the dependence of material strength on volume. Or, alternatively, there may exist a scaling effect of material defects.

In fiber-reinforced composites, manufacturing or fabrication defects may come in several forms: matrix voids, matrix microcracks, fiber misalignment, broken fibers, interface disbonds, just to mention a few. These are interacting and competing defects in the sense that one type of defect may become dominant under one stress condition and another type of defect may become dominant under a different stress condition. This happens because the fiber reinforcement network, together with the distribution of defects, constitutes the prime microstructure of the composite, and there exist continued interactions between the evolving microstructure and the distribution of defects. In the process, the scaling effects of defects are complicated by this interaction.

In this presentation, the scaling effects of defects in fiber-reinforced composites will be briefly discussed with the introduction of the concept of effective defects. It is then shown with the aid of some actual experimental and analysis results that the scaling effects are very much present, but they are regulated by the characteristic dimension of the composite microstructure due to the aforementioned microstructure-defect interaction effect.

(Original photographs unavailable at time of publication)

SCALING EFFECTS ON MATERIAL STRENGTH IS AN AGE-OLD PROBLEM:

* The Griffith Experiment of 1920 - glass rods under tension (rods of constant length)

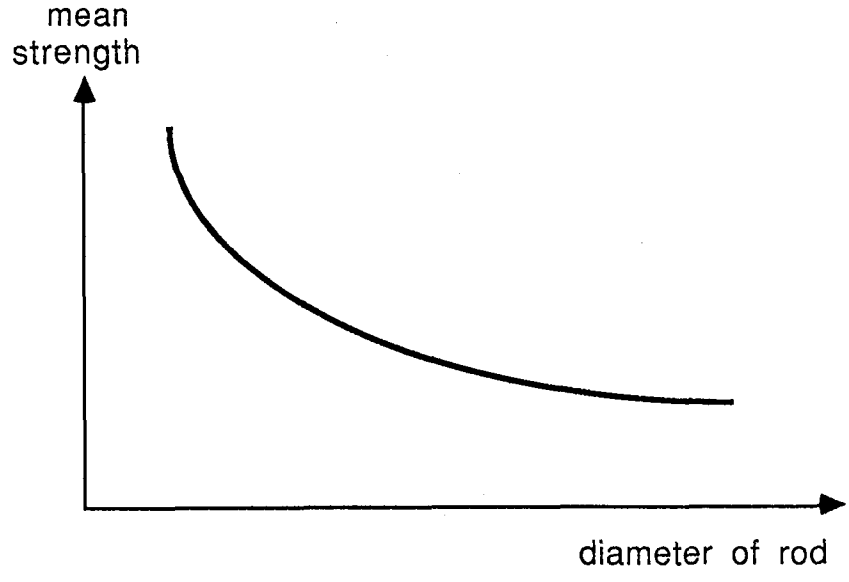

* The Weibull Experiment of 1939 - glass rods under tension (rods of const. diameter)

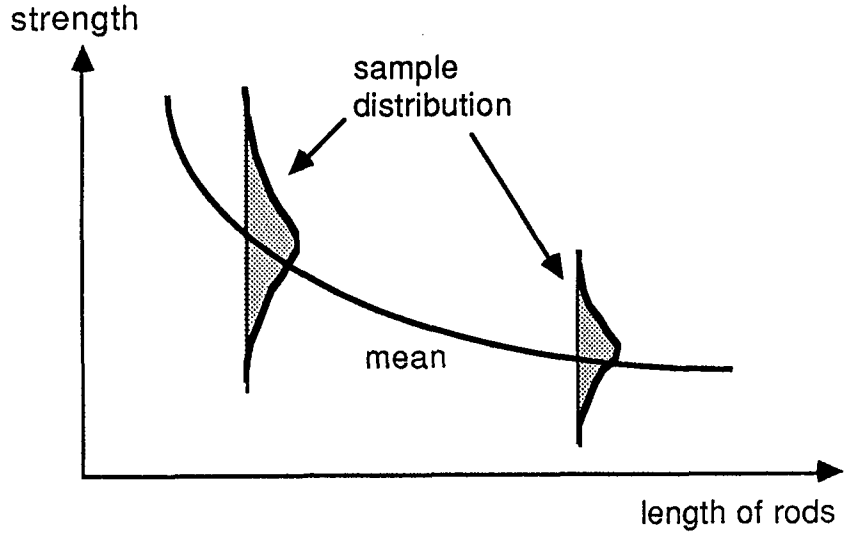

MATERIAL DEFECT WAS THE CULPRIT

- The fractured surface of a sample -
(due to Don Adams, 1974)

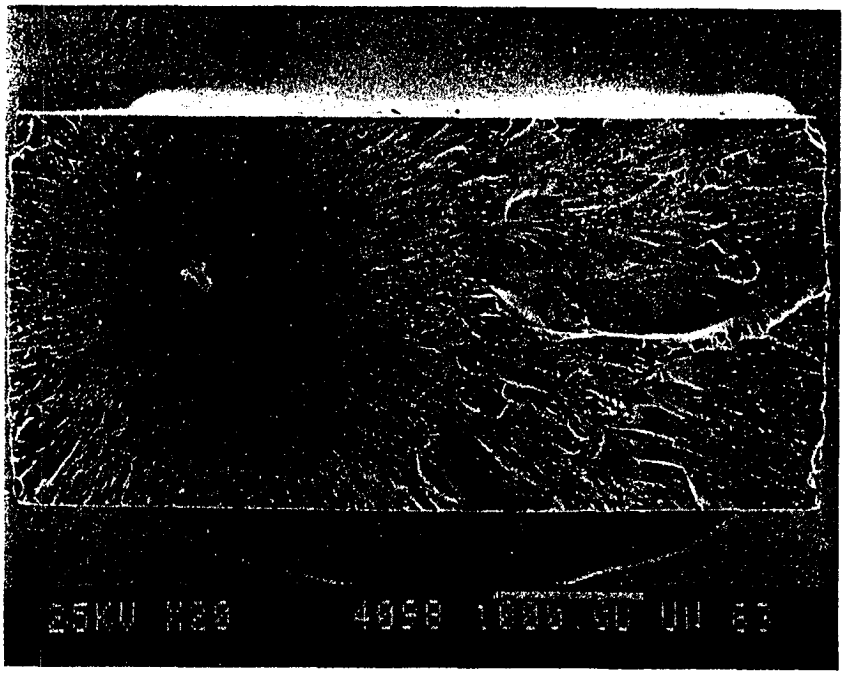

fractured surface of an epoxy rod at 20x

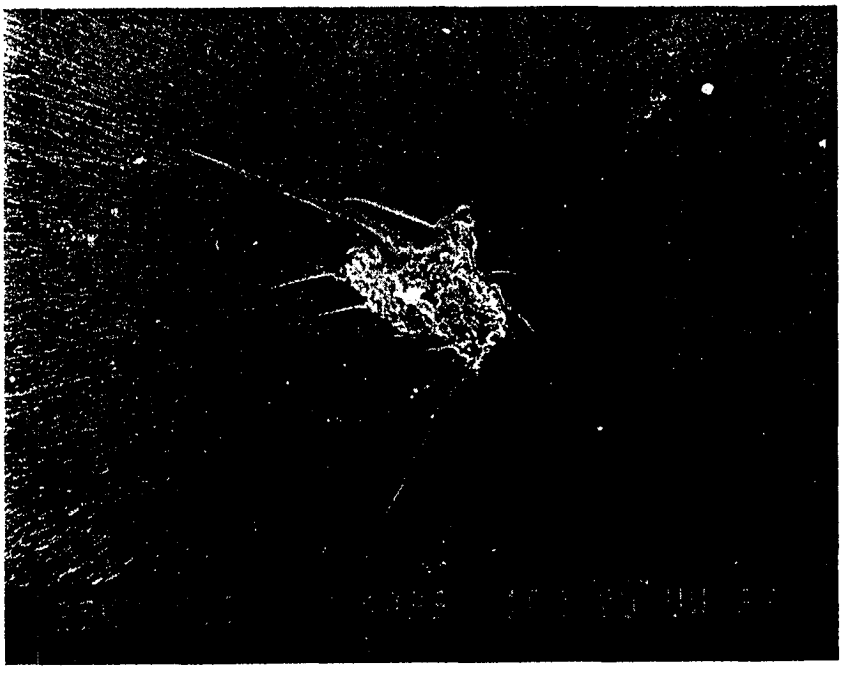

the same fractured surface at 100x

SCALING EFFECT ON FIBROUS COMPOSITES IS MORE THAN JUST DEFECTS

* The Rosen Experiment of 1964 - fiber breakage in matrix

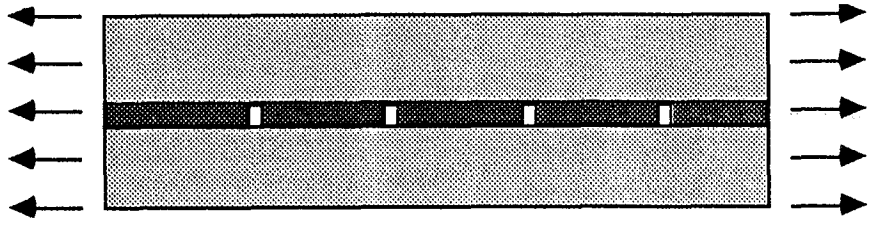

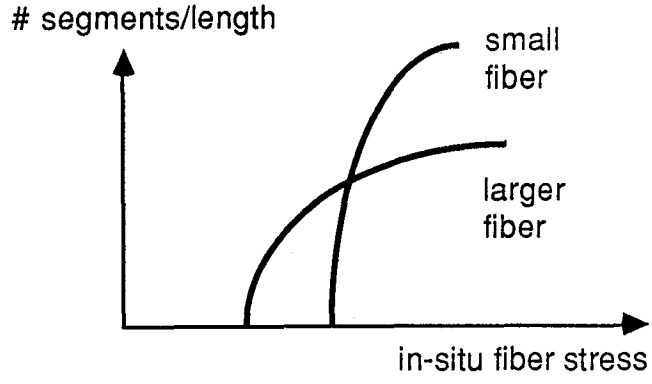

Added Factors:

1. Defects distribution along the fiber
2. Fiber-matrix interface bonding condition
3. Presence of residual stresses
4. Evolving effects of local failures

These are all integral parts of the composite microstructure.

Composites are a manifold of microstructures

For every 10X - 100X magnification, ...
there is a distinctly defined microstructure!

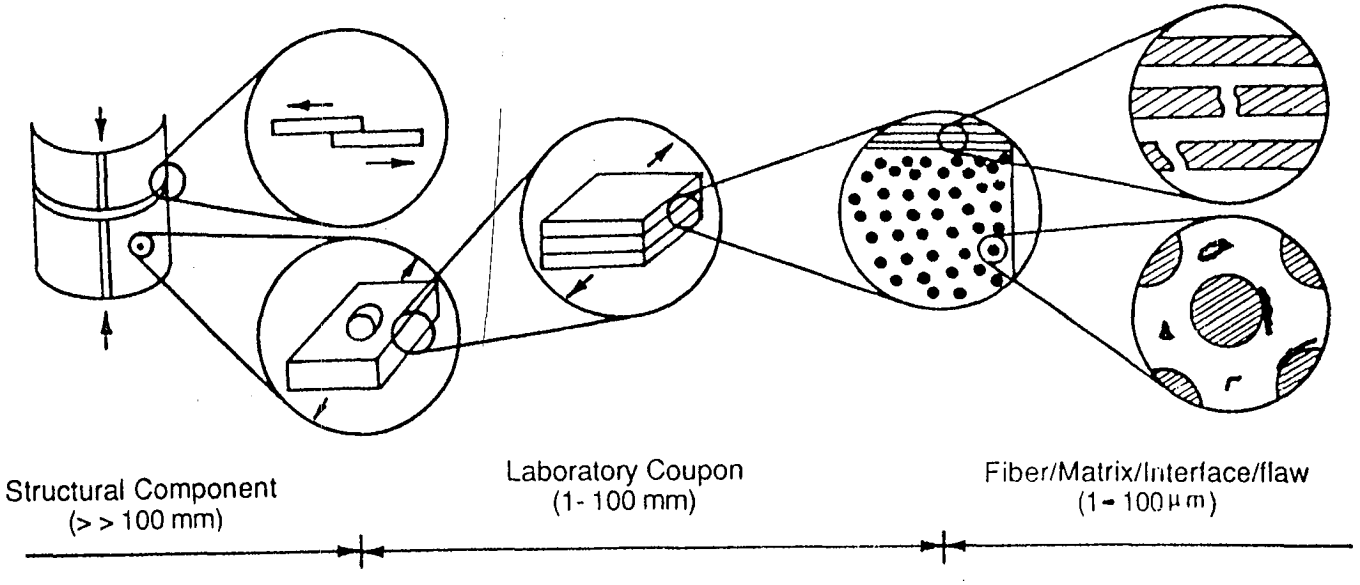

DEFECTS IN WHICH MICROSTRUCTURE LEVEL?

* Matrix cracking in UD CMC (Wang & Barsoum, 1992)

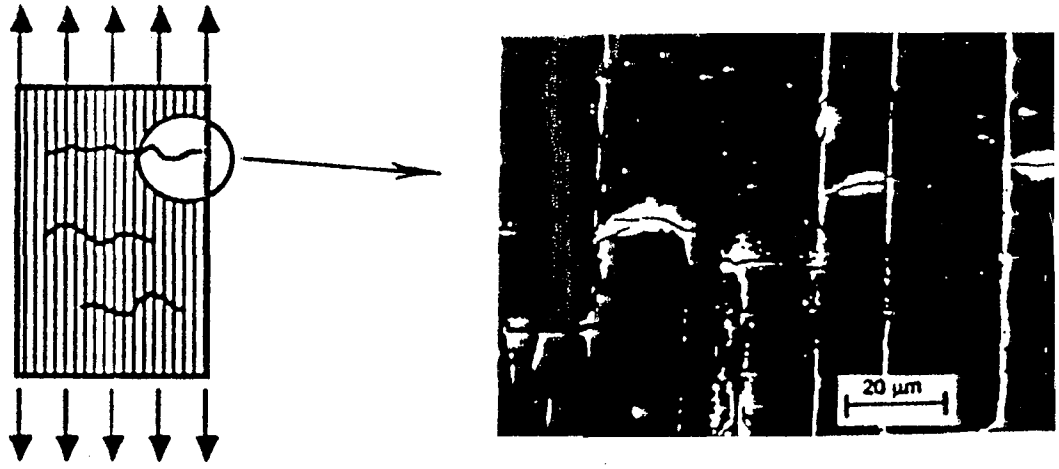

* Data: SCS-6 (140µm) and SCS-9 (140µm) fibers
Borosilicate matrix (in room temperature)

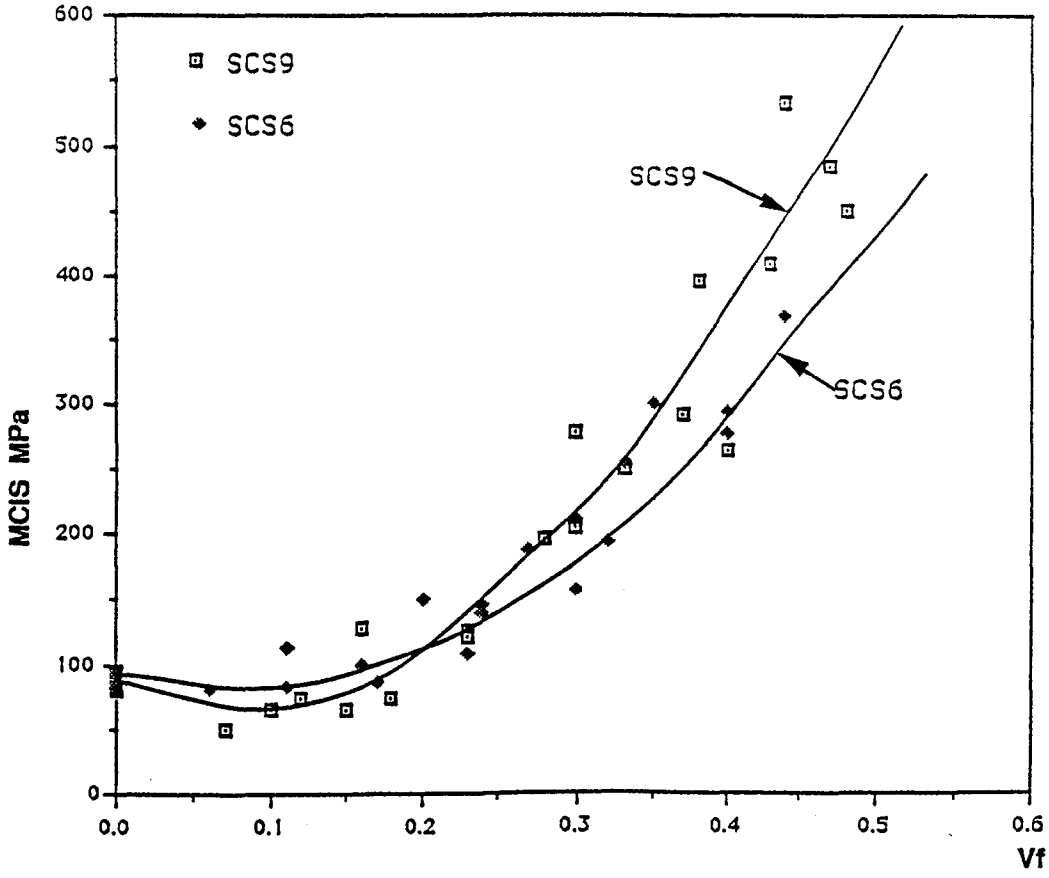

DEFECTS IN WHICH MICROSTRUCTURE LEVEL?

Transverse Cracking in [0/90]s Laminates (Crossman & Wang, 1982)

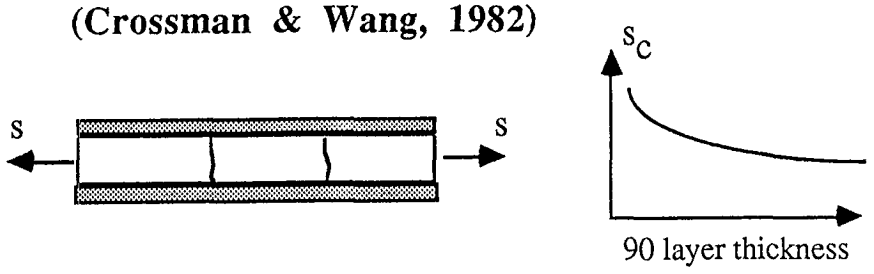

* Data: Multiple cracks in graphite-epoxy $[0/90_n]_S$ laminates

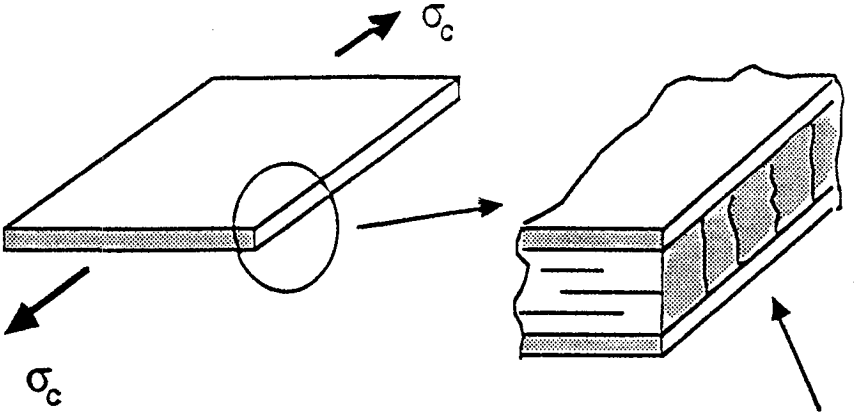

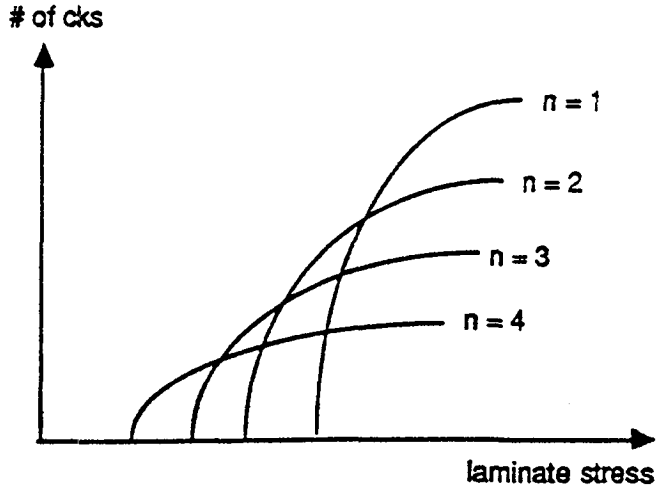

THE CONCEPT OF EFFECTIVE DEFECT

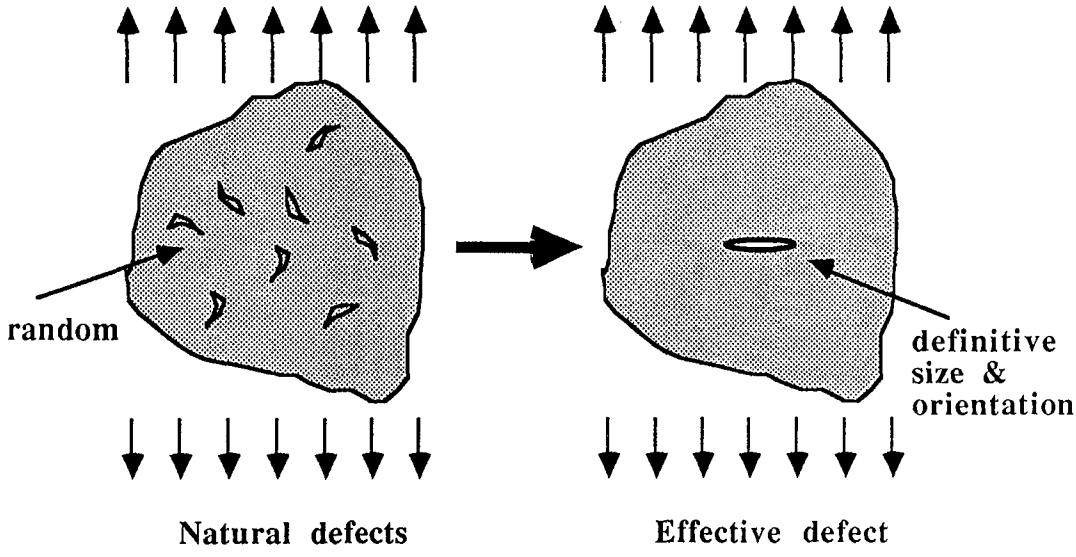

* About the "effective" defect:

  - defect orientation - adjudicated by material failure mode
  - defect size - by failure stress, material toughness & failure criterion

  For example: tensile failure of a brittle material

  - defect orientation is normal to the applied tension;
  - defect is crack-like & its size is:

$$a_{eff} = \lambda\,(K_c/\sigma_{cr})^2$$

* Scaling effect:

$$a_{eff} \propto \int_v (\text{natural defect density})dv$$

EFFECTIVE DEFECTS IN COMPOSITES

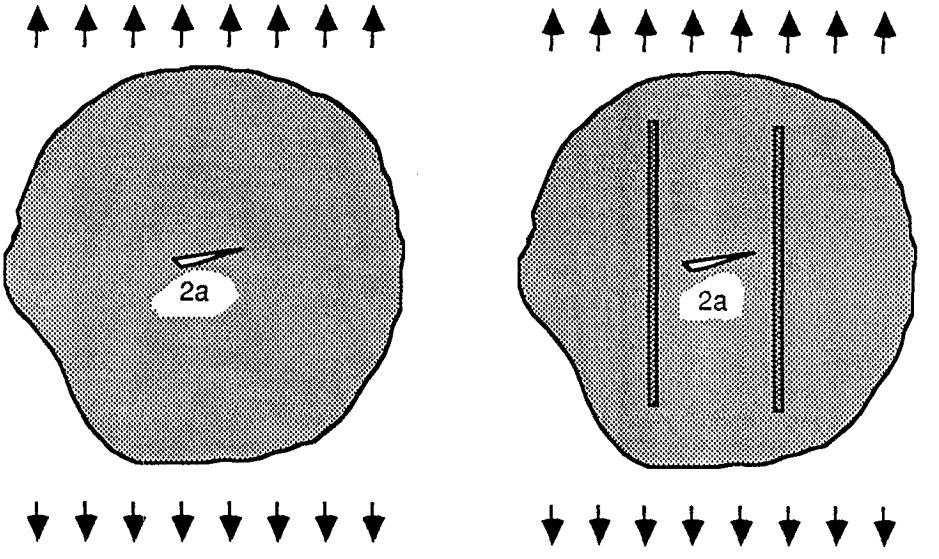

* Reinforcing fibers are a part of composite microstructure

  - defect and microstructure interactions

- Positive effects on defects:
  - defect size limiting (fiber spacing)
  - crack shielding (fiber spacing, stiffness)
  - crack arrest/deflection (fiber spacing, interface)
  - multiple cracking (fiber spacing, interface)
    (increased material toughness)
- Negative effects on defects:
  - more manufacturing defects
  - residual stresses

* Scaling Effect on Defect:

- governed by the characteristic size of the microstructure

SCALING EFFECTS ON DEFECTS

- A physical Example -

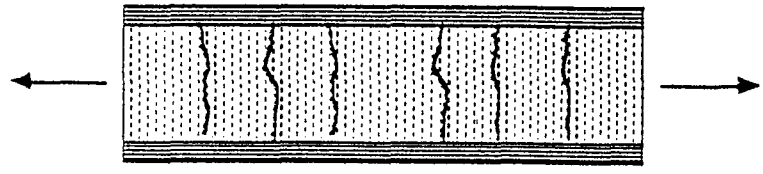

*** probable source of cracking: inter-fiber flaws**

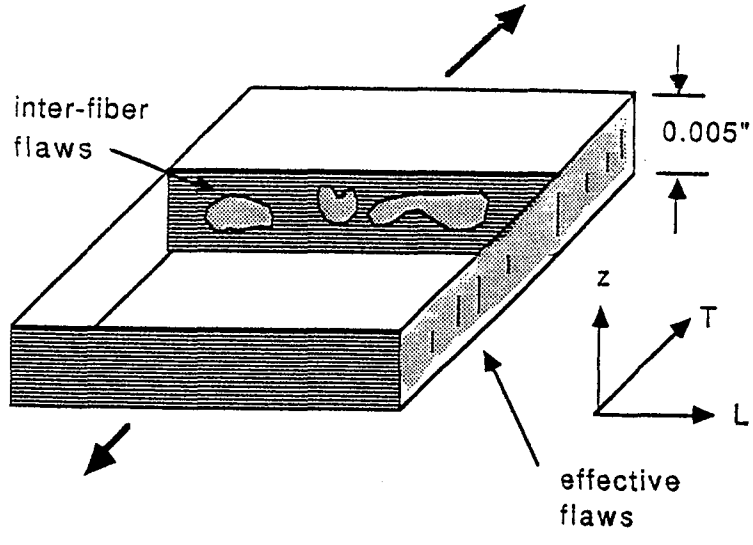

*** Idealization: effective flaws**

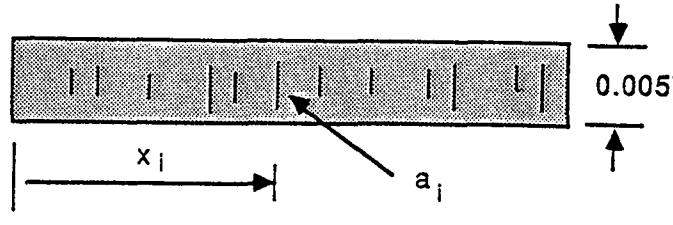

a_i : flaw size distn. x_i : flaw location distn.

Suggest A Proper Scaling Law for n 90^{o} Plies

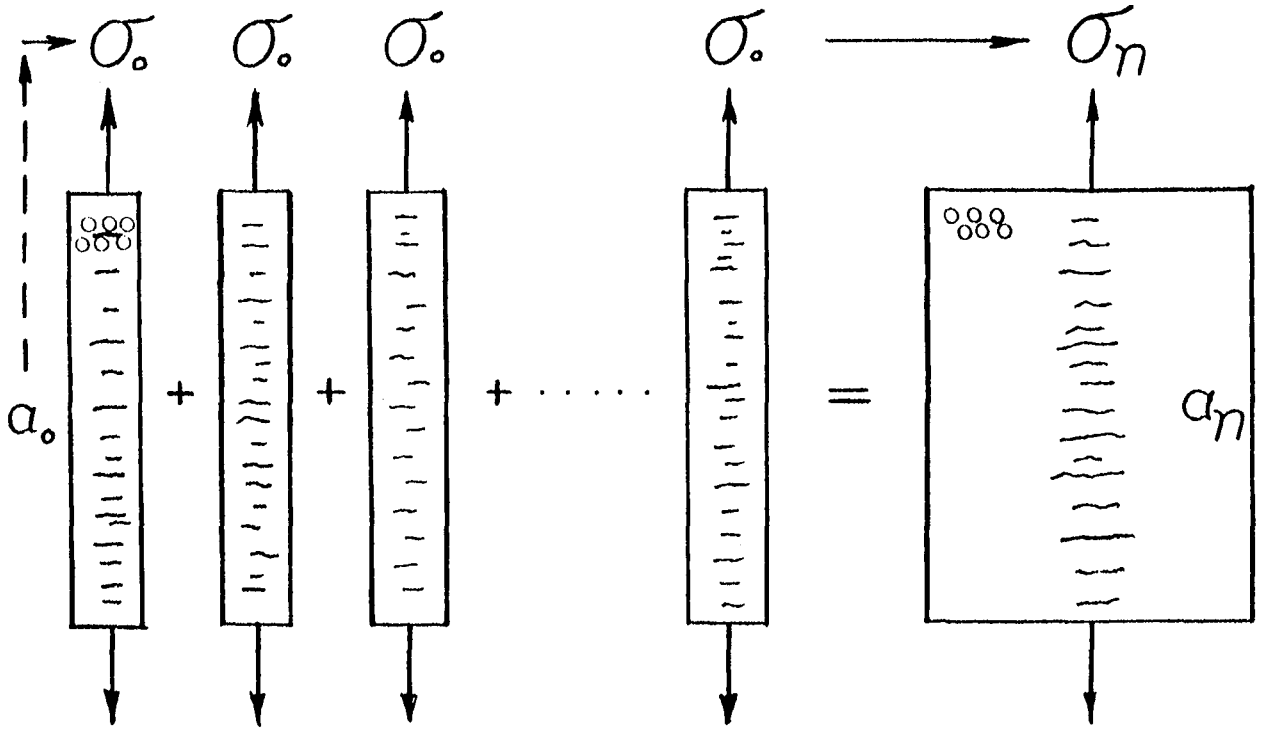

$$\sigma_o = K\sqrt{a_o}$$

$$\sigma_n = K\sqrt{a_n}$$

$$a_n \cong a_o n^{2/\alpha_o}$$

Application of Fracture Mechanics

* Treat effective flaws as distributed cracks - (Wang and Lei, 1985)

Mechanisms : fracture of microflaws

Model : random flaw distribution

Simulation : Monte-Carlo search

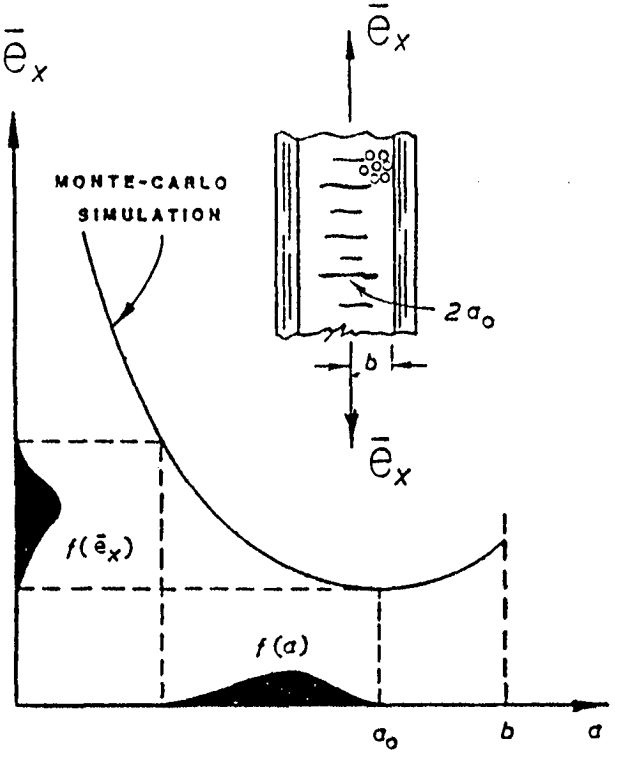

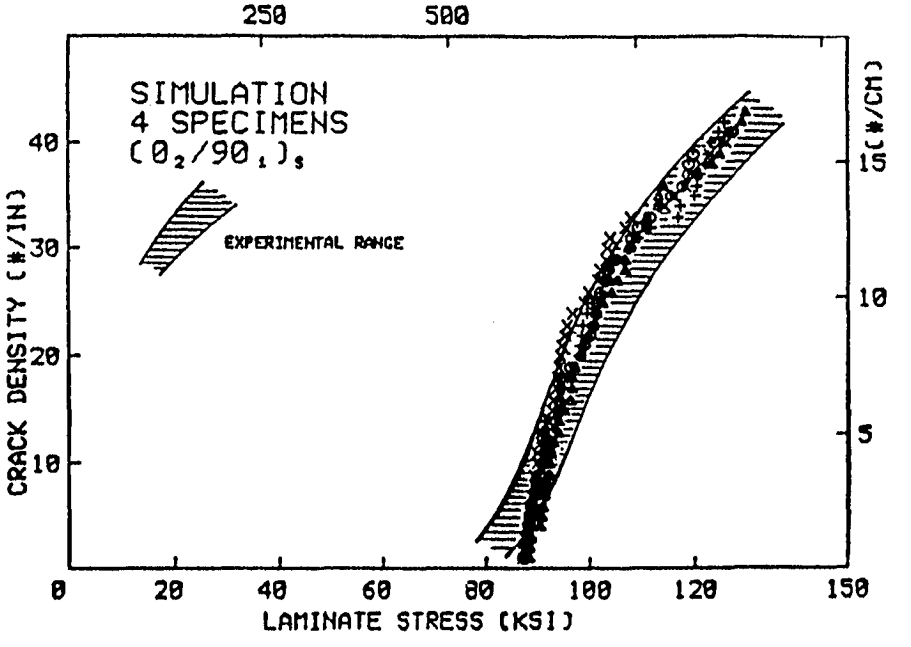

SCALING EFFECTS ON DEFECTS

- Another physical Example

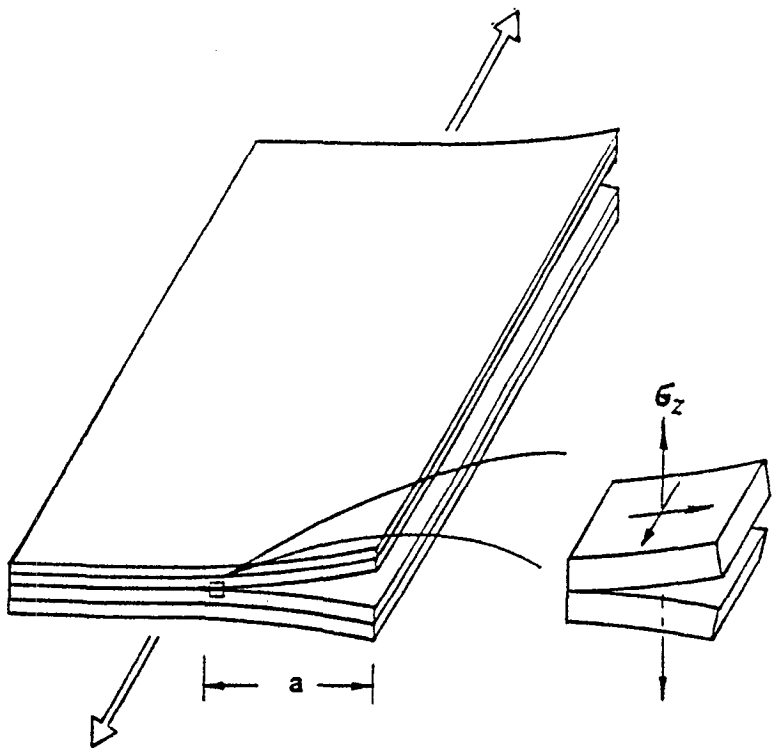

*** probable source of cracking: inter-ply flaws**

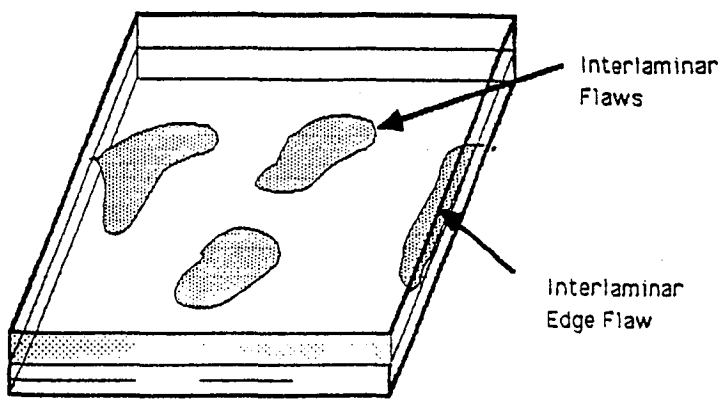

*** Idealization: <u>effective</u> edge flaw**

Application of Fracture Mechanics

* (generally) mix-mode, self-similar: (Wang & Crossman, 1980)

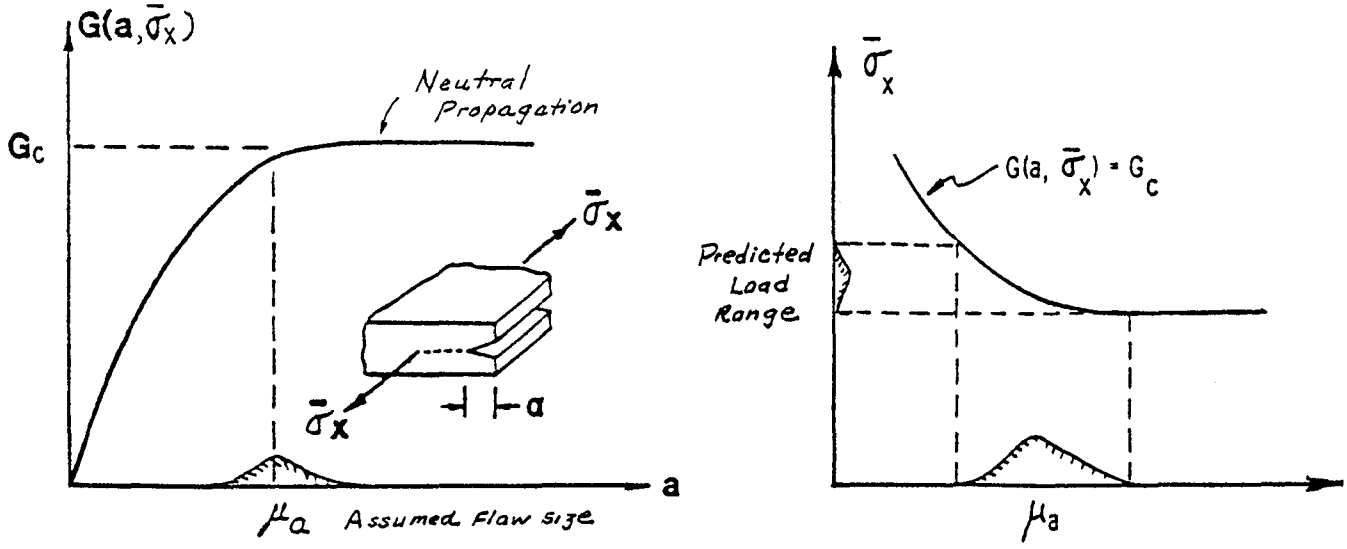

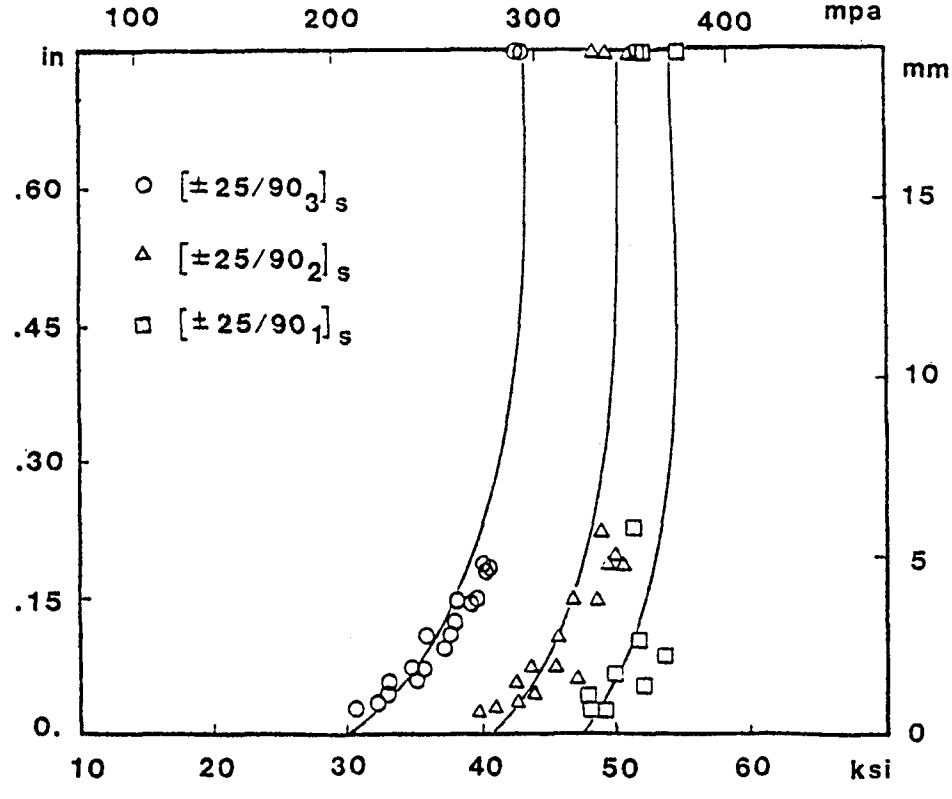

SCALING EFFECTS ON DEFECTS

A physical Example -

*** Interactive microcracking in CMC: (Wang & Barsoum, 1992)**

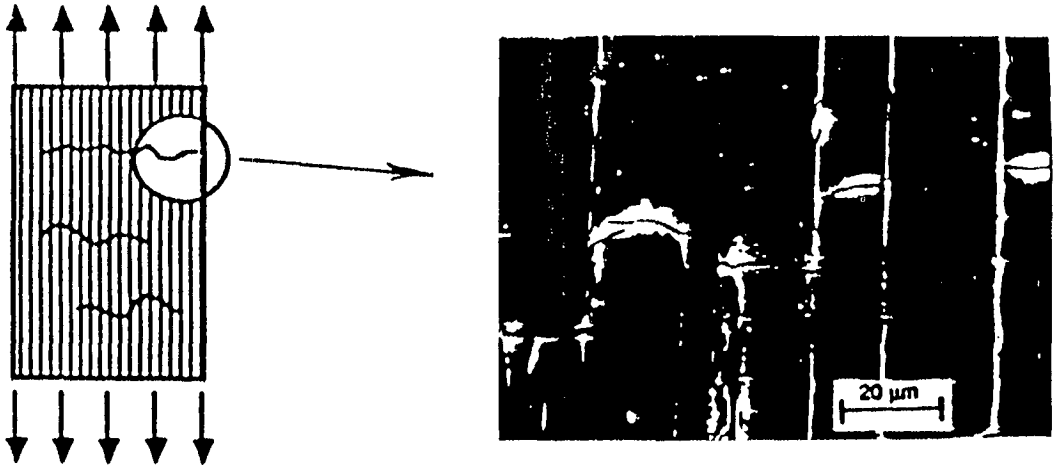

*** Inferred source(s) of initiation:**

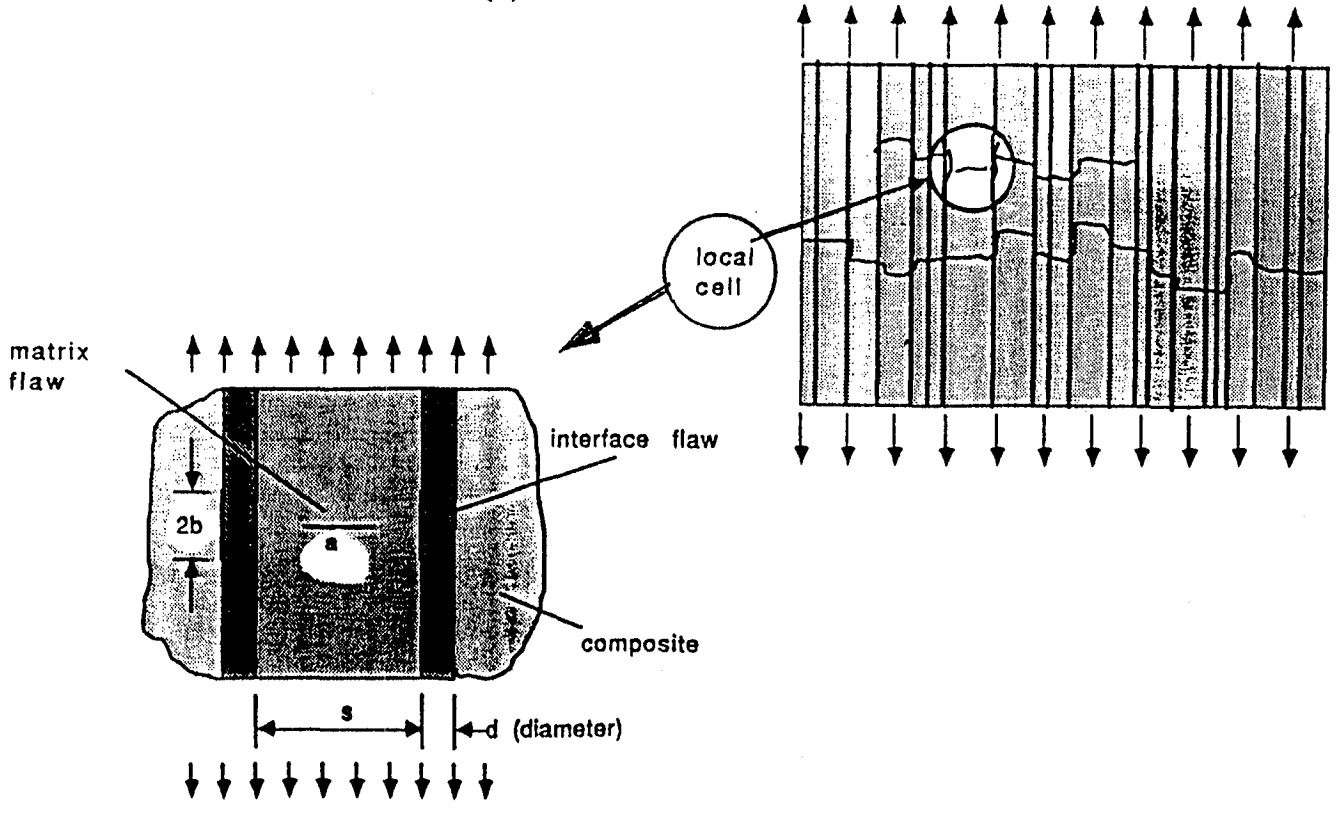

Experimental & Predicted Matrix Cracking Stress

Wang & Barsoum, 1992

SCS-6/7740

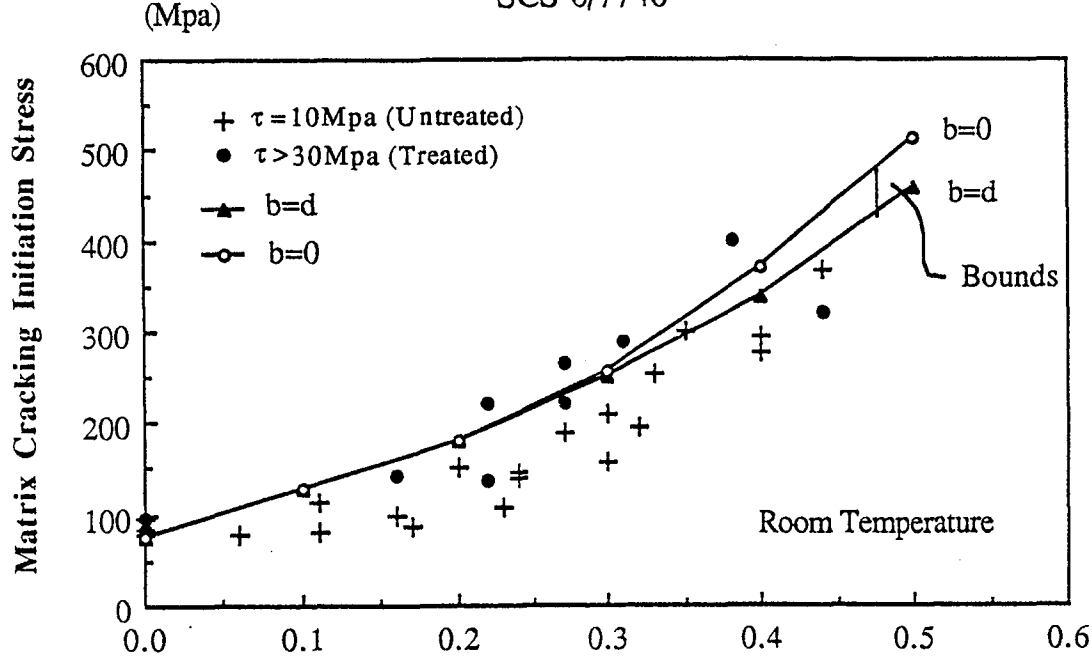

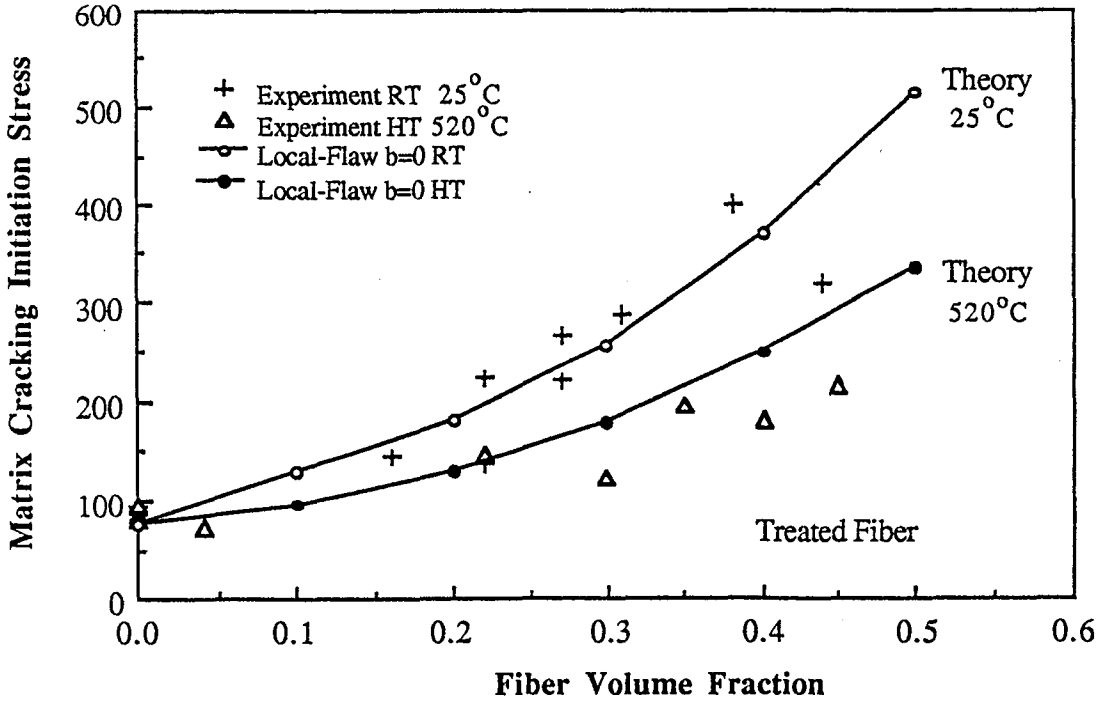

CONCLUDING REMARKS

* material defects exist, especially in fibrous composites

* scaling effect is due to random distribution in volume

* physical defects are difficult to identify or describe

* the concept of "effective defects" serves a useful purpose

* in monolithic medium, the dominant one(s) control failure

* in composites, multiple (localized) failures can occur

* scaling effect is regulated by the characteristic size of the reinforcement microstructure

* experimental evidences have been consistent with this axiom;

* the axiom can be quantitatively & qualitatively applied to simulate the damage processes in composites

* the examples cited are simple yet revealing

SIZE EFFECT IN COMPOSITE MATERIALS AND STRUCTURES: BASIC CONCEPTS AND DESIGN CONSIDERATIONS

Carl Zweben
Advanced Technology Manager and Division Fellow
Martin Marietta Astro Space
King of Prussia, Pennsylvania

INTRODUCTION

It has long been known that the strength of brittle materials like ceramics depends on the volume of stressed material and the nature of the stress distribution. Both of these effects arise because brittle materials are flaw sensitive, and flaw severity and distribution are generally statistical in nature. As the probability of finding a serious flaw increases with increasing material volume, large brittle bodies tend to fail at lower stress levels than smaller ones when both are subjected to the same kind of uniform stress field, such as pure tension. This is known as "Size Effect".

The significant influence of size and stress distribution on strength of ceramics has a major effect on methods used to determine strength properties. Because of the brittle nature of ceramics, measuring tensile strength is not a simple task, and flexural testing is common. The resulting flexural strength is often referred to as "modulus of rupture". It is widely recognized that the modulus of rupture is much higher than the strength of a coupon having the same dimensions loaded in pure tension, because the region of high tensile stress in a flexural specimen is much smaller. This fact is usually accounted for by use of Weibull statistical methods to determine allowable tensile strength properties when flexure tests are used (Ref. 6).

Plastic deformation in metals tends to reduce stress concentrations arising from defects, and these materials display much less strength scatter and Size Effect than ceramics. In practice, the influence of size on the strength of metallic structures is rarely, if ever, considered, whereas it is a key consideration for ceramics.

Polymer matrix composite (PMC) materials reinforced with continuous fibers have a number of characteristics which are typical of brittle materials. One of the most important similarities to ceramics is that PMCs lack plasticity to reduce the influence of stress concentrations arising from defects. Components subjected to tensile and compressive loads in the fiber direction have more or less linear tensile stress-strain curves and strengths which display significantly more scatter than ductile metals. In light of these facts, it is natural to ask whether the strength of composite materials depends on material volume. That is, **is there a Size Effect in composite materials and structures?** The issue here is one of inherent material strength dependence on volume, independent of the influence of manufacturing process variability. The question is well defined in Ref. 12. To paraphrase, would small specimens cut from a large structure have the same strength characteristics as the structure itself when subjected to the same state of uniform stress?

Considering that large composite structures have been reliably used in service for some time, the question naturally arises that if there is a significant Size Effect, why has it not been identified?

It seems entirely possible that there may be a significant Size Effect in composite materials and structures, but it has not been detected or recognized as such for a variety of reasons. First, local stress concentrations arising from joints and cutouts often dominate strength considerations, rather than the stresses in the bulk of the structure. Second, unless one is looking for a Size Effect, the critical tests required to detect it may not be run. Third, in the event that tests do show up a reduction in strength with increasing size, the phenomenon may be attributed to other sources,

such as manufacturing process variability (which may in fact be the cause in many instances). Finally, in the development of large structures it is common to rely extensively on subcomponent tests to modify preliminary designs, so that design allowables defined by coupon tests may not be the arbiters of the final design.

EVIDENCE FOR A SIZE EFFECT

There is a significant, but inconclusive body of evidence that there is a Size Effect in composites:

- the mean tensile strengths of glass, carbon (graphite), boron and aramid filaments decrease with increasing length (Refs. 1,18,19,20). This is a form of Size Effect.
- the mean tensile strength of untwisted fiber bundles is less than that of filaments and decreases with increasing length (Ref. 1)
- the mean tensile strength of twisted fiber bundles also decreases with increasing length, but at a lower slope than for untwisted bundles (Ref. 1)
- tensile failure of unidirectional composites is associated with a statistical accumulation of fiber breaks (Refs. 7,21)
- unidirectional tensile coupons are 18-51% weaker than impregnated strands which have smaller volumes (Ref. 5)
- unidirectional tensile rings are 23% weaker than tensile coupons which have smaller volumes (Ref. 12)
- flexural strengths of unidirectional coupons can exceed tensile strengths by as much as 44% and compressive strengths by as much as 56% (e.g. Refs. 2,3,5,13)
- the flexural strength of 100-ply unidirectional coupons is 15% weaker than for 25-ply coupons (Ref. 14)

- the reduction in laminate strength caused by circular holes increases with increasing hole size (possibly because the volume of material subjected to a stress concentration increases with increasing hole diameter) (Ref. 15)
- the burst strength of pressure vessels tends to decrease with increasing volume of material, although there are notable exceptions (Ref. 4)
- the static compression strength of specimens with three holes in series is 11% lower than for a coupon with one hole, and the fatigue life (cycles to failure) is 69% lower (Ref. 16).

Figures in the presentation charts that accompany this extended abstract show the length-strength dependence of a number of fibers and twisted and untwisted fiber bundles, and the variation of pressure vessel strength with material volume.

Here, we can only briefly summarize some of the key pieces of evidence suggesting there may be a Size Effect. Obviously, each bit of data needs to be carefully scrutinized for accuracy and to see whether there may be other reasons for the observed effects.

STATISTICAL ANALYSIS METHODS

The statistical methods of analysis used for composite strength can be divided into two main categories. In the first, the material is treated at the macroscopic level as if it were an effectively homogeneous material. The most common macroscopic approach to model composite strength is use of classical Weibull theory, as in Refs. 5 and 16.

The second class of analytical methods is based on micromechanical statistical failure models, as in Refs. 7 to 11. At least some of the micromechanics models predict a Size Effect similar to that based on Weibull theory (e.g. Ref. 17). The micromechanics twisted fiber bundle model of Ref. 1, which provides good agreement with experimental data for aramid fibers, also predicts a Size Effect.

SIZE EFFECT IMPLICATIONS

If there is a significant Size Effect, an important implication is that use of standard test coupons to establish design allowables for large structures could be very nonconservative. To illustrate, assume that the strength of a composite material is reasonably represented by classical Weibull theory (Ref. 6). Let $\bar{S}$ be the mean strength of a volume V subjected to a uniform state of stress, and $\bar{S}_o$ the corresponding mean strength of volume V_o. Using Weibull theory, the ratio of the two strengths is given by

$$\frac{\bar{S}}{\bar{S}_o} = \left(\frac{V_o}{V}\right)^{1/m}$$

where m is the Weibull shape parameter, also called the Weibull modulus. This formula is illustrated by the figure in the attached presentation that shows the reduction in strength with increasing volume predicted by Weibull theory.

For example, consider a material whose strength coefficient of variation, C, is 5%, which is a reasonable number for a well made composite. The Weibull modulus m for this material is about 24 (m is approximately given by m = 1.2/C). The volume of large structures can easily be four to six orders of magnitude greater than that of standard

coupons used to define strength properties. For structures in this size range, Weibull theory predicts strength reductions of about 25 to 40 %, which are obviously quite significant.

Another consideration is that if there is a significant Size Effect, in analyzing the strength of large composite structures it would be necessary to use statistical methods that take into account both size and stress distribution. This is very different from the way we do business at the present time.

SUMMARY AND CONCLUSIONS

Composite materials display strength characteristics that are similar to those of brittle ceramics, whose strengths are known to decrease with increasing volume for a uniform state of stress (Size Effect) and also are dependent on stress distribution. These similarities raise the question of whether there is also a Size Effect in composite materials and structures. There is significant, but inconclusive experimental evidence for the existence of a Size Effect in composites. Macroscopic and micromechanical statistical models have been developed which predict a Size Effect and are in general agreement with experimental data.

The existence of a significant Size Effect in composites would be of great importance. For example, it would mean that use of standard test coupons to establish design allowables for large structures could be very nonconservative. Further, it would be necessary to analyze the strength of large composite structures using statistical methods, as is done for ceramics.

The question of the existence of a Size Effect is of great theoretical and practical importance. The issue can only be resolved by a very careful experimental program.

ACKNOWLEDGMENT

I am grateful to Mr. Michael Bader and Dr. Keith Kedward for valuable discussions during the preparation of this paper.

REFERENCES

1. C. Zweben, W. S. Smith and M. W. Wardle, "Test Methods for Fiber Tensile Strength, Composite Flexural Modulus and Properties of Fabric-Reinforced Laminates", Composite Materials: Testing and Design - Fifty Conference, ASTM STP 674, American Society for Testing and Materials, Philadelphia, 1979, pp. 228-262.

2. B. E. Kaminski, "Effects of Specimen Geometry on the Strength of Composite Materials", Analysis of the Test Methods for High Modulus Fibers and Composites, ASTM STP 521, American Society for Testing and Materials, Philadelphia, 1973.

3. C. Zweben, "The Flexural Strength of Aramid Fiber Composites", Journal of Composite Materials, Vol. 12, 1978, pp. 422-430.

4. L. A. Riedinger, M. H. Kural, and G. W. Reed, Jr., "Evaluation of the Potential Structural Performance of Composites", Mechanics of Composite Materials, F. W. Wendt, H. Liebowitz, and N. Perrone, Editors, Pergamon Press, Oxford, 1970, pp. 481-525.

5. R. E. Bullock, "Strength Ratios of Composite Materials in Flexure and in Tension", Journal of Composite Materials, Vol. 8, 1974, pp. 200-206.

6. W. Weibull, "A Statistical Theory of Strength of Materials", Ing. Vetenskaps. Akad. Handl. NR 151, 1939.

7. B. W. Rosen, "Mechanics of Fiber Strengthening", Fiber Composite Materials, American Society for Metals, Metals Park, Ohio, 1965.

8. C. Zweben, "A Bounding Approach to the Strength of Composite Materials", Engineering Fracture Mechanics, Vol. 4, 1972, pp. 1-8.

9. S. L. Phoenix, "Probabilistic Concepts in Modeling the Tensile Strength Behavior of Fiber Bundles and Unidirectional Fiber Matrix Composites", Composite Materials: Testing and Design, ASTM STP 546, American Society for Testing and Materials, Philadelphia, 1974, pp. 130-151.

10. D. G. Harlow, "Properties of the Strength Distribution for Composite Materials", Composite Materials: Testing and Design - Fifth Conference, ASTM STP 674, American Society for Testing and Materials, Philadelphia, 1979.

11. C. Zweben, "Tensile Strength of Hybrid Composites", Journal of Materials Science, Vol. 12, No. 7, 1977, pp. 1325-1337.

12. J. W. Hitchon and D.C. Phillips, "The effect of specimen size on the strength of cfrp", Composites, Vol. 9 April, 1978, pp. 119-124.

13. K. R. Berg and J. Ramsey, " Metal Aircraft Structural Elements Reinforced with Graphite Filamentary Composites", NASA CR - 112162, August 1972.

14. M. R. Wisnom, "On the Decrease in Strength of Carbon Fibre-Epoxy with Size Effect".

15. M. E. Waddoups, J. R. Eisenmann and B. E. Kaminski, "Macroscopic Fracture Mechanics of Advanced Composite Materials", J. Composite Materials, Vol. 5, October 1971, pp. 446-454.

16. P. C. Chou and R. Croman, "Scale Effect in Fatigue of Composite Materials", J. Composite Materials, Vol. 13, July 1979, pp. 178-194.

17. C. Zweben, "The Effect of Stress Nonuniformity and Size on the Strength of Composite Materials", Composites Technology Review, Vol. 3, No. 1, 1981, pp. 23-26.

18. A. G. Metcalfe and G. K. Schmitz, Proceedings, American Society for Testing and Materials, Vol. 64, 1964, p. 1075.

19. H. W. Herring, "Selected Mechanical and Physical Properties of Boron Filaments", NASA TN D-3202, National Aeronautics and Space Administration, Langley, Virginia, 1966.

20. R. J. Diefendorf and E. Tokarsky, Polymer Engineering and Science, Vol. 15, No. 3, 1975, pp. 150-159.

21. P. W. Manders and M. G. Bader, "The strength of hybrid glass/carbon fibre composites, Part 2 A statistical model", J. of Materials Science, Vol. 16, 1981, pp. 2246-2256.

OUTLINE

- Introduction
- Evidence for Size Effect
- Analysis of Size Effect
- Implications of Size Effect
- Summary and conclusions

INTRODUCTION

- Metals
  - Plasticity minimizes flaw sensitivity
  - Little strength scatter
  - Strength little affected by size
- Ceramics
  - No plasticity
  - Flaw sensitive
  - Large strength scatter
  - Strength decreases with increasing volume - "Size Effect"

INTRODUCTION

- Polymer Matrix Composites (PMCs)
  - No plasticity
  - Flaw sensitive?
  - Strength scatter between ceramics and metals

IS THERE A SIZE EFFECT IN COMPOSITE MATERIALS?

- If Size Effect exists, why isn't it obvious?
  - Local stress concentrations typically dominate design
  - Extensive use of subcomponent tests
  - We may not have been looking for it
  - May be attributed to something else - e.g. process variability

INTRODUCTION

- Since ignoring Size Effect apparently hasn't hurt us, why should we care?
  - Structure size increasing - e.g. bridges
  - Critical to basic understanding of composites
  - Important to separate basic effects - e.g. materials vs. processes

QUESTION

Does the failure stress level of a composite structure

subjected to a uniform state of stress

depend on the volume of material in the structure ?

That is:

Is there a "Size Effect" in composites?

EVIDENCE FOR SIZE EFFECT

- Evidence suggestive, but not conclusive
- Filament strength decreases with increasing length and diameter
  - Glass, boron, carbon, aramid, alumina, etc.
- Untwisted bundle strength is weaker than filament strength and decreases with increasing length (Zweben, et al.)
- Twisted bundle strength decreases with increasing length at lower slope (Zweben, et al.)

GRAPHITE FIBER LENGTH - STRENGTH DEPENDENCE
(After Diefendorf and Tokarsky)

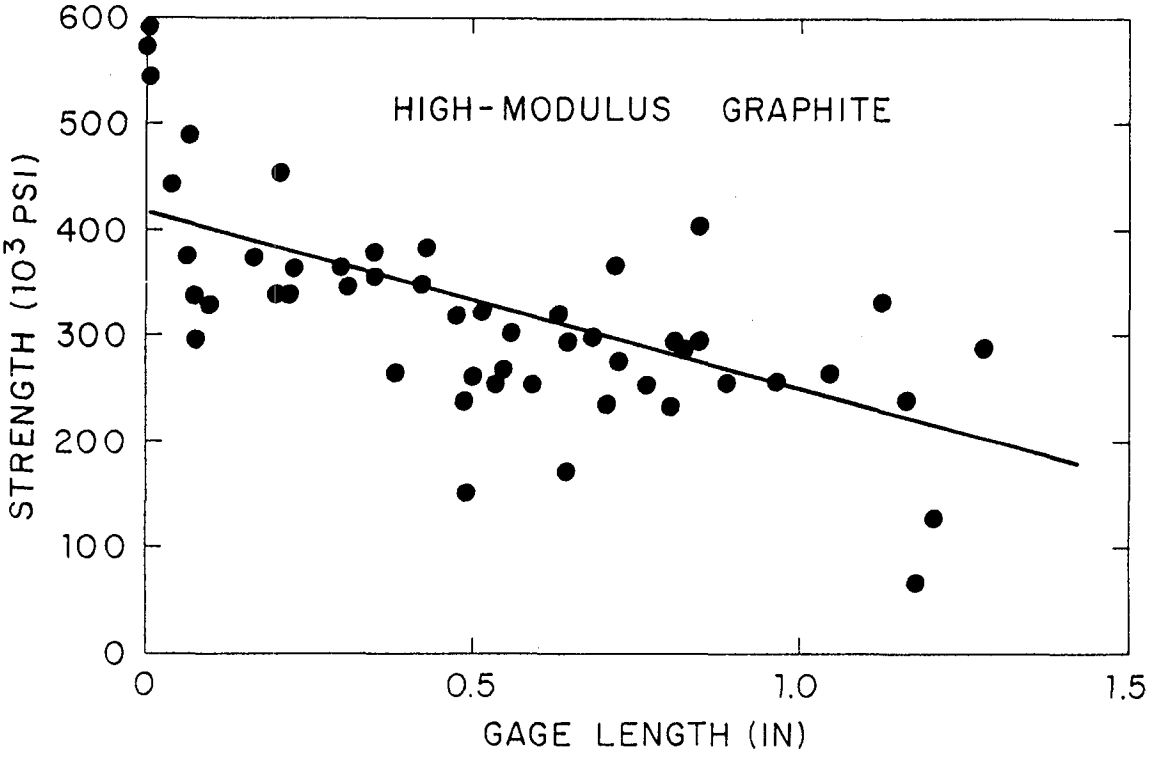

BORON FIBER LENGTH - STRENGTH DEPENDENCE
(After Herring)

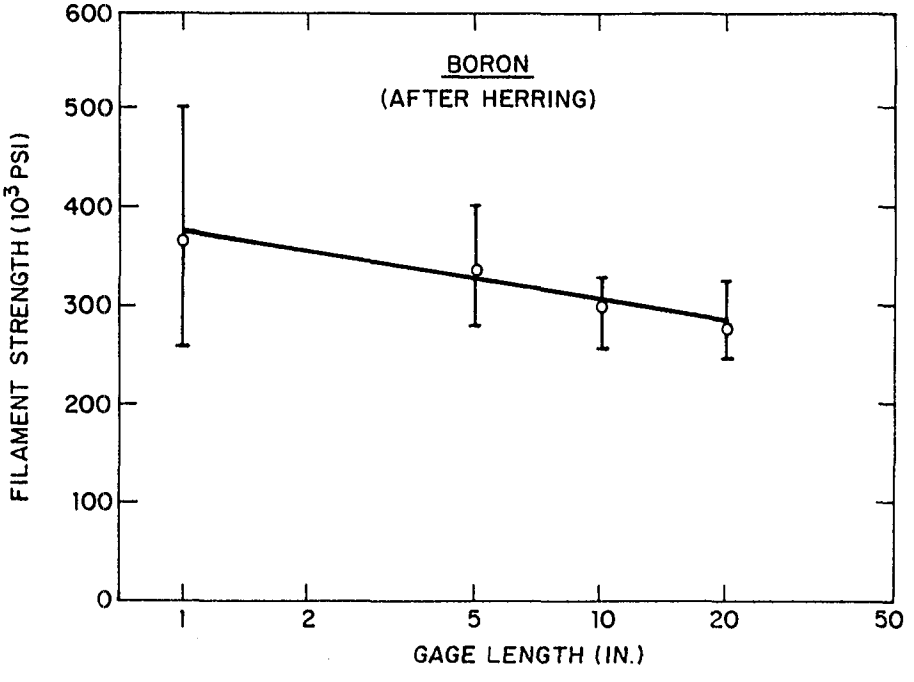

GLASS FIBER LENGTH - STRENGTH DEPENDENCE
(After Metcalfe and Schmitz)

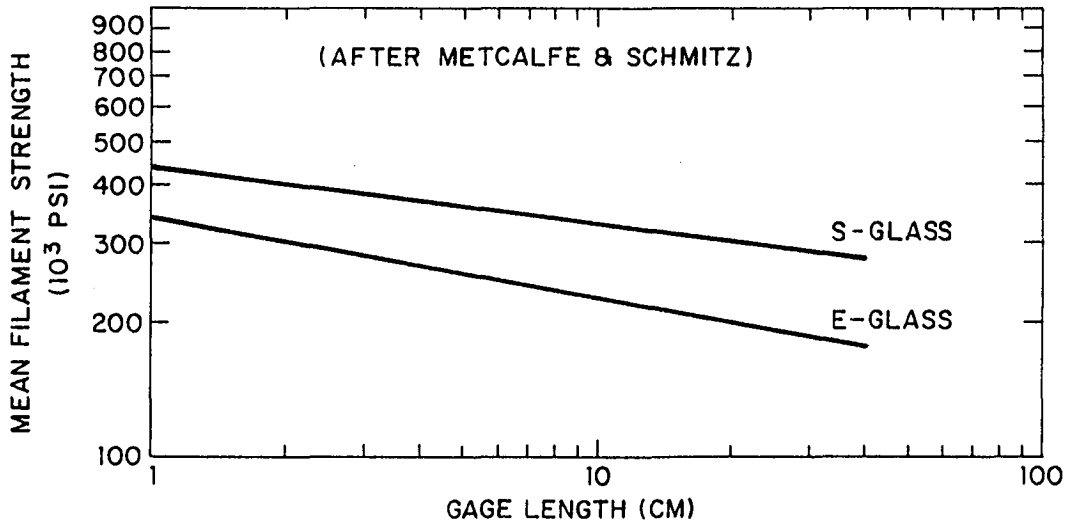

LENGTH - STRENGTH DEPENDENCE OF ARAMID FIBERS AND UNTWISTED AND TWISTED YARNS
(Zweben, Smith and Wardle)

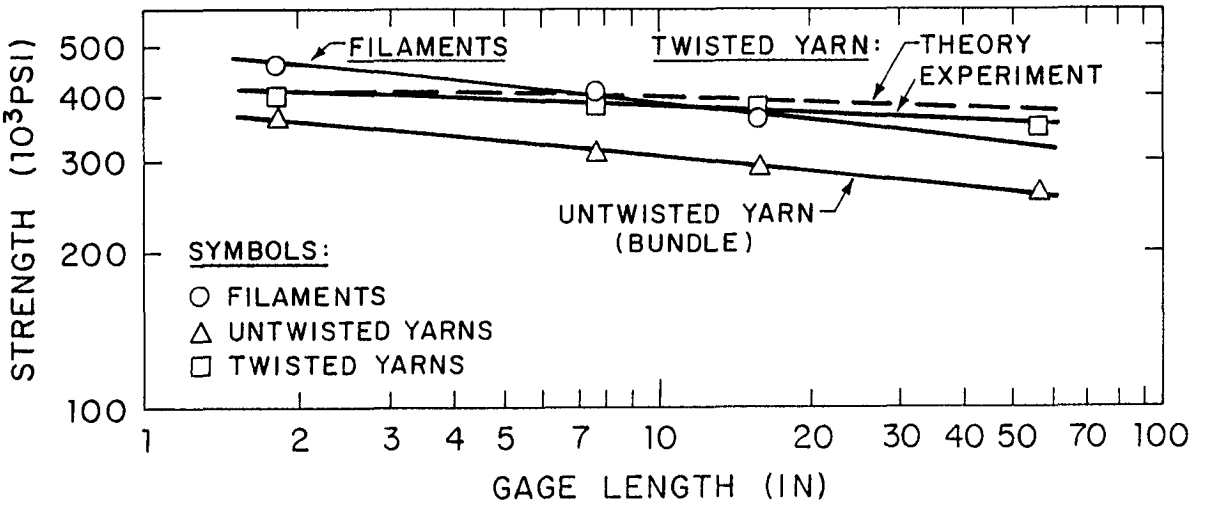

TWISTED YARN STRENGTH MODEL
(Zweben, Smith and Wardle)

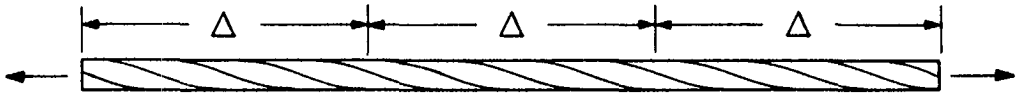

TWISTED YARN

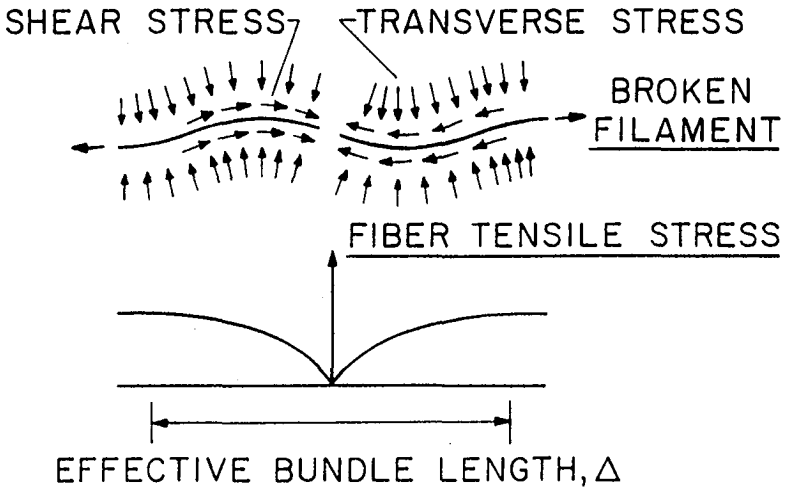

EVIDENCE FOR SIZE EFFECT

- Composite tensile failure associated with statistical fiber break accumulation (Rosen)
- Tensile coupons 18-51% weaker than impregnated strands (Bullock)
- Tensile rings 23% weaker than coupons (Hitchon and Phillips)
- Flexural strength can exceed
  - tensile strength by 44%
  - compression strength by 56% (e.g. Berg & Ramsey, Bullock)
- Four-point bend strength:
  - 100-ply coupon 15% weaker than 25-ply (Wisnom)
- Laminate strength decreases with increasing hole diameter (Waddoups, et al.)
- Pressure vessel burst strength decreases with increasing size (Riedinger, et al.)
- For compression coupons with three holes in series vs. one hole:
  - Static strength 11% lower
  - Fatigue life 69% lower (Chou and Croman)

TENSILE STRENGTH OF S-GLASS YARNS, ROVINGS, AND S-GLASS/EPOXY PRESSURE VESSELS

(After Riedinger, Kural and Reed)

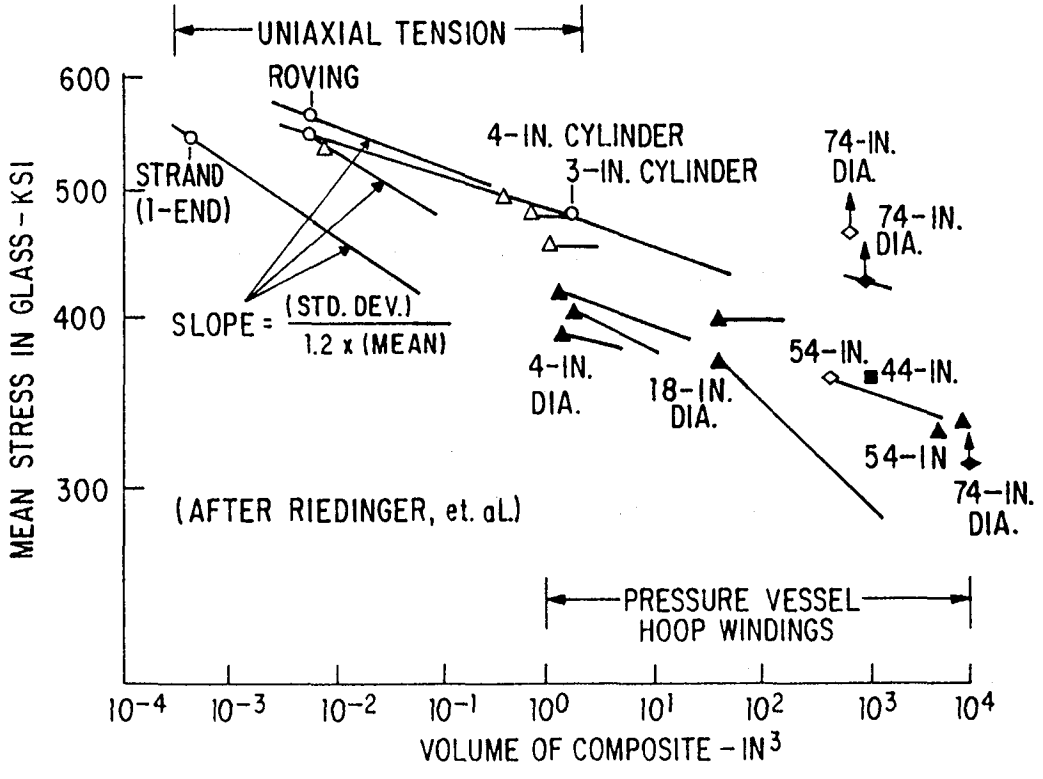

SIZE EFFECT IMPLICATIONS

- Design allowables from standard coupons may be very nonconservative
- Strength depends on stress distribution

ANALYSIS OF SIZE EFFECT

- Weibull theory (Bullock, Chou, etc.)
  - Composite treated as homogeneous material
- Micromechanics statistical models (Rosen, Zweben, Phoenix, etc.)

WEIBULL STRENGTH DISTRIBUTION FUNCTION

$$F(\sigma) = 1 - \exp\left[- \int_V \left[\frac{\sigma - \sigma_u}{\sigma_o} \right]^m dv \right]$$

σ_u = Zero Probability Strength, Threshold Strength

σ_o = Scale Parameter, Reference Strength

m = Shape Parameter, Weibull Modulus, Flaw Density Exponent

V = Material volume

COMPARISON OF PREDICTED AND EXPERIMENTAL FLEXURAL/TENSILE STRENGTH RATIOS

Weibull Theory (Bullock)	Micromechanics Statistical Model (Zweben)	Experiment (Bullock)
1.35 - 1.44	1.3 - 1.8	1.35 - 1.49

SIZE EFFECT FOR HOMOGENEOUS WEIBULL MATERIAL

For uniform state of stress

$$\frac{S}{S_o} = \left[\frac{V_o}{V}\right]^{1/m}$$

m = Weibull modulus, shape parameter
V = volume
S = mean failure stress

For composites

m = 5 - 45 (CV = 25 - 3%)

VARIATION OF STRENGTH WITH VOLUME PREDICTED BY WEIBULL THEORY ("SIZE EFFECT")

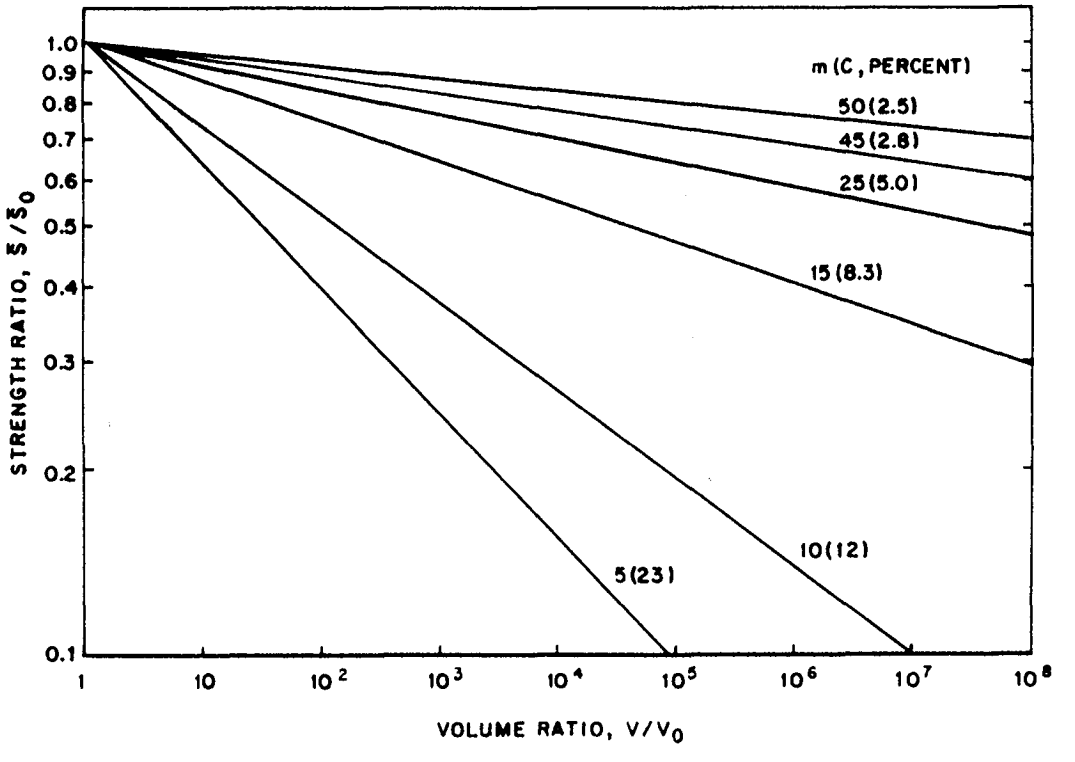

COMPARISON OF COUPON AND STRUCTURE STRENGTHS PREDICTED BY WEIBULL THEORY

- Assume
  - Classical Weibull theory (homogeneous)
  - m = 25 (c.v. = 5%)
  - Structure volume = 10^4 to 10^6 times coupon volume
- Predicted strength reduction = 25 - 40%

SUMMARY AND CONCLUSIONS

- Evidence for Size Effect significant, but inconclusive
- Weibull and some micromechanics models predict size effect
- Coupon data may be very nonconservative for large structures
  - Possible 25 - 40% strength reduction
- Careful experiments needed to prove or disprove

STATISTICAL SCALING RELATIONSHIPS AND SIZE EFFECTS IN THE STRENGTH AND CREEP RUPTURE OF FIBROUS COMPOSITES

S. Leigh Phoenix
Department of Theoretical and Applied Mechanics
Cornell University
Ithaca, New York 14853
(607) 255-8818

In this presentation we discuss a new theoretical model and supporting experimental results for the strength and lifetime in creep rupture of unidirectional, carbon fiber/epoxy matrix composites at ambient conditions. First we review the 'standard' Weibull/power-law methodology that has been standard practise. Then we discuss features of a recent model which builds on the statistical aspects of fiber strength, micromechanical aspects of stress transfer around fiber breaks, and time-dependent creep of the matrix. The model is applied to 'microcomposites' consisting of seven fibers in a matrix for which strength and creep-rupture data are available. The model yields Weibull distributions in an envelope format for both strength and lifetime. The respective shape, scale and power-law parameters depend on such parameters as the Weibull shape parameter for fiber strength, the exponent for matrix creep, the effective load transfer length (which grows in time due to matrix creep) and the critical cluster size for failed fibers. The experimental results are consistent with the theory, though time-dependent debonding appears to be part of the failure process.

STATISTICAL SCALING RELATIONSHIPS AND SIZE EFFECTS IN THE STRENGTH AND CREEP RUPTURE OF FIBROUS COMPOSITES

S. Leigh Phoenix
Department of Theoretical and Applied Mechanics
Cornell University
Ithaca New York, 14853

Credits:
Hiroshi Otani
Petru Petrina
Harold Robinson IV

Funding:
Martin Marietta, Oak Ridge, TN
Cornell Materials Science Center (NSF-DMR-MRL)

INTRODUCTION

- unidirectional graphite/epoxy composites
- applications:
  - pressure vessels, flywheels, centrifuges, beams
- scalings:
  - reliable ($P_f < 10^{-6}$), long life (yrs) under creep-rupture
  - want limited lifetime testing because of cost
  - extrapolate across many size scales (10^9)

Comments:

- Focus mainly on unidirectional graphite/epoxy composites under high tension
- Applications include:
  - filament-wound pressure vessels (NASA, DOD)
  - composite flywheels (DOD, SDI)
  - gas centrifuge cylinders (DOE)
  - structural beams
- Scaling problems:
  - want structure to reliably sustain high tensile stresses for very long time periods (many years)
  - material subject to creep rupture (stress rupture, creep fatigue)
  - high reliability means P(failure) $< 10^{-6}$
  - want to do very limited creep-rupture testing because of cost; do mainly strength testing
- want to extrapolate across size scale increases of up to nine orders of magnitude (eg. microcomposites to strands to vessels to centrifuges)

SOME ISSUES AND FOCUS

- fiber statistics, micromechanics
- time dependence via matrix creep and debonding
- reliability and distribution lower tails
- role of Weibull distribution (new distributions?)
- size scalings and power-laws
- QC spool screening (strength as a predictor of lifetime)
- new theory and 'micro' experiments

Elaboration on issues:

- fiber flaw statistics interacting with micromechanics
- time dependence largely through matrix creep and progressive debonding
- reliability modeling and statistics for lower tails of failure distributions
- role of the Weibull distribution for both strength and lifetime
- possible new distributional forms arising from micromechanics and statistics
- strength as a predictor for lifetime
- size scalings and power-law models for stress versus lifetime
- screening tests to reveal fiber spool-to-spool variations with respect to fiber and tow damage
- links of performance to quality control

- Focus of presentation:
  - focus on theoretical advances as well as experimental verification on 'micro' composites
  - tie to general features of creep-rupture data as well as limited QC issues for spools

APPROACH OF PAST 25 YEARS

- brute force
- load strands and observe lifetimes (a few data sets)
- a few NOL rings and vessels; high cost
- fit Weibull distributions and power-law
- extrapolate in size and time (eg. DOE AGC)

- Previous modeling and testing approach:
  - brute force
  - hang weights on hundreds of epoxy-impregnated strands at specified stress levels (LLNL, Toray, ORNL); costly and relatively few lifetime data sets exist
  - sometimes test NOL rings and pressure vessels; extremely costly and only a handful of data sets exist
  - fit Weibull distributions to strength data and lifetime data
  - determine power-law curve for stress level versus mean lifetime
  - extrapolate using power-law for stress level coupled with Weibull size effect relationship (eg. DOE Advanced Gas Centrifuge)

MODEL EQUATIONS

$$H_V(\sigma) = 1 - \exp\{-(\sigma/\sigma_{c,V})^{\zeta_c}\}, \quad \sigma \geq 0$$

$$\sigma_{c,V} = \sigma_{c,V_0}(V/V_0)^{-1/\zeta_c}$$

$$H_V(t,\sigma) = 1 - \exp\{-(t/t_{c,V}(\sigma))^{\beta_c}\}, \quad t \geq t_0$$

$$t_{c,V}(\sigma) = t_0(\sigma/\sigma_{c,V})^{-\rho}, \quad \sigma < \sigma_{c,V}$$

- The above viewgraph gives the equations of previous methodology
- In these equations

  ζ_c is the Weibull shape parameter for composite strength

  $\sigma_{c,V}$ is the Weibull scale parameter for composite strength
  V is the structural material volume
  V_0 is the base volume (say of epoxy impregnated strands)

  β_c is the Weibull shape parameter for composite lifetime

  $t_{c,V}(\sigma)$ is the Weibull scale parameter for composite lifetime

  ρ is the power-law exponent
  t_0 is a time constant
- Typical values of the parameters are

  $20 < \zeta_c < 30$

  $0.15 < \beta_c < 0.4$

  $70 < \rho < 120$ (ρ_f is about 300)
  seconds $< t_0 <$ hours

QUESTIONS

- **no micromechanical accounting of failure process**
- **dangers in extrapolation**
- **parameter values generic?**
- **QC on strand strength good enough ?**
- **accuracy of lower tail extrapolation for high reliability?**

Questions with the procedure:

- No micromechanical accounting of the failure process and no fundamental model in terms of fiber (mechanics, statistics), matrix, interface and micromechanical stress redistribution
- Thus, effects of material or processing changes cannot be predicted
- Cannot assess dangers in extrapolation to long times and large volumes as stress levels and times of interest are outside data range
- Are parameter values 'generic' for a material type or can they vary with the spool-to-spool or lot-to-lot 'quality' of the constituents?
  Example: Unpublished case of 'good' and 'bad' spools of Hercules AS4 fiber where ρ appeared to differ by a factor of 1.5.
- Are quality control tests on strand strength alone sufficient to ensure proper creep-rupture performance?
- How accurate are Weibull strength and lifetime lower tails required for reliability assessment (eg. P(failure) = 10^{-6})?

THEORETICAL ADVANCES FOR STRENGTH

- Seek out major scalings
- Build on Chain-of-Bundles model (Zweben, Rosen,...)
- Key Features
  - effective load transfer length δ
  - fiber load-sharing constants around broken fibers
    1, K_1, K_2, K_3, K_4,..., K_k,...
  - material volume is V = mn (10^6 to 10^{10})
    m = L/δ is number of bundles
    n is number of fibers

Comments on theoretical advances for strength:

- New theoretical and computational advances allow more realistic load-sharing calculations
- Also can relax chain-of-bundles assumption
- New developments beyond Weibull for nature of the strength distribution
- Will apply to microcomposite of six fibers in a hexagonal array

CHAIN-OF-BUNDLES MODEL FOR MICROCOMPOSITES

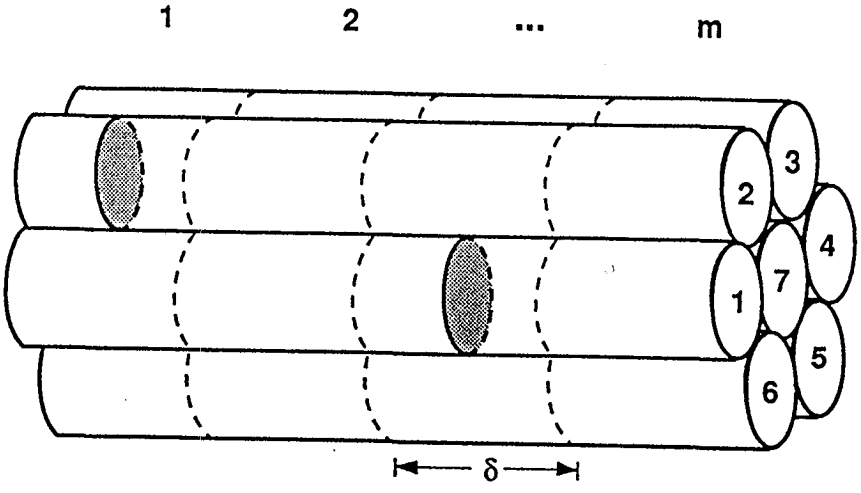

δ - Fiber element length

m - Number of bundles

◍ - Single fiber break

Comments on model for microcomposites

- **this is an idealized structure for composites of 7 fibers actually fabricated and tested**

SOME BUNDLE LOAD-SHARING CONFIGURATIONS

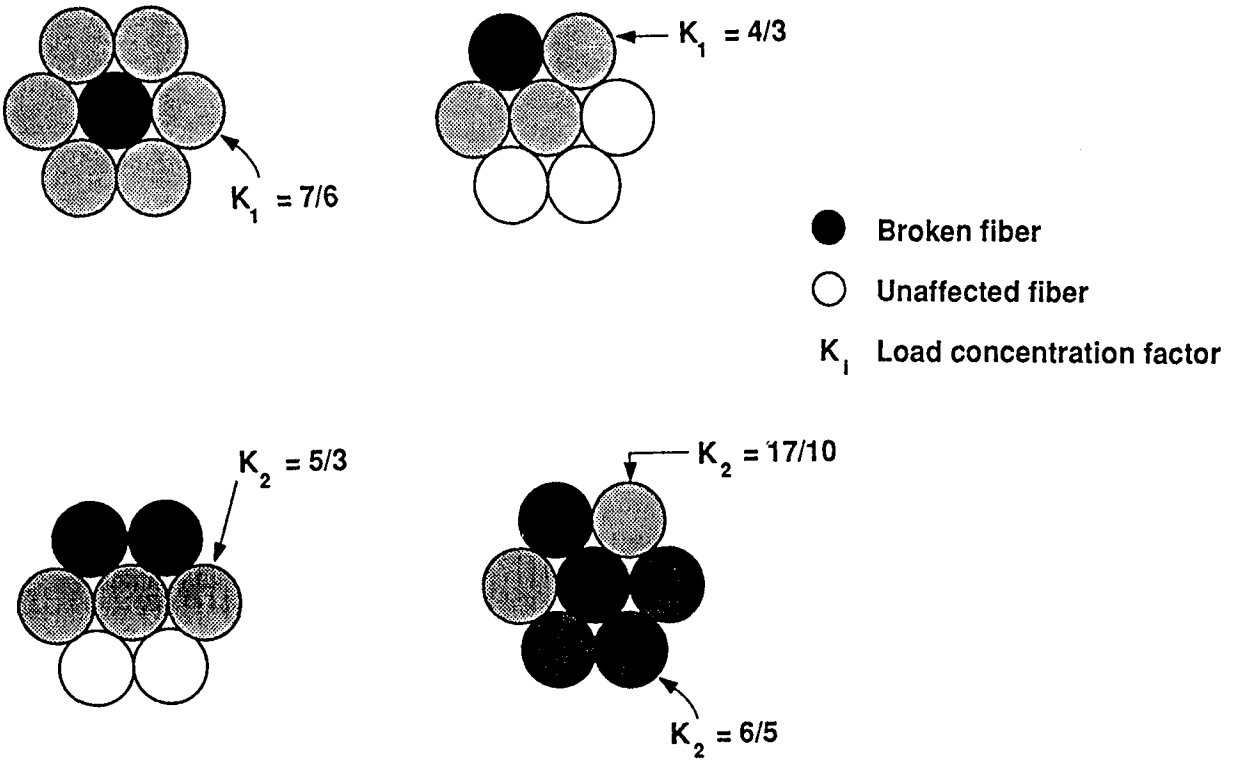

Comments on load-sharing:

- **This figure shows several configurations of failed and surviving fibers**
- **Loads induced on surviving fibers are calculated using a simple rule based on geometric adjacency**
- **More complicated rules based on shear lag assumptions change the calculated probabilities very little**
- **Bundle failure probabilities are based on failure progression through the bundles**

WEIBULL ENVELOPE DISTRIBUTION FOR COMPOSITE STRENGTH

for $1/K_k < \sigma / \sigma_\delta < 1/K_{k-1}$

$$H_{m,7}(\sigma) \approx 1 - \exp[- (\sigma / \sigma_{k,m,7})^{k\zeta}]$$

$$d'_1 = 1 \qquad d'_2 = (1/7)[6(7/6)^{\zeta} + 18(4/3)^{\zeta}]$$

$$d'_3 = (1/7)[36(4/3)^{\zeta}(5/3)^{\zeta} + 12(7/6)^{\zeta}(17/10)^{\zeta} + 18(7/6)^{\zeta}(6/5)^{\zeta} + 12(4/3)^{\zeta}(17/10)^{\zeta} + 18(7/6)^{\zeta}(6/5)^{\zeta}] .$$

Comments on Weibull Envelope:

- **Resulting Weibull envelope in decreasing load has exponents $\zeta, 2\zeta, \ldots, k\zeta, \ldots$ based on the idea of the critical cluster size k (critical number of adjacent breaks) at which a bundle collapses**
- **The constant d'_k contains information on the progression of failure configurations**
- **σ_δ and ζ are the Weibull scale and shape parameters respectively for a fiber element of size δ**
- **m is the number of bundles in the chain**

DOMINANT WEIBULL DISTRIBUTION FOR STRENGTH

$$H_{m,7}(\sigma) \approx 1 - \exp[-(\sigma/\sigma_c)^{\zeta_c}]$$

$$\sigma_c = \sigma_{k^*,m,7}$$

$$\zeta_c = k^*\zeta$$

Comments on dominant Weibull distribution:

- **One value of k denoted k* becomes dominant for the probability distribution**
- **The 'effective' Weibull shape parameter is ζ_c and the effective Weibull scale parameter is σ_c**
- **important to emphasize that the true distribution will have a downward concave shape relative to this distribution, i.e., Weibull distribution is conservative**

WEIBULL/WEAKEST-LINK SCALING FOR FIBERS

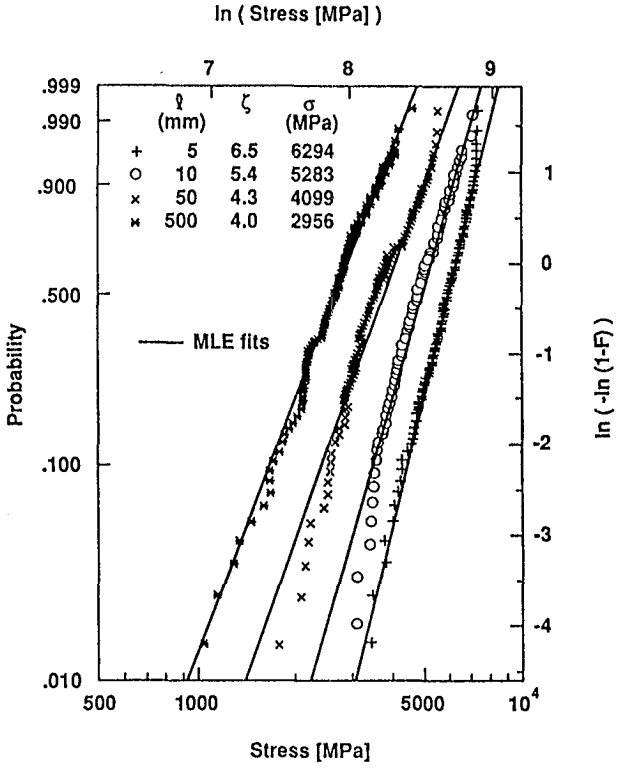

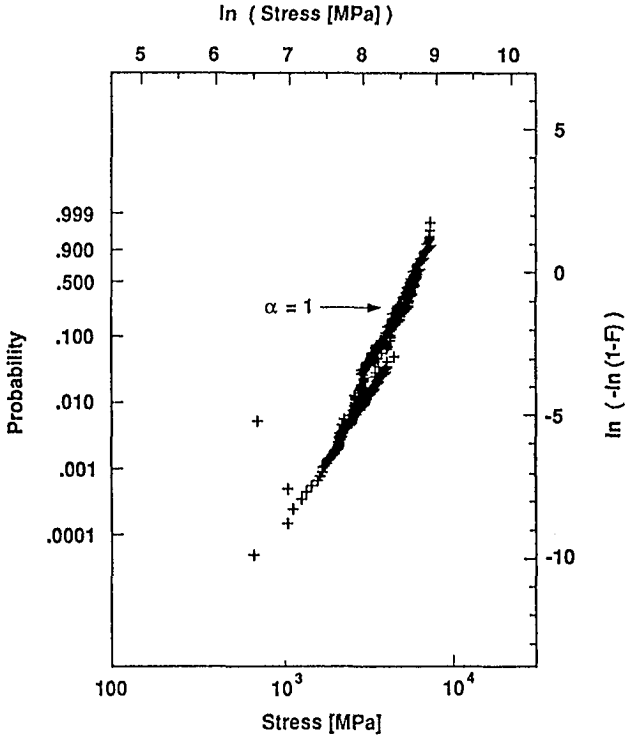

Comments on fiber distributions:

- **Here we show the results of fiber strength tests measured at gauge lengths of from 5mm to 500 mm representing a change of two orders of magnitude**
- **Sample sizes were about 100**
- **The graph on the right shows the data merged on the basis of a weakest link transformation (reference length 5mm)**
- **Note that the strength is very close to Weibull over a decade of strength**
- **These results scaled to length δ become inputs for the microcomposite model**
- **The parameter α is a Weibull length-strength sensitivity factor and is about one for these fibers**

CREEP-RUPTURE SCALING FOR FIBERS: WEIBULL PLOTS

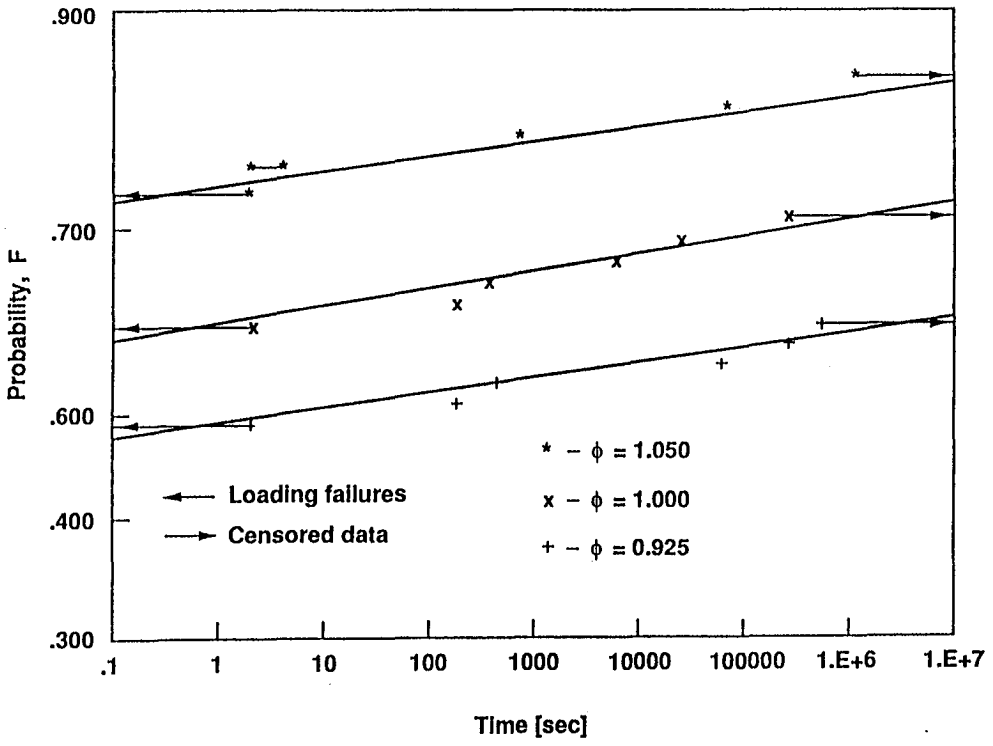

Comments:

- creep-rupture tests were run on single fibers at room temperature and three load levels ϕ = 1.05, 1.00 and 0.925 times the scale parameter for fiber strength
- The gage length was 50mm and the effective number of samples at each stress level was 36, 43 and 48 respectively
- A stepwise testing procedure was used based on a Coleman/Weibull/power-law formulation
- The results are plotted on Weibull coordinates, and the Weibull shape parameter was about 0.02

CREEP-RUPTURE SCALING FOR FIBERS: POWER LAW SCALING

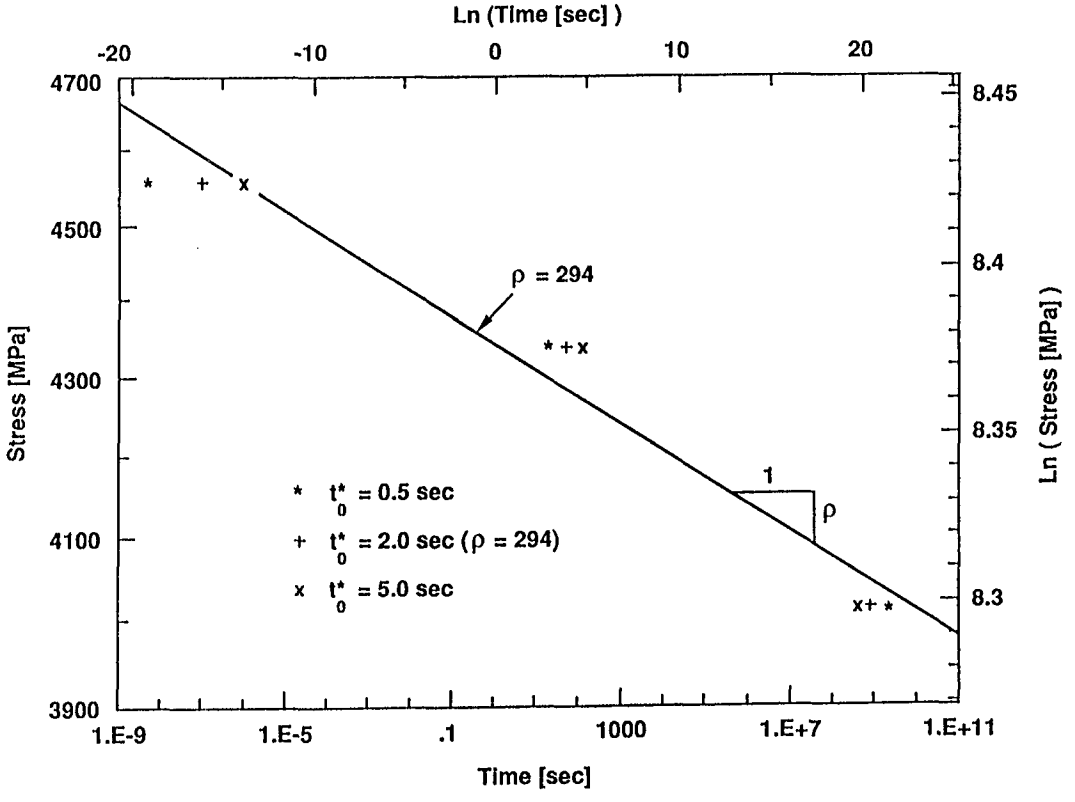

Comments:

- Analysis of data yields conclusion that fiber lifetime depends on stress level approximately as a power law with exponent $\rho = 294$
- Various assumptions are shown as to the time constant (the data did not have enough resolution to be more precise)
- As the power-law exponent for *composite* lifetime will turn out to be almost two orders of magnitude smaller, we will be able to ignore creep-rupture in the fibers

STRENGTH OF 7-FIBER MICROCOMPOSITES

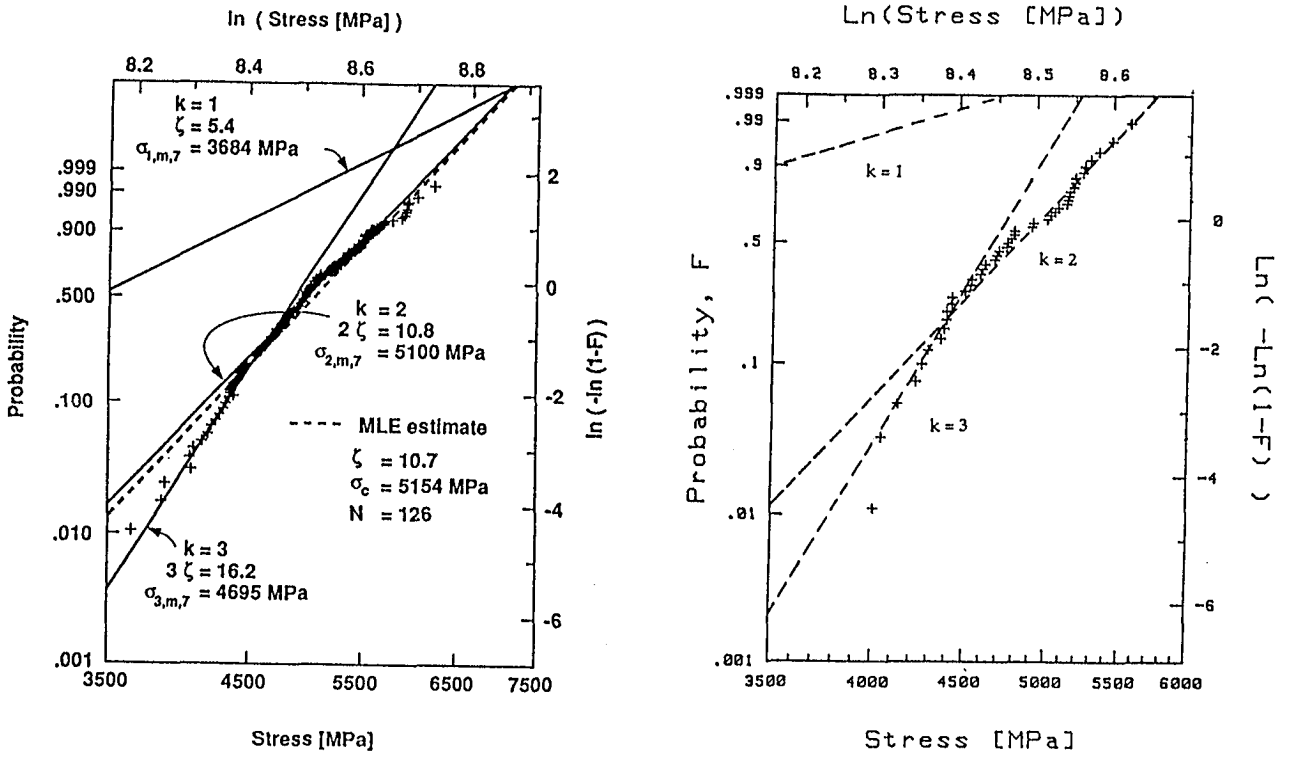

Comments:

- **Here we show strength results on seven fiber microcomposites**
- **We show results from two data sets involving two different epoxies**
- **The Weibull features discussed earlier are clearly shown**
- **The data does <u>not</u> follow the k = 1 line meaning that the composite does <u>not</u> fail when the first fiber fails**
- **In the middle stress range k = 2 means that the composite fails when the second fiber fails**
- **In the lower stress range k = 3 means that the composite fails when the third fiber fails**
- **Had an order of magnitude more fibers been tested we might have seen a k = 4 region**
- **Note multiples of the Weibull shape parameter almost exactly**
- **The conclusion is that for scaling purposes in strength and composite size a simple Weibull framework is an oversimplification -- though conservative**
- **Nevertheless there does tend to be a dominant Weibull distribution which in this case corresponds to k = 2.**
- **The dotted line in the leftmost plot shows a maximum likelihood estimate of this Weibull distribution based on all the data, and the parameters agree closely with those of the k=2 line**

THEORETICAL MODEL FOR LIFETIME: ELEMENTS

$$J_m(t) = J_0[1 + (t/t_0)^{\theta}] , \qquad t \geq 0,$$

$$\underline{\delta}_i(t) = \delta_i[1 + (t/t_{0i})^{\theta}]^{1/2} , \quad t \geq 0 ,$$

$$F_{\delta}(t;\sigma_i) = 1 - \exp\{ - (\sigma_i/\sigma_{\delta})^{\zeta} (1 + (t/t'_0)^{\theta})^{\alpha/2}\} , \quad t \geq 0,$$

Comments:

- **The first equation gives a power-law creep model for the matrix in shear under linear elasticity (though a nonlinear law gives a comparable parametric formulation)**
- **The second equation (Lagoudas, Hui and Phoenix 1989) shows how the effective load transfer length is affected**
- **The third equation gives an equivalent lifetime distribution for an 'element' of the composite**

THEORETICAL MODEL FOR LIFETIME: GENERAL RESULTS

$$1/\mathcal{K}_k < \sigma/\sigma_\delta < 1/\mathcal{K}_{k-1}$$

$$H_{m,7}(t;\sigma) = 1 - \exp[\,-m7\ \phi_k(t;\sigma)]$$

$$\phi_k(t;\sigma) = \begin{cases} d'_k\,(\sigma/\sigma_\delta)^{k\zeta}, & 0 < t < t^*_{0,k-1} \\ \quad \cdots & \\ d'_k(\sigma/\sigma_\delta)^{k\zeta}(t/t^*_{0,k-1})^{(k-1)\alpha\theta/2}, & t^*_{0,k-1} < t < t^{\#}_{k-1} \\ d'_{k-1}(\sigma/\sigma_\delta)^{(k-1)\zeta}(t/t^*_{0,k-2})^{(k-2)\alpha\theta/2} & t^{\#}_{k-1} < t < t^{\#}_{k-2} \\ \quad \cdots & \\ d'_2(\sigma/\sigma_\delta)^{2\zeta}(t/t'_0)^{\alpha\theta/2}, & t^{\#}_2 < t < t^{\#}_1 \\ d'_1(\sigma/\sigma_\delta)^{\zeta}, & t^{\#}_1 < t\,. \end{cases}$$

- **The main result is that for a given load range, a segmented Weibull lifetime distribution occurs in time depending on certain transition times**
- **The effective Weibull shape parameter in time for the corresponding segments decreases with increasing time**
- **The first and last segments correspond respectively to initial 'static' composite failure and no fiber failure whereby the composite lasts indefinitely**
- **The lifetime parameters depend on the load range**
- **The conclusion is that for scaling purposes in lifetime and composite size a simple Weibull framework is an oversimplification -- though conservative**
- **Nevertheless, for larger composites one Weibull distribution tends to dominate depending on the load range and composite size scale.**
- **However under larger size and load level extrapolations, the effective Weibull parameters change**

THEORETICAL MODEL FOR LIFETIME: WEIBULL/POWER-LAW APPROXIMATION

$$H_{m,7}(t;\sigma) \approx 1 - \exp\{ - [t/t_c(\sigma)]^{\beta}\}$$

where

$$t_c(\sigma) = t^*_{0,k^\#}(\sigma/\sigma_{k^\#+1,m,7})^{-\rho^*}$$

$$\beta = k^\# \alpha\theta/2 , \qquad k^\# \sim k^*$$

$$\rho^* = [(k^\#+1)/k^\#]\rho$$

and

$$\rho = 2\zeta / (\alpha\theta) .$$

Comments:

- **The first equation is the dominant Weibull distribution for the lifetime of the composite**
- **The second equation is the lifetime Weibull scale parameter, which is a power-law in stress level with the following parameters:**
  - **a time constant (involving the parameters of the model)**
  - **scale constant for stress (approximately the Weibull scale parameter for strength)**
  - **a power exponent which depends mildly on the critical cluster size for time, is proportional to the fiber Weibull shape parameter for strength, inversely proportional to the matrix creep exponent, and proportional to a fiber weakest-link scale factor (taken as one here)**
- **Next we show that these features occur in the lifetime data on microcomposites**

APPARATUS AND THREE LOAD LEVELS FOR MICROCOMPOSITE EXPERIMENTS

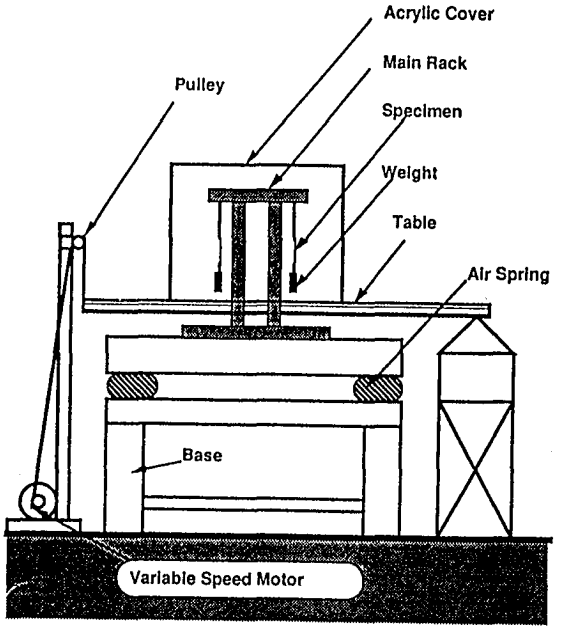

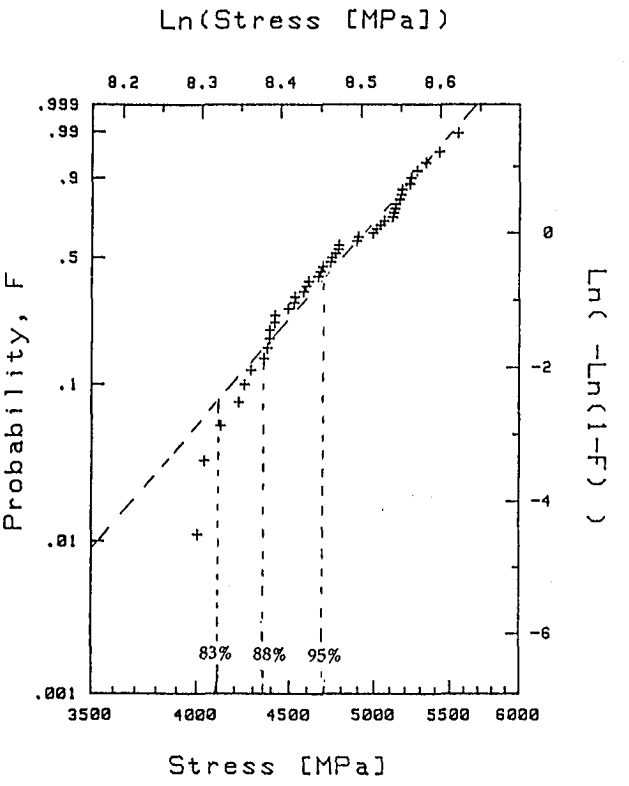

Comments:

- **The left figure shows the basic creep-rupture apparatus involving hanging weights and an air table**
- **The right figure shows the stress levels used in the experiment where % means percentage of the scale parameter for strength**
- **Note that the 95% stress level is well into the k = 2 range for strength, the 83% stress is well into the k = 3 range and the 88% is at the transition (see earlier figure)**

LIFETIME DISTRIBUTIONS FOR UPPER TWO LOAD LEVELS

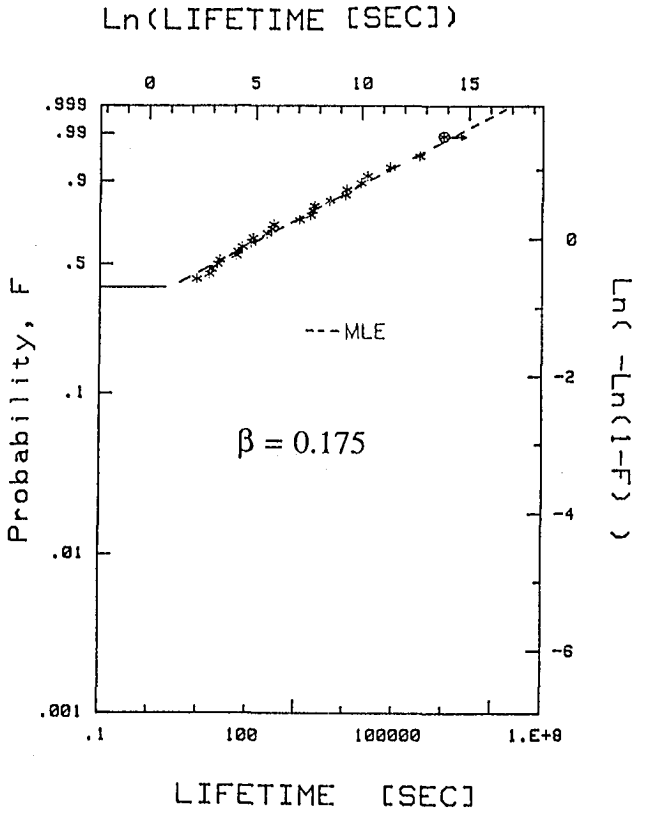

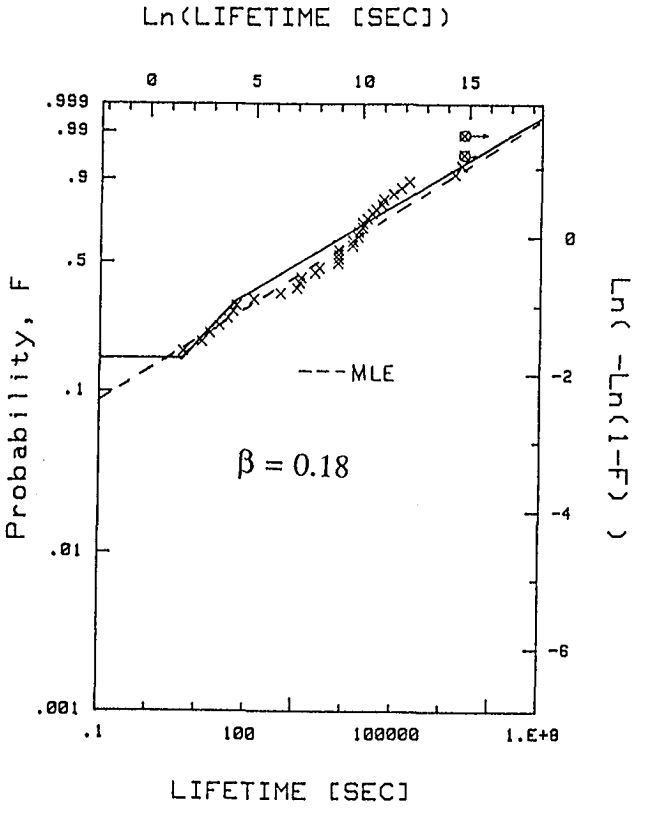

Comments:

- **The left figure shows lifetime results at the 95% stress level where the shape parameter for an MLE Weibull fit is $\beta = 0.175$**
- **The right figure shows lifetime results at the 85% stress level, where the shape parameter for an MLE Weibull fit is $\beta = 0.18$**
- **The solid segments in the right figure are predictions from the theory (only fitted parameters being δ and τ)**

LIFETIME DISTRIBUTION FOR LOWEST LOAD LEVEL AND POWER LAW FOR LIFETIME VERSUS STRESS

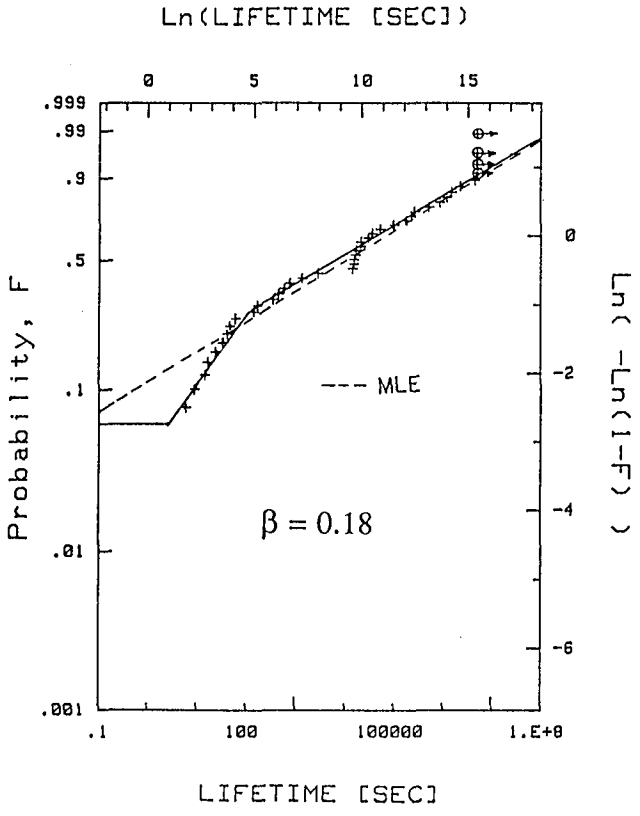

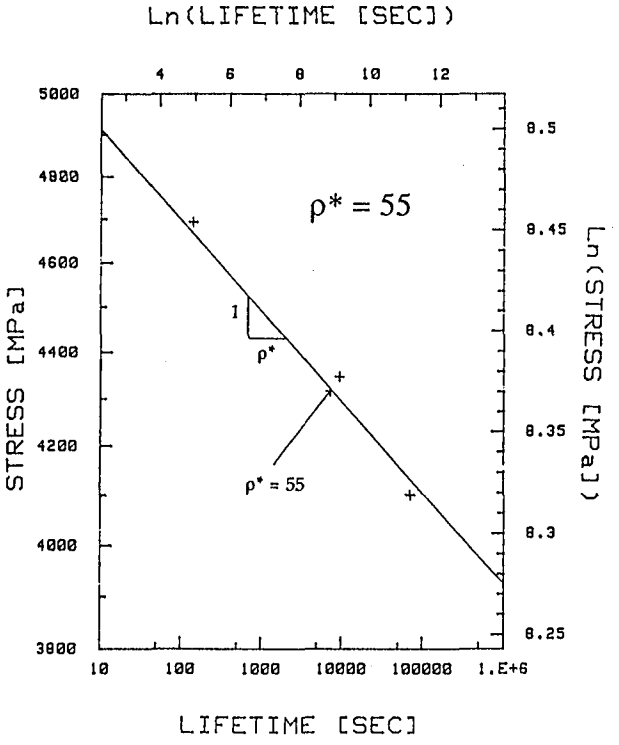

Comments:

- **The left figure shows lifetime results at the 83% stress level where the shape parameter for the upper tail is β = 0.18**
- **The solid segments in the right figure are predictions from the theory**
- **As theory would predict, the lower tail has shape parameter about 0.36**
- **Lower stress levels would continue to show increasing dominance of this lower tail as would larger composites and tails of even higher shape parameter would emerge**
- **Thus a simple Weibull/power-law framework fails to model the complex scalings in size, time and stress level**
- **The right figure shows a power law relating scale parameter for lifetime to stress level. The power-law exponent ρ* is 55 in reasonable accordance with theory**
- **A key point is that the exponent for a large composite will be only a little larger than half of this value**

MODEL PARAMETERS: FIBERS AND EPOXIES

	PSR(1988)	OPP(1989)
epoxy:	DER331/DEH26	DER331/Jeff.T403
E	2000 MPa	2000 MPa
σ_{ult}	65 MPa	50 MPa
ε_f	7-9% (dbn.)	5-6% (dbn.)
(θ	0.22	0.36 [0.49])
(t_0'	2 sec	3 sec)
fiber:		
α	1	1
ζ	5.4	6.8
σ_{10}	5283 MPa	6234 MPa
β	0.02	0.025 (?)
ρ	300	300 (?)

Comments:

- **The above are mechanical and statistical parameters for two systems that have been tested to varying degrees as discussed earlier**
- **PSR is Phoenix, Schwartz and Robinson (Composites Sci. and Tech.,1988)**
- **OPP is Otani, Phoenix and Petrina (J. Materials Sci., 1991)**

MODEL PARAMETERS: MICROCOMPOSITES

	PSR(1988)	OPP(1989)
composite:		
δ (k = 2)	0.15 mm	0.57 mm
δ (k = 3)	0.25 mm	0.81 mm
σ_δ	11,500 MPa	9500 MPa
β	0.11	0.18 [0.24]
θ	0.22	0.36 [0.49]
t_0'	2 sec	3 sec
ρ^*	98	73 [55]
ρ	49	37 [28]

Comments:

- **The above are the resulting best fit parameters to the microcomposites in strength and creep rupture as discussed earlier**
- **The above are mechanical and statistical parameters for two systems that have been tested to varying degrees as discussed earlier**
- **Note that the second matrix DER331/Jeffamine T403 seemed to give much longer load transfer lengths and a higher creep exponent**
- **Note that a large composite would have a power-law exponent closer to ρ**

IMPACT SESSION

C.C. Poe Jr., Moderator

Scaling of Impact Damage in Fiber Composites

Stephen R. Swanson
Department of Mechanical Engineering
University of Utah
Salt Lake City, Utah 84112

ABSTRACT

Impact damage in fiber composite structures remains of much concern, and is often the limiting factor in establishing allowable strain levels. The complexity of impact damage formation usually dictates that experiments are required, but scaling of results from small laboratory scale specimens to large structures introduces additional uncertainty into the analysis. This presentation gives the results of an analytical and experimental investigation intended to develop procedures for prediction of damage formation and subsequent strength loss, with particular emphasis on scaling of results with respect to structure size.

The experimental investigation involved both drop-weight and airgun impact on carbon/epoxy plates and cylinders. Five sizes of plates ranging from 50 by 50 by 1.072 mm to 250 by 250 by 5.36 mm, and two sizes of cylinders with diameters of 96.5 and 319 mm, were employed in the experimental program. Impact tests were carried out over a range of impact conditions, and specimens were inspected for damage by C-scan and de-plying. Analysis procedures were developed for both quasi-static and dynamic impacts for both the plates and cylinders. As has been reported previously, comparison of predicted structural response and measured surface strains was quite good over the entire range of sizes employed in the program.

The damage formation and strength loss after impact showed a number of interesting features that are significant with respect to scaling of size. The extent of delamination was observed to increase with specimen size more than would be expected if stresses controlled the delamination extent. This was explained on the basis that delamination is controlled by energy release rates, and thus incorporates the usual dependence on the absolute size characteristic of fracture mechanics. Additionally, the experiments indicated that delamination initiated at matrix cracks and is dependent on the absolute size of the ply group thicknesses. Both the initiation and propagation of delamination are seen to be controlled by fracture mechanics parameters, and thus show specific dependence on size that must be accounted for in extrapolating results from laboratory scale tests to full size structures.

Regions of broken fibers were observed in the impacted specimens. In contrast to delamination, the fiber breaks were best correlated with the calculated specimen strains. Results in the literature indicate that delivered fiber tensile strength (as opposed to the strength of dry fibers) is at most a very weak function of volume. However compressive strength is influenced strongly by a number of parameters such as stress gradients that would be expected to give strong size effects.

INTRODUCTION

- Scaling of experimental results from small scale to large composite structures remains a relatively unexplored subject

- Scaling of damage and failure appears particularly complicated, and is not well understood

- This paper will consider the results of damage observed in scaled impact tests on carbon/epoxy specimens

- We have performed impact tests that provide experimental evidence on scaling:
  - Plates and cylinders
  - Airgun and pendulum impacts
  - Scaling of results was examined with 5 sizes of plates and 2 sizes of cylinders

- This paper will:
  - Summarize the damage response
  - Address effects of size on damage formation

OVERVIEW

- Review of impact experiments

- Summary of damage formation

- Highlight effect of scaling (size effects) on
  - Delamination initiation
  - Delamination propagation
  - Fiber breakage

REPRESENTATIVE PREVIOUS WORK ON SCALING

- Nature of damage in impact
  - Boll et al., 1986
- Scaling of structural and failure response
  - Jackson, 1990, 1992,1993
  - Morton, 1988, 1991, 1993
  - Swanson, Smith, and Qian, 1991
  - Qian et al., 1990
  - Qian and Swanson, 1990
  - Wisnom, 1993

POSSIBLE MODELS FOR SCALING OF DAMAGE AND FAILURE IN FIBER COMPOSITES

- **Weibull**

$$P_f = 1 - \exp\left[-\int_V \left(\frac{\sigma - \sigma_u}{\sigma_0}\right)^m dV\right]$$

- **Fracture mechanics**

$$\sigma\sqrt{a} = constant$$

- **Stress gradients**
  - **Neuber**
  - **Point and average stress, Whitney and Nuismer**
  - **Point strain, Poe**
  - **Compression model of Swanson et al.**

- **Different models have different implications for scaling of damage and failure**

- **Understanding of the damage and failure process appears to be vital to understand scaling**

SCALING OF STRUCTURAL RESPONSE

- Scale behavior of structural response obtained by examination of governing differential equations, and forming dimensionless coefficients
- This procedure followed for both plates and cylinders
- Experimental test plan based on these results. The test plan then utilized geometric scaling of both specimen and impactor, with constant impact velocity independent of size.
- Experimental results over 5 plate sizes and 2 cylinder sizes confirm structural scaling procedures

II. Scaling Rules

- Scaling rules were developed from the equations of motion governing impact response of orthotropic plates

$$D_{11}\frac{\partial^2\bar{\alpha}}{\partial x^2}+D_{66}\frac{\partial^2\bar{\alpha}}{\partial y^2}+(D_{12}+D_{66})\frac{\partial^2\bar{\beta}}{\partial x\partial y}-A_{55}(\bar{\alpha}+\frac{\partial w}{\partial x})=\frac{\rho h^3}{12}\frac{\partial^2\bar{\alpha}}{\partial t^2} \quad (1)$$

$$(D_{12}+D_{66})\frac{\partial^2\bar{\alpha}}{\partial x\partial y}+D_{66}\frac{\partial^2\bar{\beta}}{\partial x^2}+D_{22}\frac{\partial^2\bar{\beta}}{\partial y^2}-A_{44}(\bar{\beta}+\frac{\partial w}{\partial y})=\frac{\rho h^3}{12}\frac{\partial^2\bar{\beta}}{\partial t^2} \quad (2)$$

$$A_{55}(\frac{\partial\bar{\alpha}}{\partial x}+\frac{\partial^2 w}{\partial x^2})+A_{44}(\frac{\partial\bar{\beta}}{\partial y}+\frac{\partial^2 w}{\partial y^2})+p(t,x,y)=\rho h\frac{\partial^2 w}{\partial t^2} \quad (3)$$

- Assume that the prototype and model are scaled according to $T_p = \lambda_T T_m$ In which the T are typical variables such as displacements, strains, etc.

- Substitute this relationship into the equations of motion, and requiring similitude gives the
  - Geometric scaling, both of structure and Impactor
  - Constant velocity of Impact
  - Time scales as λ
  - Impact force scales as λ^2

- Note that energy scales as λ^3 , while thickness scales as λ,thus energy should not be normalized by thickness

IMPACT EXPERIMENTS

- Plates made from AS4/3501-6 Carbon/epoxy prepreg, in 5 sizes ranging from 50 by 50 by 1.072 mm (2 by 2 by .042 in, 8 plies) to 250 by 250 by 5.36 mm (10 by 10 by .211 in, 40 plies). Layup $[(\pm 72)\lambda/0_2\lambda]_S$
- Cylinders filament wound from IM7/55A carbon/epoxy, in 96.5 and 319 mm ID. Layup $[\pm 18/90_2]_S$
- Specimens scaled geometrically, along with impact projectiles
- Specimens instrumented with strain gages
- Dynamic impacts carried out with air gun, using cylindrical projectiles with hemispherical ends that were 1, 1/2, and 1/4 of the projectile diameter

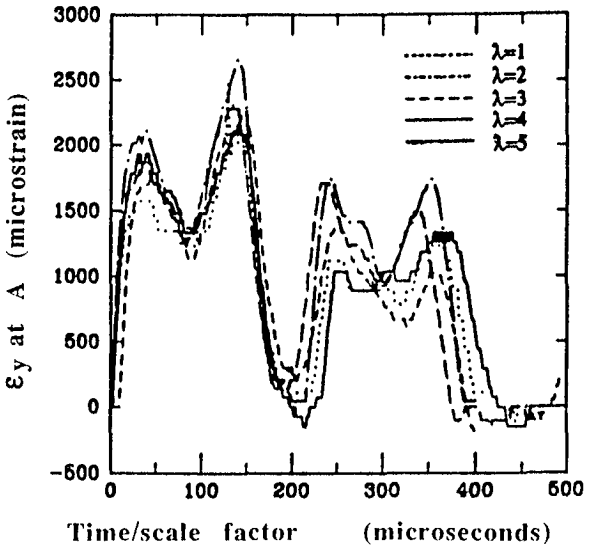

Scaling of strain response in impact tests on five different plate sizes

V0=4.57 m/s, location A

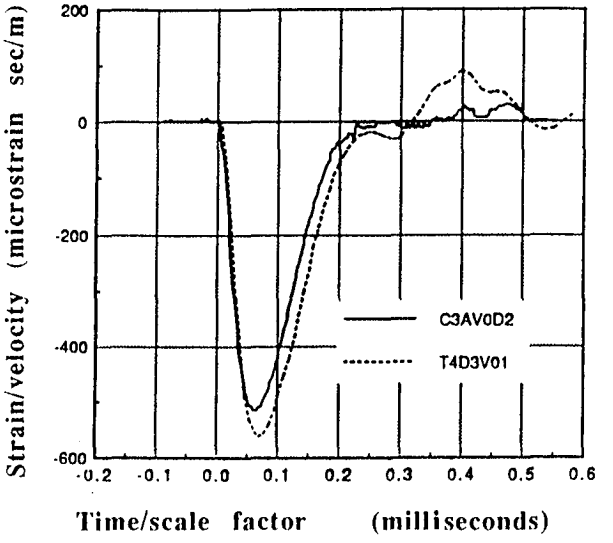

Scaling of strain response in impact tests of 96.5 mm and 319 mm diameter cylinders

Position H2

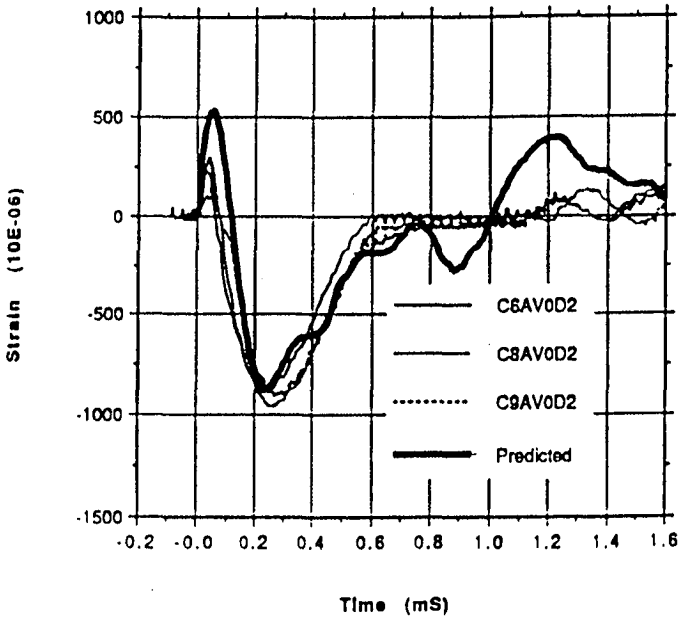

Comparison of measured and predicted hoop #1 strain gage reading for large cylinder

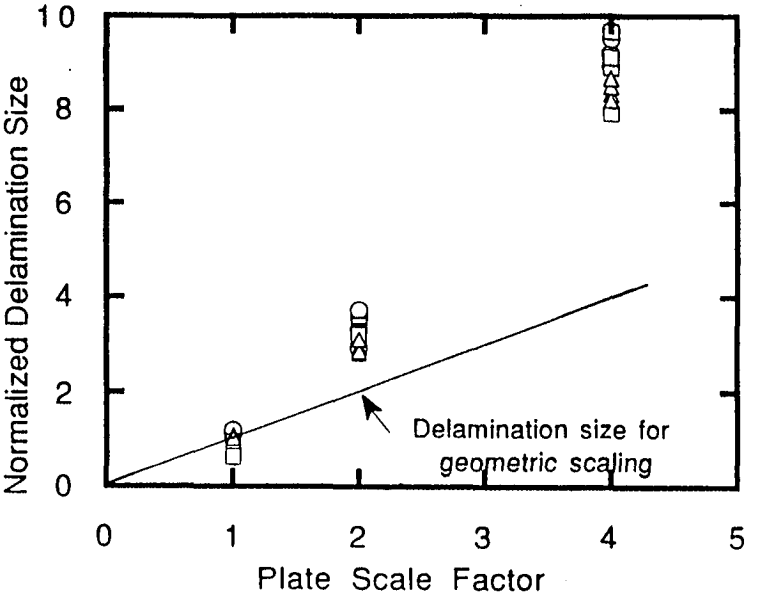

Scaling of delamination propagation in plate impact tests

DELAMINATION PROPAGATION, FRACTURE MECHANICS SCALING

- General expression for energy release rate given by

$$G=\sigma_0^2 \pi a f(a/w)/Q$$

- Includes absolute size effect.
  - If usual scaling followed, delamination size at constant impact velocity should scale with specimen size.
  - Experiments showed much larger increase in delamination with specimen size

- Delamination initiation also has a size effect

Delamination Doesn't Scale Geometrically

Geometric Scaling:

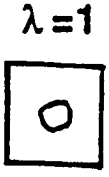

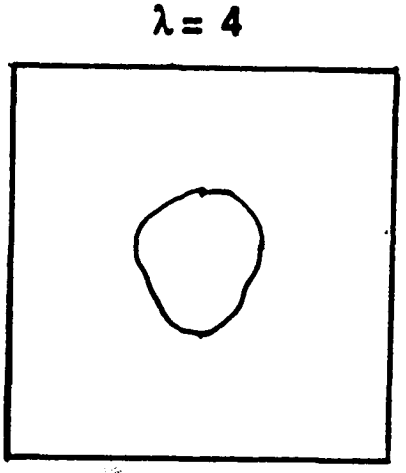

V_o = constant

Experiment:

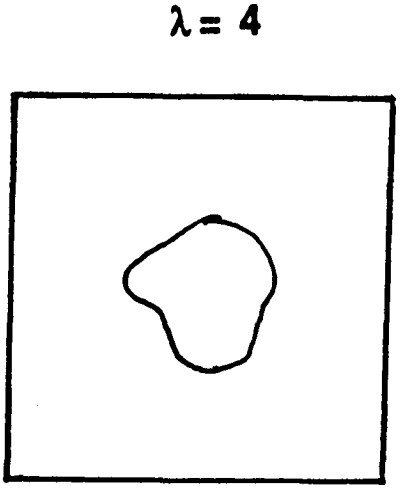

V_o=24.4 m/s

V_o = 12.2 m/s

DELAMINATION INITIATION SCALING

- Delamination initiation also has a size effect

- Experimental Evidence:
  - Delamination appears to occur at stresses lower than presumed allowables, in both plates and cylinders
  - Initiation stresses are function of absolute size

- Size effect likely due to delamination initiation at matrix cracks
  - Mechanism reported in the literature
  - Sectioning shows delamination away from neutral axis, where interlaminar shear stress is highest
  - Size of ply groups determines size of matrix crack, and thus energy release rate for delamination
  - Ply group thickness scaled in our experiments

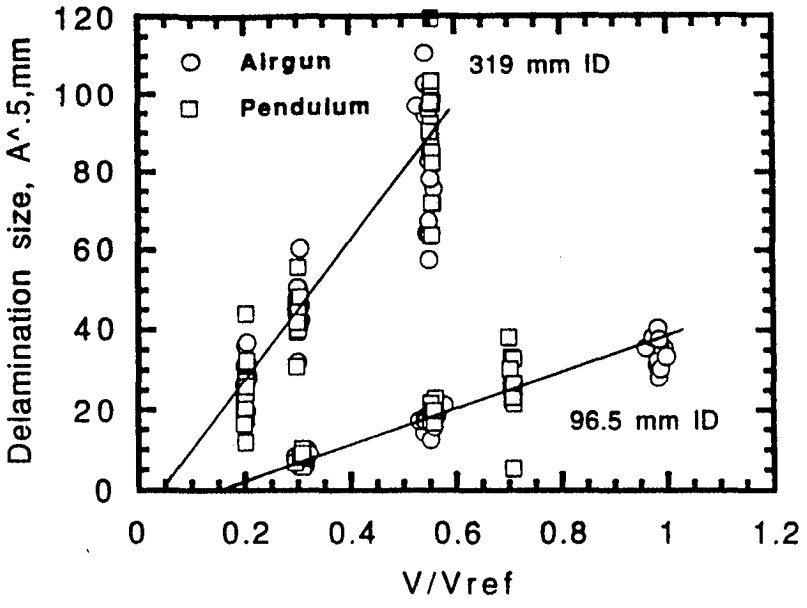

Estimation of delamination initiation in cylinder impact tests

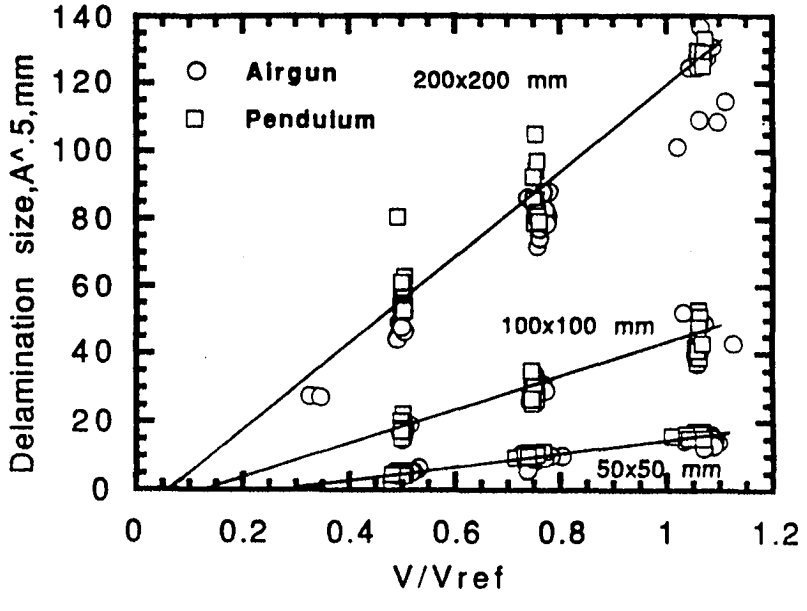

Estimation of delamination initiation in plate impact tests

FIBER BREAKAGE

- Fiber breaks observed in sectioning of plates and cylinders
- Prediction technique compares calculated fiber strains with allowable fiber strains (using maximum fiber direction strain failure criterion)
- Simple prediction for size of broken fiber zones compares linear analysis prediction with allowables, neglects nonlinear damage effects and propagation effects
- Predicted fiber breakage in general agreement with experiment, but does not show nonlinear effects
- Fiber breakage follows applied strains, does not appear to follow fracture mechanics type scaling
- Loss of strength due to fiber breaks has been correlated with residual strength by Tian and Swanson; fracture mechanics scaling to be expected

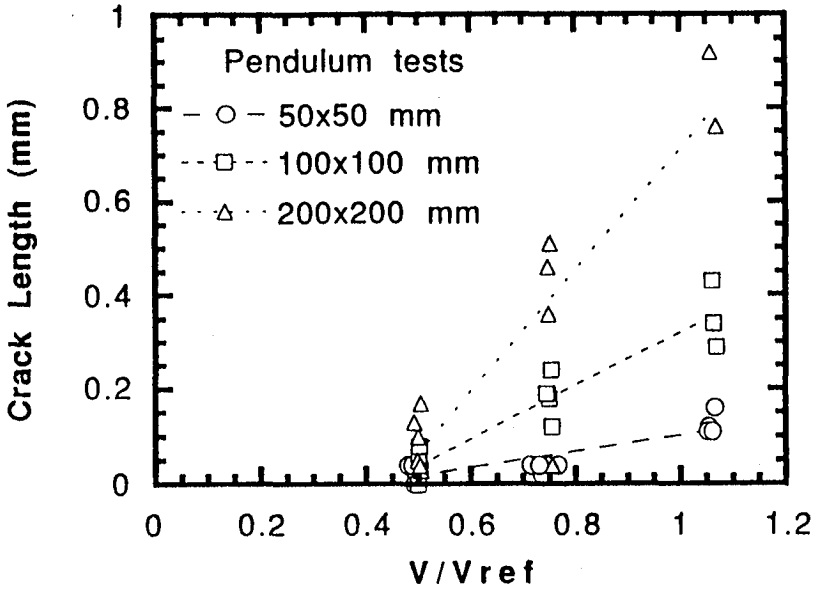

Broken fiber regions in impact tests of 50, 100, and 200 mm (2, 4, and 8 in.) plates

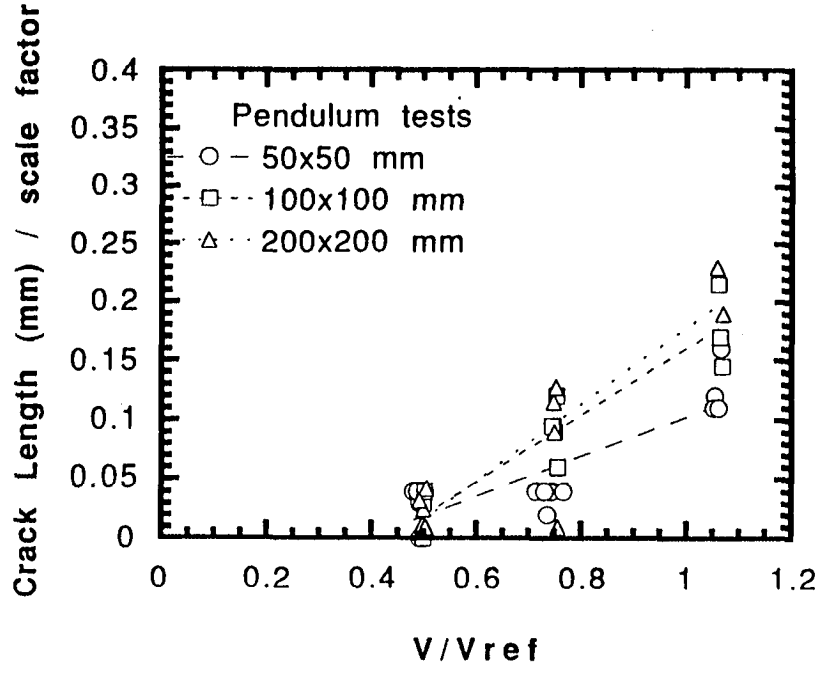

Effect of plate size on broken fiber regions in impact tests of 50, 100, and 200 mm (2, 4, and 8 in.) plates

SCALING OF FIBER TENSILE STRENGTH

- Apparently at most a small scaling effect on tensile strength
- As reported in "Strength Design Criteria for Carbon/Epoxy Pressure Vessels," Swanson, 1990, industry results indicate no more than 20% strength loss from all effects, in going from small specimens to very large pressure vessels, changing stressed volume by a factor of 10^6
- Thus tensile strength under uniform stress has extremely weak size effect

SCALING OF COMPRESSIVE STRENGTH

- Scaling of compressive strength appears to be very complicated
- Literature indicates possible larger scaling effects on compressive strength
- Apparent strong stress gradient effects, e.g. compressive strength in bending higher than in uniform stress
- Models considering support of adjacent fibers influencing fiber microbuckling support these gradient effects ("A Micro-Mechanics Model for In-Situ Compression Strength of Fiber Composite Laminates," Swanson, 1992). Models like this predict stress gradient, and therefore scaling effects.

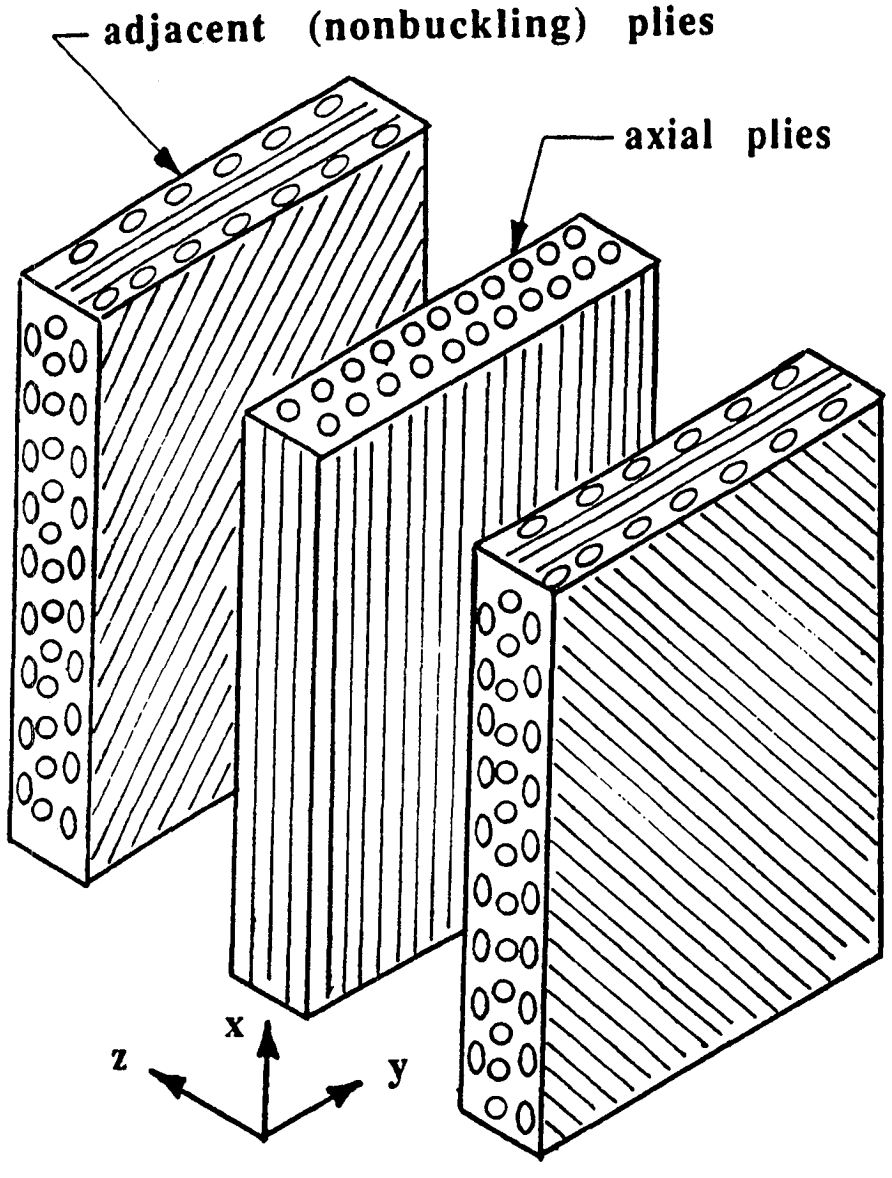

Model of axial plies laminated with non-buckling adjacent plies.

Swanson, S.R., "A Micro-Mechanics Model for In-Situ Compression Strength of Fiber Composite Laminates," ASME J. Eng Mtls Tech, 114, pp 8-12 (1992).

Shear mode of fiber microbuckling, with shear resistance offered by the matrix

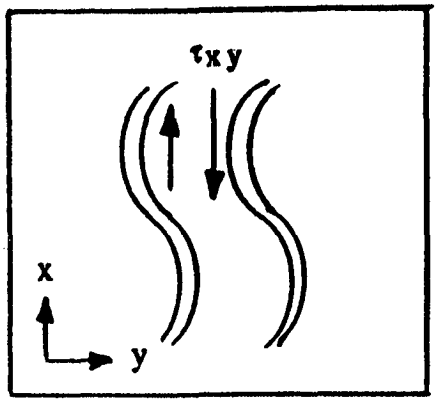

Additional shear resistance to fiber microbuckling offered by adjacent plies in compression failure of a laminate

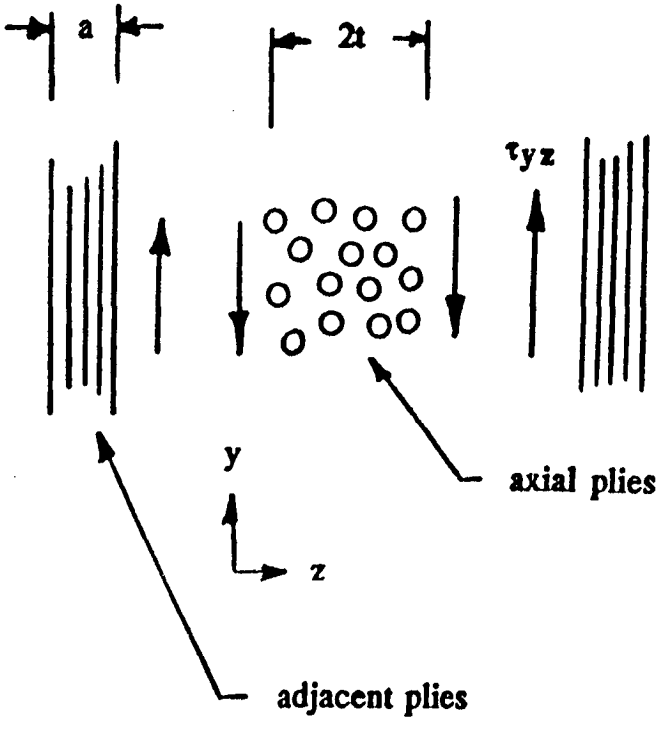

Swanson, S.R., "A Micro-Mechanics Model for In-Situ Compression Strength of Fiber Composite Laminates," ASME J. Eng Mtls Tech, 114, pp 8-12 (1992).

OTHER COMMENTS

- Accuracy of 2-d stress analysis near impact site
  - Cairns and Lagace used 3-d elasticity solution near impact
  - For flexible structures, spreading contact stress over the appropriate area using contact law provides reasonable acccuracy with 2-d (plate, shell) analyses

- Dynamic effects
  - Division of impacts into "quasi-static" and "dynamic" regimes can be accomplished on the basis of the ratio of impact mass to effective structure mass
  - Both analysis results and damage observations support this conclusion in the present experiments

SUMMARY AND CONCLUSIONS

- Impact experiments carried out over 5 plate and 2 cylinder sizes
- Scaling of damage formation can be understood if the damage mechanism is known
- Delamination propagation has a square root size effect as predicted by energy release rate
- Delamination initiation has size effect as predicted by energy release rate, presumably from initiation at matrix cracks
- Fiber breakage appears to follow calculated strains, without fracture mechanics effects
- Scaling of compression failure expected to be different than for tension fiber failure

Scaling Effects in the Tensile and Flexure Response of Laminated Composite Coupons

David P. Johnson
John Morton
Virginia Polytechnic Institute and State University

Sotiris Kellas
Lockheed Engineering and Sciences Co.

Karen E. Jackson
U.S. Army Vehicle Structures Directorate, ARL

Sponsored by NASA Langley Research Center
Landing and Impact Dynamics Branch

Outline

- Motivation/Objectives
- Scaling Issues
- Experimental Program
- Preliminary Tension Results
- Preliminary Flexure Results
- Conclusions

Motivation

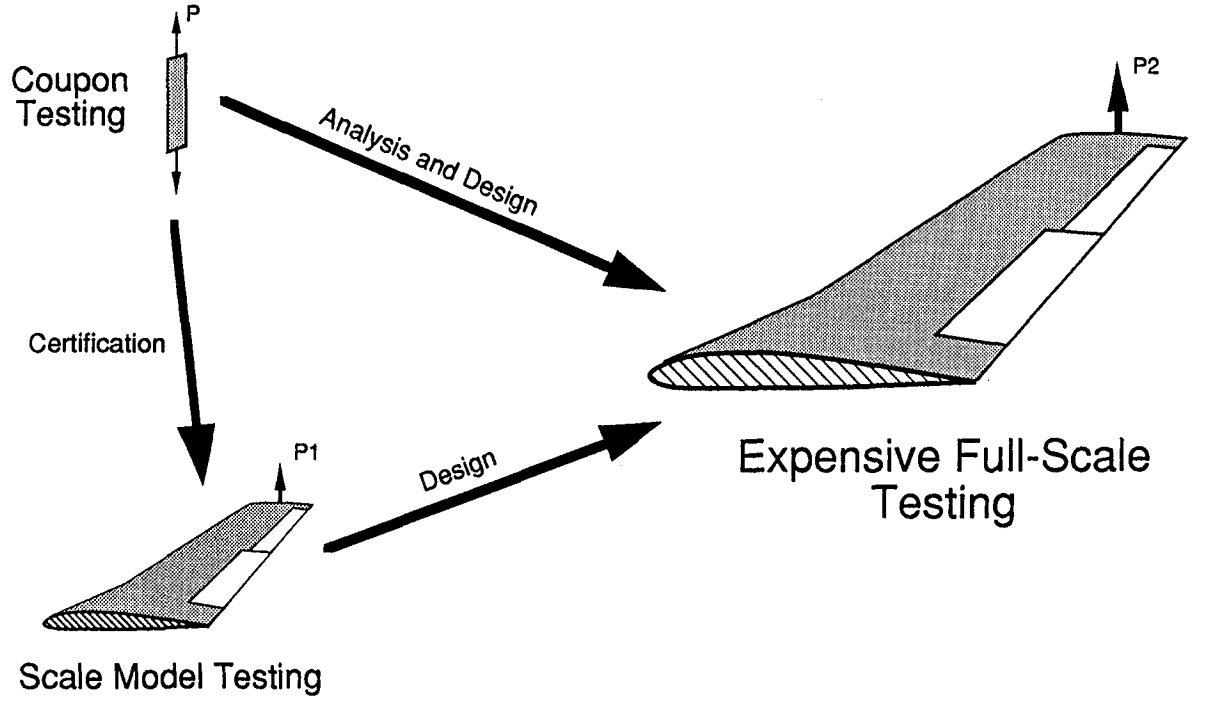

Objectives

- Investigate scaling effects in laminated composite coupons loaded in tension
- "Scaling effects" defined as variations, with size, in:

  Stress/strain response (shape)

  Strength

  Strain to failure

  Damage initiation and propagation

- Correlate damage modes with stress/strain plots

Outline

- Motivation/Objectives
- → Scaling Issues
- Experimental Program
- Preliminary Tension Results
- Preliminary Flexure Results
- Conclusions

Scaling of Coupon Dimensions

- 1-D
- 2-D
- 3-D

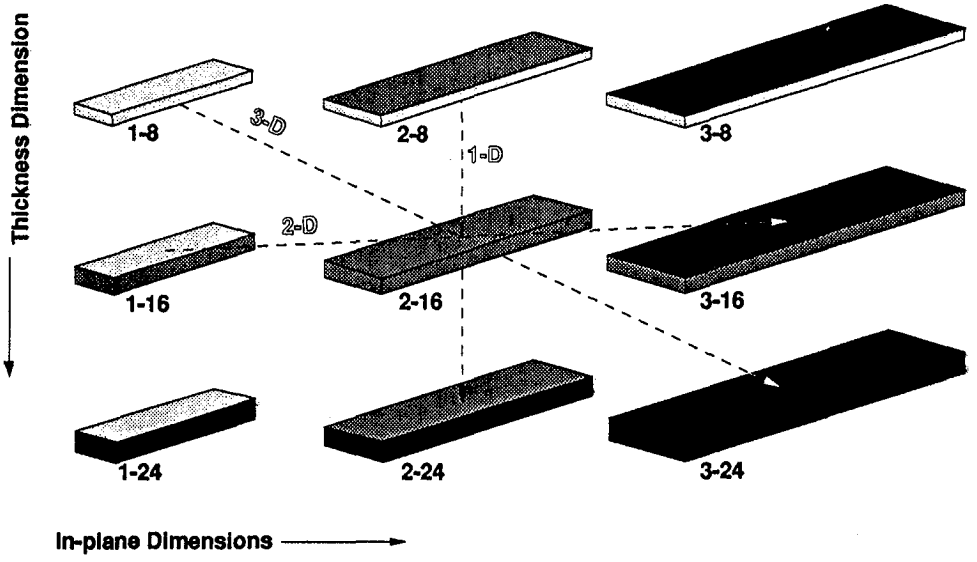

Scaling Laminate Thickness

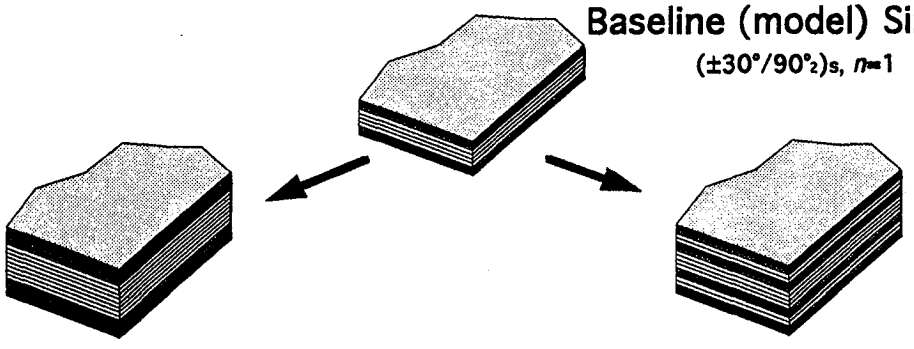

Baseline (model) Size

$(\pm 30°/90°_2)_S$, $n=1$

Ply-level (blocked plies)

$(\pm 30°_n/90°_{2n})_{2S}$, $n=2$

Sublaminate-level (distributed plies)

$(\pm 30°/90°_2)_{2S}$, $n=2$

Outline

- Motivation/Objectives
- Scaling Issues
- Experimental Program
- Preliminary Tension Results
- Preliminary Flexure Results
- Conclusions

Material Systems

- AS4/3502 graphite/epoxy
  - Widely used thermoset resin
  - Typically "brittle" in its response
- APC-2 graphite/PEEK (AS4 fiber)
  - Semi-crystalline thermoplastic resin
  - Typically "tough" in its response

Mechanical Response

- Load/deflection curves

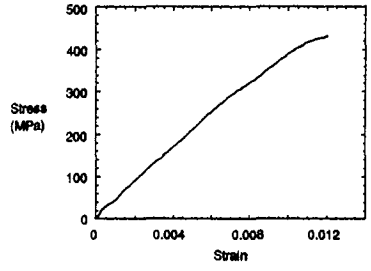

- Photo microscopy

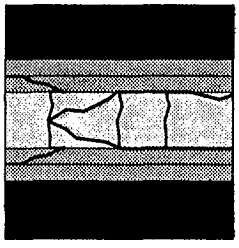

- Dye penetrant enhanced radiography

Outline

- Motivation/Objectives
- Scaling Issues
- Experimental Program
- ➔ Preliminary Tension Results
- Preliminary Flexure Results
- Conclusions

Mechanical Testing

- Specimen geometry (n = 1,2,3,4)

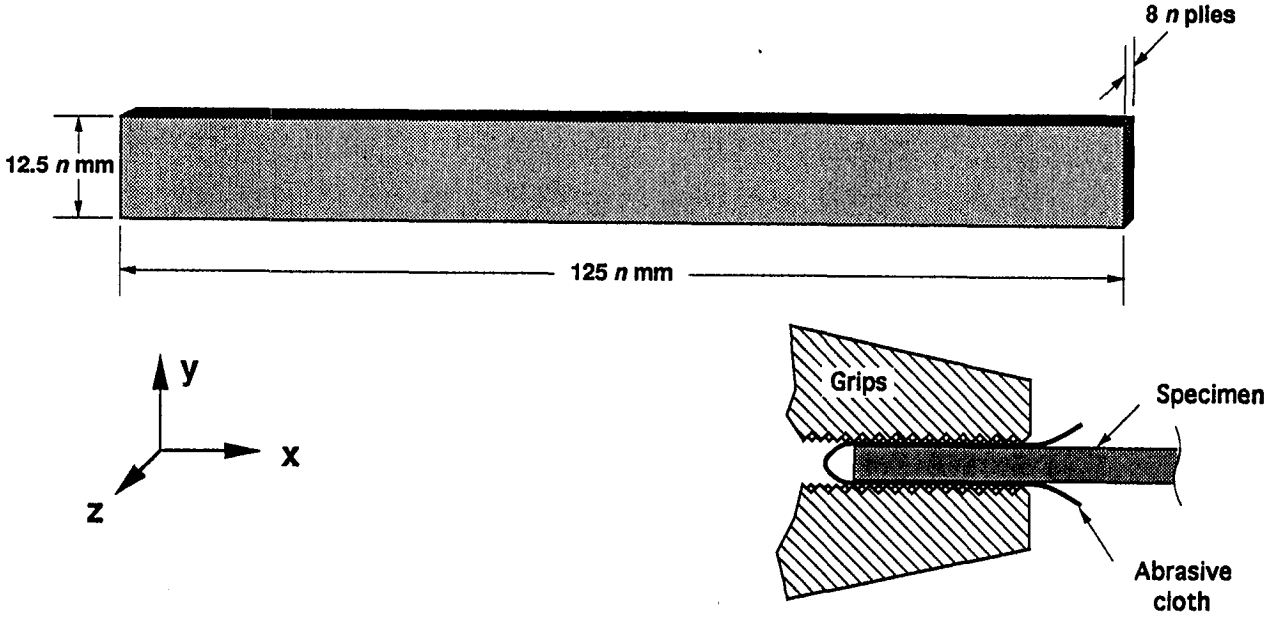

Stacking Sequences (AS4/3502)

- Lay-up A

  $[30/-30/90/90]_{ns}$

  $[30_n/-30_n/90_n/90_n]_s$

- Lay-up B

  $[45/-45/0/90]_{ns}$*

  $[45_n/-45_n/0_n/90_n]_s$

- Lay-up C

  $[90/0/90/0]_{ns}$

  $[90_n/0_n/90_n/0_n]_s$

- Lay-up D

  $[45/-45/45/-45]_{ns}$

  $[45_n/-45_n/45_n/-45_n]_s$

n = 1,2,3,4

*APC-2 panels

3-D Scaled Stress/strain Response (AS4/3502)

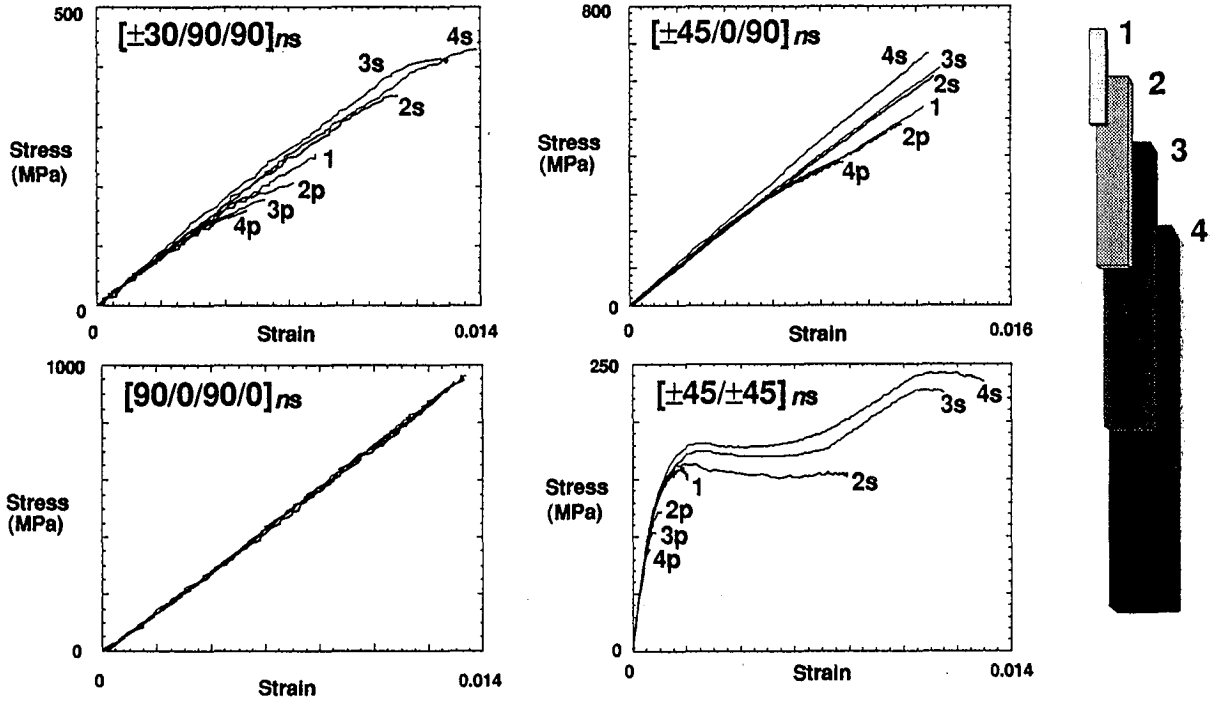

3-D Scaled Stress/strain Response (AS4/3502)

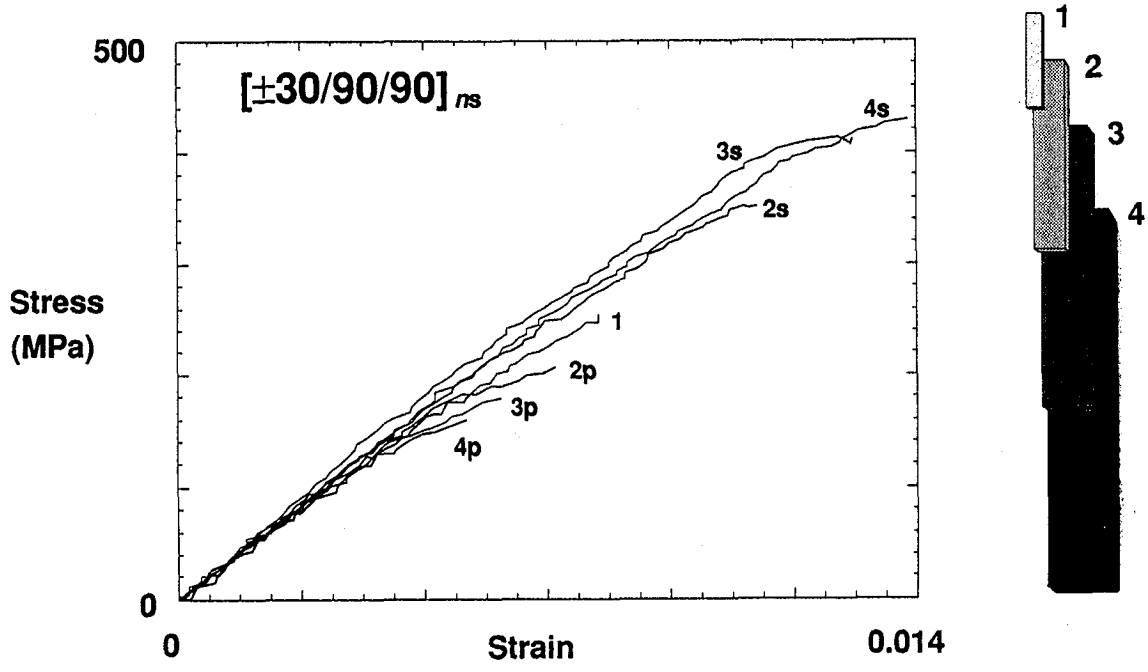

3-D Scaled Stress/strain Response (AS4/3502)

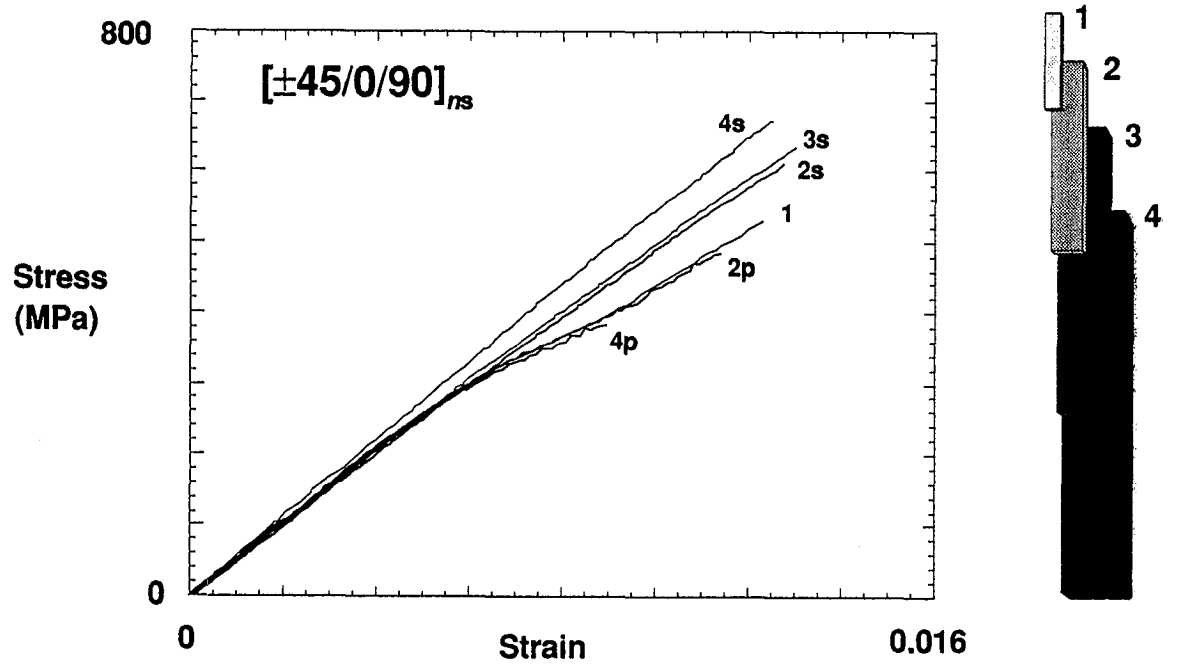

3-D Scaled Stress/strain Response (AS4/3502)

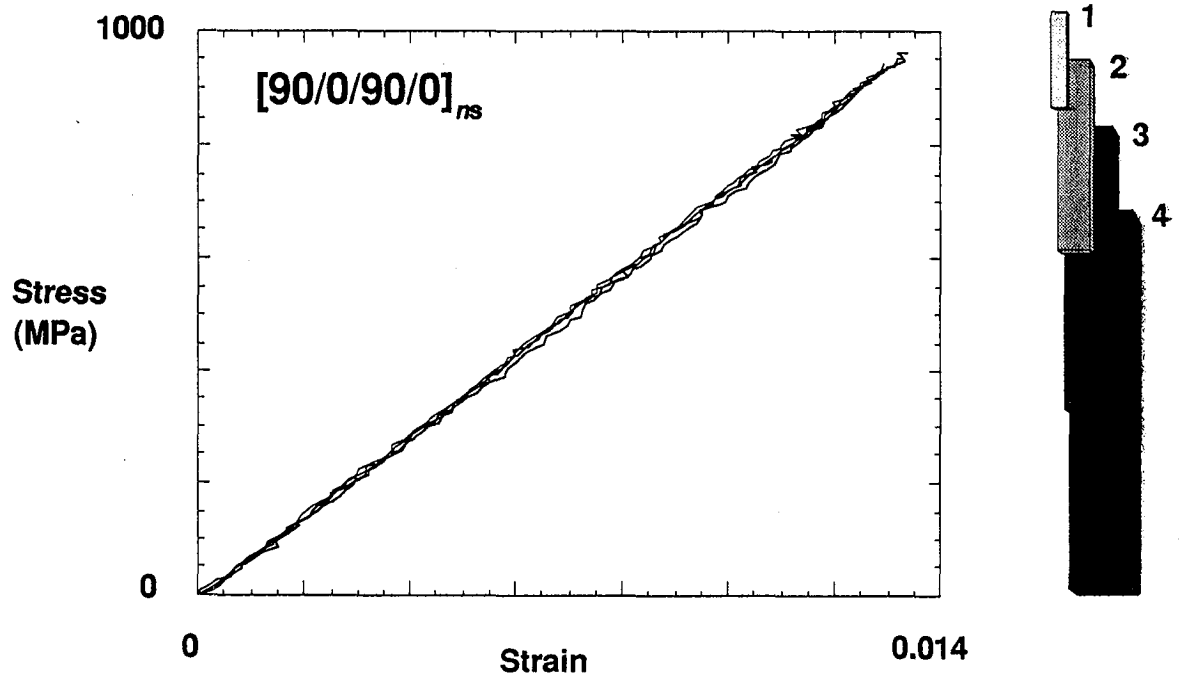

3-D Scaled Stress/strain Response (AS4/3502)

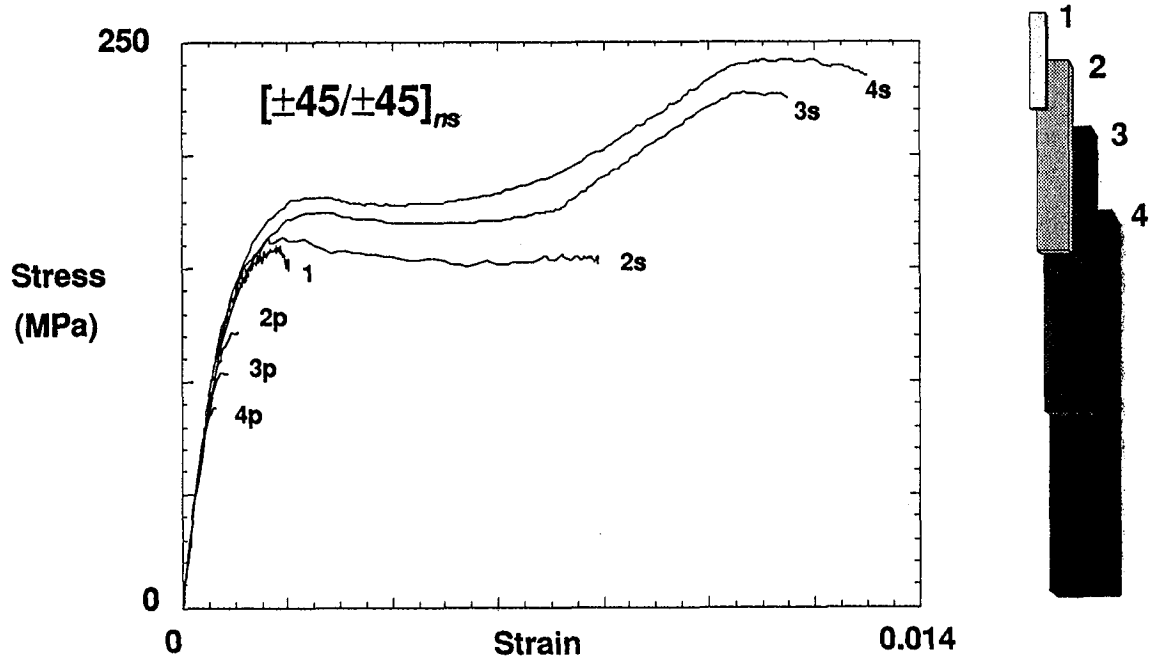

$[\pm 30/90/90]_{ns}$ 1- and 2-D Scaling (AS4/3502)

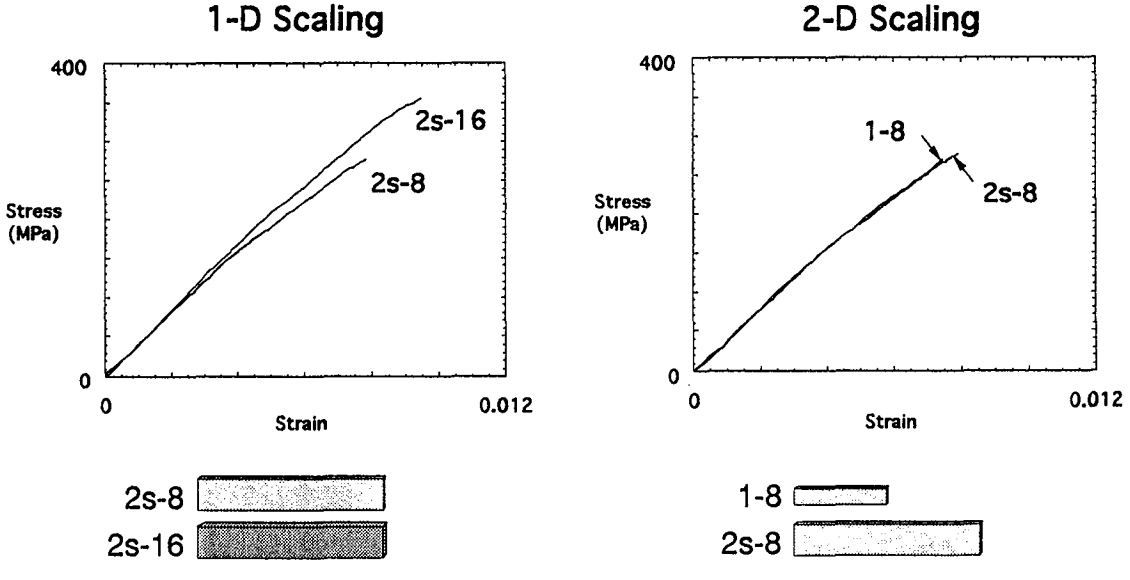

$[\pm 45/0/90]_{ns}$ 3-D Scaling (AS4/3502 vs. APC-2)

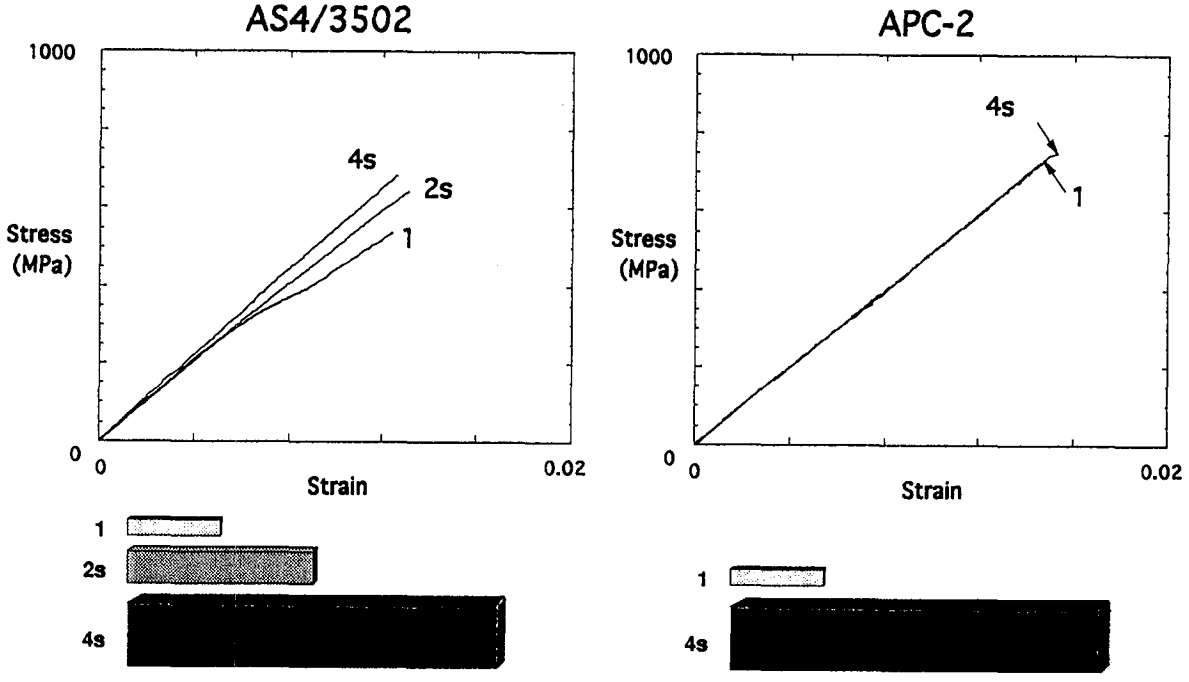

$[\pm 30/90/90]_{ns}$ (AS4/3502) Damage Propagation

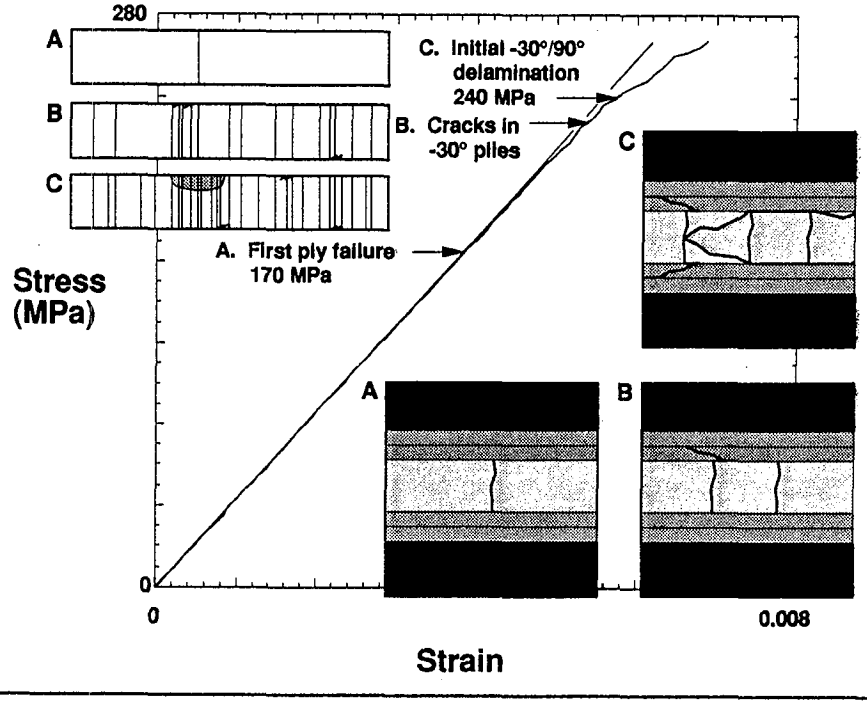

$[\pm 45/0/90]_{ns}$ (AS4/3502) Damage Propagation

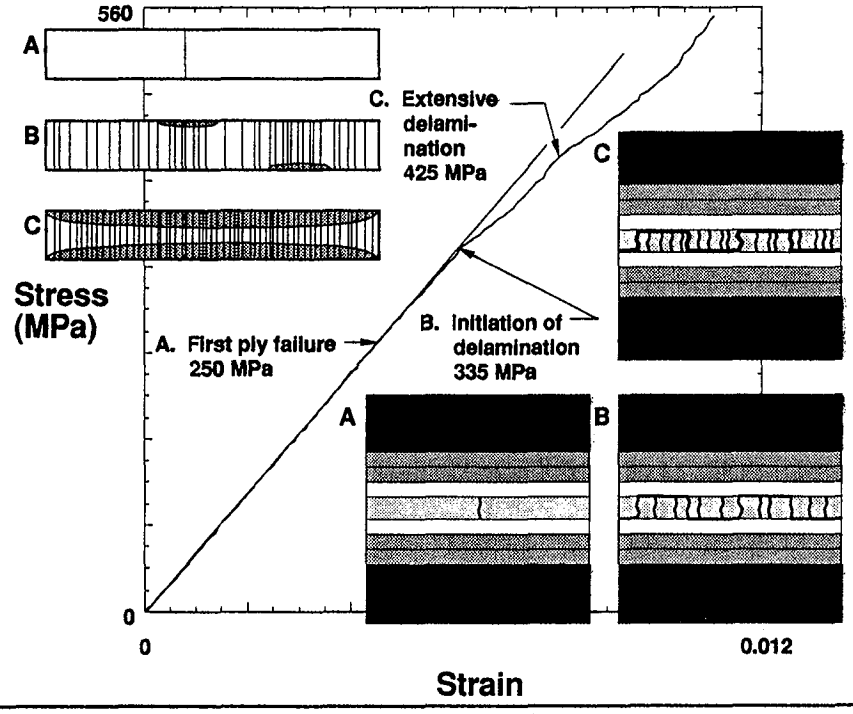

Normalized Properties (Strength)

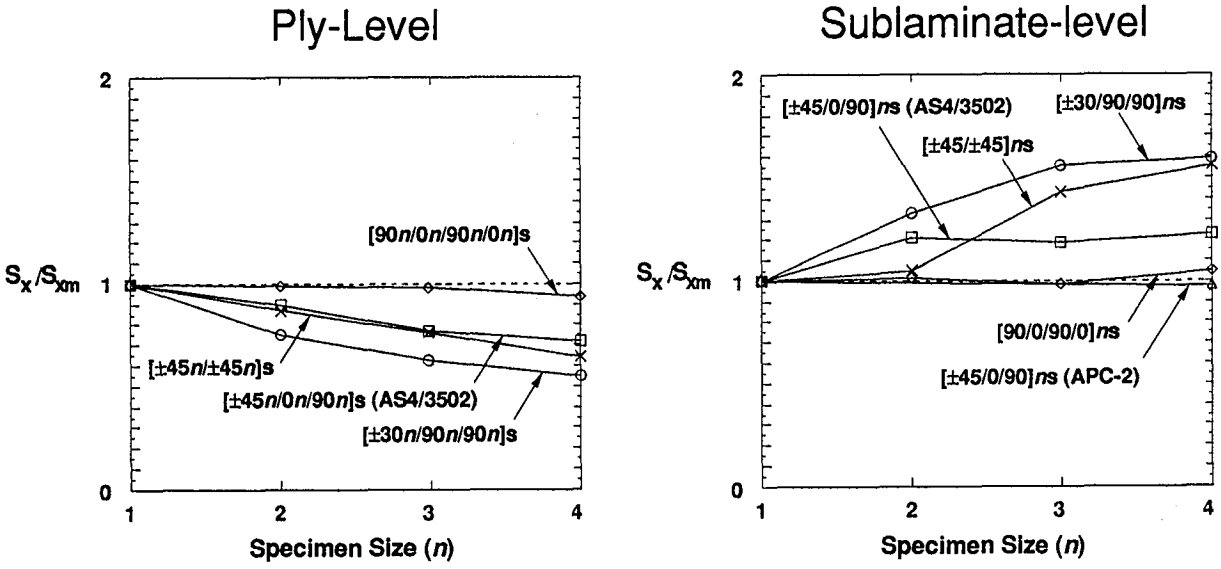

Normalized Properties (Failure Strain)

Ply-Level

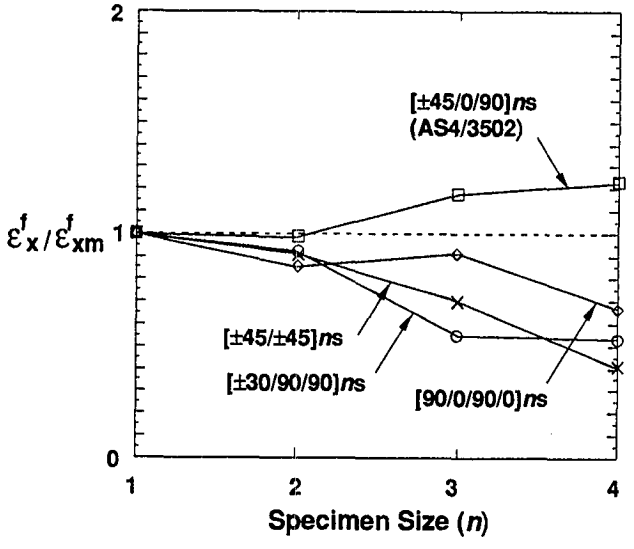

Sublaminate-level

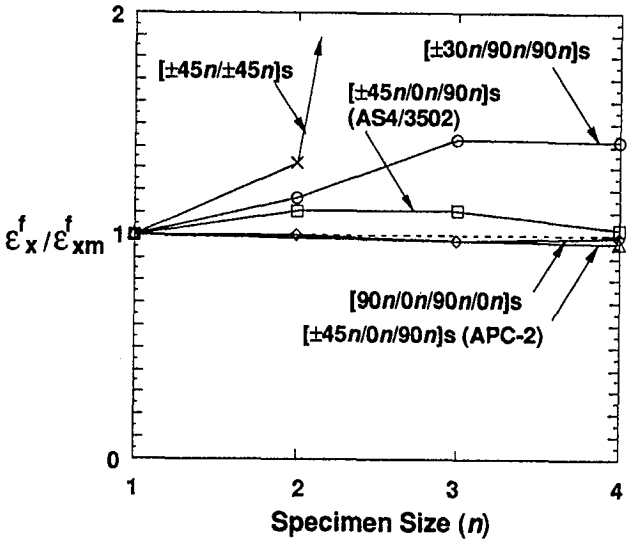

Normalized Properties

First Ply Failure
Sublaminate-level

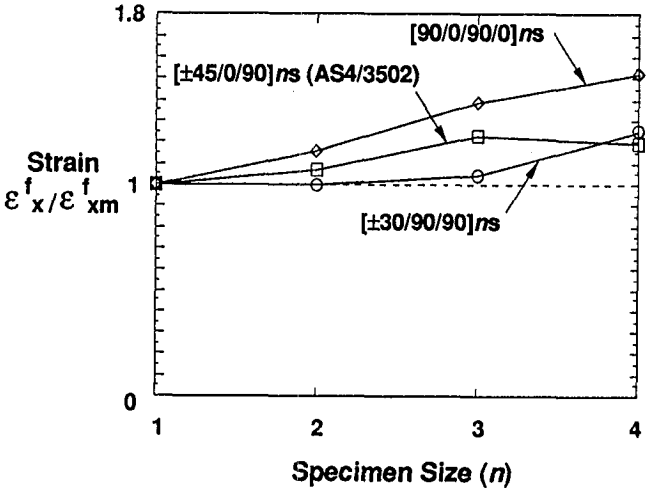

Delamination Onset
Sublaminate-level

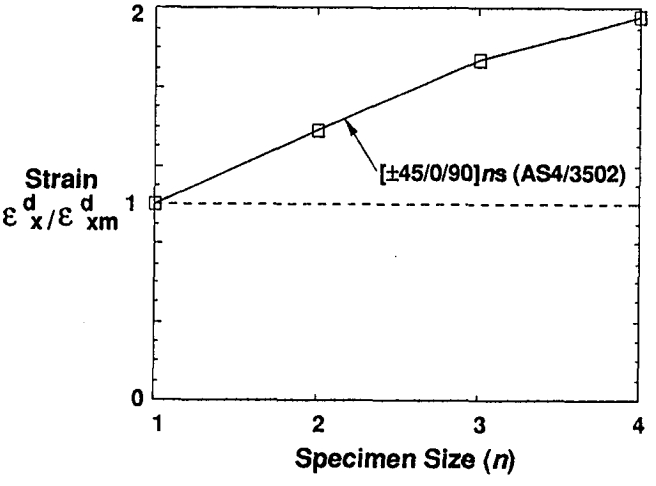

Outline

- Motivation/Objectives
- Scaling Issues
- Experimental Program
- Preliminary Tension Results
- ➔ Preliminary Flexure Results
- Conclusions

Mechanical Testing

- Specimen geometry (n = 1,2,4)

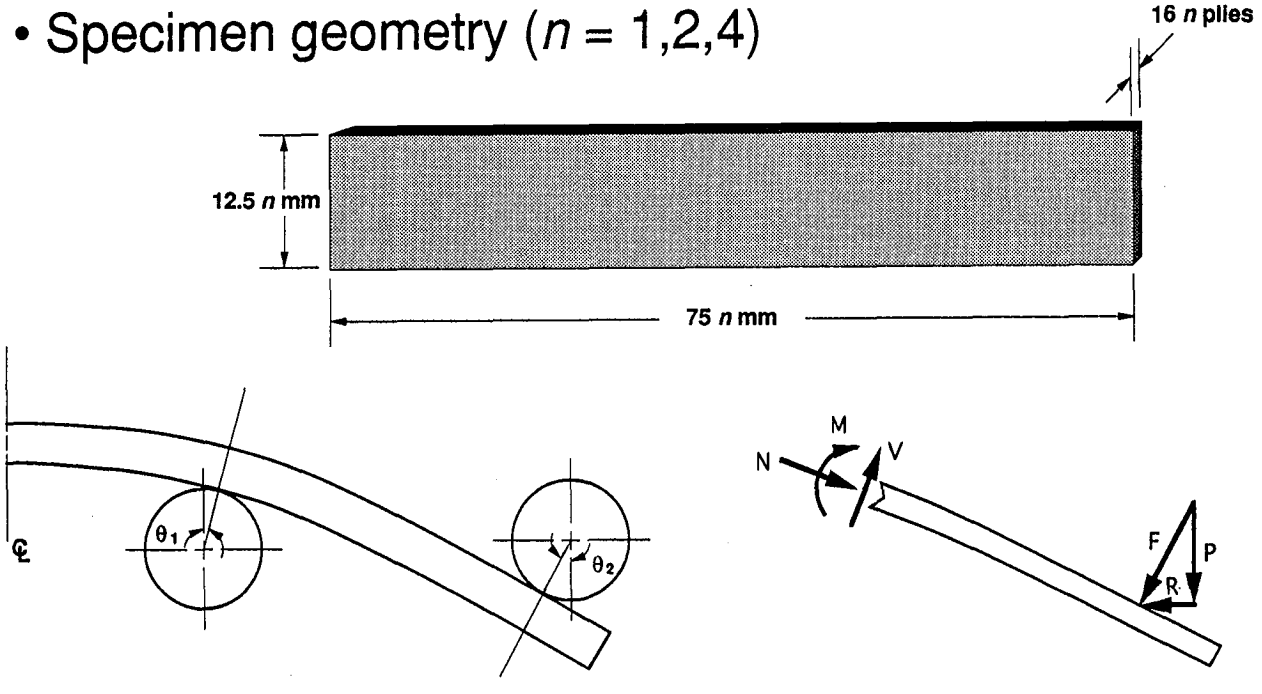

Stacking Sequences

- Lay-up B

  $[45/-45/0/90]_{2ns}$

  $[45_n/-45_n/0_n/90_n]_{2s}$

- Lay-up C

  $[0/90/0/90]_{2ns}$

  $[0_n/90_n/0_n/09_n]_{2s}$

- Lay-up D

  $[45/-45/45/-45]_{2ns}$

  $[45_n/-45_n/45_n/-45_n]_{2s}$

$[45/-45/0/90]_{2ns}$ and $[45_n/-45_n/0_n/90_n]_{2s}$ 3-D Scaled Response

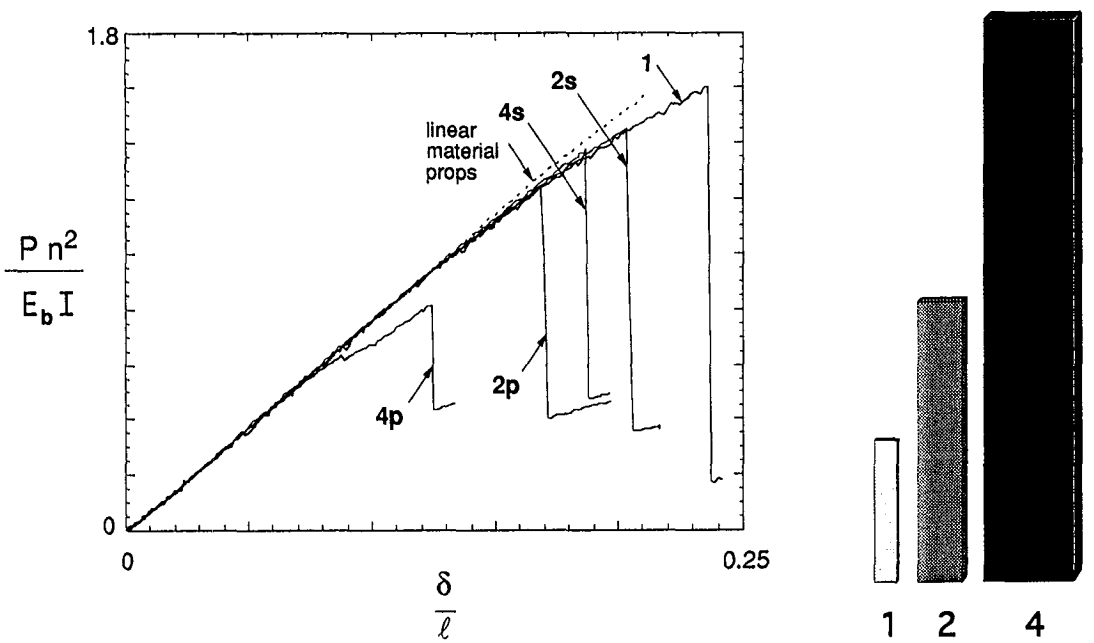

$[0/90/0/90]_{2ns}$ and $[0_n/90_n/0_n/90_n]_{2s}$ 3-D Scaled Response

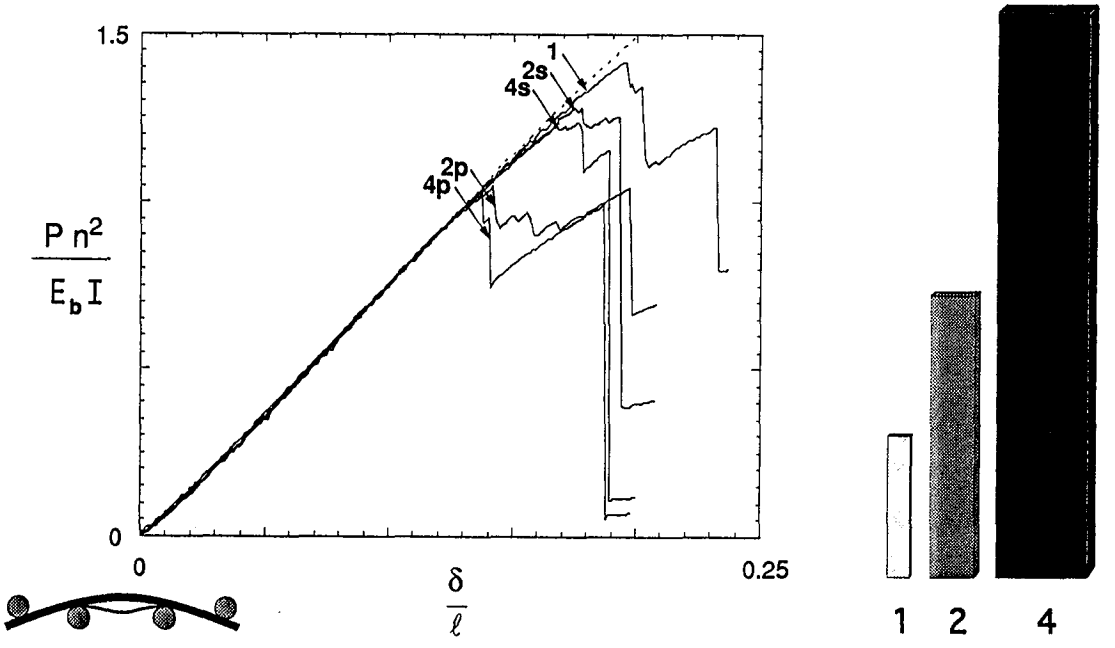

$[45/-45/45/-45]_{2ns}$ and $[45_n/-45_n/45_n/-45_n]_{2s}$ 3-D Scaled Response

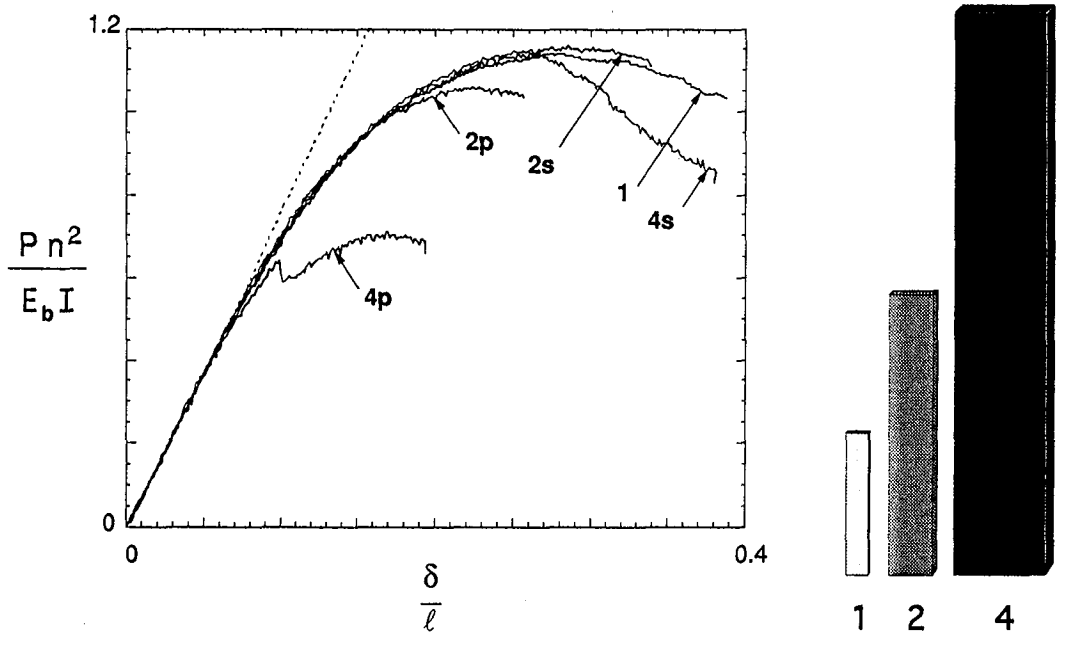

Outline

- Motivation/Objectives
- Scaling Issues
- Experimental Program
- Preliminary Tension Results
- Preliminary Flexure Results
- ➔ Conclusions

Conclusions (Tension)

- Distributed plies superior to blocked plies
- Matrix toughness can reduce/eliminate scaling effects
- Delamination may play a significant roll
- Presence of 0° plies lessens scaling effects

Conclusions (Flexure)

- Non-uniform loading changes the nature of scaling
- Surface 0° plies fail by compressive buckling
- Load introduction/structural effects important

SCALING EFFECTS IN THE IMPACT OF COMPOSITE BEAMS AND PLATES

John Morton

Department of Engineering Science and Mechanics
Virginia Polytechnic Institute and State University

MATERIAL AND STRUCTURAL SCALING

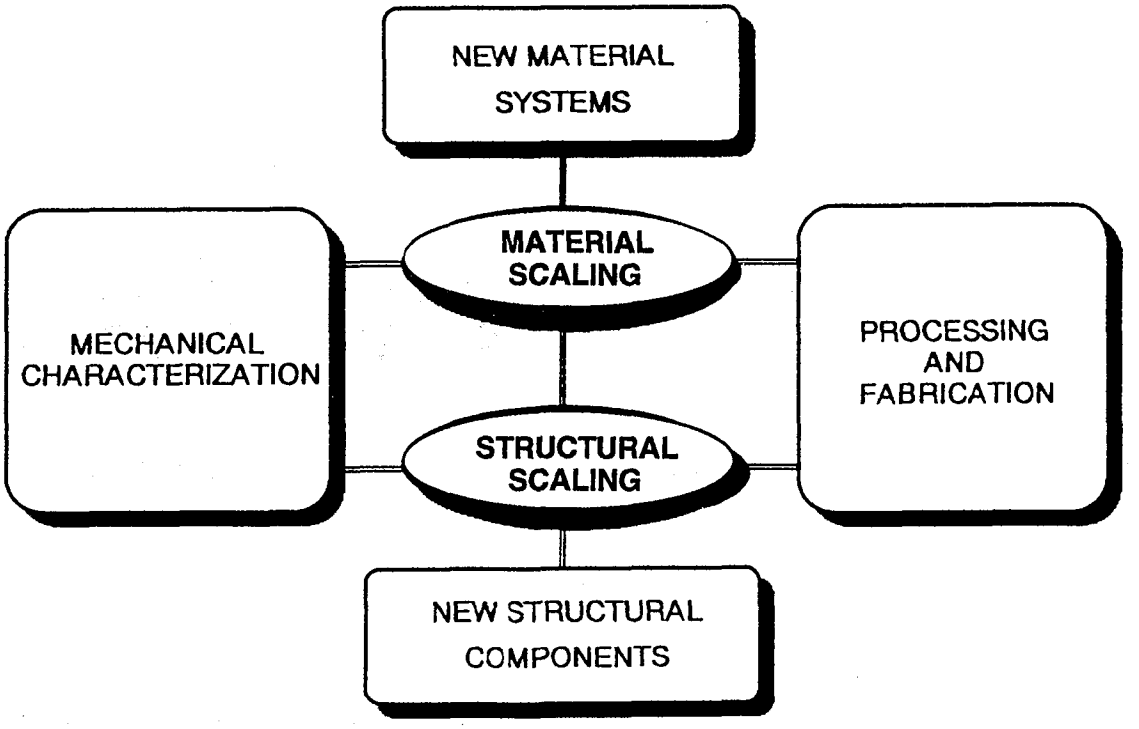

SCALING LEVELS

- FIBER DIAMETER – Not Practical
- PLY THICKNESS – Residual stress effects
- SUBLAMINATE – Pertinent scaling parameters
- SPECIMEN – Rules of similitude

SPECIMEN SCALE-UP

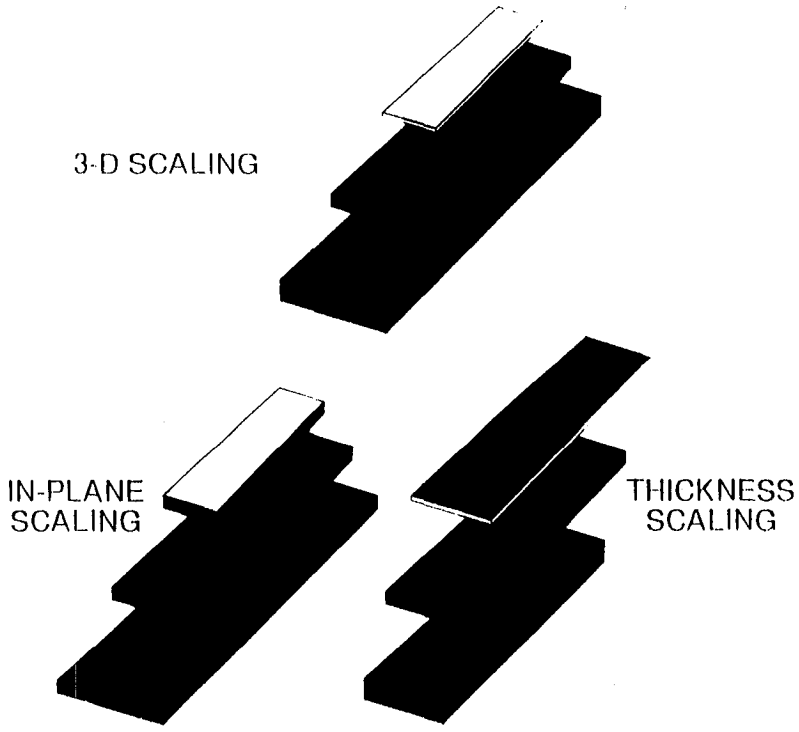

LAMINATE THICKNESS INCREASE

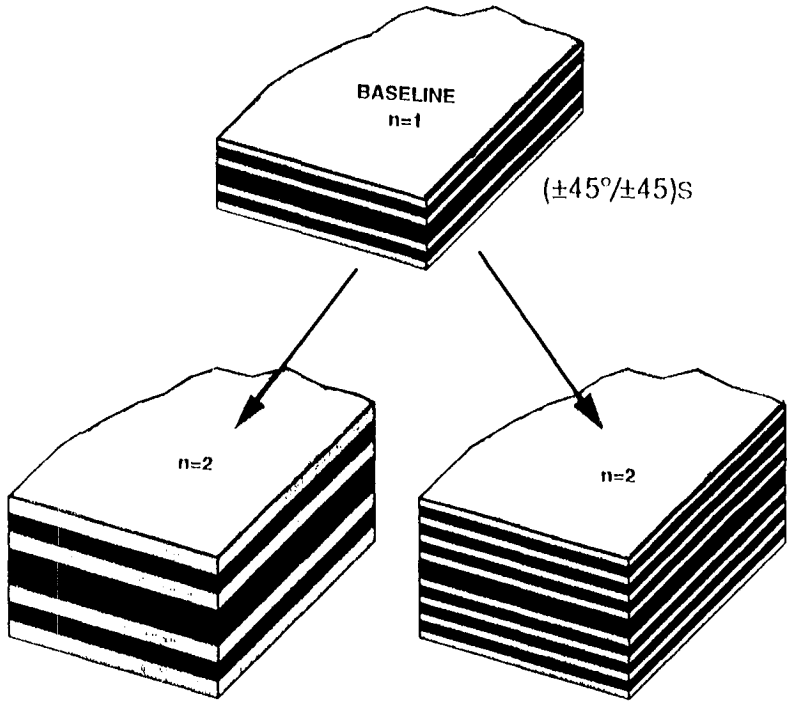

RESEARCH OBJECTIVES

- TO IDENTIFY SCALE EFFECTS IN ADVANCED COMPOSITE MATERIAL SYSTEMS
- TO FORMULATE MECHANICS BASED RULES FOR SCALE- UP OF COMPOSITE MATERIALS AND STRUCTURES

SOURCES OF SCALE EFFECTS

- LAMINATE FREE-EDGE EFFECTS
- RESIDUAL FABRICATION STRESSES
- DAMAGE
- SIZE-VOLUME EFFECTS
- INCOMPLETE SIMILITUDE

LAGACE, 1987. BATDORF, 1988

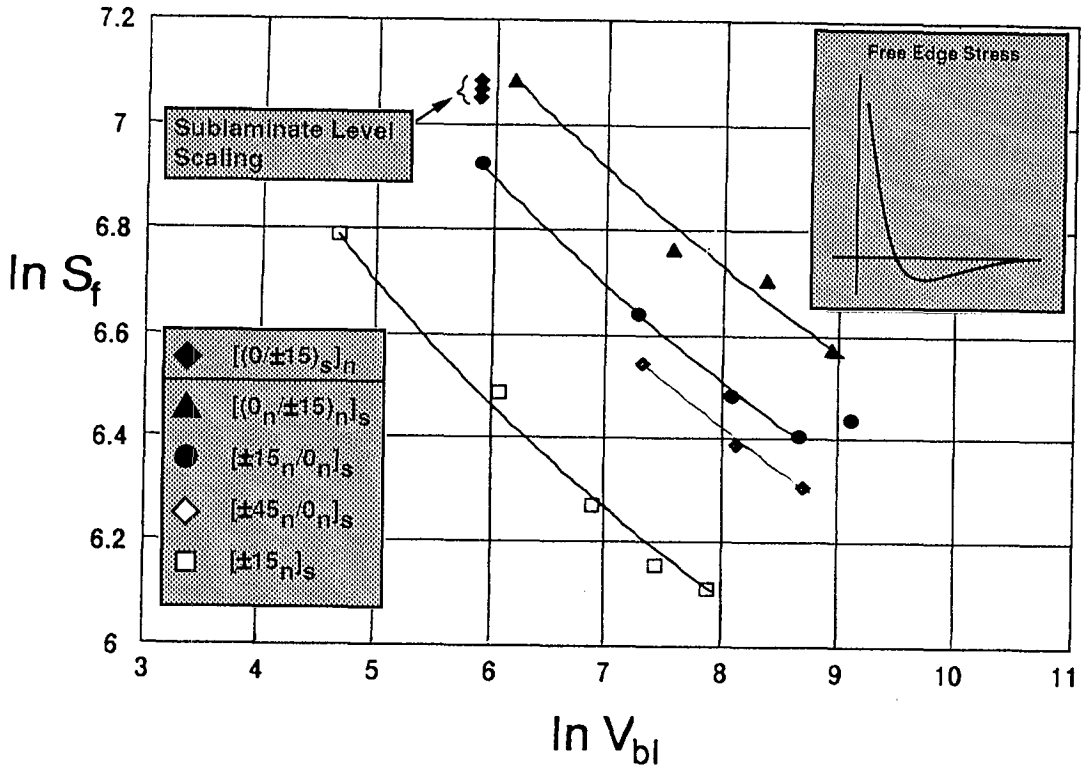

BATDORF, 1988

WEIBULL DISTRIBUTION

$$\ln S_f = A - B \ln \ln V_{bl}$$

S_f = Failure Stress

V_{bl} = Boundary Layer Volume

A, B = Weibull's Shape Parameters

Laws and Dvorak, 1988

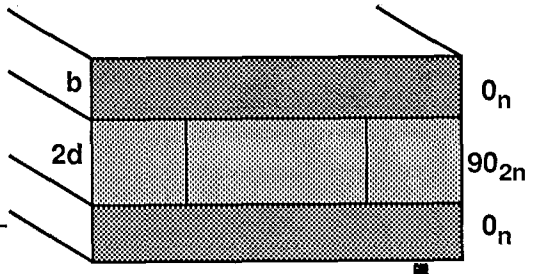

$$\frac{\sigma}{E} = \left(\frac{\xi \, b \, E_l \, G_c}{d(b+d) \, E \, E_t} \right)^{1/2} - \frac{\sigma_t^R}{E_t}$$

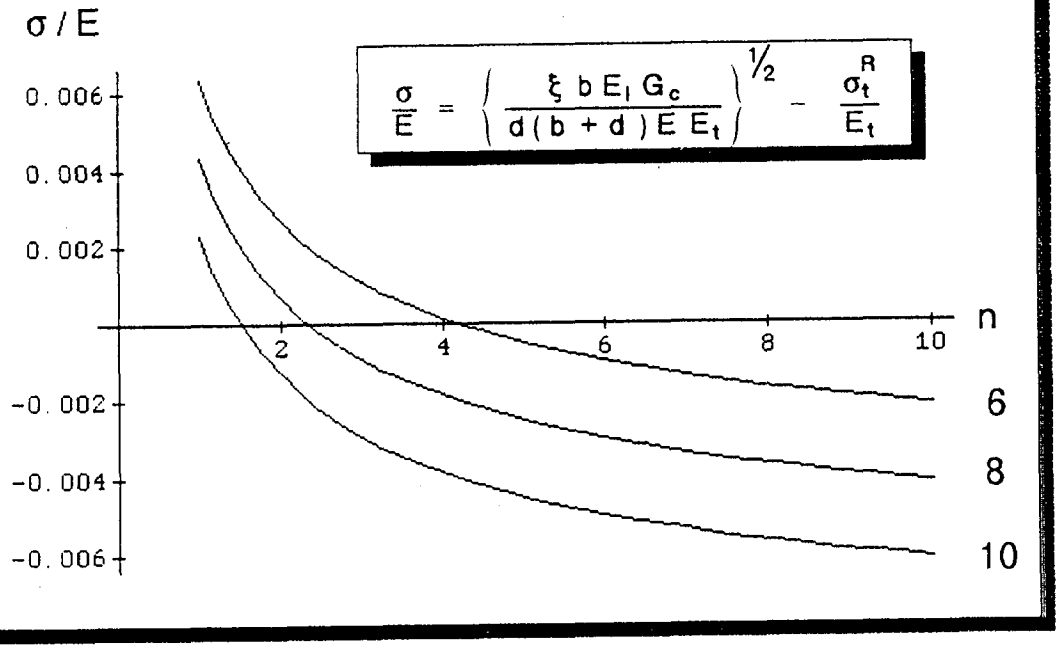

Similarity

- Geometric – exact replica
- Kinematic – homologous pcles...pts...times
- Kinetic (Dynamic) – homologous parts...forces
- Constitutive
  - rate effects
  - fracture mechanics
  - residual stresses

Dimensional Analysis

Non-dimensional Groups

$$\pi_1 = \frac{w}{h} \qquad \pi_2 = \frac{L}{h} \qquad \pi_3 = \frac{D}{h} \qquad \pi_4 = \frac{S}{h}$$

$$\pi_5 = \frac{Vt}{h} \qquad \pi_{10} = \frac{g\,t^2}{h}$$

$$\pi_5 = \frac{F\,h}{D_{eff}} \qquad \pi_6 = \frac{E}{D_{eff}}$$

$$\pi_9 = \frac{\rho\,h^3}{m} \qquad \pi_7 = \frac{K_Q}{\sigma\,h_2^{\frac{1}{2}}} \qquad \pi_8 = \frac{\tau}{t}$$

Scale Models

Scale factors $\lambda_\alpha = \dfrac{\alpha_{model}}{\alpha_{prototype}}$

Conflicts:

Impact–analysis suggests

$$\lambda_V = 1$$

But, if strain rate effects are important

$$\lambda_V = \lambda_h$$

Notch-sensitive materials will show size strength effects

$$\lambda_\sigma = \frac{\lambda_K}{\lambda_{h2}^{\frac{1}{2}}}$$

Jackson, 1989

Ply-level Scaling

Eccentrically loaded composite beam-column.

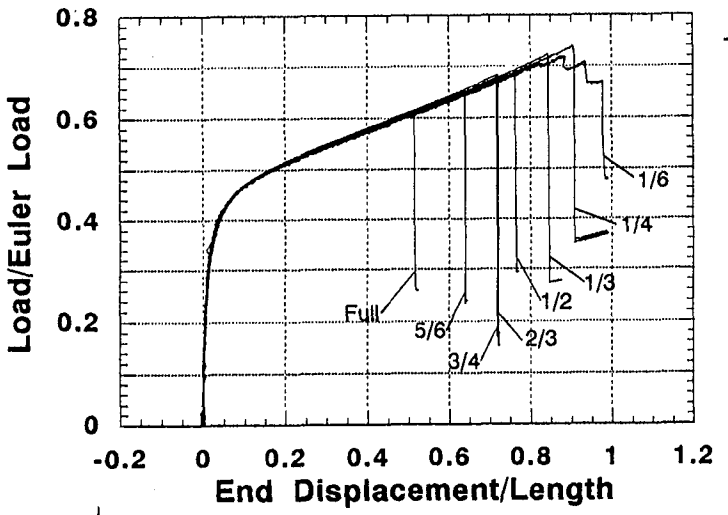

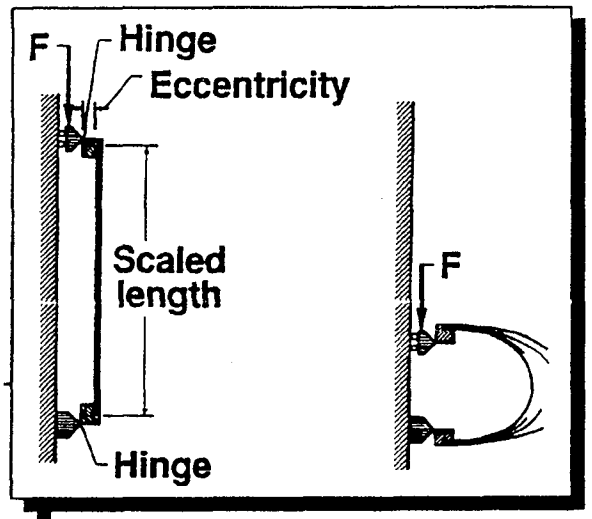

Unidirectional graphite-epoxy

Eccentrically loaded composite beam-column.

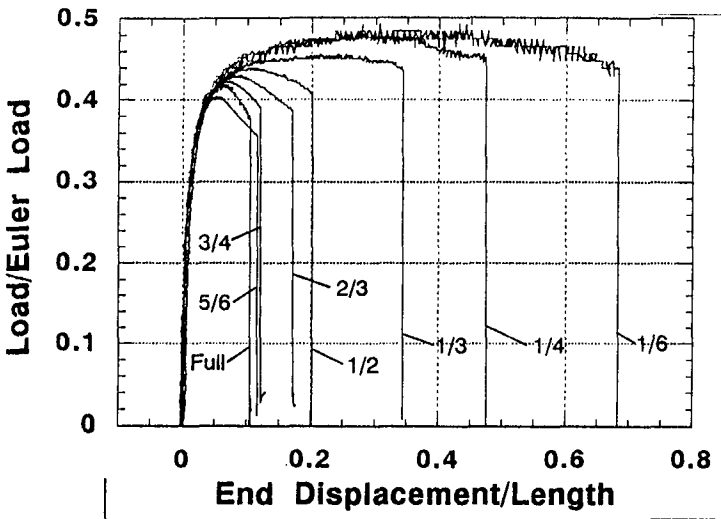

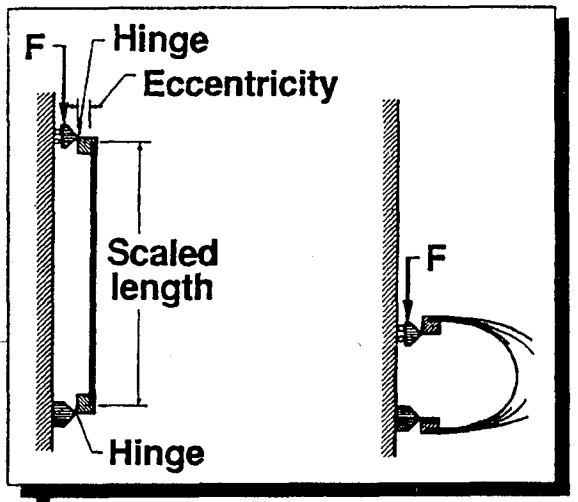

Angle ply graphite-epoxy

KELLAS AND MORTON, 1990

PLY LEVEL SCALING OF GRAPHITE-EPOXY TENSILE SPECIMENS

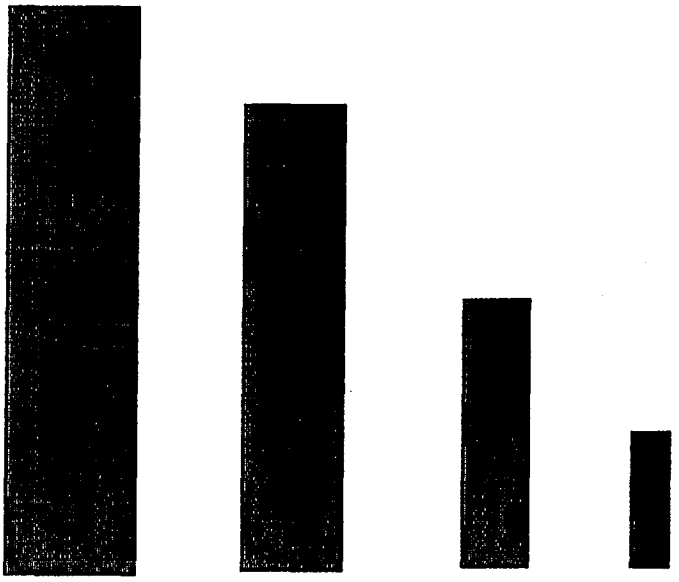

$[\pm 30°_n / 90°_{2n}]_s$

$[\pm 45°_n / \pm 45°_n]_s$

$[90°_n / 0°_n / 90°_n / 0°_n]_s$

$[\pm 45°_n / 0°_n / 90°_n]_s$

OBJECTIVE

- TO STUDY THE EFFECT OF SPECIMEN SIZE, STACKING SEQUENCE, AND MATERIAL SYSTEM UPON THE FAILURE RESPONSE OF ±45° LAMINATES.

EXPERIMENTAL DETAILS

- MATERIAL SYSTEM
  - AS4/3502
  - AS4/PEEK
- STACKING SEQUENCE
  - (+45°n/-45°n/+45°n/-45°n)s - Blocked Plies (n=1-4)
  - (+45°/-45°/+45°/-45°)ns - Distributed Plies (n=1-4)
- SPECIMEN SIZE
  - Length = 5.0 x n inches (n=1-4)
  - Width = 0.5 x n inches (n=1-4)
- LOADING RATE
  - 0.1 x n in/min (n=1-4) - Constant strain rate
- DAMAGE EXAMINATION
  - Enhanced X-radiography
  - Optical Microscopy

Stress/Strain Behavior - AS4/3502

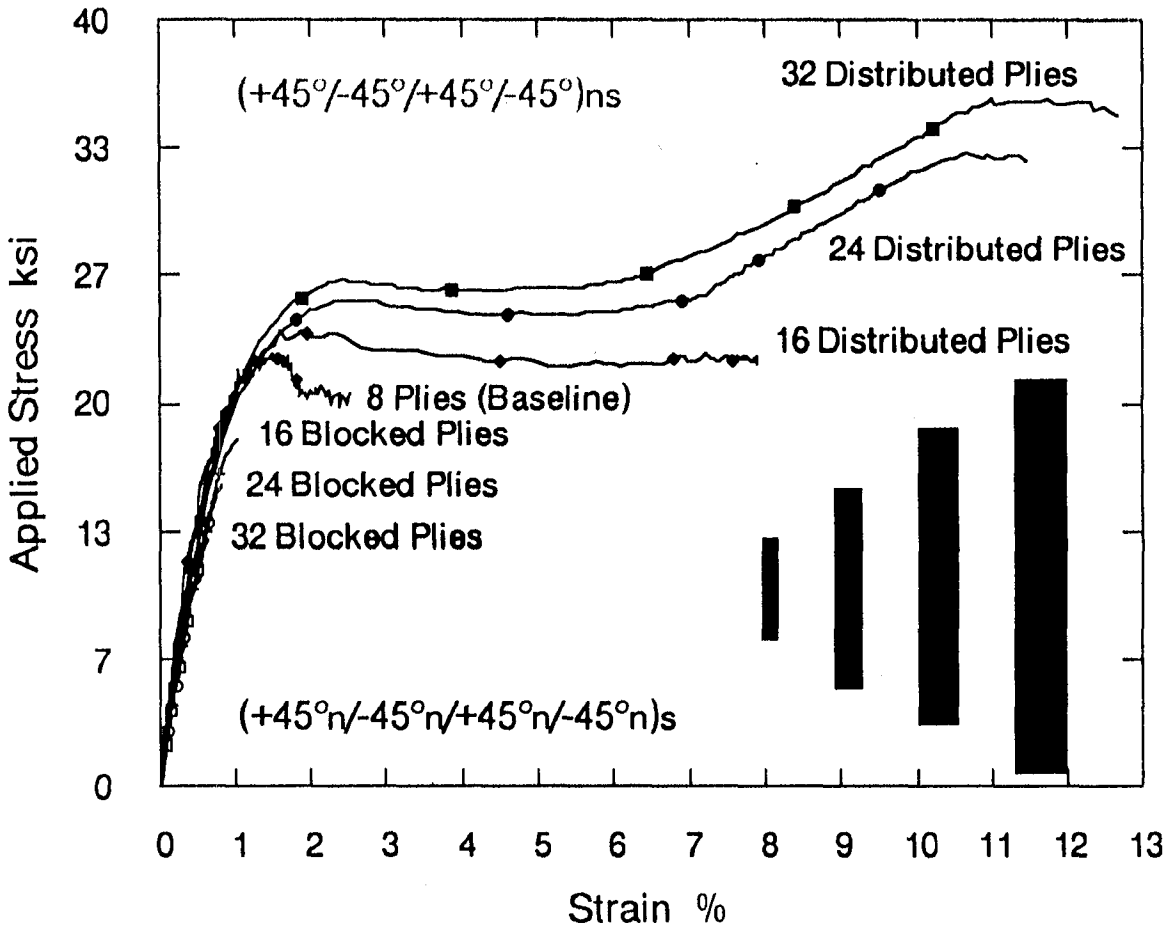

RADIOGRAPHS OF VIRGIN SPECIMENS

$(\pm 45°_n/\pm 45°_n)_s$

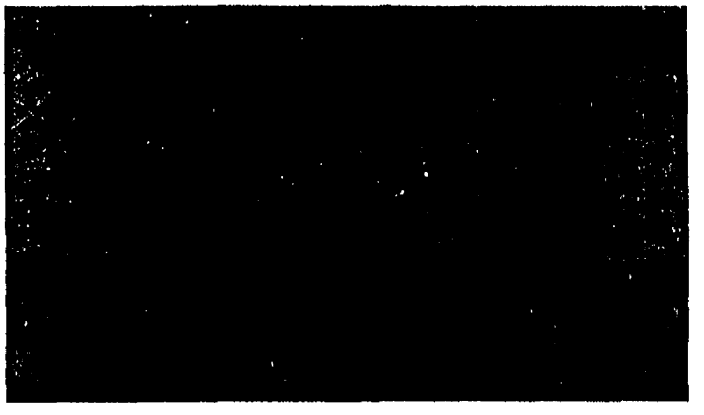

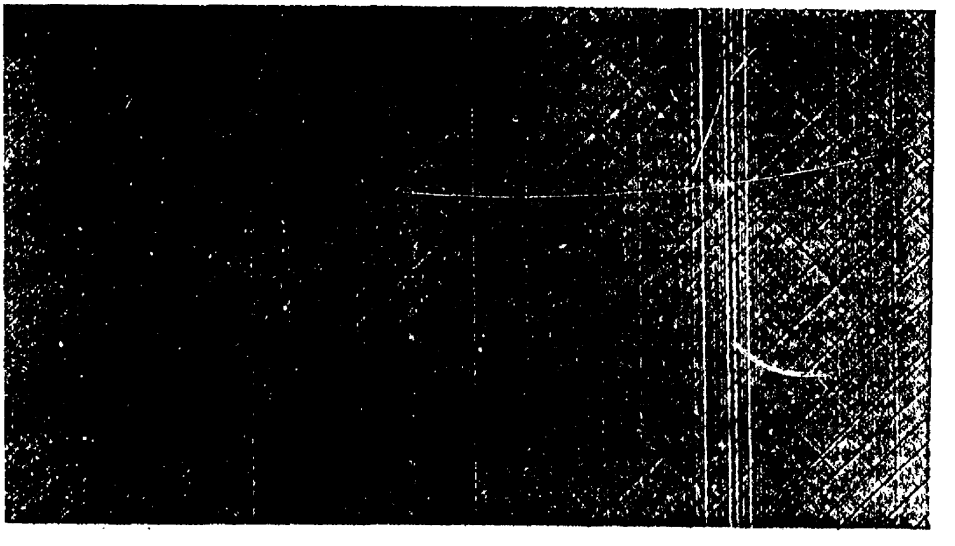

FIRST AND SECOND PLY FAILURES - AS4/3502

8 Ply Laminates - Size a

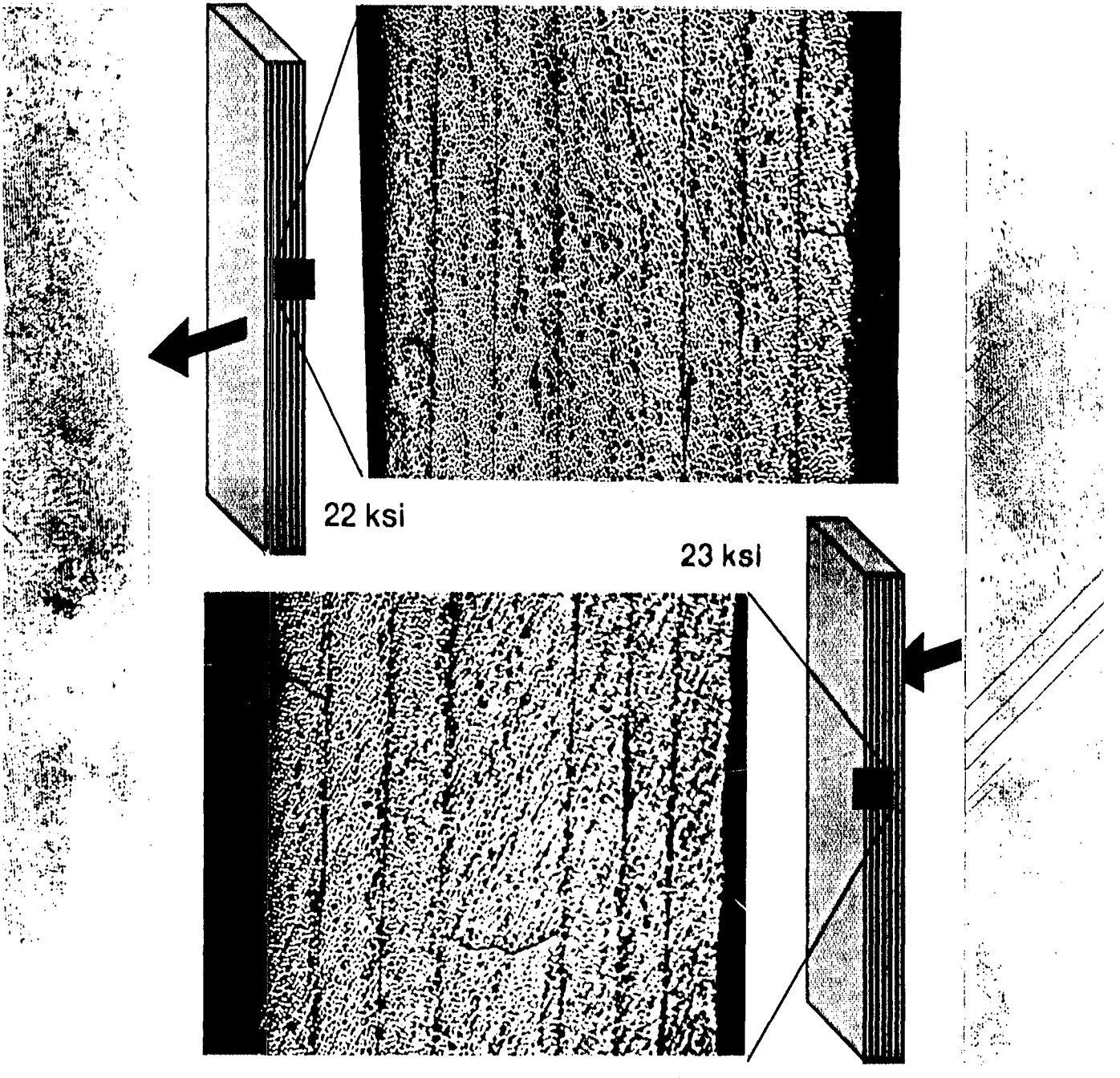

(Original figure unavailable at time of publication)

EDGE EFFECTS IN ±θ LAMINATES

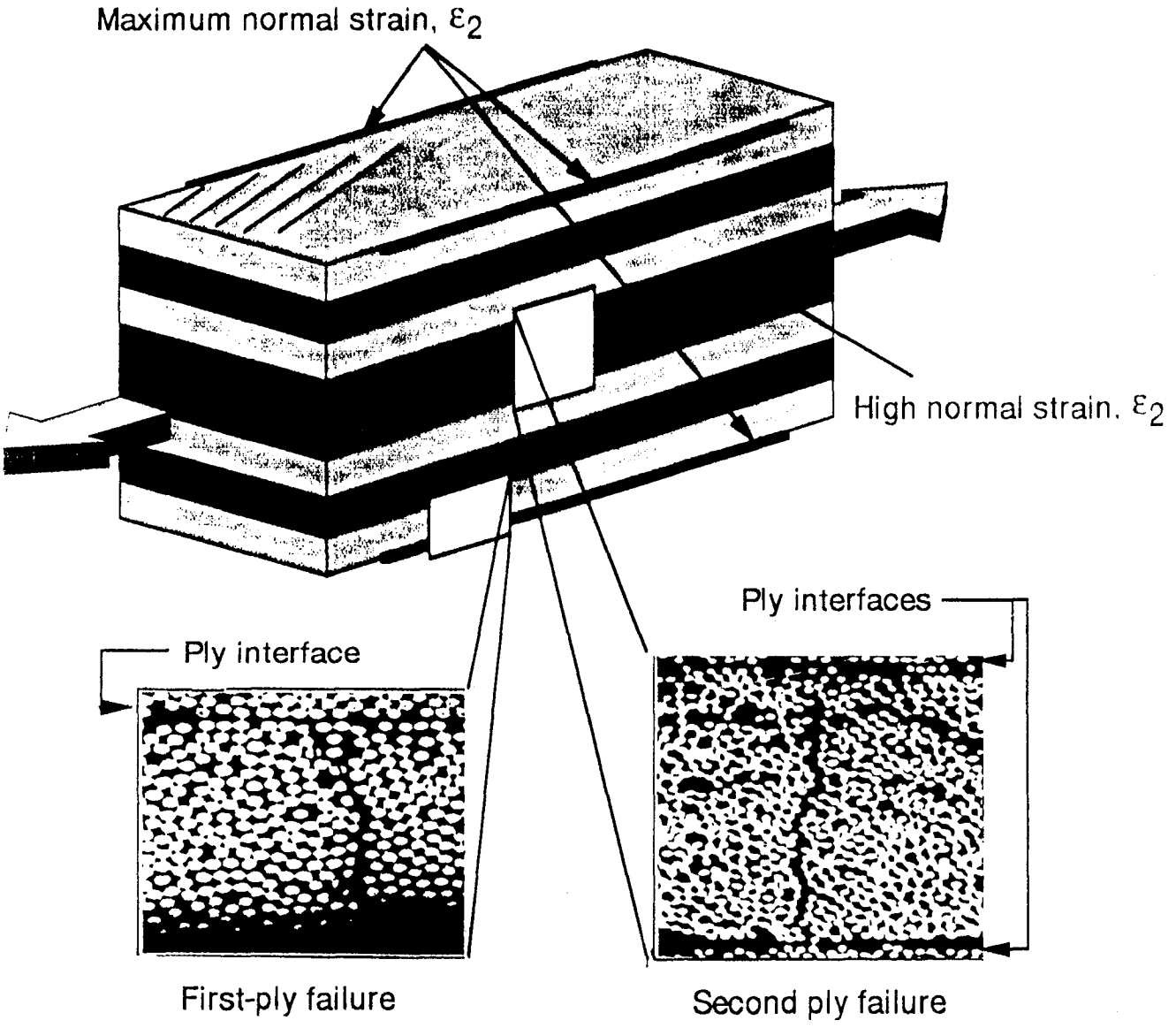

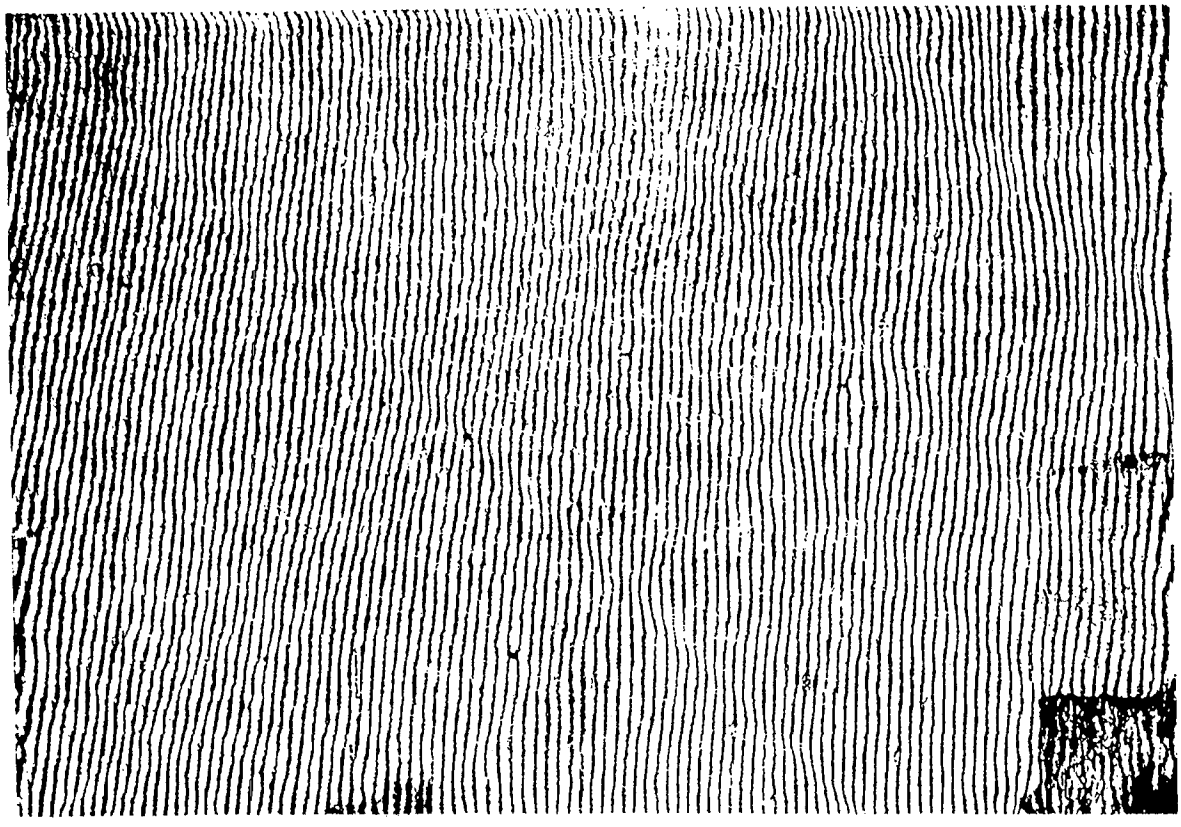

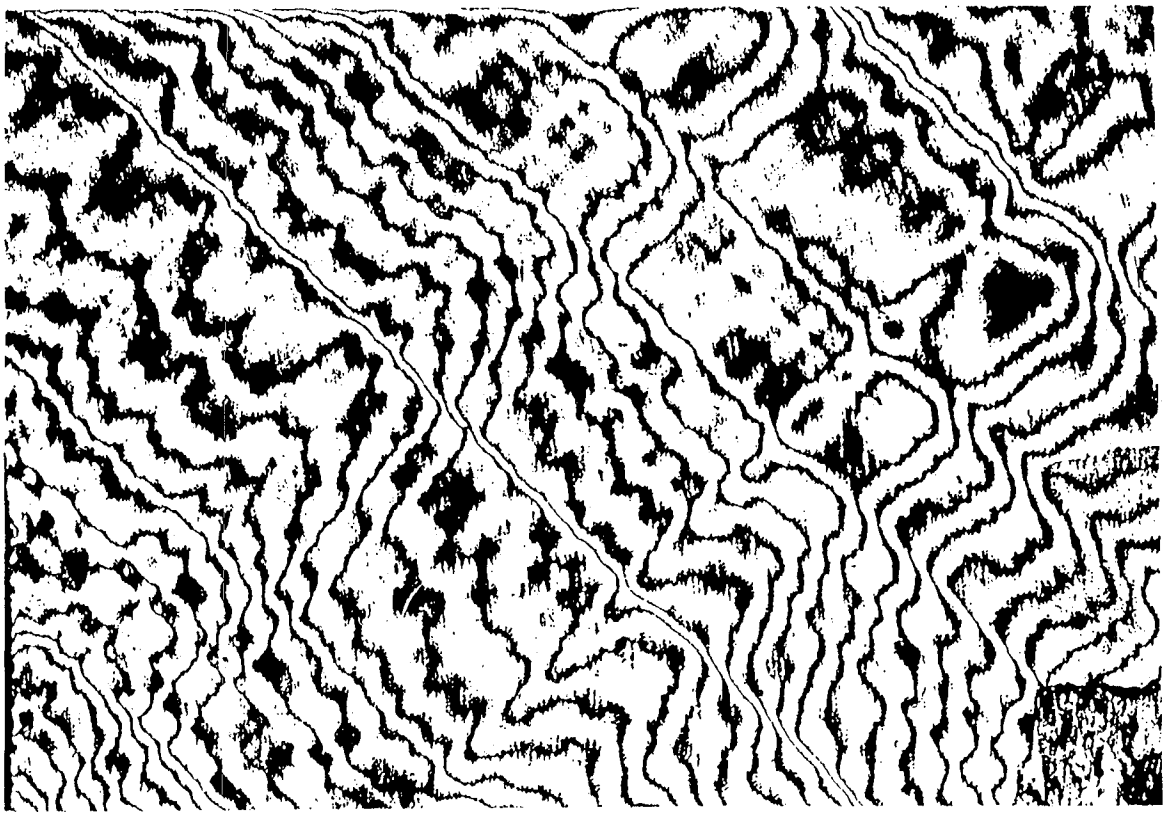

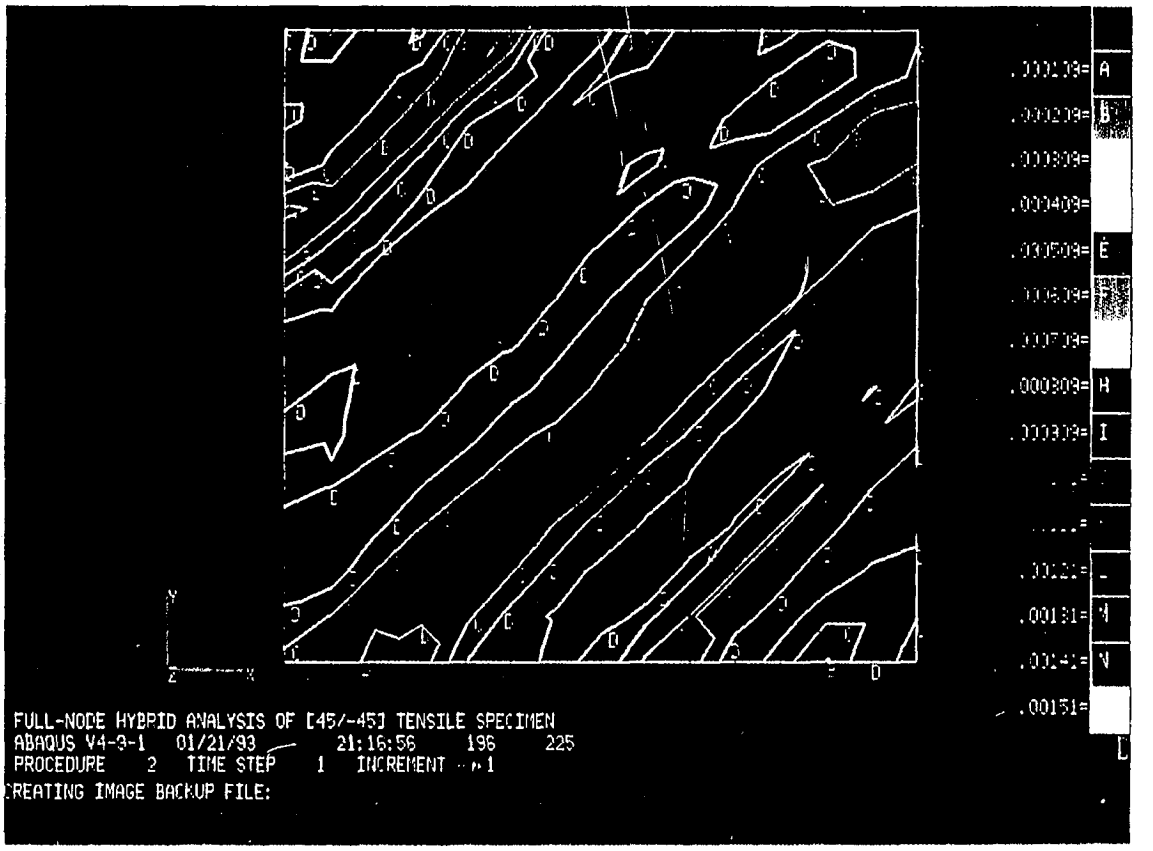
.000109= A
.000209= B
.000309=
.000409=
.000509= E
.000609=
.000709=
.000809= H
.000909= I
.00101= J
.00111= K
.00121= L
.00131= M
.00141= N
.00151=
FULL-NODE HYBRID ANALYSIS OF [45/-45] TENSILE SPECIMEN
ABAQUS V4-9-1 01/21/93 21:16:56 196 225
PROCEDURE 2 TIME STEP 1 INCREMENT 1
CREATING IMAGE BACKUP FILE:

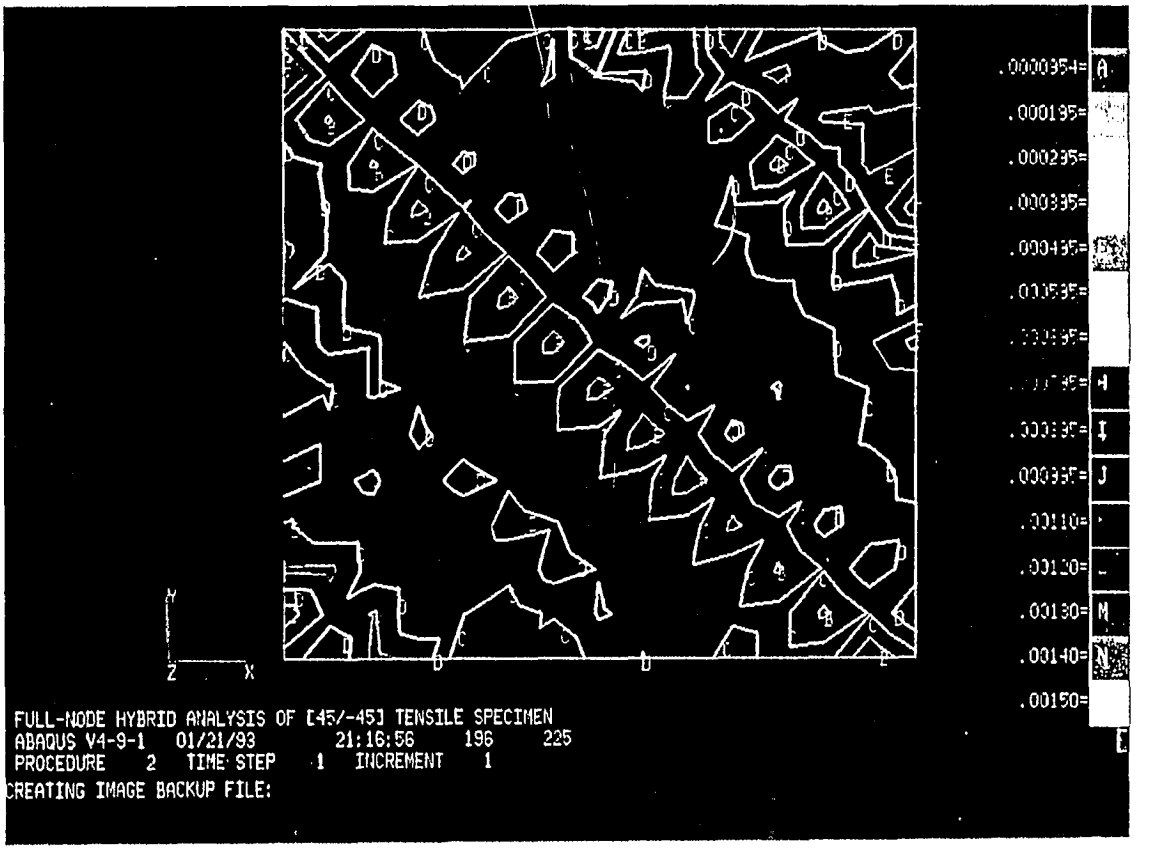
.0000354= A
.000195= B
.000295=
.000395=
.000495= E
.000595=
.000695=
.000795= H
.000895= I
.000995= J
.00110= K
.00120= L
.00130= M
.00140= N
.00150=
FULL-NODE HYBRID ANALYSIS OF [45/-45] TENSILE SPECIMEN
ABAQUS V4-9-1 01/21/93 21:16:56 196 225
PROCEDURE 2 TIME STEP 1 INCREMENT 1
CREATING IMAGE BACKUP FILE:

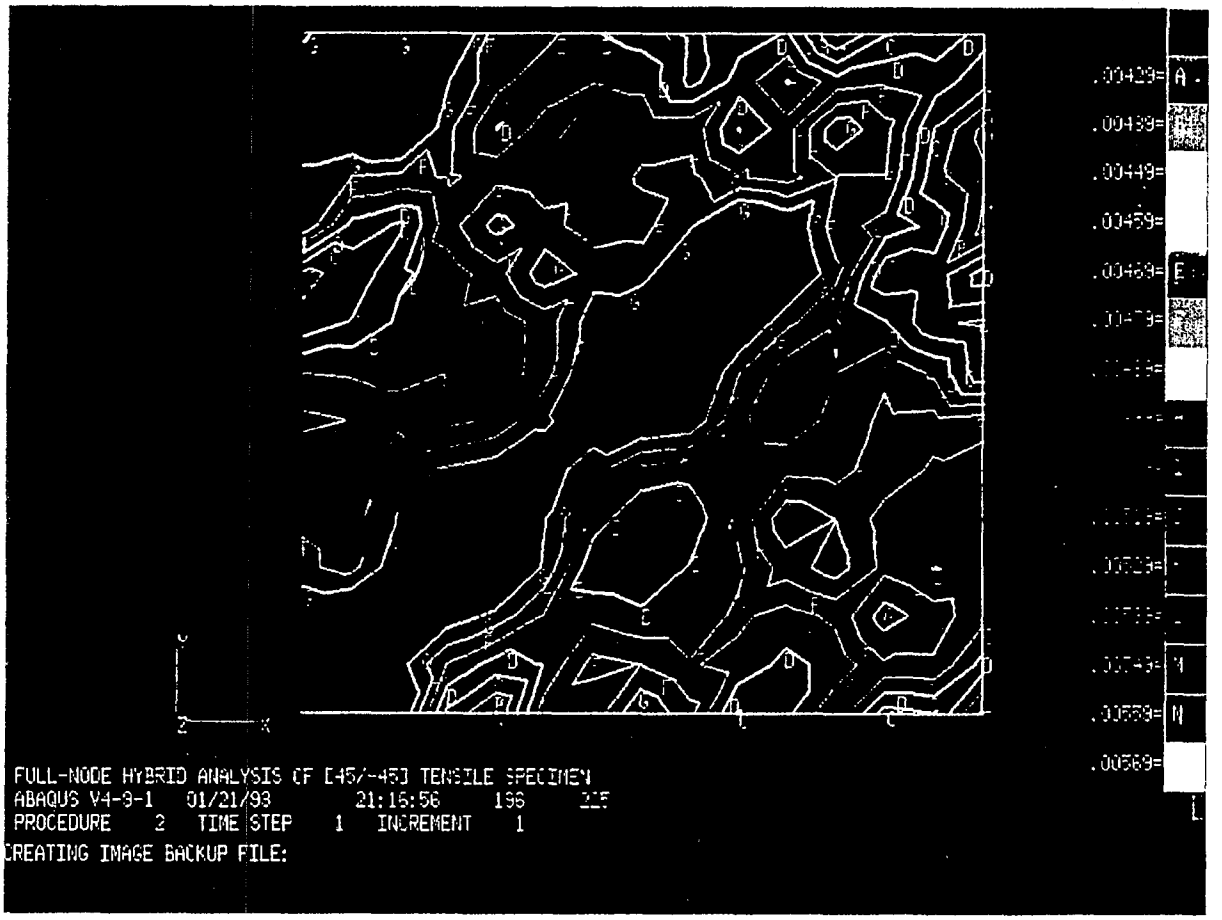
.00429=
.00439=
.00449=
.00459=
.00469=
.00569=
FULL-NODE HYBRID ANALYSIS OF [45/-45] TENSILE SPECIMEN
ABAQUS V4-9-1 01/21/93 21:16:56 196 225
PROCEDURE 2 TIME STEP 1 INCREMENT 1
CREATING IMAGE BACKUP FILE:

PINTADO AND MORTON, 1991

Scaling of Impact Loaded Composite Beams

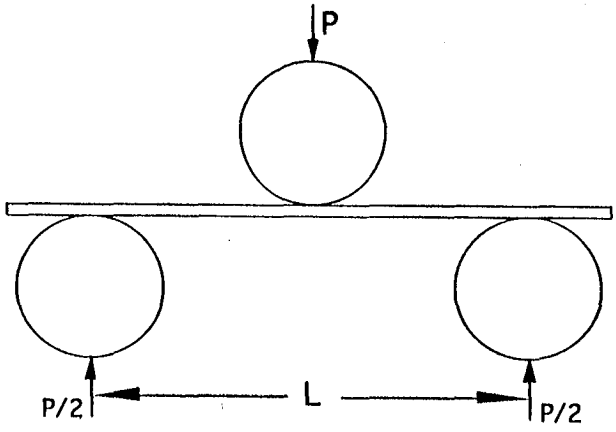

Quasi-isotropic AS//3502
Sublaminate Level Scaled Coupons

$(+45°, -45°, 0°, 90°)_{ns}$ n = 2, 3, 4

Stiffness parameter β

IMPACT SET-UP SCHEMATIC

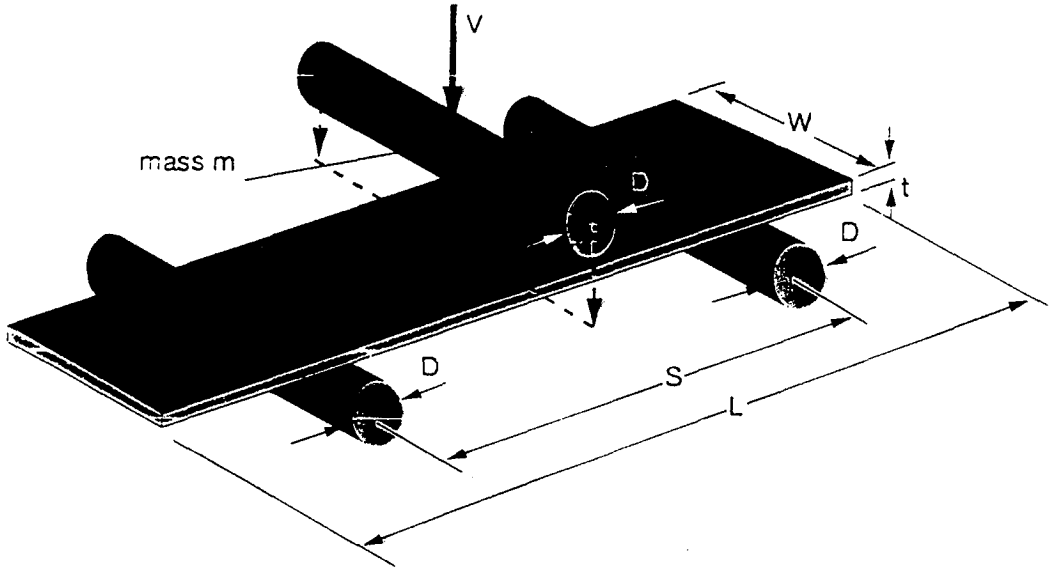

Scale Geometry: λD, λW, λt, λS, λL.
Scale Mass: λ^3m .
Scale Impact Energy: λ^3E , where the velocity V is constant.
λ is the Scale Factor.

STATIC THREE POINT BEND

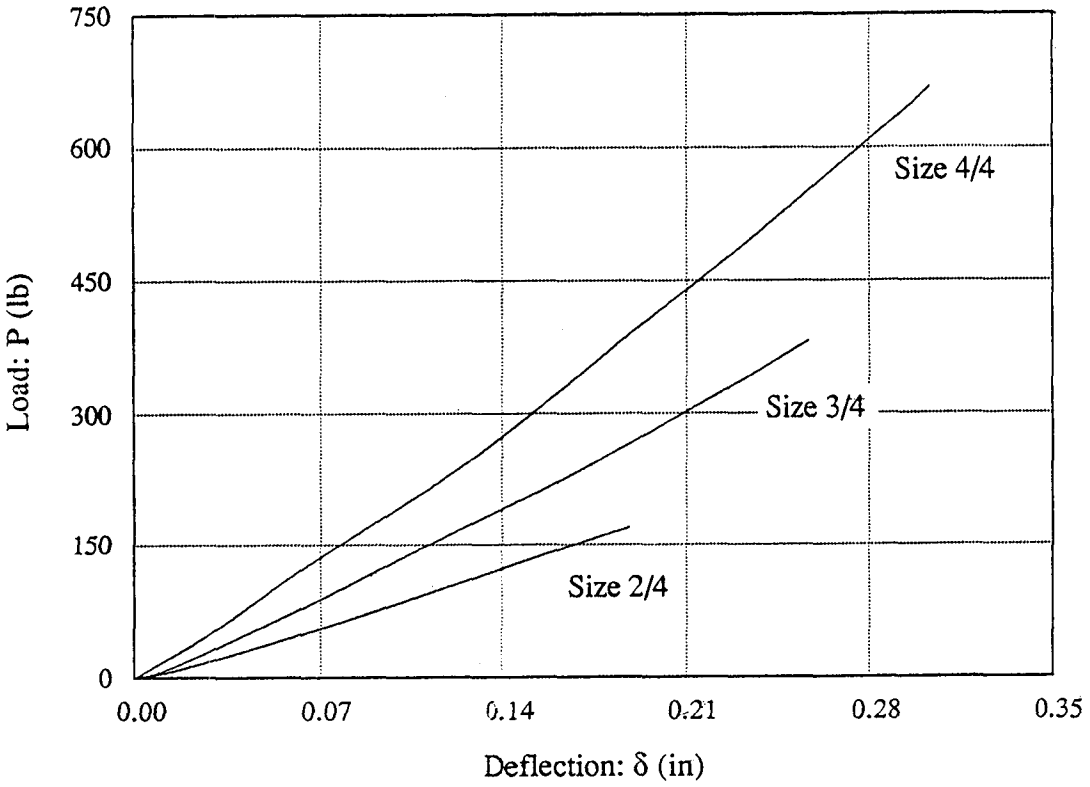

SCALED STATIC RESPONSE

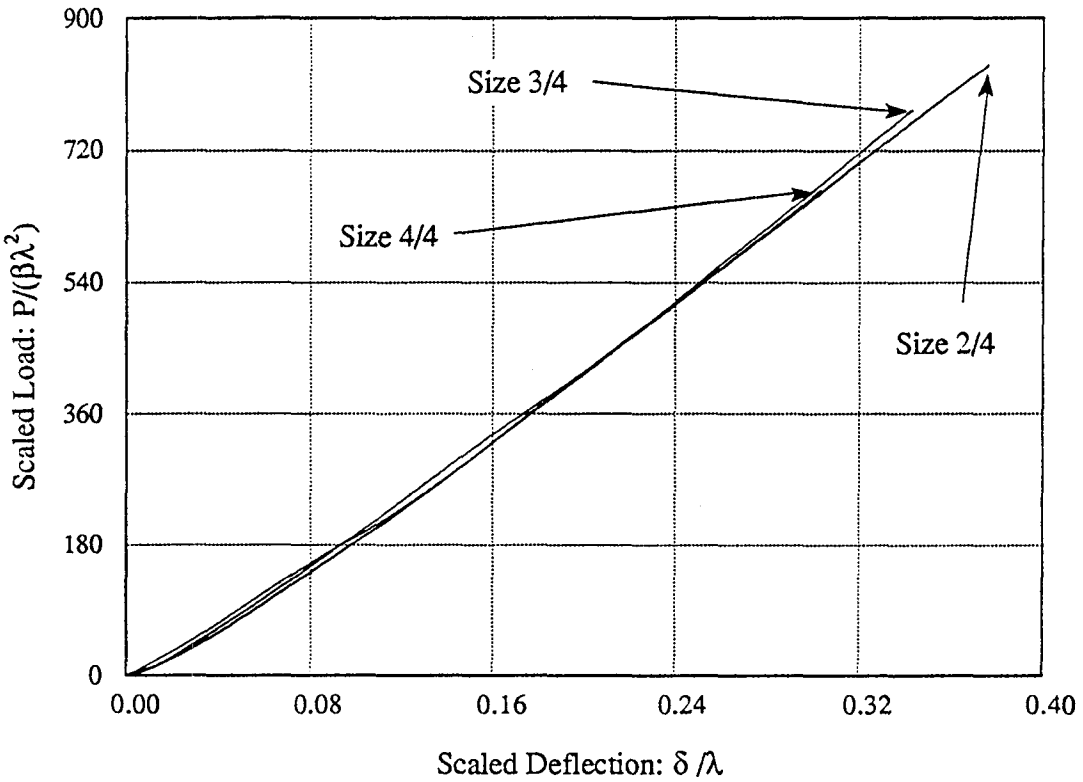

IMPACT RESPONSE (NO DAMAGE)

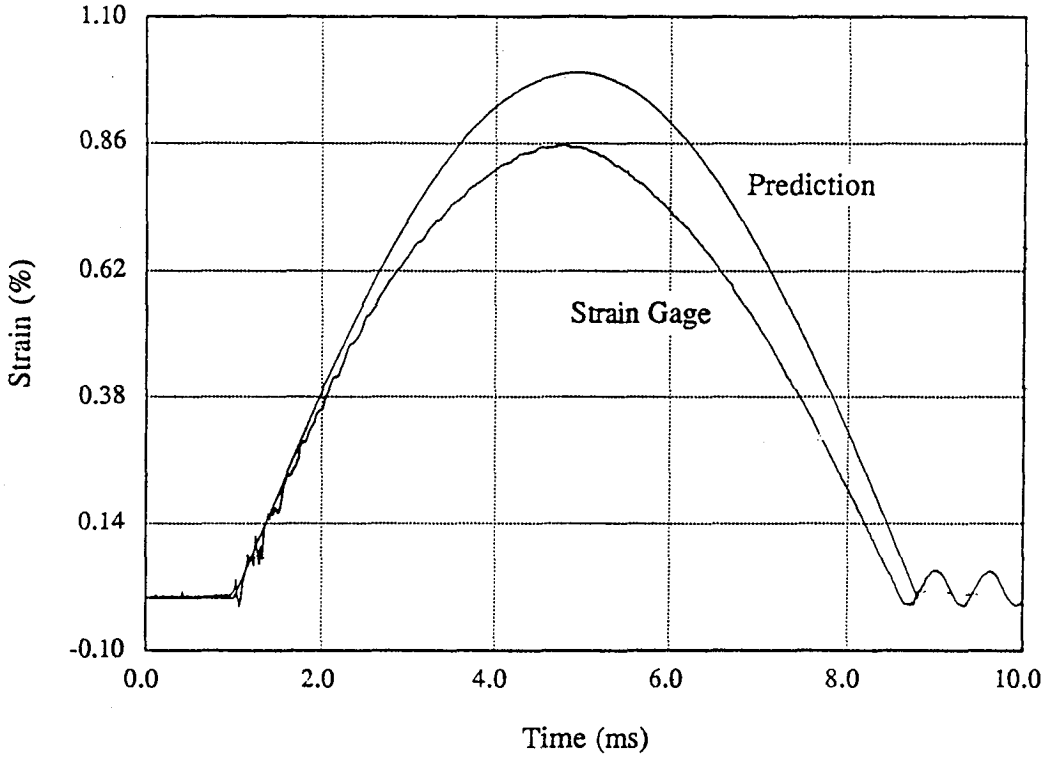

IMPACT RESPONSE WITH DAMAGE

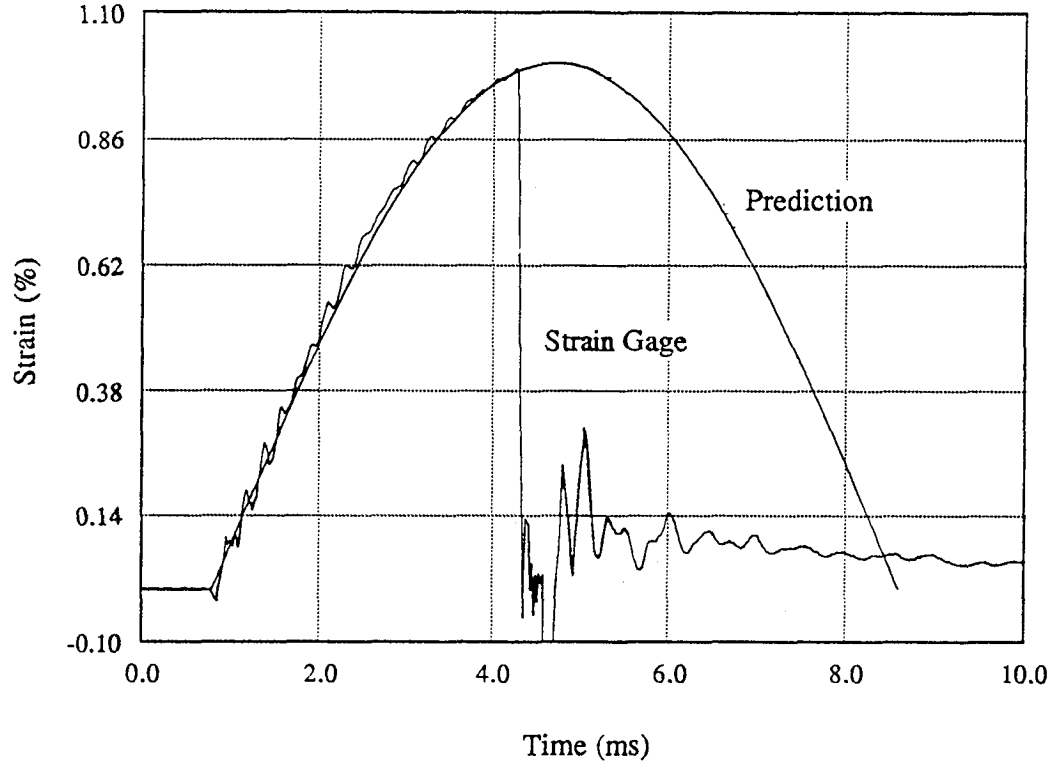

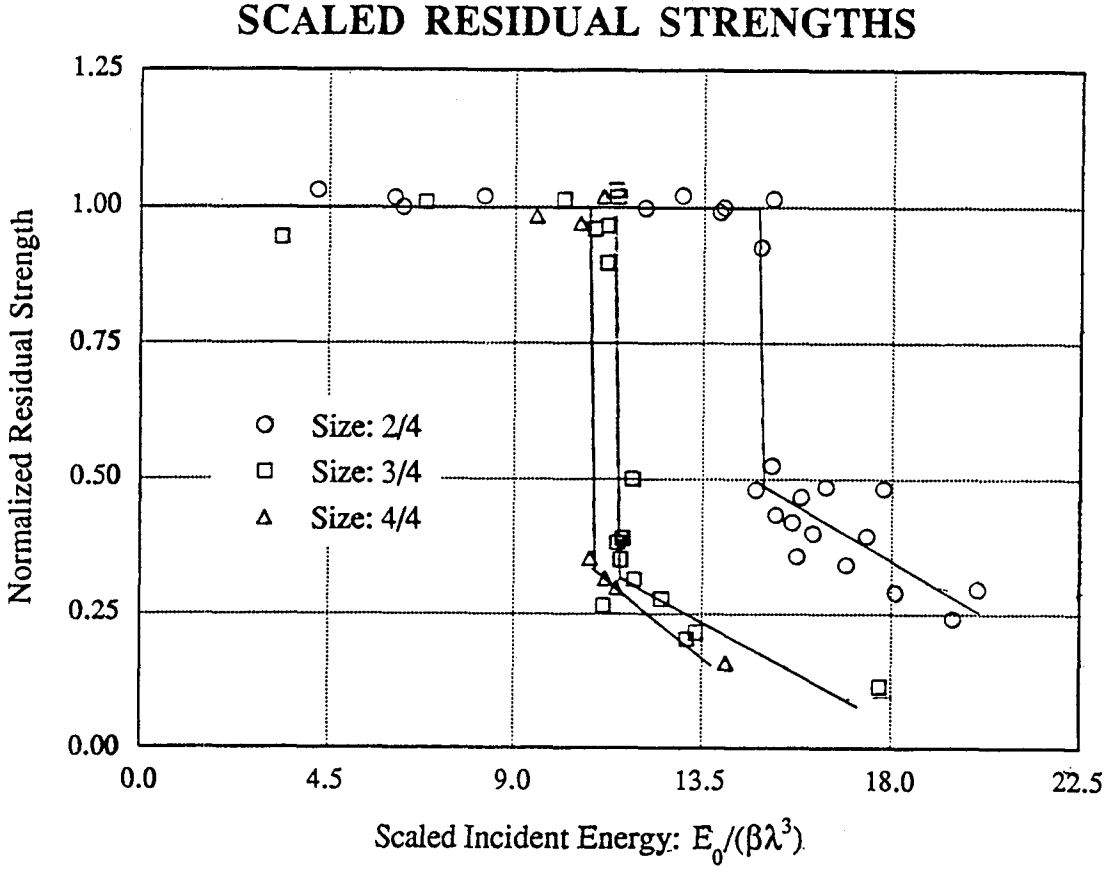
SCALED RESIDUAL STRENGTHS
Normalized Residual Strength
1.25
1.00
0.75
0.50
0.25
0.00
0.0
4.5
9.0
13.5
18.0
22.5
Size: 2/4
Size: 3/4
Size: 4/4
Scaled Incident Energy: $E_0/(\beta\lambda^3)$

TYPICAL X-RAY RADIOGRAPHS OF IMPACT LOADED SCALED SPECIMENS

$$E=\left(\frac{4}{4}\right)^3 E\left(\frac{4}{4}\right) = 18.0J$$

$$E=\left(\frac{3}{4}\right)^3 E\left(\frac{4}{4}\right) = 7.6J$$

$$E=\left(\frac{2}{4}\right)^3 E\left(\frac{4}{4}\right) = 2.3J$$

$$E=\left(\frac{1}{4}\right)^3 E\left(\frac{4}{4}\right) = 0.28J$$

IMPACT FORCE AS A SCALING PARAMETER

C. C. Poe, Jr.
NASA Langley Research
Hampton, VA

and

Wade C. Jackson
US Army Vehicle Structures Directorate
NASA Langley Research
Hampton, VA

ABSTRACT

The Federal Aviation Administration (FAR PART 25) requires that a structure carry ultimate load with nonvisible impact damage and carry 70 percent of limit flight loads with discrete damage. The Air Force has similar criteria (MIL-STD-1530A). Both civilian and military structures are designed by a building block approach. First, critical areas of the structure are determined, and potential failure modes are identified. Then, a series of representative specimens are tested that will fail in those modes. The series begins with tests of simple coupons, progresses through larger and more complex sub components, and ends with a test on a full-scale component, hence the term "building block." In order to minimize testing, analytical models are needed to scale impact damage and residual strength from the simple coupons to the full-scale component. Using experiments and analysis, the present paper illustrates that impact damage can be better understood and scaled using impact force than just kinetic energy. The plate parameters considered are size and thickness, boundary conditions, and material, and the impact parameters are mass, shape, and velocity.

View Graph No. 1

OUTLINE

I. **QUASI-STATIC IMPACT RESPONSE -**
Large Impacter Mass

II. **TRANSIENT IMPACT RESPONSE -**
Large & Massive Targets

- **Damage Initiation**
- **Damage Resistance**
- **Plate Size & Thickness**
- **Nonstructural Mass**
- **Impacter Radius**

- This paper is divided into two parts based on the target responding in one of two ways -- quasi-static and transient, which are characterized by large impacter mass and by large target mass, respectively.

- The parameters to be discussed are shown in the list at the bottom of the view graph.

View Graph No. 2

ENERGY BALANCE MODEL

Equating the kinetic energy and work done by the impacter,

$$\frac{1}{2}m_i v_i^2 = \int_0^{\delta_{max}} F d\delta + \int_0^{\alpha_{max}} F d\alpha \qquad (1)$$

where the force-displacement relationship is

$$F = k\delta \qquad (2)$$

and the force-indentation relationship is

$$F = n_0 R_i^{1/2} \alpha^{3/2} \qquad (3)$$

Substituting equations (2) and (3) into (1),

$$\frac{1}{2}m_i v_i^2 = \frac{1}{2}k^{-1}F_{max}^2 + \frac{2}{5}(n_0 R_i^{1/2})^{-2/3} F_{max}^{5/3} \qquad (4)$$

- A relationship can be developed between impacter mass m_i and velocity v_i and impact force F_{max} by equating the kinetic energy of the impacter and the work done on the plate, equation (1).
- The work is the sum of that associated with the flexural displacement δ and with the local Hertzian indentation α.
- Quasi-static force-displacement relationships given by equations (2) and (3) were used for flexure and indentation, respectively. In equation (2), k is the flexural stiffness; and, in equation (3), n_0 is a function of the elastic constants of the plate [1] and R_i is the radius of the indenter.

View Graph No. 3

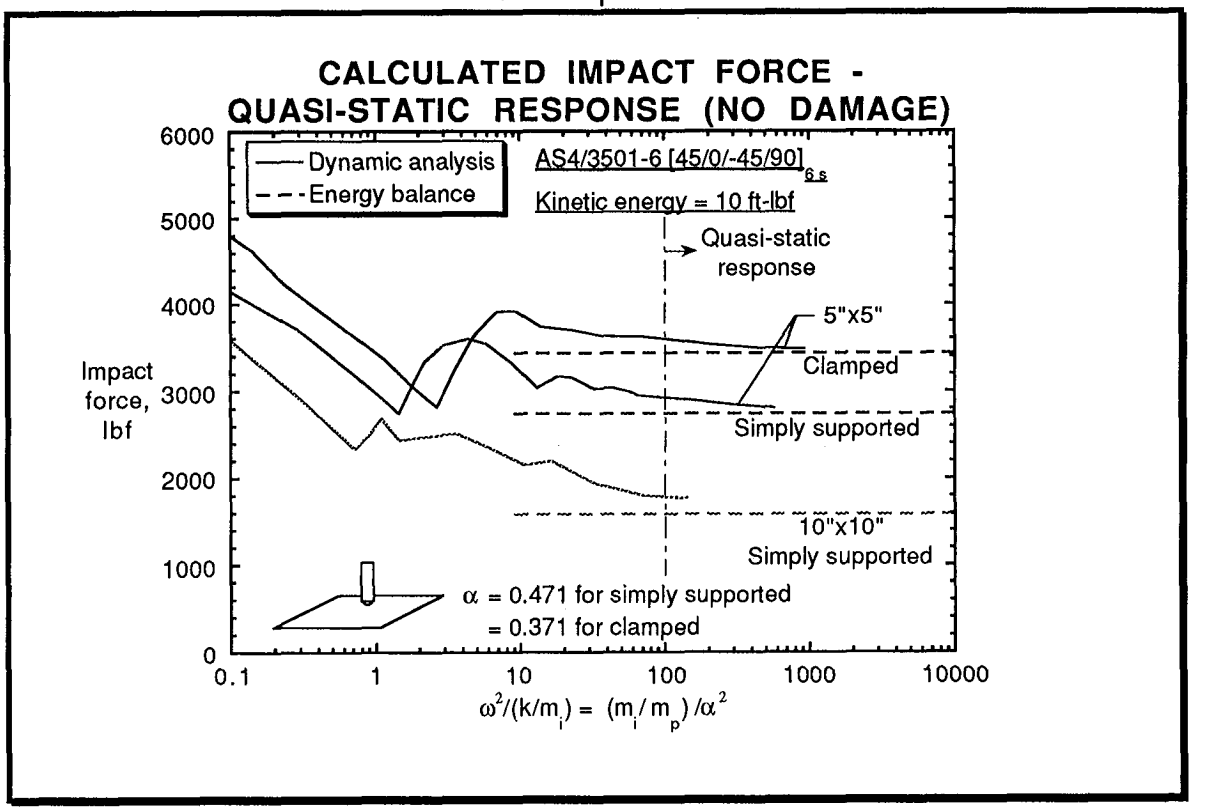

- For three square composite plates and a kinetic energy of 10 ft-lbf, impact force is plotted against the fundamental frequency squared divided by the ratio of flexural stiffness to impacter mass. For a uniformly thick plate, the abscissa reduces to the ratio of impacter mass to plate mass divided by a factor α that depends on boundary conditions. Two plates have the same size but different boundary conditions and two have same boundary conditions but different sizes. The solid lines were calculated using a finite element code that includes the equations of motion [1], and the dashed lines were calculated using the energy balance equation in View Graph No. 2.

- The finite element results approach those from the energy balance equation for large values of the mass ratio, indicating quasi-static response. For quasi-static response, impact force increases with increasing plate stiffness as evidenced by the effects of plate size and boundary conditions.

View Graph No. 4

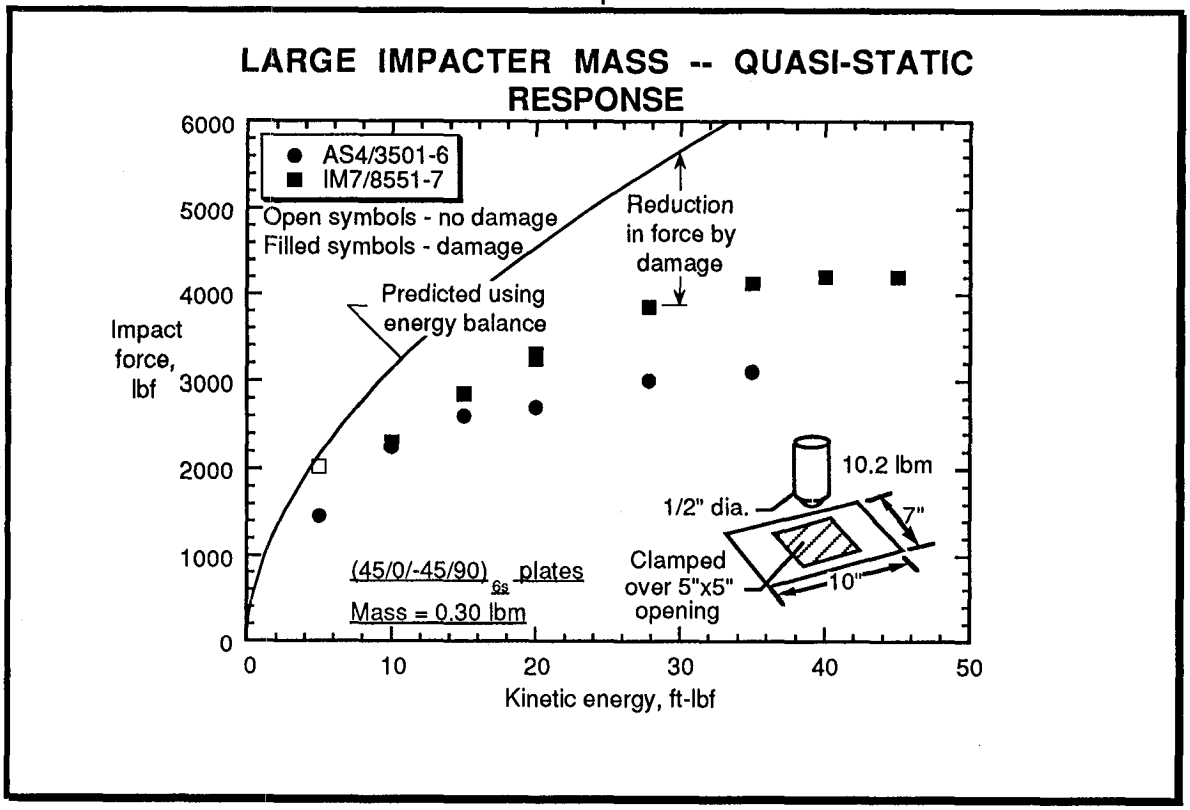

- Impact force is plotted against kinetic energy as circular and square symbols for tests of AS4/3501-6 and IM7/8551-7 composite plates. Open symbols indicate no damage, and filled symbols indicate damage in C-scans.

- The solid line was calculated using the energy balance equation. One curve represents both materials since the flexural stiffnesses were essentially equal. The ratio of $(m_i/m_p)/\alpha^2$ was 250, indicating that the response was quasi-static. See View Graph No. 3.

- The predicted and measured impact forces agree when there was no measurable damage. Damage reduced the impact force by cushioning the impact. The impact forces for AS4/3501-6 were less than those for IM7/8551-7 because the damage was smaller as will be shown subsequently.

View Graph No. 5

TYPICAL C-SCAN AFTER IMPACT

$[45/0/-45/90]_{6s}$ AS4/3501-6 Laminate

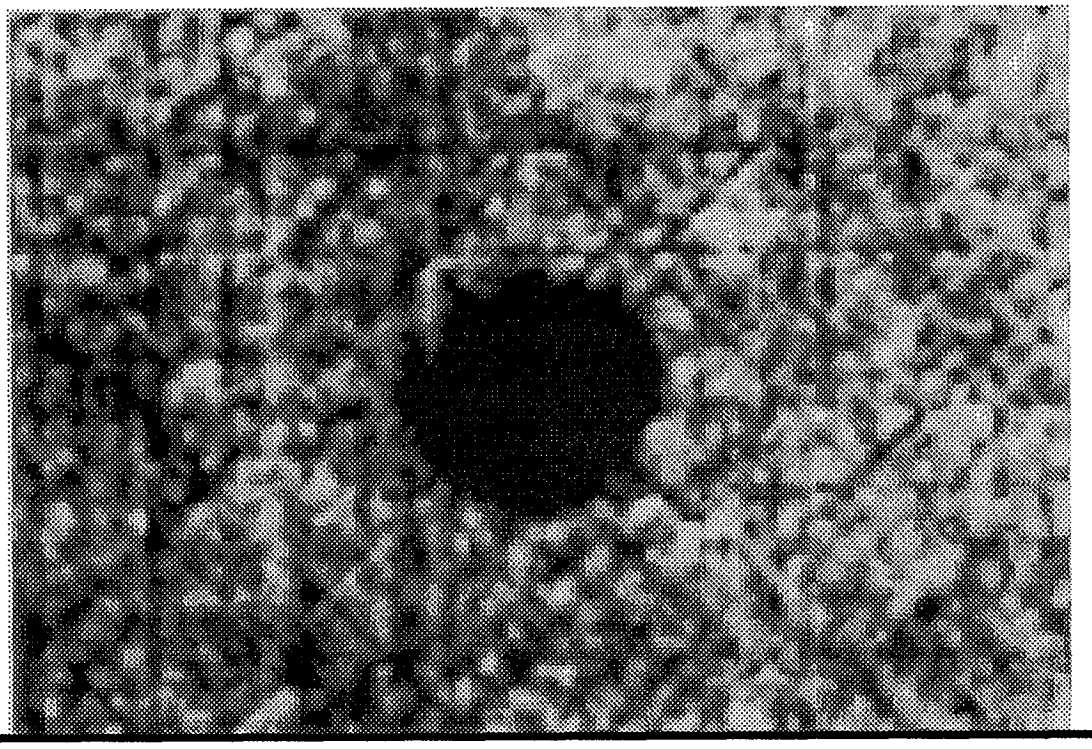

- A C-scan of a quasi-isotropic laminate after impact is shown. The dark circular region at the center indicates high attenuation caused by impact damage. The damage consists of cracked resin, broken fibers, and delaminations between plies. The region circumscribed by all the delaminations is circular but not the individual delaminations [2].
- The damaged region was assumed to be circular, and the diameter was calculated from the area A using $d_0 = \sqrt{4A / \pi}$.

View Graph No. 6

STRESSES IN ISOTROPIC PLATES WITH QUASI-STATIC IMPACT RESPONSE

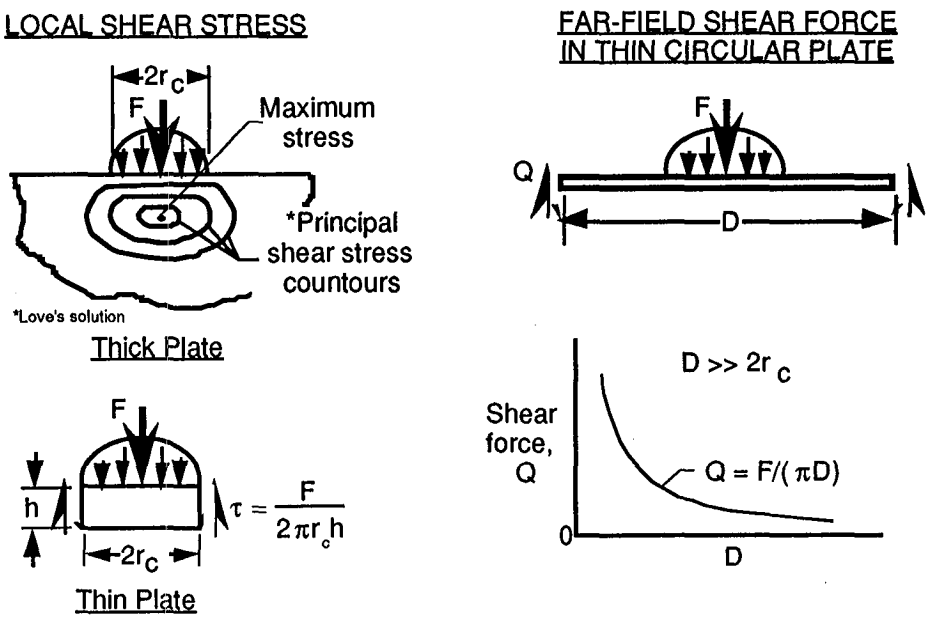

- The diagrams on the left illustrate the shear stresses that cause damage in the contact region for thick [3] and thin [4] circular plates, respectively. Here, $2r_C$ is the contact diameter given by $2r_C = 2(FR_i / n_0)^{1/3}$ and n_O is defined in View Graph No. 2
- The diagrams on the right illustrate the transverse shear force Q that causes damage at some distance from the contact region in thin circular plates [1].
- These results should apply to plates of any shape as long as the contact radius $2r_C$ or distance D is large compared to plate size.

View Graph No. 7

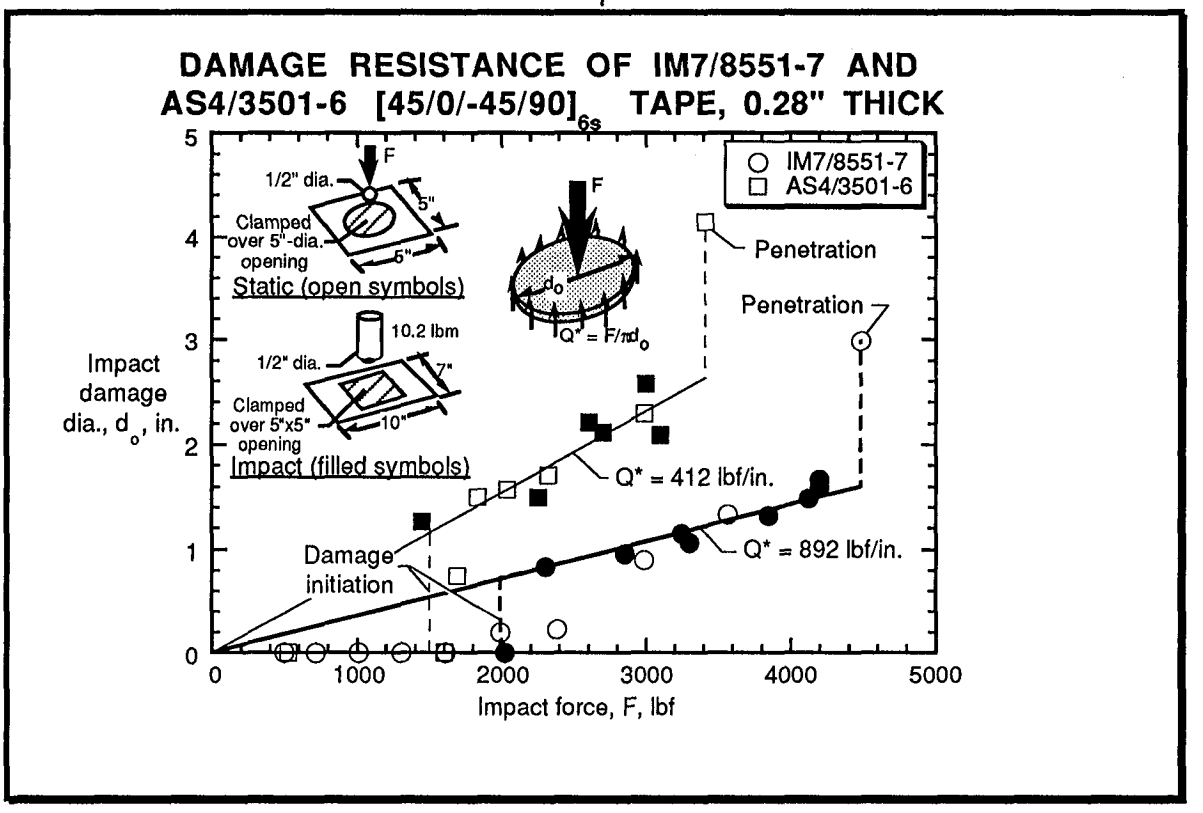

- The diameter of impact damage is plotted against impact force for AS4/3501-6 and IM7/8551-7 laminates. Test results are shown for both falling weight and static indentation tests.
- The results for the falling weight and static indentation tests agree well. The damage was not visible in C-scan images until a critical impact force was exceeded. Then, the damage spread instantaneously, probably as delamination growth. Afterward, the damage diameter increased in proportion to impact force until penetration.
- The constant of proportionality is Q^*/π, indicating that the damage increased in size when a critical value of transverse shear force per unit width was exceeded. Thus, Q^* is a metric for damage resistance.
- The value of Q^* for the toughened IM7/8551-7 was over twice that of AS4/3501-6.

View Graph No. 8

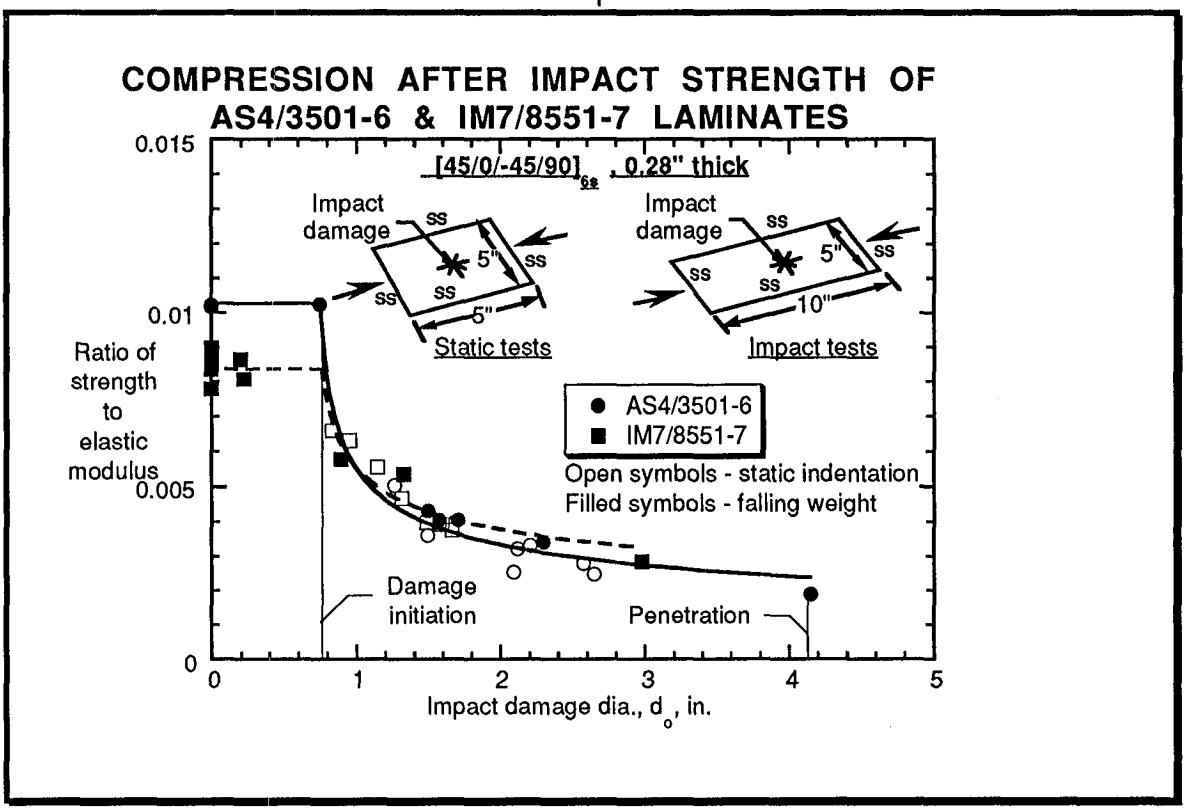

- Residual compression strength is plotted against damage diameter for the laminates in View Graph No. 7. Strengths were divided by elastic modulus to give nominal far-field failing strains and to normalize strengths for small differences between fiber volume fractions.

- Strengths do not decline until damage diameter exceeds about 0.8". Afterward, the normalized strengths for the AS4/3501-6 and IM7/8551-7 were essentially equal for a given size of damage. Thus, residual strengths can possibly be scaled in terms of damage size, irrespective of resin.

View Graph No. 9

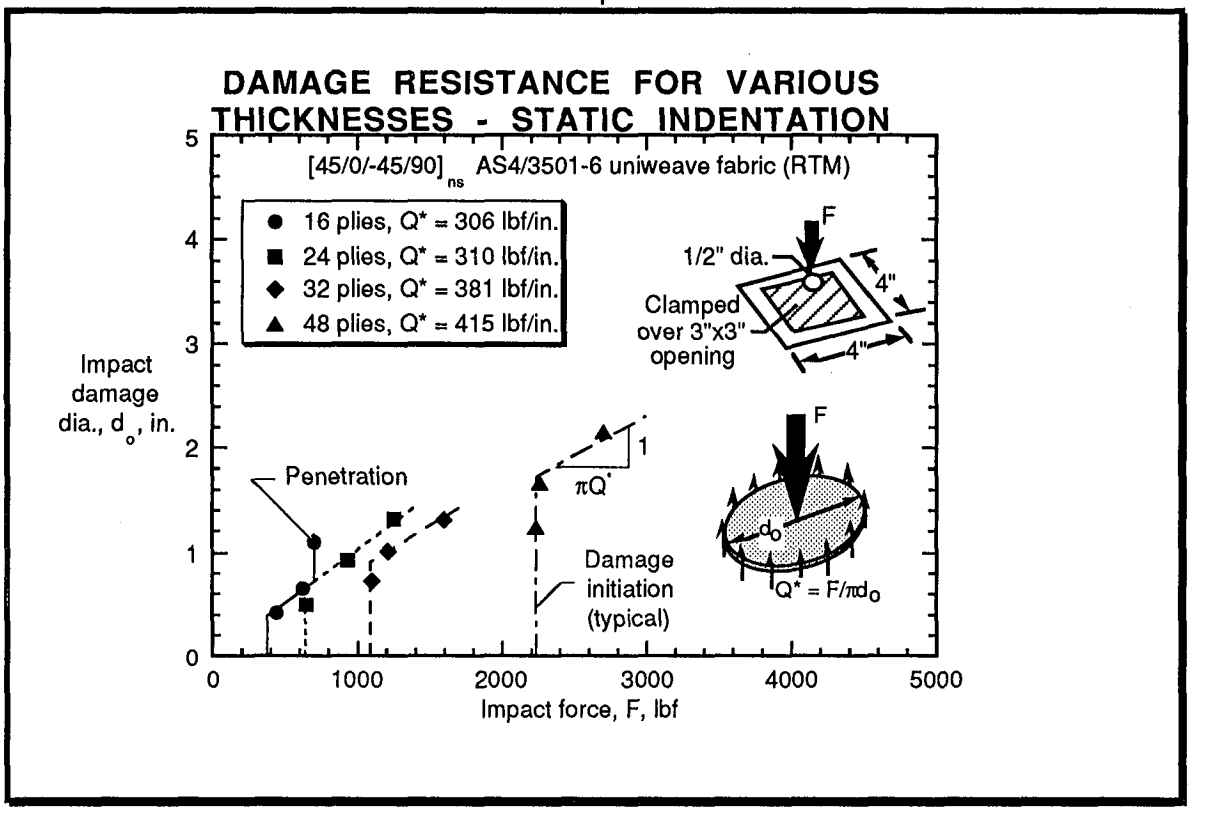

- Damage diameter is plotted against impact force for static indentation tests of 16-, 24-, 32-, and 48-ply quasi-isotropic laminates.
- The impact force for damage initiation and the value of Q^* increase with increasing thickness.

View Graph No. 10

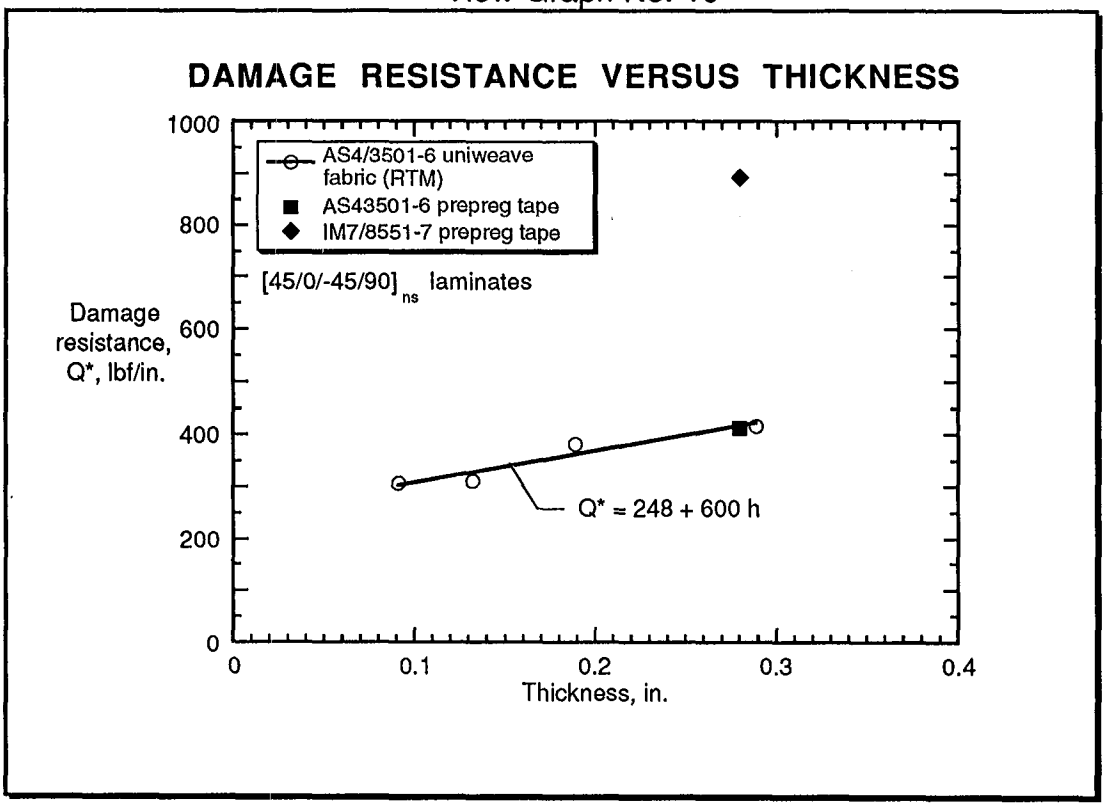

- Damage resistance Q^* is plotted against laminate thickness for the test data in View Graph No. 9.
- The values of Q^* increase linearly with increasing thickness.
- Values of Q^* for the data in View Graph No. 7 are also plotted for comparison. The values of Q^* for the AS4/3501-6 prepreg tape and resin transfer molded (RTM) laminates were equal. As noted in View Graph No. 7, the value of Q^* for the IM7/8551-7 laminate was more than twice that for the AS4/3501-6 laminates.

View Graph No. 11

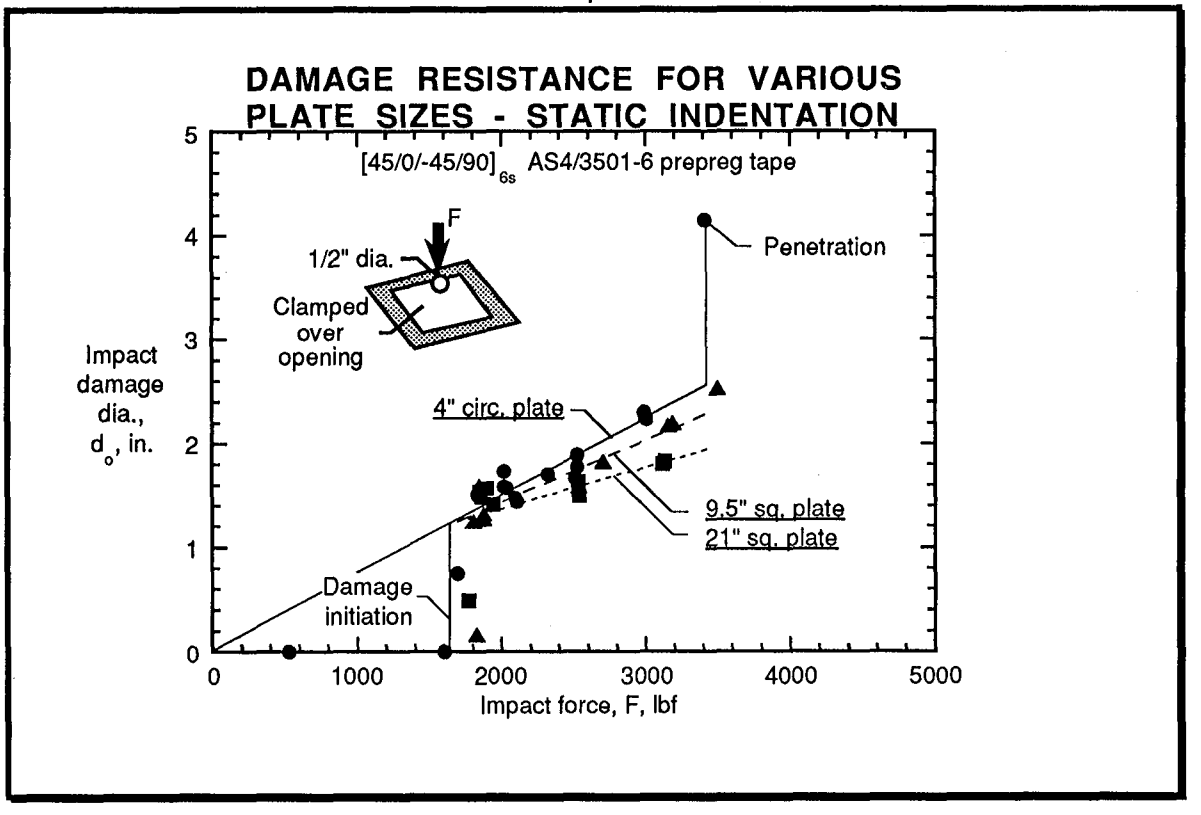

- Values of damage diameter are plotted against impact force for static indentation tests of AS4/3501-6 quasi-isotropic plates of three sizes - 4" circular, 9.5" square, and 21" square.
- The damage diameter decreased with increasing plate size. For 2"-, 3"-, and 4"-circular plates [1], the damage diameter was independent of plate size.

View Graph No. 12

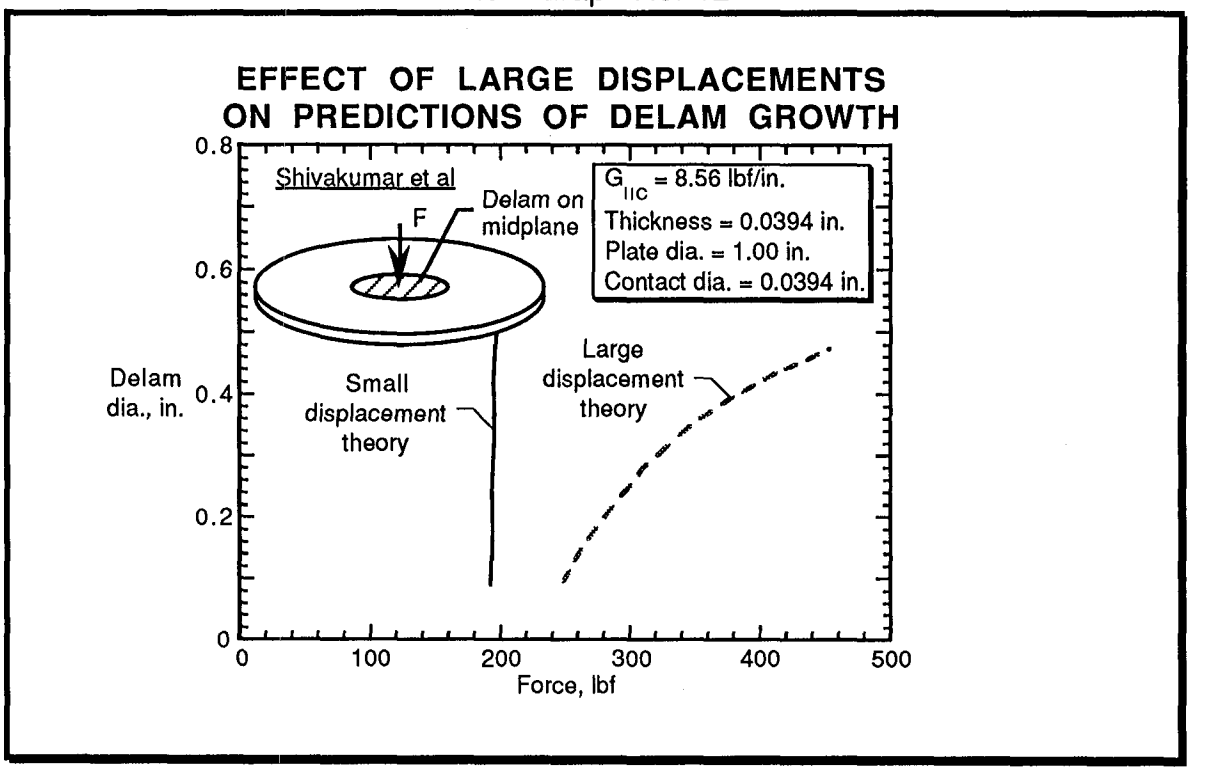

- The diameter of a circular delamination is plotted against force for a circular isotropic plate. The calculations are from reference 5 assuming a constant value of mode II strain energy release rate G_{IIc} = 8.56 lbf/in.

- For small displacement theory, the delamination is predicted to extend across the plate with no increase in force once a critical force is attained. But for large displacement theory, the delamination is predicted to extend only with increasing force. The increase in force to extend the delamination (damage resistance) is due to large displacements. Thus, the increase in damage resistance with increasing plate size in View Graph No. 11 is likely due to large displacements. It is believed that the transverse shear force at the delamination front is reduced by a membrane force that develops with the large displacements.

View Graph No. 13

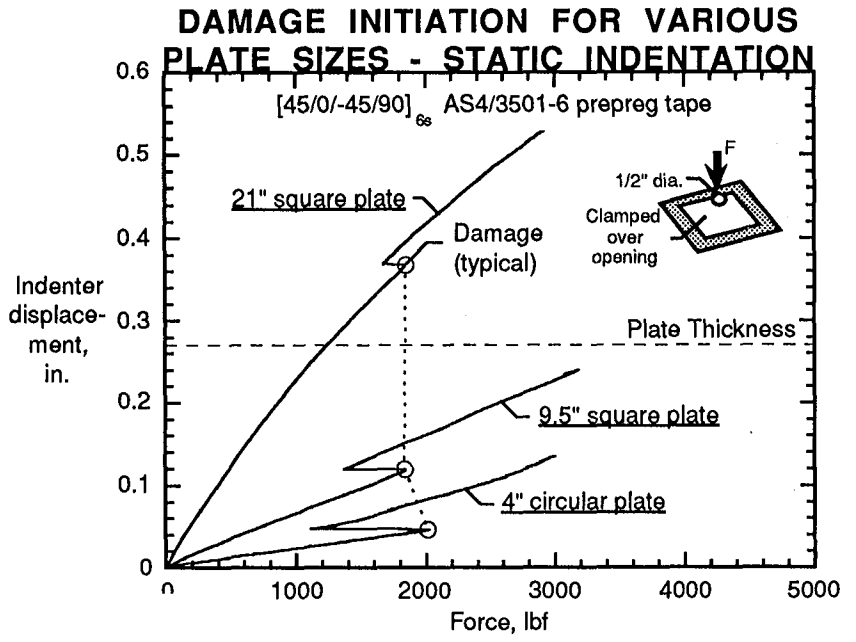

- Indenter displacement is plotted against impact force for the static indentation tests of the plates in View Graph No. 11.
- For a given force, displacement increases with increasing plate size as expected. Displacements exceed plate thickness for the largest plate.
- Damage initiation is indicated by the drops in force for the displacement controlled tests. The forces for damage initiation were relatively independent of plate size as indicated by the dashed line.
- The magnitude of the drops in force decreases with increasing plate size because the magnitude of the increase in displacement due to damage decreases relative to the displacement of the plate. Thus, the decrease in impact force due to damage should decrease with increasing plate size.

View Graph No. 14

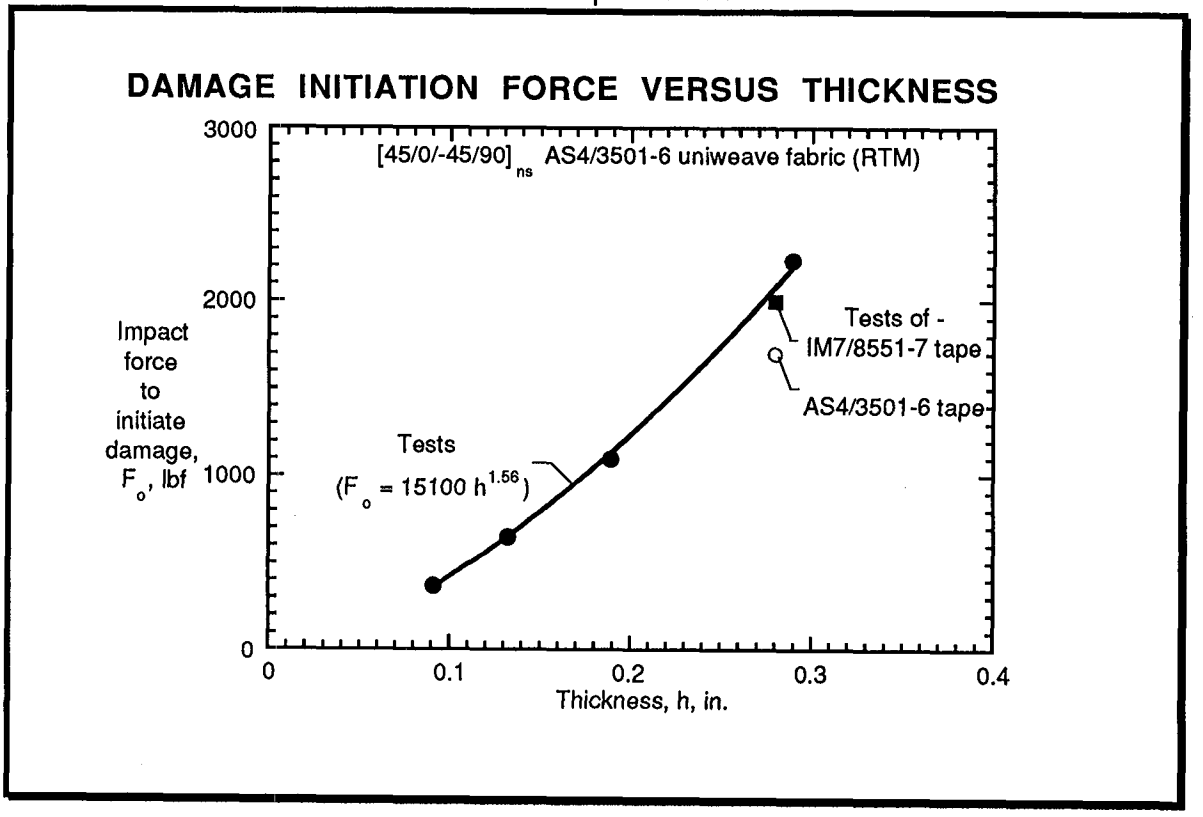

- Impact force to initiate damage is plotted against laminate thickness for the test data in View Graph No. 9.
- The impact force to initiate damage increases with increasing thickness to the 1.56 power.
- Test data for the laminates in View Graph No. 7 is plotted for comparison. Although the damage resistance of the IM7/8551-7 was more than twice that of the AS4/3501-6, the force to initiate damage was only 1.2 times that of the AS4/3501-6.

View Graph No. 15

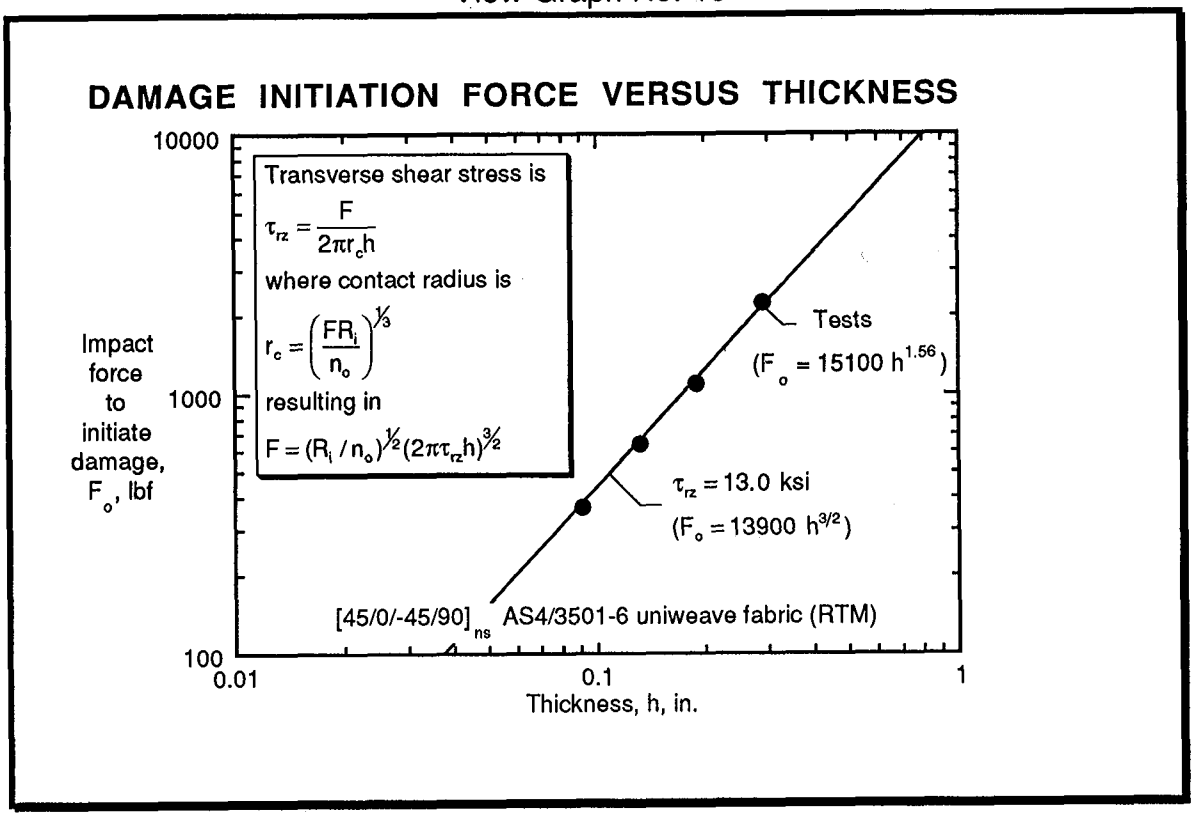

- The test data in View Graph No. 14 is replotted with logarithm scales. Calculations are also plotted for a constant value of transverse shear stress $\tau_{rz}|_{r=r_c}$. A value of τ_{rz} = 13.0 ksi was chosen to fit the data.

- The test data and calculations agree well indicating that the initiation of damage is associated with the transverse shear stress. As noted previously, this damage initiation is likely delamination initiation and growth. For these thin laminates, it is likely that matrix cracking initiates at smaller forces due to flexural tension and shear.

View Graph No. 16

II. TRANSIENT IMPACT RESPONSE
- *Large, Massive Targets*

- The following view graphs involve impact response of large, massive targets.

View Graph No. 17

TWO-MASS/HERTZIAN-SPRING MODEL

Applying Newtonian mechanics to the impacter and plate,

$$m_i \frac{dv_i}{dt} = -F, \quad \text{and} \quad m_p \frac{dv_p}{dt} = -F, \tag{1}$$

where the force-indentation relationship is

$$F = n_0 R_i^{1/2} \alpha^{3/2} \tag{2}$$

and the indentation rate is

$$\dot{\alpha} = v_i + v_p \tag{3}$$

Solving equations (1) - (3),

$$F_{max} = (n_o R_i^{1/2})^{2/5} (\frac{5}{4} M v_i^2)^{3/5} \tag{4}$$

where

$$M = (m_i^{-1} + m_p^{-1})^{-1} \tag{5}$$

- Using Newtonian mechanics and assuming that indentation is governed by Hertz's equation, a relationship can be derived between the impact force and the masses of the impacter and plate [6]. Flexural type deformations are assumed to be negligible.
- The reciprocal of the mass term *M* in equation (5) is the sum of the reciprocals of the impacter and plate. Therefore, equation (4) indicates that the impact force is limited by the smallest of the impacter and plate masses.

View Graph No. 18

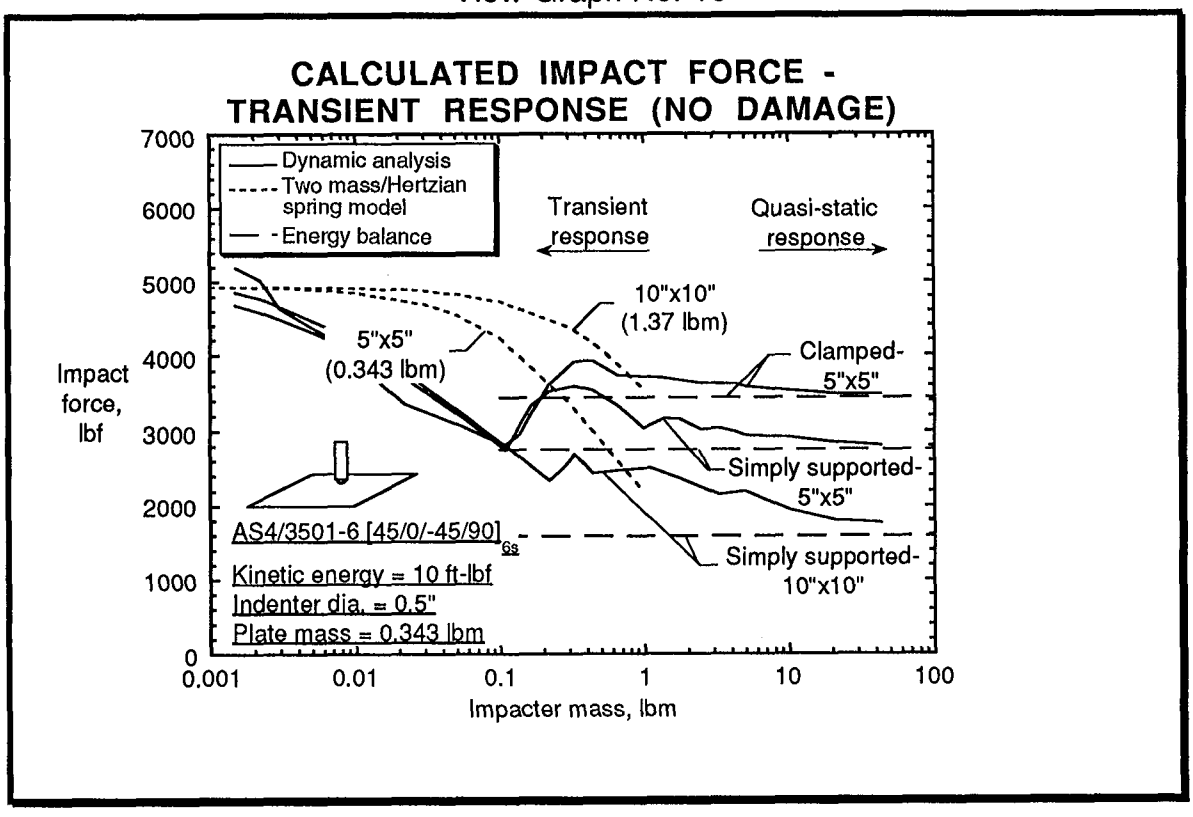

- The impact forces in View Graph No. 3 are replotted against the impacter mass. Calculations using the two mass/Hertzian spring model in View Graph No. 17 are plotted also.

- For impacter masses less than 0.1 lbm, the impact forces from the dynamic analysis are equal because the duration of the impact is less than the time for the waves to reflect from the boundaries [1]. Thus, the impact force is unaffected by the boundaries.

- Impact forces calculated using the two mass/Hertzian spring model for the 10"-square plate were greater than those for the 5"-square plate because impact force increases with increasing M, which increases with increasing plate mass.

- Calculations using the two mass/Hertzian spring model and the dynamic analysis agree only when the impacter mass is less than 0.002 lbm. For impacter masses greater than 0.002 lbm, the calculated values are greater than those from the dynamic analysis because flexural displacements increase with increasing impacter mass.

View Graph No. 19

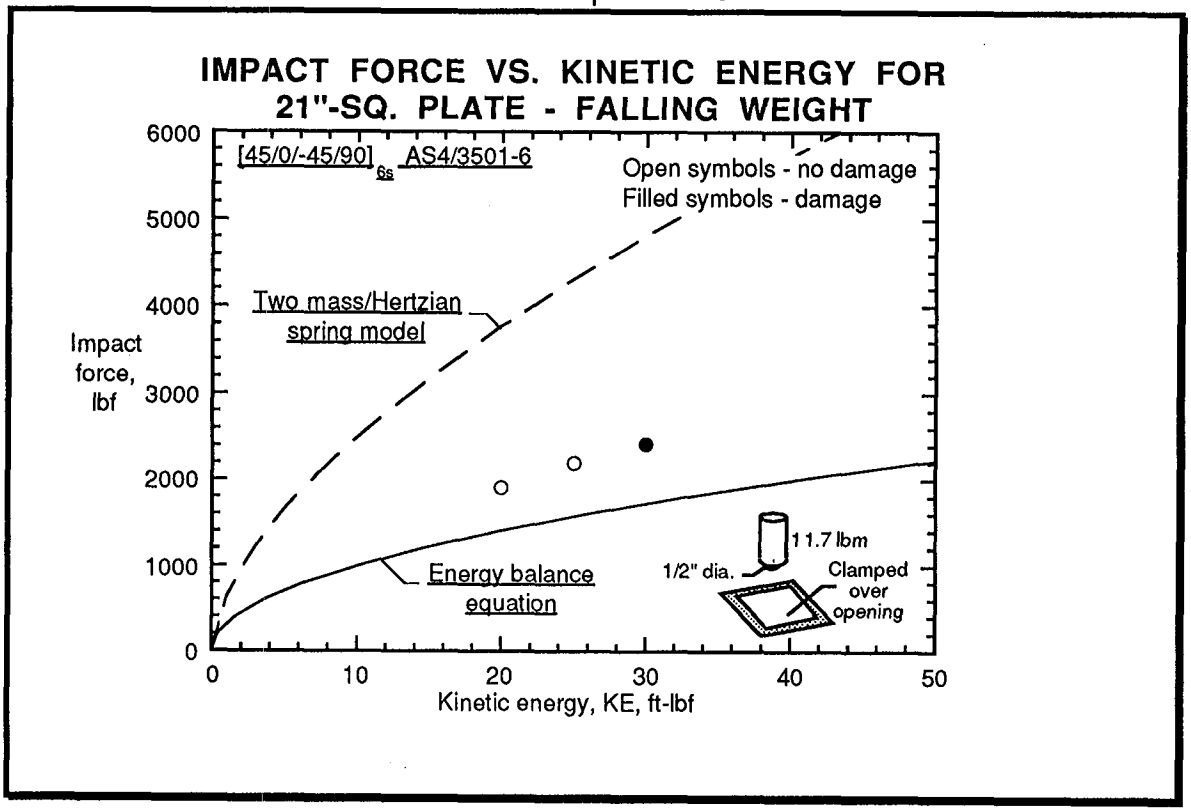

- Impact force is plotted against kinetic energy for falling weight tests of the 21"-square plate. Damage was revealed in C-scan images of only one of the three plates. It appears that the damage did not have a significant effect on the impact force. Damage caused only a small drop in load for the static indentation test of a plate of the same size in View Graph No. 13, indicating that damage would only reduce impact force slightly.

- Calculations are also plotted for the energy balance equation and the two mass/Hertzian spring model. The measured impact forces were about 40% greater than those calculated using the energy balance equation. For the 21"-square plate, the mass ratio $(m_i/m_p)/\alpha^2$ is 15. In View Graph No. 3, the impact force from the dynamic analysis for the 10"x10"-square plate at $(m_i/m_p)/\alpha^2 = 15$ is also about 40% greater than that calculated using the energy balance equation. On the other hand, the measured impact forces were about 50% less than those calculated using the two mass/Hertzian spring model, indicating that the flexural displacements were significant though less than quasi-static values.

View Graph No. 20

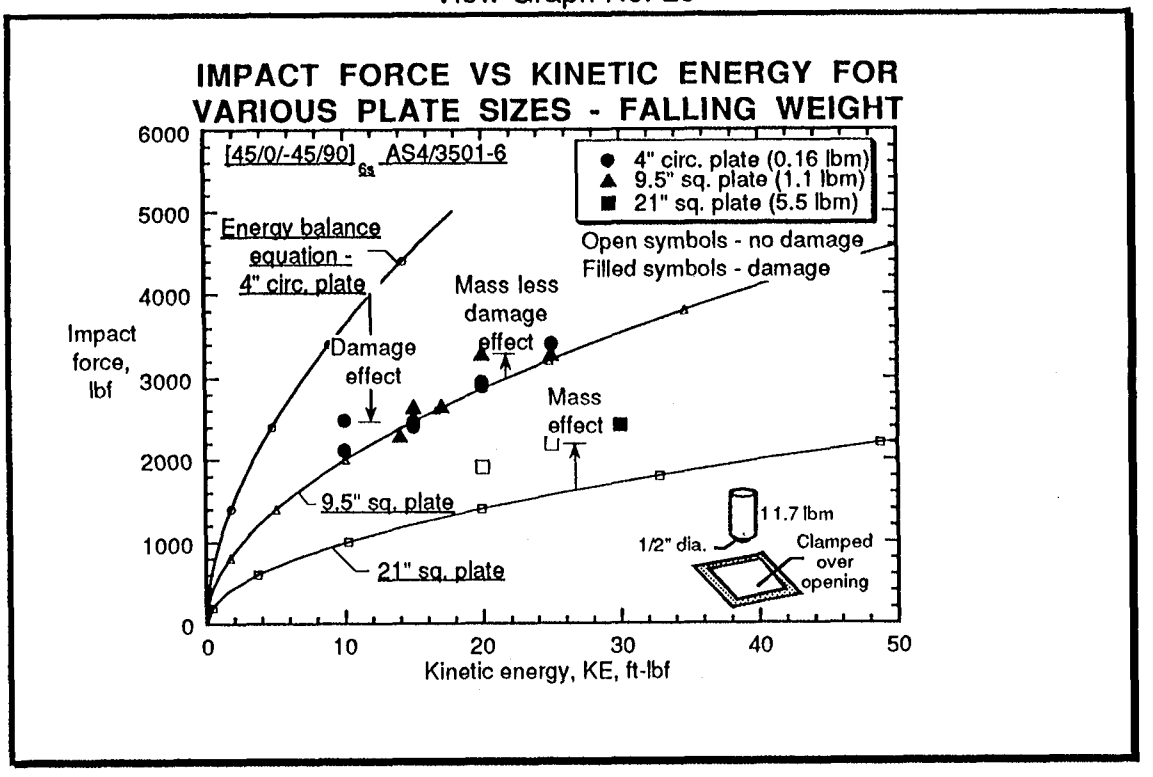

- Impact force is plotted against kinetic energy for falling weight tests of the 4"-circular and 9.5"-square plates. Damage was visible in the C-scan images of all these plates. The data in View Graph No. 19 for the 21"-square plates is included for comparison. The impact forces for the 21"-square plate were less than those for the 4"-circular and 9.5"-square plates, which were about equal.

- Calculations are also plotted for the energy balance equation. The mass ratio $(m_i/m_p)/\alpha^2$ is 530 and 77 for the 4"-circular and 9.5"-square plates, respectively. Thus, the dynamic analysis results in View Graph No. 3 for a kinetic energy of 10 ft-lbf indicate that the response to the falling weight should have been quasi-static for the 4"-circular plates and nearly quasi-static for the 9.5"-square plates. Although impact force increases with increasing kinetic energy, the type of response and hence the difference between impact forces calculated with the dynamic analysis and energy balance equation was not significantly affected by variations in kinetic energy [1].

- The impact forces measured for the 4"-circular plates were about 40% less than those calculated using the energy balance equation, whereas those measured for the 9.5"-square plates were equal to those calculated using the energy balance equation. Since the impact response for the 4"-circular plates was quasi-static, the 40% difference between measured and calculated impact forces was caused by the damage, much as in View Graph No. 4. For the 9.5"-square plates, the damage and transient effect appear to have canceled one another resulting in no difference between measured and calculated impact forces. Thus, damage can offset plate size effects and confound interpretation of experimental results.

View Graph No. 21

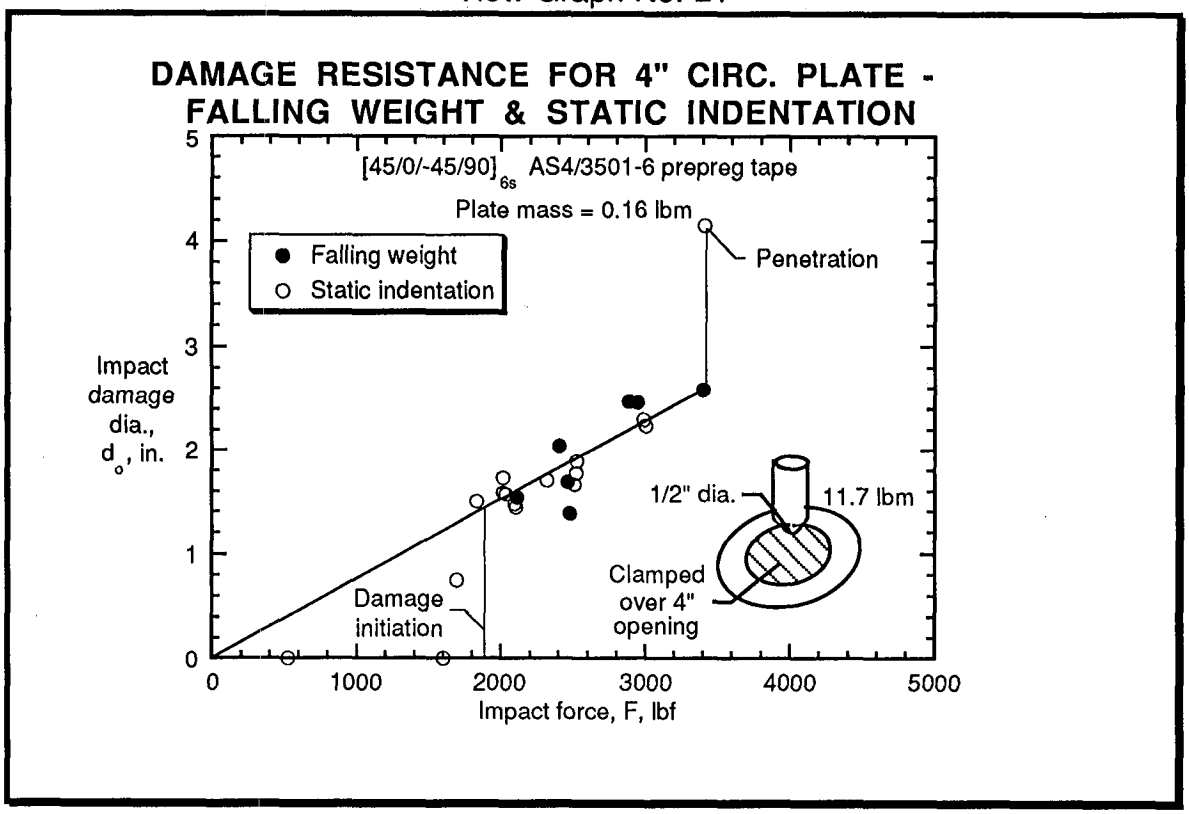

- Impact damage is plotted against impact force for falling weight tests of 4"-diameter circular plates. Static indentation results from View Graph No. 11 are plotted for comparison.

- The falling weight and static indentation data coincide, much as those in View Graph No. 7. As discussed in View Graph No. 20, the response to the falling weight should have been quasi-static.

View Graph No. 22

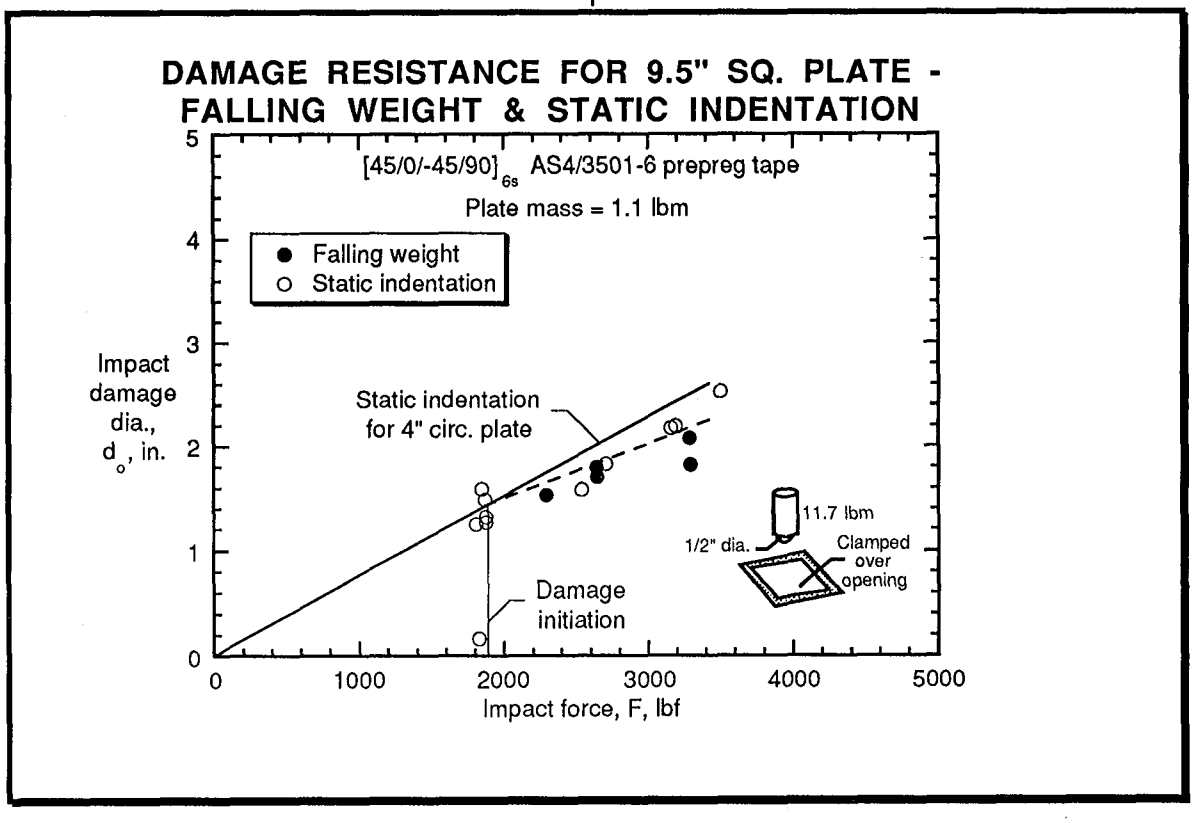

- Impact damage is plotted against impact force for falling weight tests of 9.5"-square plates. Static indentation results from View Graph No. 11 are plotted for comparison.
- The falling weight and static indentation data coincide, much as in View Graph No. 21. As discussed in View Graph No. 20, the response to the falling weight should have been nearly quasi-static.

View Graph No. 23

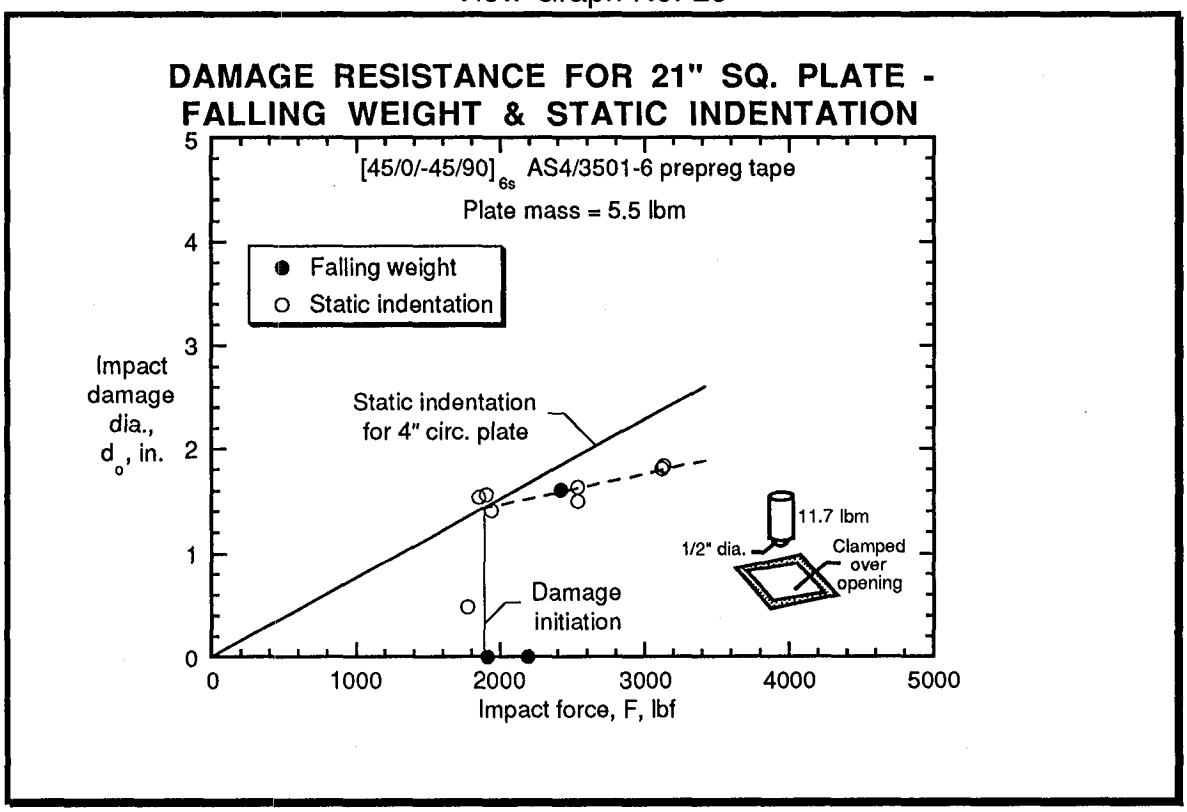

- Impact damage is plotted against impact force for falling weight tests of 21"-square plates. Static indentation results from View Graph No. 11 are plotted for comparison.

- As discussed in View Graph No. 20, the response to the falling weight should have been transient. Nevertheless, the falling weight and static indentation data coincide, much as in View Graphs No. 21 and 22. Thus, the relationship between damage size and impact force was not noticeably affected by the type of response.

View Graph No. 24

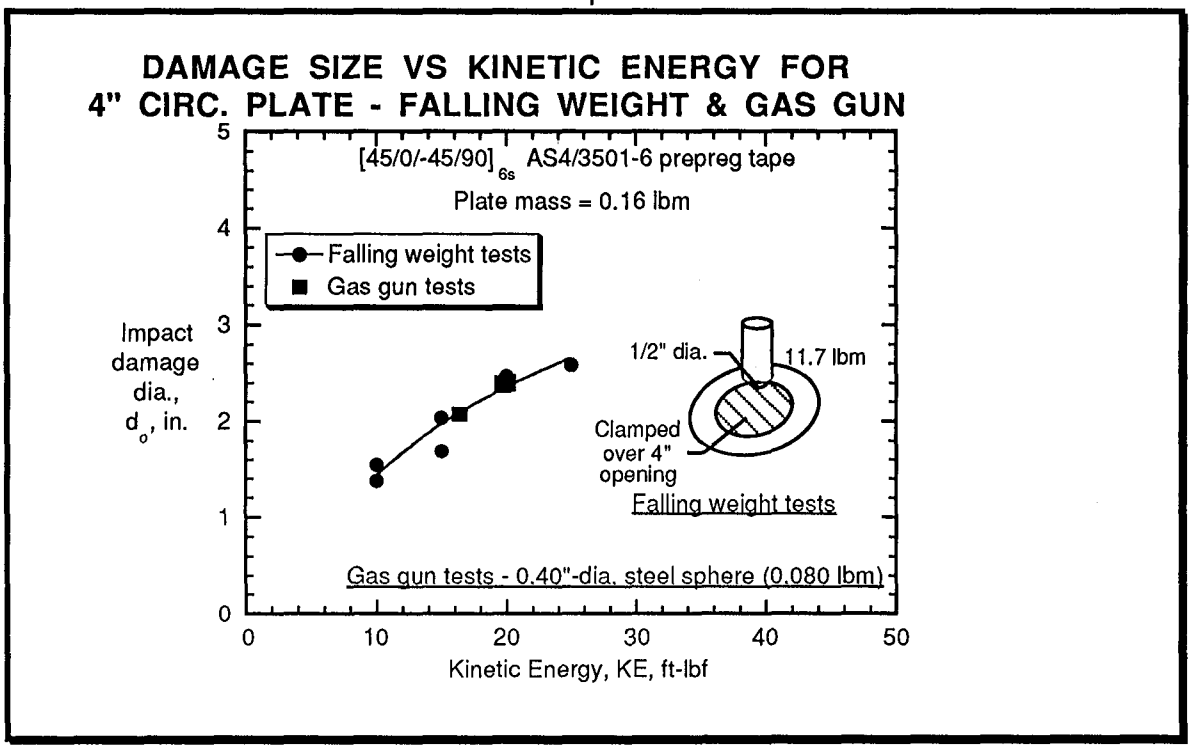

- Damage size for gas gun tests is plotted against kinetic energy for the 4"-circular plates. Impact forces could not be measured. The falling weight results in View Graph No. 21 are plotted against kinetic energy for comparison.

- The damage sizes for the gas gun and falling weight tests were equal. The mass ratio $(m_i/m_p)/\alpha^2$ is 3.6 for a 4"-circular plate. For this mass ratio, the dynamic analysis indicates a transient response for a 5"-square plate in View Graph No. 3, but resulting in an impact force nearly equal to that calculated by energy balance. One would expect the response of a 4"-circular and 5"-square plate to be similar, indicating that the damage size for the gas gun and falling weight tests should have been equal.

View Graph No. 25

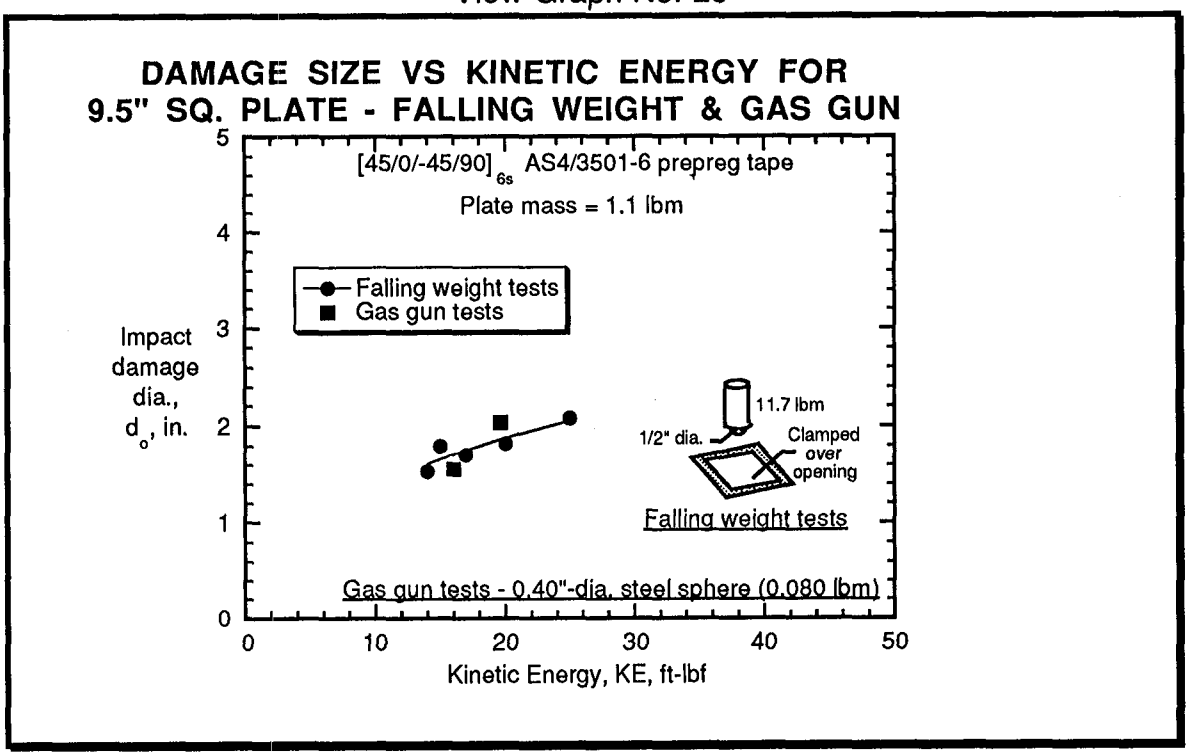

- Damage size for gas gun tests is plotted against kinetic energy for the 9.5"-square plates. The falling weight results in View Graph No. 22 are plotted against kinetic energy for comparison.

- The mass ratio $(m_i/m_p)/\alpha^2$ is 0.53 for a 9.5"-square plate. For this mass ratio, the dynamic analysis response is transient for a 10"-square plate in View Graph No. 3, resulting in an impact force nearly 60% greater than that calculated by energy balance. One would expect the response of a 9.5"- and 10"-square plate to be essentially the same. Even though impact forces should have been greater for the gas gun tests, the damage sizes for the gas gun and falling weight tests were equal. Thus, the difference between calculated impact forces was probably moderated by the damage.

View Graph No. 26

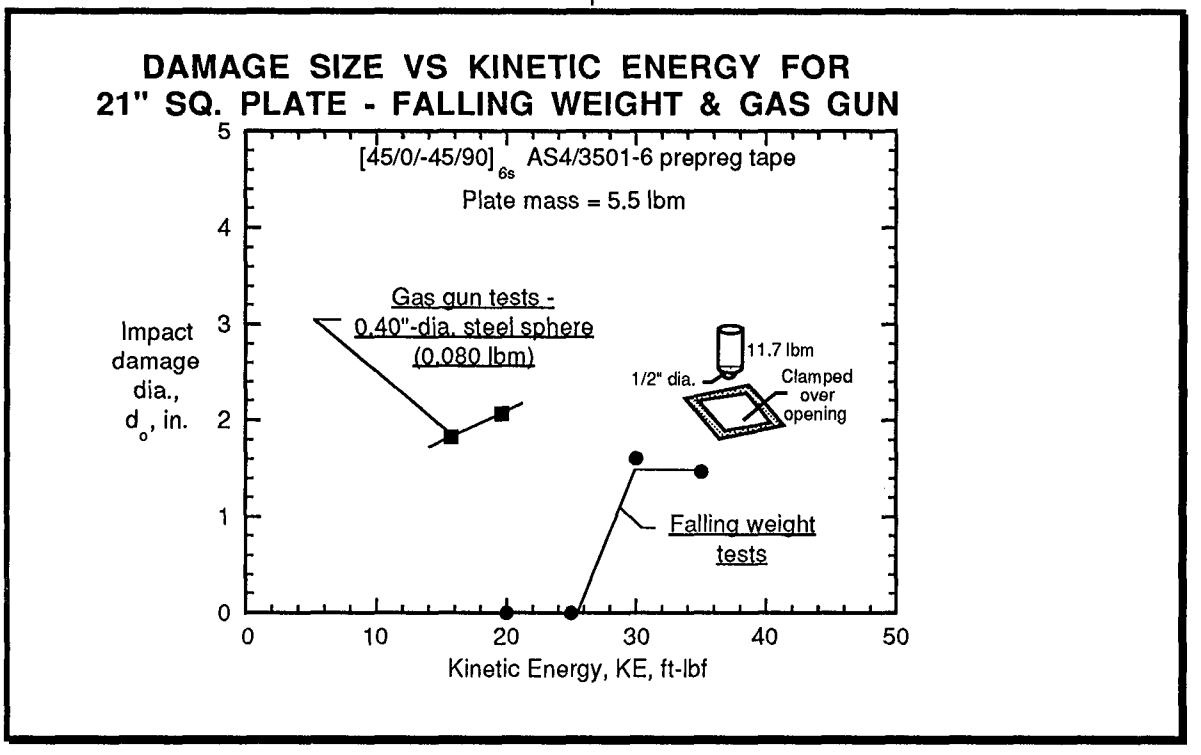

- Damage size for gas gun tests is plotted against kinetic energy for the 21"-square plates. The falling weight results in View Graph No. 23 are plotted against kinetic energy for comparison.

- The mass ratio $(m_i/m_p)/\alpha^2$ is 0.11 for a 21"-square plate. For this mass ratio, the dynamic analysis response is transient for a 10"-square plate in View Graph No. 3, resulting in an impact force more than 100% greater than that calculated by energy balance. One would expect the difference between calculated impact forces for a 21"-square plate to be even greater without damage. Greater values of kinetic energy were necessary to produce damage for the falling weight tests than the gas gun tests, indicating that the damage did not completely moderate the differences between impact force as in View Graph No. 25.

View Graph No. 27

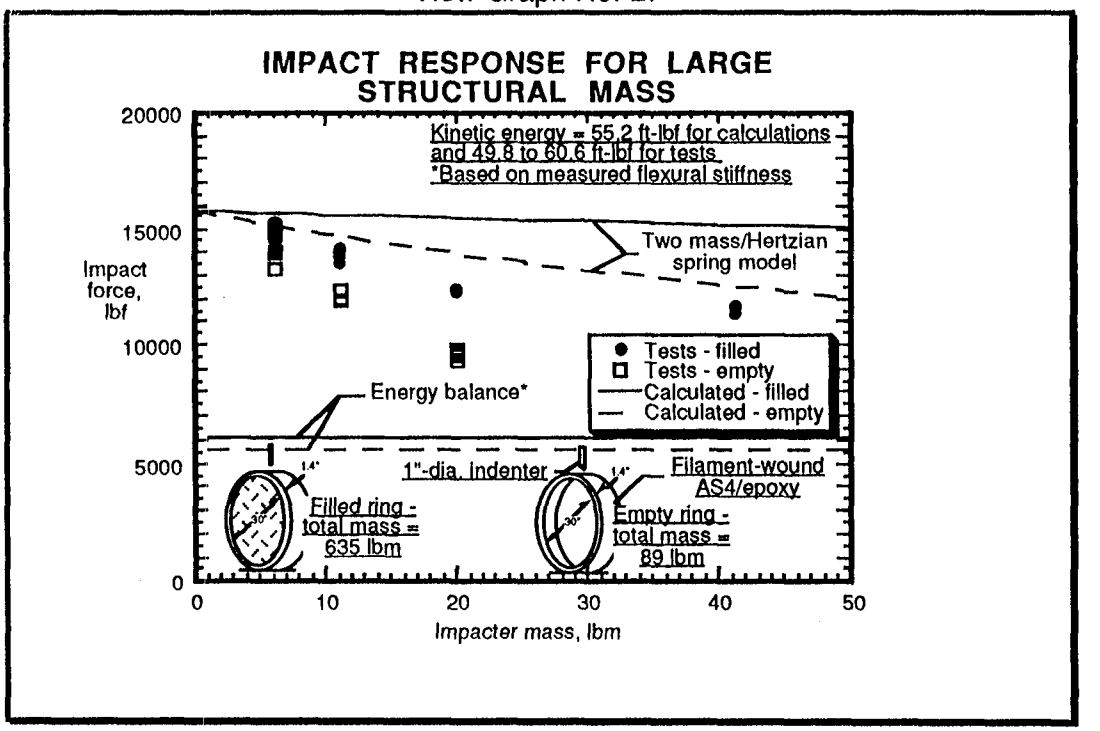

- Impact force is plotted against impacter mass for falling weight tests of two filament-wound rings [7]. The kinetic energies varied over a fairly narrow range of 49.8 to 60.6 ft-lbf. One of the rings was filled with inert propellant and one was empty. As a result of the inert propellant, the mass of the filled ring was about seven times that of the empty ring. The rings represented 12-ft. diameter, 25-ft. long cases of the same thickness for solid rocket motors.

- The impact forces decreased with increasing impacter mass and were greater for the filled ring than the empty ring. These values of force are much greater than those shown in the previous view graphs for relatively thin plates. No damage was visible in C-scan images for these values of kinetic energy and indenter diameter.

- Calculations with the energy balance equation and the two mass/Hertzian spring model are plotted for comparison. A static indentation test was also conducted on each specimen to measure flexural stiffness. These values were used in the energy balance equations. The inert propellant resulted in only a 25% increase in flexural stiffness.

- For the smallest impacter mass, the forces from the tests were within 10% and 15% of those calculated with the two mass/Hertzian spring model for the filled and empty rings, respectively. With increasing impacter mass, the forces asymptotically approached those calculated with the energy balance equation -- more closely for the empty ring than the filled ring. Calculations with the two mass/Hertzian spring model correctly account for the differences between ring masses.

- The ratios of impacter mass to ring mass varied from 0.068 to 0.46 for the empty ring and from 0.0096 to 0.065 for the filled ring, indicating also that the response was transient. For the smallest impacter mass and filled ring, the mass ratio was smaller than that for the gas gun test of the 21"-square plate in View Graph No. 26.

View Graph No. 28

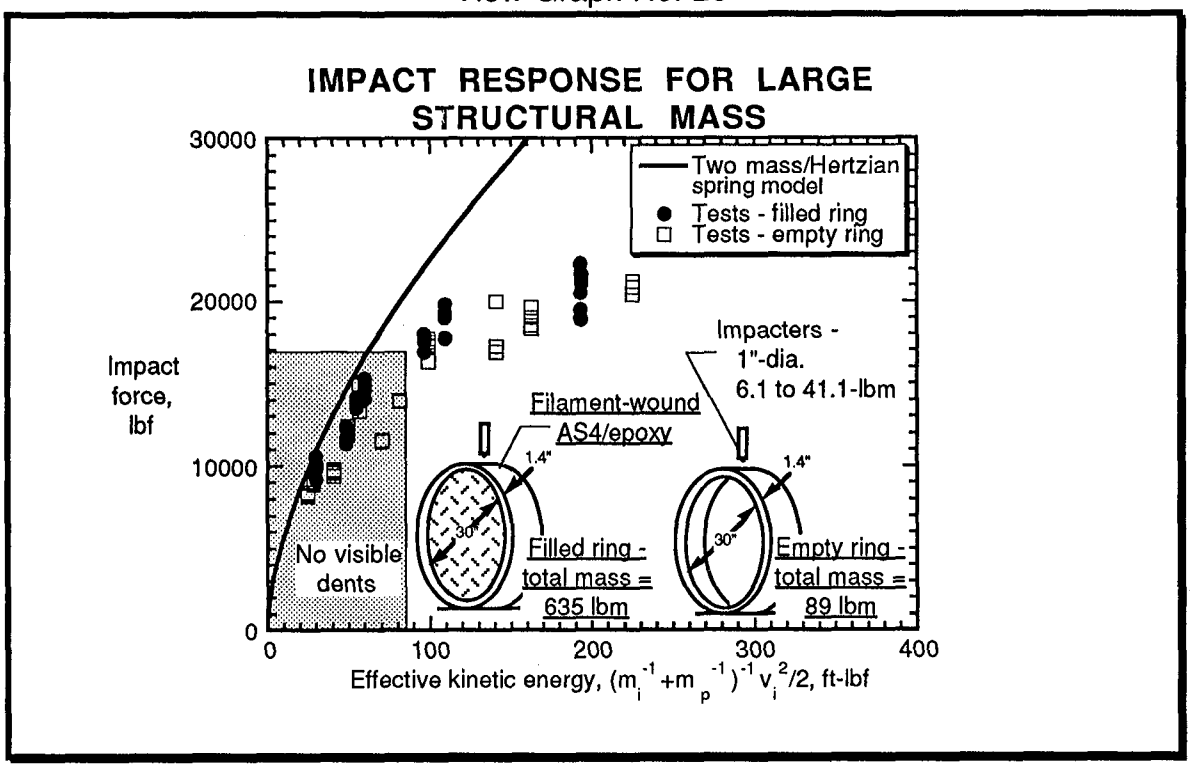

- Impact force is plotted against effective kinetic energy $Mv_i^2/2$ for the filled and empty rings. Damage was not visible in C-scans nor dents on the surface for tests within the shaded region. The use of effective kinetic energy causes the data for the filled and empty rings to coincide.

- Calculations with the two mass/Hertzian spring model agree with the test data only for the smallest values of kinetic energy, which correspond to the smallest values of impacter mass. Some of the discrepancy outside the shaded region is due to damage; however, most is due to flexural displacements, which are not included in the two mass/Hertzian spring model. Of course, these flexural displacements are much smaller than quasi-static values as indicated by the large discrepancy between the impact forces from tests and those calculated with energy balance in View Graph No. 27.

View Graph No. 29

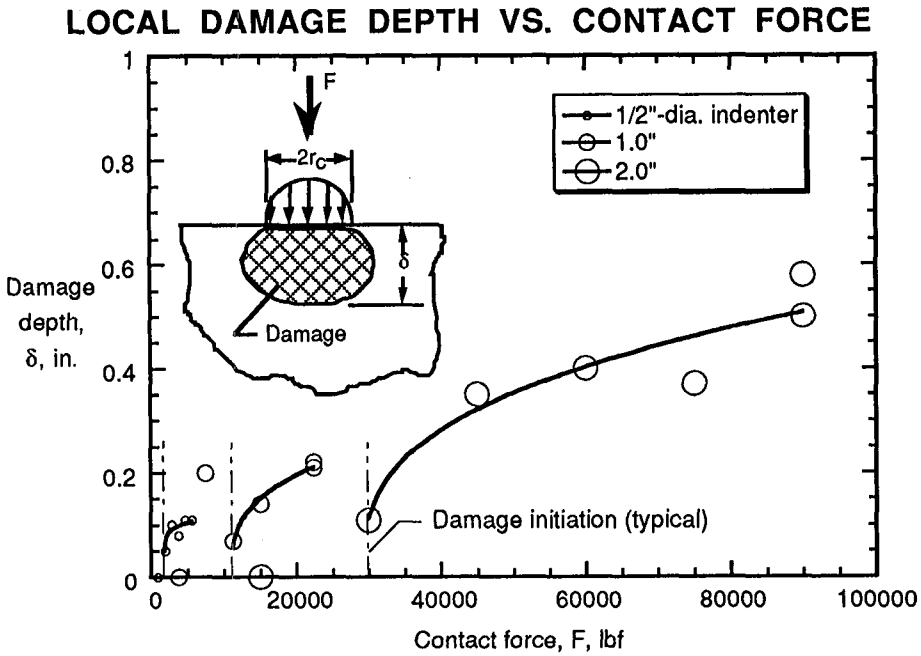

- Depth of fiber damage is plotted against contact force for static indentation tests of coupons cut from filament-wound rings like those in View Graph Nos. 27 and 28. Results are shown for 1/2"-, 1"-, and 2"-diameter hemispherical indenters. The damage consisted of matrix cracks and broken fibers; no delaminations were observed. The extent of fiber damage was determined by pyrolyzing the coupons and examining the layers of carbon fibers.

- The force to initiate the damage and the depth to which it grew increased with increasing indenter diameter.

View Graph No. 30

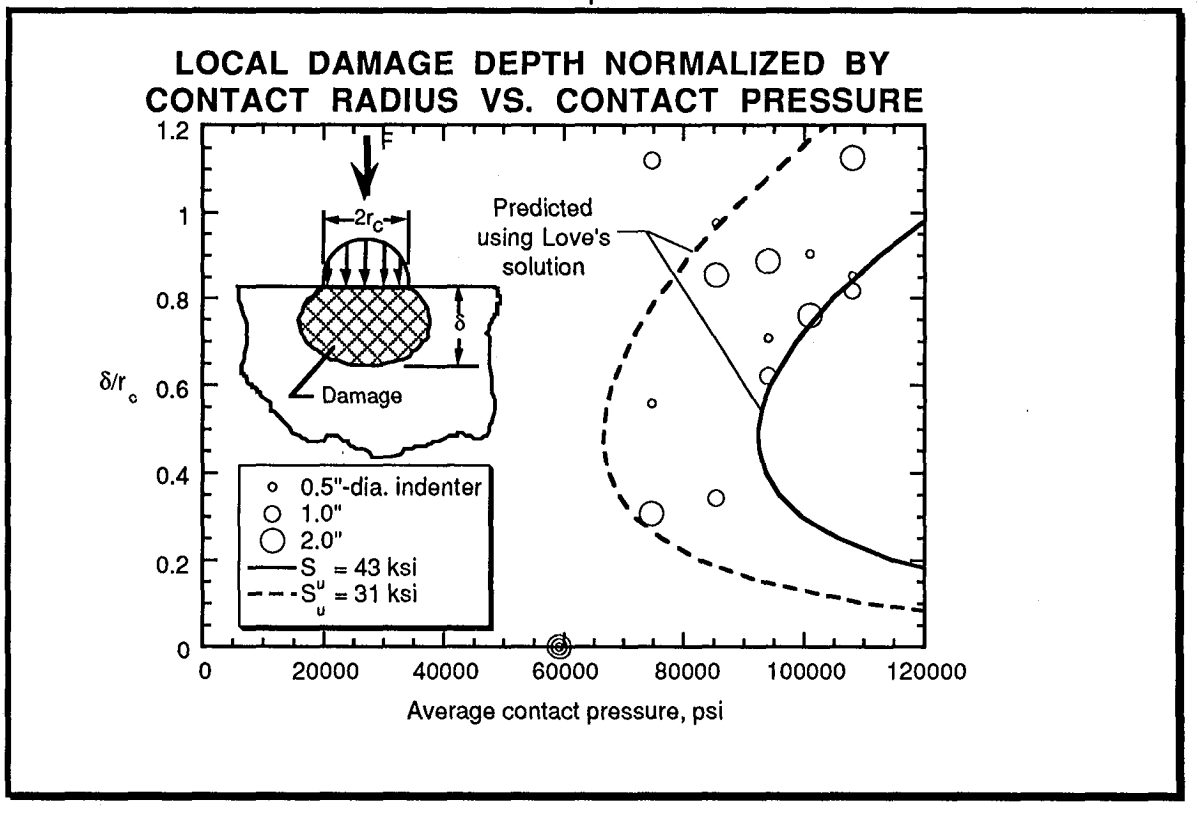

- The damage depths in View Graph No. 29 were divided by the contact radius and plotted against the average contact pressure, which was calculated by dividing the contact force by πr_c^2. The contact radius r_c was calculated using Hertz's equation in View Graph No. 15. The data for the various indenter diameters coalesce.

- Two contours of principal shear stress from Love are plotted for values of 43 and 31 ksi to bound the data [7]. Agreement between the tests and calculations indicates that a principal shear stress criterion can be used to predict the onset and growth of local damage in thick laminates. The contact pressure to initiate damage is 2.15 times the principal shear stress.

View Graph No. 31

GENERAL CONCLUSIONS

- For large impacter mass, response is quasi-static, and impact force can be predicted using energy balance.

- For large target size or mass
  - response is transient and impact force predicted using energy balance is too small.
  - Impact force predicted using the two mass/hertzian spring model is upper bound.

- Impact damage reduces impact force.

View Graph No. 32

CONCLUSIONS FOR THIN PLATES

- Impacts caused delaminations.
- Delaminations initiated when a critical transverse shear stress was exceeded.
- Delamination size
  - increased linearly with increasing impact force.
  - corresponded to critical value of transverse shear stress per unit width (damage resistance).
- Damage resistance
  - increased with increasing plate thickness.
  - increased somewhat with increasing plate size.
  - appears to be associated with large displacements.

View Graph No. 33

CONCLUSIONS FOR THICK PLATES

- Impacts caused only local damage in 1.4"-thick plate - no delaminations.

- Damage initiated when a critical contact pressure was exceeded.

- Damage size
  - increased with increasing impact force.
  - corresponded to a critical value of principal shear stress.
  - increased with increasing impacter diameter.

REFERENCES

1. Jackson, Wade, C.; and Poe, Jr. C. C.: The Use of Impact Force as a Scale Parameter for the Impact Response of Composite Laminates. NASA TM 104189 and AVSCOM TR 92-B-001, January 1992

2. Gosse, J. H.; and Mori, P. B. Y.: Impact Damage Characterization of Graphite/Epoxy Laminates. Proceedings of the American Society for Composites - Third Technical Conference, Sept. 25-29, 1988, pp. 344-353.

3. Poe, Jr., C. C.: Simulated Impact Damage in a Thick Graphite/Epoxy Laminate Using Spherical Indenters. *Proceedings of American Society for Composite Materials*, Technomic Publishing, Lancaster, PA, Nov. 1988.

4. Sjöblom, Peter: Simple Design Approach Against Low-Velocity Impact Damage. 32nd International SAMPE Symposium, April 6-9, 1987, pp. 529-539.

5. Shivakumar, K. N.; and Elber, W.: Delamination Growth Analysis in Quasi-Isotropic Laminates under Loads Simulating Low-Velocity Impact. NASA TM 85819, June 1984.

6. Greszczuk, Longin B.: Damage in Composite Materials due to Low Velocity Impact. Impact Dynamics, John Wiley & Sons, Inc., 1982, pp. 55-94.

7. Poe, Jr., C. C.: Impact Damage and Residual Tension Strength of a Thick Graphite/Epoxy Rocket Motor Case. *Journal of Spacecraft and Rockets*, Vol. 29, No. 3, May-June 1992, pp. 394-404.

REPORT DOCUMENTATION PAGE

Form Approved
OMB No. 0704-0188

1. AGENCY USE ONLY *(Leave blank)*	2. REPORT DATE	3. REPORT TYPE AND DATES COVERED
	July 1994	Conference Publication

4. TITLE AND SUBTITLE
Workshop on Scaling Effects in Composite Materials and Structures

5. FUNDING NUMBERS
WU 505-63-50-09

6. AUTHOR(S)
Karen E. Jackson, Compiler

7. PERFORMING ORGANIZATION NAME(S) AND ADDRESS(ES)
NASA Langley Research Center
Hampton, VA 23681-0001

8. PERFORMING ORGANIZATION REPORT NUMBER
L-17414

9. SPONSORING/MONITORING AGENCY NAME(S) AND ADDRESS(ES)
National Aeronautics and Space Administration
Washington, DC 20546-0001

10. SPONSORING/MONITORING AGENCY REPORT NUMBER
NASA CP-3271

11. SUPPLEMENTARY NOTES
Jointly sponsored by the Engineering Science and Mechanics Department of Virginia Tech, Blacksburg, VA and the Institute for Mechanics and Materials, University of California at San Diego.

12a. DISTRIBUTION/AVAILABILITY STATEMENT
Unclassified–Unlimited

Subject Category 39

12b. DISTRIBUTION CODE

13. ABSTRACT *(Maximum 200 words)*
This document contains presentations and abstracts from the Workshop on Scaling Effects in Composite Materials and Structures jointly sponsored by NASA Langley Research Center, Virginia Tech, and the Institute for Mechanics and Materials at the University of California, San Diego, and held at NASA Langley on November 15–16, 1993. Workshop attendees represented NASA, other government research labs, the aircraft/rotorcraft industry, and academia. The workshop objectives were to assess the state-of-technology in scaling effects in composite materials and to provide guidelines for future research.

14. SUBJECT TERMS
Scaling effects; Similitude; Composite materials; Dimensional analysis; Structural analysis; Strength

15. NUMBER OF PAGES
357

16. PRICE CODE
A16

17. SECURITY CLASSIFICATION OF REPORT	18. SECURITY CLASSIFICATION OF THIS PAGE	19. SECURITY CLASSIFICATION OF ABSTRACT	20. LIMITATION OF ABSTRACT
Unclassified	Unclassified	Unclassified	

National Aeronautics and
Space Administration
Langley Research Center
Mail Code 180
Hampton, VA 23681-00001